جامعة سيدي محمد بن عبد الله بفاس
ⵜⴰⵙⴷⴰⵡⵉⵜ ⵙⵉⴷⵉ ⵎⵓⵃⵎⴷ ⴱⵏ ⵄⴱⴷⵍⵍⴰⵀ ⴰ ⴼⴰⵙ
UNIVERSITÉ SIDI MOHAMED BEN ABDELLAH DE FES

كلية العلوم ظهر المهراز فاس
ⵜⴰⵖⵡⵍⵎⵜ ⵏ ⵜⵣⵔⴼⵜ ⵉⵎⵣⵔⵉ ⴼⴰⵙ
FACULTE DES SCIENCES DHAR EL MAHRAZ FES

N° d'ordre : 53/2024

Centre des Études : ***Sciences et Techniques et Sciences Médicales***

Formation Doctorale : ***Mathématiques et Applications***.

Discipline : ***Mathématiques.***
Spécialité : ***Mathématiques Appliquées.***
Laboratoire : ***Analyse Mathématiques et Applications.***

THÈSE DE DOCTORAT

Contributions to Exploring Memory Effects in Fractional Calculus : Insights into Vesicle Dynamics, Microswimmer Behavior, and Epidemiological Models

Présentée par :

Ghizlane DIKI

Soutenue le 26/10/2024 devant le jury :

Pr. MELIANI Said	***Faculté des Sciences et Techniques - Beni Mellal***	***Président***
Pr. SEAID Mohammed	***Université de Durham – Royaume Uni***	***Rapporteur***
Pr. ALAOUI Aziz	***Université Le Havre Normandie - France***	***Rapporteur***
Pr. AKDIM Youssef	***Faculté des Sciences Dhar El Mahraz - Fès***	***Rapporteur***
Pr. EL ALAOUI Fatima-Zahra	***Faculté des Sciences - Meknès***	**Examinatrice**
Pr. HACHIMI Hanaa	***École National des Sciences Appliquées - Kénitra***	**Examinatrice**
Pr. BARBARA Abdelkarim	***Faculté des Sciences Dhar EL Mahraz - Fès***	**Examinateur**
Pr. AZROUL Elhoussine	***Faculté des Sciences Dhar El Mahraz - Fès***	**Directeur de thèse**
Pr. GUEDDA Mohammed	***Université de Picardie Jule Verne – Amiens - France***	**Co-Directeur de thèse**

Année Universitaire : 2024-2025

Dedication




To my dear parents, Omar and Amina, whose unwavering love
and endless support have been the cornerstone of my path.
Your sacrifices and encouragement have been
my strength throughout this entire process

To my sister, Hiba, whose unwavering support and be-
lief in me have been a constant source of inspiration.
Your presence has made every step of this endeavor more meaningful.

To my brother, Mouhcine, whose camaraderie and en-
couragement have been a true source of strength.
Your support has been invaluable and
has helped shape this accomplishment.

This thesis represents not only years of hard work
but also the immeasurable support of my family.
Each page is a testament to your love and be-
lief in my dreams. Thank you for being my guid-
ing light and for sharing this achievement with me.




ACKNOWLEDGEMENTS

The completion of this thesis marks the culmination of a long and challenging journey, one that I could not have accomplished without the support, encouragement, and guidance of many remarkable individuals. It has been a demanding experience, but also one filled with growth, learning, and moments of profound inspiration. I owe this achievement to the collective effort of all those who have stood by me during this time.

I would like to begin by expressing my deepest gratitude to my thesis supervisor, **Prof. EL Houssine AZROUL**. Their intellectual guidance, insightful feedback, and unwavering support have been essential to my progress throughout this research. His belief in my abilities and their commitment to excellence pushed me to go beyond my limits, and for that, I will always be deeply appreciative.

A heartfelt thank you also goes to my co-supervisor, **Prof. Mohamed GUEDDA**, whose expertise, critical advice, and attention to detail helped shape the direction of my work. His encouragement and constant availability for discussion were invaluable in refining my research and driving it toward completion.

I would like to express my profound gratitude to my Ph.D. thesis committee members. I am particularly honored to extend my heartfelt appreciation to **Prof. MELIANI Said** from Sultan Moulay Slimane University-Beni-Mellal for graciously accepting the role of President of the defense committee. His leadership and expertise have been invaluable throughout this journey.

I would also like to sincerely thank **Prof. SEAID Mohammed** from Durham University, UK, **Prof. ALAOUI Aziz** from Le Havre Normandy University, France, and **Prof. AKDIM Youssef** from Sidi Mohamed ben Abdellah University, Fez, for their commitment as Rapporteurs. Their insightful evaluations and constructive feedback have significantly enriched the quality of my thesis and advanced my research.

Additionally, I wish to acknowledge the Examiners of my thesis: **Prof. EL ALAOUI Fatima-Zahra** from the Faculty of Sciences, Meknès, **Prof. HACHIMI Hanaa** from the National School of Applied Sciences, Kénitra, and **Prof. BARBARA Abdelkrim** from Sidi Mohamed ben Abdellah University, Fez. Their critical evaluations and thoughtful insights have been instrumental in shaping my academic development and enhancing the overall quality of this work.

Finally, I would like to express my gratitude to **Prof. Nabil KABBAJ**, Vice-Dean in charge of scientific research and cooperation, for his humility, availability, support, and encouragement.

To my colleagues and fellow researchers, who have become much more than collaborators; they have become like family. I extend my deepest thanks. **Sara BOUDA**, **Houria EL-YAHYAOUI**, **Meryem ELLEKHLIFI Nezha KAMALI**, **Safae L'KIMA**, and **Nassira MADANI**, your friendship, encouragement, and shared passion for knowledge have made this journey far richer and more meaningful. Together, we have faced both challenges and victories, and your support has made the process infinitely more rewarding. It has been a privilege to work alongside such talented individuals, and I will always cherish the moments we have shared, both inside and outside the academic setting.

I would also like to honor the former members of our Department of Mathematics who have now become esteemed professors; their encouragement and mentorship have left a lasting impact on our community, inspiring us all to reach new heights in our research endeavors. Special thanks to **Omar BENSLIMANE**, **Athmane BOUMAZOURH**, **Omar KCHIT**, **Mohammed SHIMI**, and **Mohammed SRATI**. Your steadfast support and friendship have transformed the challenges of research into deeply rewarding experiences. Among them is someone whose presence fills my life with warmth and light in the most beautiful way. The bonds we've formed will always hold a cherished place in my heart, enriching my experience in ways I will forever treasure.

To my dear friends **Imane**, **Wiam**, **Mojahid**, and **Hasnae**, and my esteemed colleagues at Laboratoire LAMA, your unwavering support and collaboration have been the guiding light of this incredible journey. I am genuinely grateful for the stimulating discussions, shared knowledge, and laughter we've experienced together.

Finally, my deepest love and gratitude are reserved for my family. To my parents, **Omar** and **Amina**, words cannot fully capture the depth of my appreciation for your unconditional love, patience, and unwavering belief in me. Your constant support has been the foundation of everything I have achieved. To my siblings, **Hiba** and **Mouhcine**, thank you for being my pillars of strength, my confidants, and my greatest sources of encouragement. You have been with me every step of the way, and this accomplishment would not have been possible without your love and care.

In conclusion, I extend my heartfelt thanks to all those who have played a role, whether directly or indirectly, in the completion of this thesis. Your contributions, no matter how large or small, have left an indelible mark on this work, and I am forever grateful.

INDEX OF SYMBOLS AND NOTATIONSV

Functions

$\Gamma(\alpha)$	The Gamma function.
$\beta(p,q)$	The Beta function.
$E_\alpha(z)$	The one-parameter Mittag-Leffler function.
$E_{\alpha,\beta}(z)$	The two-parameter Mittag-Leffler function.
$\mathscr{L}\{f(t)\}$	The Laplace transform of the function f.
$\psi(t)$	The orientation angle for the vesicle.
$\mathscr{R}(t)$	The shape deformation of the vesicle

.

Derivative and Integral

$D^n = \frac{d^n}{dt^n}$	Ordinary derivative with respect to t of integer order n.
I_a^α	Riemann-Liouville fractional integral of order α.
${}^{\mathscr{RL}}D_a^\alpha$	Riemann-Liouville fractional derivative of order α.
${}^{C}D_a^\alpha$	Caputo fractional derivative of order α.
${}^{\mathscr{J}}D_a^\alpha f$	Jumarie fractional derivative of order α.

Abbreviations

RBCs	Red Blood Cells.
TT	Tank-treading.
TB	Tumbling.
VB	Vacillating Breathing.
OD-TT	Over-damped tank-treading.
UD-TT	Under-damped tank-treading.
R-L	Riemann-Liouville.
M-L	Mittag-Leffler.
ODEs	Ordinary differential equations.

ABSTRACT

Fractional calculus offers a robust mathematical framework for modeling systems with memory effects, enabling a deeper understanding of dynamic processes that exhibit non-local behaviors over time. This thesis investigates the impact of memory effects through fractional calculus across diverse dynamic systems, with a particular focus on vesicle dynamics, microswimmers in shear flows, and drug transmission in epidemiological models. Vesicle dynamics and microswimmer behavior are analyzed using fractional models, specifically the Caputo and Jumarie's modified Riemann-Liouville derivatives, revealing novel tank-treading modes and the role of memory effects in vesicle deformation. Analytical and numerical methods, such as solutions based on the Mittag-Leffler function, provide precise results for the orientation and deformation of vesicles and red blood cells. Furthermore, the transition from flipping to stationary motion in red blood cells under varying viscosity ratios is explored using the modified Riemann-Liouville derivative, advancing the understanding of particle behavior in complex fluid environments. Additionally, a compartmental drug transmission model, formulated using the Caputo fractional derivative, evaluates the influence of family and public health education on reducing drug transmission, incorporates sensitivity analysis to evaluate how variations in model parameters affect drug transmission outcomes. This work significantly contributes to applied mathematics by offering novel insights into both vesicle dynamics and epidemiological modeling through the lens of fractional derivatives, with implications for future research in these fields.

Keywords: Fractional calculus, Caputo fractionnal derivative, Jumarie's modified Riemann-Liouville fractional derivative, Memory effects, Vesicle dynamics, Red Blood Cells, Microswimmers, Drug transmission, Epidemiological models.

RÉSUMÉ

Le calcul fractionnaire offre un cadre mathématique puissant pour modéliser des systèmes avec effets de mémoire, permettant une compréhension plus approfondie des processus dynamiques présentant des comportements non locaux au fil du temps. Cette thèse explore l'impact des effets de mémoire via le calcul fractionnaire à travers divers systèmes dynamiques, en se concentrant notamment sur la dynamique des vésicules, les microswimmers dans des flux cisaillants, et la transmission de drogues dans des modèles épidémiologiques. La dynamique des vésicules et le comportement des microswimmers sont analysés à l'aide de modèles fractionnaires, en particulier les dérivées de Caputo et la dérivée modifiée de Riemann-Liouville de Jumarie, révélant de nouveaux modes de tank-treading et l'influence des effets de mémoire sur la déformation des vésicules. Des méthodes analytiques et numériques, telles que les solutions basées sur la fonction de Mittag-Leffler, fournissent des résultats précis sur l'orientation et la déformation des vésicules et des globules rouges. De plus, la transition entre les mouvements de basculement et stationnaire des globules rouges sous différents rapports de viscosité est étudiée à l'aide de la dérivée modifiée de Riemann-Liouville, améliorant ainsi la compréhension du comportement des particules dans des environnements fluides complexes. Parallèlement, un modèle compartimental de transmission de drogues, formulé à l'aide de la dérivée fractionnaire de Caputo, évalue l'influence de l'éducation familiale et de santé publique sur la réduction de la transmission de drogues, intègre une analyse de sensibilité pour évaluer comment les variations des paramètres du modèle affectent les résultats de transmission de drogues. Ce travail apporte une contribution significative aux mathématiques appliquées en offrant de nouvelles perspectives tant sur la dynamique des vésicules que sur la modélisation épidémiologique à travers l'usage des dérivées fractionnaires, avec des implications pour la recherche future dans ces domaines.

Mot clés: Calcul fractionnaire, La dérivée fractionnaire de Caputo, La dérivée fractionnaire modifiée de Riemann-Liouville, L'effets de mémoire, Globules rouges, La dynamique des vésicules, micro-nageur, La transmission de drogues, Les modèles épidémiologiques.

ARABIC ABSTRACT

الملخص

يوفر الحساب الكسري إطارًا رياضيًا قويًا لنمذجة الأنظمة ذات تأثيرات الذاكرة، مما يمنح فهمًا أعمق للعمليات الديناميكية التي تظهر سلوكًا غير محلي على مر الزمن .تستكشف هنه الأطروحة تأثيرات الذاكرة من خلال الحساب الكسري عبر أنظمة ديناميكية مختلفة ,مع التركيز على ديناميكيات الحويصلات والسباحين المجهريين في التدين التدفقات المجهريين باستخدام النماذج الكسرية، وخاصة مشتقات كابوتو ومشتقة ريمان-ليوفيل المعدلة لجوماري، لكشف عن أنماط جديدة في حركة الجسيمات وتأثير الذاكرة على تشوه الحويصلات .يتم تقديم نتائج دقيقة لتوجهات وتغيرات شكل الحويصلات وكريات الدم الحمراء باستخدام الطرق التحليلية والعددية، بما في ذلك الحلول المستندة إلى دالة ميتاج الح ليفلر .علاوة على ذلك، تمت دراسة الانتقال من الحركة المتقلبة إلى الحركة الثابنة لكريات الدم الحمراء في التدفقات القصية باستخدام مشتقة ريمان-ليوفيل المعدلة، مما يساهم في فهم أعمق لسلوك الجسيمات في البيئات السائلة المعقدة .بالتوازي مع ذلك، تم تطوير نموذج مقسم لانتقال المخدرات باستخدام مشتقة كابوتو لتحليل تأثير التثقيف هذا العمل في الرياضيات التطبيقية من خلال تقديم رؤى جديدة في كل من نمذجة الأوبئة وديناميكيات الحويصلات باستخدام المشتقات الكسرية

الكلمات المفتاحية: الحساب الكسري، تأثيرات الذاكرة، ديناميكيات الحويصلات، السباحين المجهريين، التدفقات القصية، انتقال المخدرات، النماذج الوبائية، مشتقة كابوتو، مشتقة ريمان-ليوفيل المعدلة، الرياضيات التطبيقية، دالة ميتاج-ليفلر، التحليل العددي، الانتقال المتقلب

SCIENTIFIC PRODUCTION

This Ph.D. Thesis is based on the following papers:

1. Alla Hamou, A., Azroul, E., **Diki, G.**, Guedda, M. (2023). Effect of family and public health education in drug transmission: an epidemiological model with memory. Modeling Earth Systems and Environment, 9(2), 2809-2828. DOI: 10.1007/s40808-022-01662-6

2. Azroul, E., **Diki, G.**, Guedda, M. (2023). Exploring the interplay between memory effects and vesicle dynamics: A five-dimensional analysis using rigid sphere models and mapping techniques. Studies in Applied Mathematics. DOI: 10.1111/sapm.12648

3. E. AZROUL, S.BOUDA, **G. Diki**, M. GUEDDA. (2024)" Analytical Solutions and Classification of Vesicle Motion and Deformation in Shear Flow: Uncovering New Tank-Treading Modes " . Chaos: An Interdisciplinary Journal of Nonlinear Science 34.3 (2024). DOI: 10.1063/5.0189923

4. E. AZROUL, **G. Diki**, " Analytical investigation of vesicle dynamics via the modified Riemann–Liouville fractional derivative: Mittag-Leffler function solution and comparative analysis with Caputo's derivative." Chaos: An Interdisciplinary Journal of Nonlinear Science 34.6 (2024). DOI: 10.1063/5.0208993

5. E. AZROUL, **G. Diki**, " Motion of an Ellipsoidal Particle in Shear Flow: Analyzing Memory Effect Influence Through Exact Solutions Investigation" ICDS 2024 (International Conference On Intelligent Computing in Data Sciences). (Accepted)

6. E. AZROUL, **G. Diki**, " Dynamic Insights on the Caputo Derivative's Impact in Unraveling Vesicle Behavior ". ICFCA 2024 (International Conference on Fractional Calculus and Applications). (Accepted)

7. E. AZROUL, **G. Diki**, " Unveiling Memory-Driven Dynamics: Fractional Calculus and Microswimmer Trajectories in 1D Shear Flow " (Submitted) .

LIST OF FIGURES

FIGURE **Page**

0.1 Timeline of Fractional Calculus during 1640–1930 3
0.2 Red blood cells observed under an electron microscope, distinctly showing their characteristic biconcave shape [1]. 4
0.3 (a) 3D model of a red blood cell (RBC), highlighting its biconcave shape. (b) Cross-sectional view of an RBC, emphasizing its geometry. (c) Surface mesh of an RBC, crucial for computational modeling and simulations [10]. 5
0.4 Diagram of a red blood cell (RBC) illustrating its dimensions along with the standard viscosities of hemoglobin and plasma. A section of the RBC is enlarged to highlight the composition of the lipid bilayer in the RBC membrane [93]. 5
0.5 Illustration of vesicles showing the detailed structure of the lipid bilayer and its organization [43]. 6
0.6 Detailed representation of a vesicle membrane, emphasizing the embedded proteins and their arrangement within the lipid bilayer [43]. 6
0.7 Tank-treading (a), tumbling (b), and vacillating-breathing (c) regimes of a vesicle in a shear flow, according to [26]. 7
0.8 Diagram depicting the vesicle's configuration [2]. 8
0.9 Schematic diagram for SIR model. 12
0.10 Schematic diagram for SEIR model. 13

2.1 The representation of the solutions of the fractional model obtained for the components ζ, ξ and F_{20} for four arbitrary values of fractional order. Parameters are : $\Delta = 4$ and $h = 2$ 37
2.2 The behaviour of the orientation angle ψ and the amplitude $\mathscr{R}$ for four arbitrary values of fractional order. Parameters are : $\Delta = 4$ and $h = 2$ 38
2.3 The representation of the solutions of the fractional model obtained for the classical components ζ, ξ and F_{20} for four arbitrary values of fractional order. Parameters are : $\Delta = 4$ and $h = 0.8$ 39
2.4 The behaviour of the orientation angle ψ for four arbitrary values of fractional order. Parameters are : $\Delta = 4$ and $h = 0.8$ with $\Gamma = 0.9$, $\Gamma = 2$ and $\Gamma = 1.05$. 41

2.5 The dynamic of the amplitude $\mathscr{R}$ for four arbitrary values of fractional order. Parameters are : $\Delta = 4$ and $h = 0.8$ with $\Gamma = 0.9$, $\Gamma = 2$ and $\Gamma = 1.05$. 42
2.6 The representation of the solutions of the fractional model obtained for the classical components ζ, ξ and F_{20} for four arbitrary values of fractional order. Parameters are : $\Delta = 4$ and $h = 2$ 47
2.7 The behaviour of the orientation angle ψ and the amplitude $\mathscr{R}$ for four arbitrary values of fractional order. Parameters are : $\Delta = 4$ and $h = 2$ 48
2.8 The representation of the solutions of the fractional model obtained for the classical components ζ, ξ and F_{20} for four arbitrary values of fractional order. Parameters are : $\Delta = 4$ and $h = 0.8$ 49
2.9 The behaviour of the orientation angle ψ for four arbitrary values of fractional order. Parameters are : $\Delta = 4$ and $h = 0.8$ with $\Gamma = 0.9$, $\Gamma = 1$ and $\Gamma = 1.2$. 50
2.10 The dynamic of the amplitude $\mathscr{R}$ for four arbitrary values of fractional order. Parameters are : $\Delta = 4$ and $h = 0.8$ with $\Gamma = 0.9$, $\Gamma = 1$ and $\Gamma = 1.2$. 51
2.11 The orientation angle dynamics ψ for $\alpha = 0.9$ with Caputo and Modified Riemann-Liouville Fractional Derivatives and Three Different Γ Values at $\Delta = 4$ and $h = 0.8$. . . 52
2.12 The orientation angle dynamics φ for $\alpha = 0.7$ with Caputo and Modified Riemann-Liouville Fractional Derivatives and Three Different Γ Values at $\Delta = 4$ and $h = 0.8$. . . 53
2.13 The orientation angle dynamics φ for $\alpha = 0.5$ with Caputo and Modified Riemann-Liouville Fractional Derivatives and Three Different Γ Values at $\Delta = 4$ and $h = 0.8$. . . 54
2.14 The dynamics of the shape deformation $\mathscr{R}$ for $\alpha = 0.9$ with Caputo and Modified Riemann-Liouville Fractional Derivatives and Three Different Γ Values at $\Delta = 4$ and $h = 0.8$. 55
2.15 The dynamics of the shape deformation $\mathscr{R}$ for $\alpha = 0.7$ with Caputo and Modified Riemann-Liouville Fractional Derivatives and Three Different Γ Values at $\Delta = 4$ and $h = 0.8$. 56
2.16 The dynamics of the shape deformation $\mathscr{R}$ for $\alpha = 0.5$ with Caputo and Modified Riemann-Liouville Fractional Derivatives and Three Different Γ Values at $\Delta = 4$ and $h = 0.8$. 57
2.17 The orientation angle ψ of the ellipsoidal particle for four different fractional order values when the parameter $\chi > 1$. 60
2.18 The particle's orientation angle psi for four different fractional order values when the parameter $\chi < 1$. 61

3.1 The representation of the numerical solutions of the fractional model obtained for the classical components $\boldsymbol{p}_1, \boldsymbol{p}_2$ and $\boldsymbol{p}_3$ for four arbitrary values of fractional order. Parameters are : $\chi = 0.4\sqrt{5}, \gamma = 1, a = c = 0.2\sqrt{5}$ and $b = 2\sqrt{0.1}$. 72

3.2 The representation of the numerical solutions of the fractional model obtained for the dynamics of the components of F_{21} for four arbitrary values of fractional order. Parameters are : $\chi = 0.4\sqrt{5}, \gamma = 1, a = c = 0.2\sqrt{5}$ and $b = 2\sqrt{0.1}$. 73
3.3 The shape deformation $\mathscr{R}$ of the particle for four arbitrary values of fractional order. Parameters are : $\chi = 0.4\sqrt{5}, \gamma = 1, a = c = 0.2\sqrt{5}$ and $b = 2\sqrt{0.1}$. 73
3.4 The orientation angle φ of the particle for four arbitrary values of fractional order. Parameters are : $\chi = 0.4\sqrt{5}, \gamma = 1, a = c = 0.2\sqrt{5}$ and $b = 2\sqrt{0.1}$ 73
3.5 The representation of the numerical solutions of the fractional model obtained for the classical components $\boldsymbol{p}_1, \boldsymbol{p}_2$ and $\boldsymbol{p}_3$ for four arbitrary values of fractional order. Parameters are : $\chi = 2/\sqrt{3}, \gamma = 1, a = 2\sqrt{(}11)/3$, $\Gamma = \sqrt{(11)/3}$ and $b = c = 1$. 75
3.6 The representation of the numerical solutions of the fractional model obtained for the dynamics of the components of F_{21} for four arbitrary values of fractional order. Parameters are : $\chi = 2/\sqrt{3}, \gamma = 1, a = 2\sqrt{(}11)/3$, $\Gamma = \sqrt{(11)/3}$ and $b = c = 1$. 76
3.7 The behavior of the orientation angle φ for four arbitrary values of fractional order. Parameters are : $\chi = 2/\sqrt{3}, \gamma = 1$ with $\Gamma = 0.9$, $\Gamma = 1$ and $\Gamma = 1.2$. 77
3.8 The dynamic of the particle contour for four arbitrary values of fractional order. Parameters are : $\chi = 2/\sqrt{3}, \gamma = 1$ with $\Gamma = 0.9$, $\Gamma = 1$ and $\Gamma = 1.2$. 78

4.1 The depiction of the exact solutions for the fractional mapped equation acquired for $\boldsymbol{p}_1, \boldsymbol{p}_2$ and $\boldsymbol{p}_3$ is presented for four distinct values of α , denoting the fractional order. 85
4.2 The depiction of the exact solutions for the fractional mapped equation acquired for F_{21} modes is presented for four distinct values of α , denoting the fractional order. . . 86
4.3 The projection of $\mathbf{p}$ onto the plane is denoted as $\mathbf{p}_\perp$, forming an angle φ with the e_1 axis [2]. 87
4.4 The particle's orientation angle φ for four different fractional order values. 89
4.5 The particle's shape deformation $\mathscr{R}$ for four different fractional order values. 89
4.6 The depiction of the exact solutions for the fractional mapped equation acquired for $\boldsymbol{p}_1, \boldsymbol{p}_2$ and $\boldsymbol{p}_3$ is presented for four distinct values of α , denoting the fractional order. 90
4.7 The depiction of the exact solutions for the fractional mapped equation acquired for F_{21} modes is presented for four distinct values of α , denoting the fractional order. . . 92
4.8 The particle's orientation angle φ for four different fractional order values with $\Gamma = 0.9$, $\Gamma = 1$ and $\Gamma = 1.2$. 93
4.9 The particle's shape deformation $\mathscr{R}$ for four different fractional order values with $\Gamma = 0.9$, $\Gamma = 1$ and $\Gamma = 1.2$. 95
4.10 The dynamics of the Orientation Angle φ for three arbitrary values of fractional order using Caputo and Modified Riemann-Liouville Fractional Derivatives. Parameters are : $\Lambda = 0.4\sqrt{5}, \gamma = 1$. 97

4.11 The dynamics of the particle contour $\mathscr{R}$ for three arbitrary values of fractional order using Caputo and Modified Riemann-Liouville Fractional Derivatives. Parameters are : $\Lambda = 0.4\sqrt{5}, \gamma = 1$. 98
4.12 The orientation angle dynamics φ for $\alpha = 0.9$ with Caputo and Modified Riemann-Liouville Fractional Derivatives and Three Different Γ Values at $\Lambda = 2/\sqrt{3}$. 99
4.13 The orientation angle dynamics φ for $\alpha = 0.7$ with Caputo and Modified Riemann-Liouville Fractional Derivatives and Three Different Γ Values at $\Lambda = 2/\sqrt{3}$. 100
4.14 The orientation angle dynamics φ for $\alpha = 0.5$ with Caputo and Modified Riemann-Liouville Fractional Derivatives and Three Different Γ Values at $\Lambda = 2/\sqrt{3}$. 101
4.15 The dynamics of the shape deformation $\mathscr{R}$ for $\alpha = 0.9$ with Caputo and Modified Riemann-Liouville Fractional Derivatives and Three Different Γ Values at $\Lambda = 2/\sqrt{3}$. 102
4.16 The dynamics of the shape deformation $\mathscr{R}$ for $\alpha = 0.7$ with Caputo and Modified Riemann-Liouville Fractional Derivatives and Three Different Γ Values at $\Lambda = 2/\sqrt{3}$. 103
4.17 The dynamics of the shape deformation $\mathscr{R}$ for $\alpha = 0.5$ with Caputo and Modified Riemann-Liouville Fractional Derivatives and Three Different Γ Values at $\Lambda = 2/\sqrt{3}$. 104

5.1 The depiction of the exact solutions for the fractional mapped equation acquired for $\boldsymbol{p}_x, \boldsymbol{p}_y$ and $\boldsymbol{p}_z$ is presented for four distinct values of α , denoting the fractional order. 113
5.2 The particle's orientation angle φ for four different fractional order values. 114
5.3 The depiction of the exact solutions for the fractional mapped equation acquired for $\boldsymbol{p}_x, \boldsymbol{p}_y$ and $\boldsymbol{p}_z$ is presented for four distinct values of α , denoting the fractional order. 116
5.4 The particle's orientation angle φ for four different fractional order values with four different values of α. 117
5.5 The time evolution $\boldsymbol{p}_x$ for the Modified Riemann-Liouville operator ($\chi = 0$). 118
5.6 The time evolution $\boldsymbol{p}_y$ for the Modified Riemann-Liouville operator ($\chi = 0$). 118
5.7 Example of a trajectory for the fractional case in the absence of external torque (Eqs. (5.40)-(5.42)) with four arbitrary values of α. The parameters are $C = \frac{\pi}{2}, C' = 0.5, v_s = 1$, and $\gamma = 2$. 122
5.8 Example of a trajectory for the fractional case in the absence of external torque (Eqs. (5.40)-(5.42)) with four arbitrary values of α. The parameters are $C = \frac{\pi}{3}, C' = 0.5, v_s = 1$, and $\gamma = 2$. 123

6.1 Schematic diagram of drug model and parameters with health education according to [54] 128
6.2 The depiction of the numerical solution of the fractional model produced for the the susceptible persons who do not accept the public health education $S(t)$ for four arbitrary fractional order values. 138

6.3 The depiction of the numerical solution of the fractional model produced for the susceptible persons who accept the public health education $C(t)$ for four arbitrary fractional order values. 139
6.4 The depiction of the numerical solution of the fractional model produced for the light drug addicts persons $L(t)$ for four arbitrary fractional order values. 139
6.5 The depiction of the numerical solution of the fractional model produced for the heavy drug addicts persons $H(t)$ for four arbitrary fractional order values. 140
6.6 The depiction of the numerical solution of the fractional model produced for the drug users in treatment persons $T(t)$ for four arbitrary fractional order values. 140
6.7 The depiction of the numerical solution of the fractional model produced for the permanent quit drug persons $R(t)$ for four arbitrary fractional order values. 141
6.8 Graphical illustration of the reproduction number $\mathscr{R}_0$ as a function of m and θ. 143
6.9 Graphical illustration of the reproduction number $\mathscr{R}_0$ as a function of m and χ. 143
6.10 Graphical illustration of the reproduction number $\mathscr{R}_0$ as a function of q and χ. 144
6.11 Graphical illustration of the reproduction number $\mathscr{R}_0$ as a function of q and m. 144
6.12 Graphical illustration of the reproduction number $\mathscr{R}_0$ as a function of q and θ. 144
6.13 Graphical illustration of the reproduction number $\mathscr{R}_0$ as a function of τ and χ. 145
6.14 Graphical illustration of the reproduction number $\mathscr{R}_0$ as a function of τ and m. 145
6.15 Graphical illustration of the reproduction number $\mathscr{R}_0$ as a function of τ and θ. 145
6.16 Graphical illustration of the reproduction number $\mathscr{R}_0$ as a function of τ and q. 146
6.17 Graphical illustration of $\mathscr{R}_0$ sensitivity indices for Caputo model parameters. 146

TABLE OF CONTENTS

Dedication i

Acknowledgements ii

Index of Symbols and Notations iv

Abstract v

Résumé vi

Arabic Abstract vii

Scientific Production viii

List of Figures ix

Table of Contents xiv

General Introduction: Context, Challenges, and Objectives 1

1 Preliminary Concepts and Insights 18

1.1 Background of non-integer calculus 19

1.1.1 Introduction 19

1.1.2 Special Functions 19

1.1.3 Elements on Laplace Transform 21

1.1.4 Fractional Integrals and Derivatives 22

1.2 Foundational Theorems and Lemmas for Fractional Differential Equations 26

2 Fractional Dynamics and Memory Effects: Insights into Vesicle and Ellipsoidal Particle Behavior in Shear Flow 29

2.1 Introduction 31

2.2 Analytical solutions and classification of vesicle motion and deformation in shear flow: Uncovering new tank-treading modes . . . 32
2.2.1 The vesicle model formulation and Fractional vesicle model . . . 32
2.2.2 Stability analysis . . . 33
2.2.3 Exact solutions and vesicle dynamics . . . 35
2.2.4 Tank-treading mode ($h > h_c$) . . . 36
2.2.5 The damped oscillatory modes ($h < h_c$) . . . 36
2.3 Dynamic Insights on the Caputo Derivative's Impact in Unraveling Vesicle Behavior 43
2.3.1 Formulation of the Vesicle Model and the Caputo Fractional Vesicle Model 43
2.3.2 Analysis of Existence and Uniqueness of Solutions in Caputo-Fractional Equations . . . 44
2.3.3 Equilibrium and Local Stability Analysis of the Fractional Model . . . 45
2.3.4 Numerical Computation Method . . . 45
2.3.5 Tank-treading mode ($h > h_c$) . . . 46
2.3.6 Damping tank-treading mode ($h < h_c$) . . . 46
2.4 Comparison of Caputo and the Modified Riemann–Liouville Fractional Derivatives in Vesicle Dynamics . . . 52
2.5 Motion of an Ellipsoidal Particle in Shear Flow: Analyzing Memory Effect Influence Through Exact Solutions Investigation . . . 58
2.5.1 TT-mode . . . 59
2.5.2 TB-mode . . . 60
2.6 Conclusion . . . 62

3 Exploring the interplay between memory effects and vesicle dynamics: A five-dimensional numerical analysis using rigid sphere models and mapping techniques 64
3.1 Introduction . . . 65
3.2 Fractional model . . . 65
3.3 Results . . . 66
3.3.1 Existence and uniqueness of solutions of the Caputo-fractional model . . . 66
3.3.2 Existence of equilibrium and Stability analysis . . . 68
3.3.3 Numerical method . . . 70
3.4 Discussion . . . 71
3.4.1 Tank-treading mode . . . 71
3.4.2 Tumbling and Vacillating-breathing modes . . . 74
3.4.3 The effect of initial conditions and fractional order on dynamics . . . 76
3.5 Conclusion . . . 78

4 Analytical investigation of vesicle dynamics via the modified Riemann–Liouville fractional derivative 80
4.1 Introduction . . . 81
4.2 From fractional general orientation equations to fractional five-dimensional mapping 82
4.3 Exact Solutions and Interpretation of Fractional Mapping Equations . . . 84
4.3.1 TT-mode . . . 85
4.3.2 Damping-TT modes . . . 89
4.4 Comparative analysis of the two fractional derivatives . . . 96
4.5 Conclusion . . . 105

5 Unveiling Memory-Driven Dynamics: Fractional Calculus and Microswimmer Trajectories in 1D Shear Flow 106
5.1 Introduction . . . 107
5.2 Fractional Model and Stability Analysis . . . 108
5.3 Extending Bretherton's Approach . . . 109
5.3.1 run mode . . . 112
5.3.2 Damping mode . . . 114
5.3.3 Special Case: No Preferred Swimming Direction ($\chi = 0$) . . . 118
5.4 Memory Effects on Swimming Trajectories . . . 119
5.4.1 Trajectories in the run regime . . . 119
5.4.2 Trajectories in the Tumbling regime . . . 120
5.4.3 Trajectories in the special case $\chi = 0$ . . . 121
5.5 Conclusion and Future Perspectives . . . 124

6 Effect of family and public health education in drug transmission: an epidemiological model with memory 125
6.1 Introduction . . . 126
6.2 Formulation of the fractional order model . . . 127
6.3 Results . . . 129
6.3.1 The existence, positivity and boundedness of solutions of the fractional model 129
6.3.2 The basic reproduction number, existence, and stability of equilibrium . . . 130
6.3.3 Numerical method for Caputo-fractional derivative . . . 137
6.3.4 Model parameter sensitivity analysis in relation to the basic reproduction number . . . 141
6.4 Discussion . . . 146
6.4.1 Memory effect . . . 146
6.4.2 The influence of model parameters . . . 147
6.4.3 Sensitivity analysis of model parameters . . . 148
6.5 Conclusion . . . 148

Conclusion and Perspectives **150**

References **152**

General Introduction: Context, Challenges, and Objectives

Fractional calculus, an advanced extension of classical calculus, introduces integrals and derivatives of non-integer orders, offering a robust framework for modeling complex systems with memory effects. Although its theoretical origins can be traced back to early mathematicians such as Leibniz and Riemann, fractional calculus has seen significant advancements and applications in contemporary science and engineering.

This chapter provides a comprehensive overview of fractional calculus, detailing its historical development and its growing significance in various research domains. From its early conceptualization to its modern applications, fractional calculus has emerged as a crucial tool for understanding dynamic systems that exhibit non-local behavior over time.

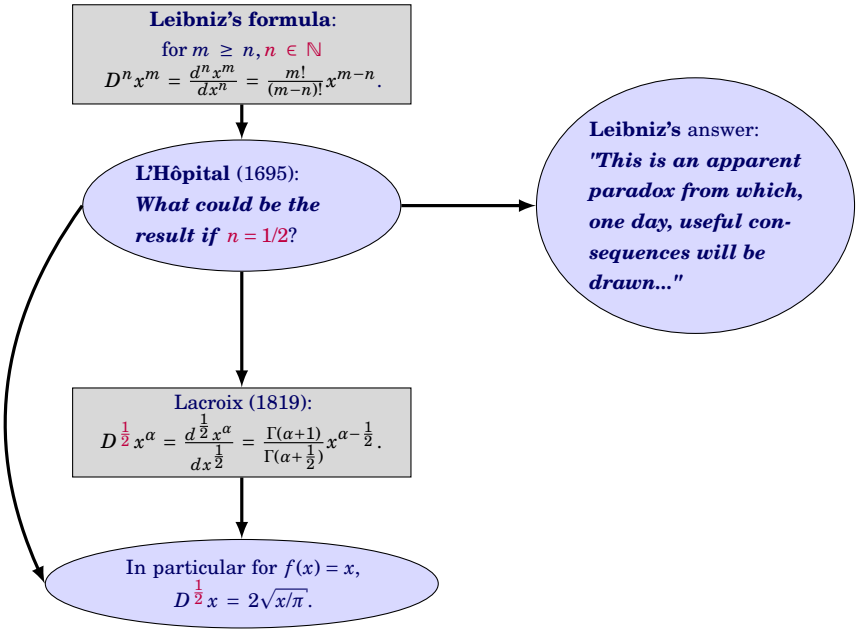
A major focus of this thesis is the application of fractional calculus to the study of deformable particles, including red blood cells and vesicles. By utilizing fractional derivatives, particularly Jumarie's modified Riemann-Liouville and Caputo derivatives, we explore complex behaviors such as tank-treading and Tumbling motions under shear flows. These investigations shed light on the intricate dynamics of these particles, enhancing our understanding of their behavior in fluid environments.

In addition to particle dynamics, this thesis extends the application of fractional calculus to epidemiological modeling, specifically in analyzing drug transmission. By developing a compartmental model using the Caputo fractional derivative, we examine the impact of family and public health education on drug spread. This model reveals how educational interventions can influence the basic reproduction number, $\mathscr{R}_0$, and thus affect drug transmission dynamics.

The subsequent sections of this chapter will elaborate on the historical evolution of fractional calculus, introduce the theoretical concepts relevant to both deformable and rigid particles, as well as epidemiological models, and outline the specific objectives and scope of this thesis. This integrated approach highlights the versatility of fractional calculus in addressing both fundamental scientific questions and practical challenges in medical and epidemiological contexts.

Fractional Calculus: History and Significance

The origins of fractional calculus are intertwined with the development of classical calculus by Newton and Leibniz. The initial question that sparked in fractional calculus was whether the n^{th} order derivative $\frac{d^n f}{dt^n}$ could be defined when n is a fraction. In a landmark correspondence in 1695, Leibniz, in a letter to the Marquis de L'Hôpital, pondered the meaning of the half-order derivative $\frac{d^{\frac{1}{2}} f}{dt^{\frac{1}{2}}}$. This query marked the beginning of formal exploration into fractional calculus and captivated the mathematical community, including luminaries such as Euler and Lagrange in the 18^{th} century, and later Liouville, Riemann, Grünwald, and Letnikov in the 19^{th} century. The contributions of these researchers established a robust foundation for the field.



Fractional calculus has a rich history, marked by the contributions of many prominent mathematicians over the centuries. This diagram provides a visual timeline of key figures who have significantly influenced the development of fractional calculus from the mid-17th century to the mid-20th century. Each of these mathematicians brought unique insights and advancements to the field, laying the groundwork for the modern applications of fractional calculus in various scientific and engineering disciplines. The timeline highlights their contributions and helps us appreciate the evolution of this mathematical domain.

Furthermore, fractional calculus distinguishes itself by its inherent "memory effect", where the history of a process influences its future behavior. This characteristic makes fractional derivatives particularly useful in modeling physical and natural systems that exhibit memory and hereditary properties. However, the non-local nature of fractional derivatives presents challenges, including significant computational demands and the need for extensive information storage. Fractional derivatives are particularly effective in capturing the memory effect of different mate-

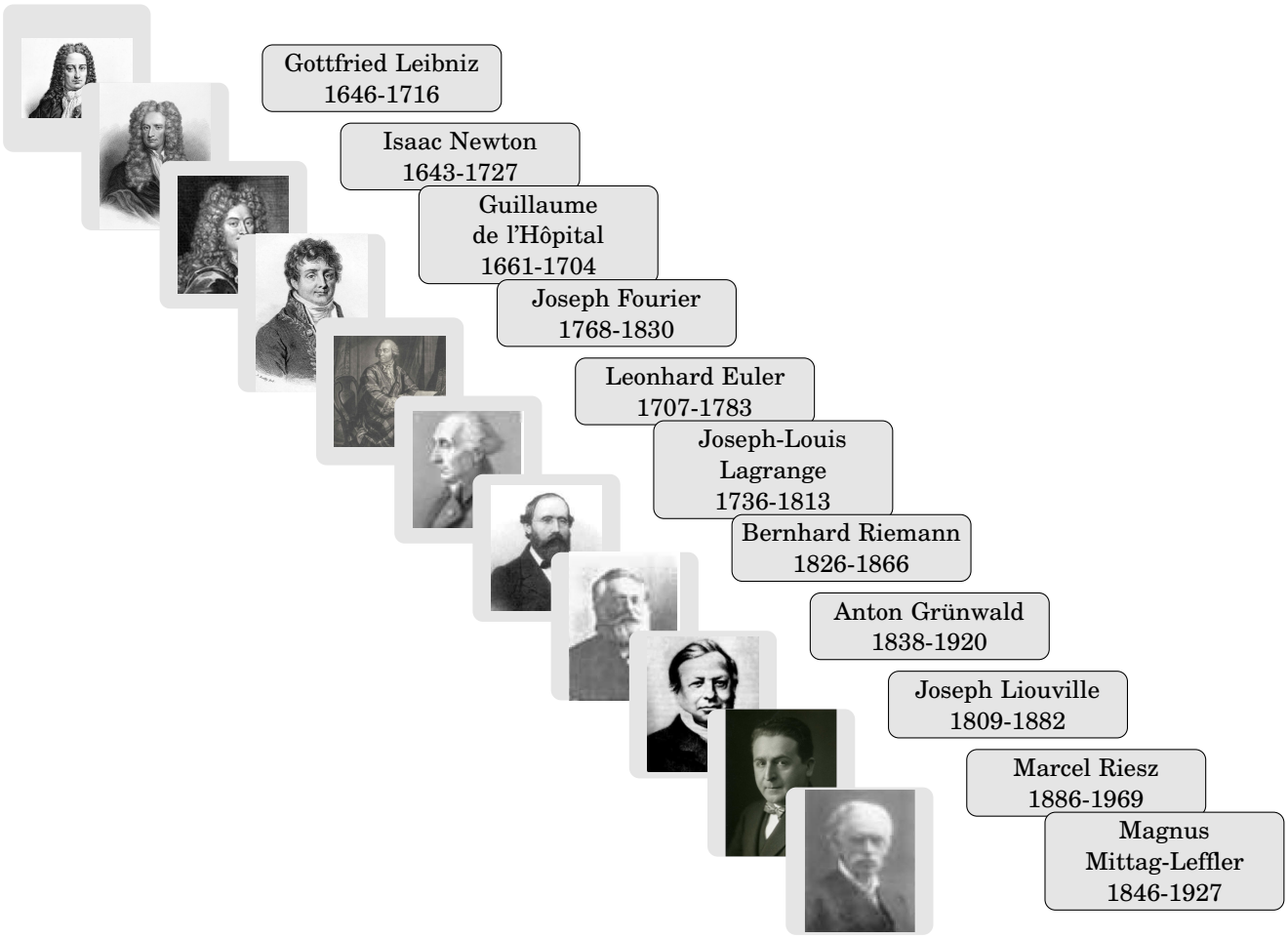


Figure 0.1: Timeline of Fractional Calculus during 1640–1930

rials and processes, as highlighted by [76]. This is the primary advantage of fractional calculus over classical integer-order systems, which essentially disregard these effects. The benefits of fractional derivatives have become evident in various areas of modeling. Today, fractional calculus is considered a mature field with a wide range of applications and continues to be an active area of research and development including epidemiological models [8, 59, 83], image processing [7, 16, 36, 69, 90], and more. In contrast, mathematical modeling using integer-order derivatives has been instrumental in understanding, predicting, and unraveling numerous real-world phenomena across various fields, including physics and biology. However, these models often fail to account for the memory effects inherent in many systems, highlighting the unique and valuable contributions of fractional calculus in modern scientific research.

Motivated by these considerations, this thesis utilizes fractional derivatives to investigate the memory effect on various models, including the behavior of rigid and deformable particles (such as red blood cells, vesicles, and microswimmers), as well as an epidemiological model of drug abuse. Before delving into these models, the following sections of this introduction will provide

a detailed overview of the characteristics of red blood cells, vesicles, and the drug abuse model, highlighting their significance and the advantages of applying fractional derivatives to each of these areas.

Deformable particles

Blood is a complex and vital fluid that plays a critical role in sustaining life by transporting oxygen and nutrients throughout the body. Among its key components, red blood cells are particularly important for ensuring that oxygen reaches all tissues and organs, making them central to the body's overall functioning. Understanding the behavior of blood flow requires careful attention to both the red blood cells and the surrounding fluids that facilitate their movement. By modeling these two elements the cells themselves and the fluids within and around them, we can gain valuable insights into the dynamics of blood flow. The following sections will provide an overview of the biological characteristics of these components, along with the models used to describe their behavior.

Red Blood Cells

The red blood cell (RBC), or erythrocyte, is among the most numerous and specialized cells in the body. Lacking a nucleus, it represents 99% of the blood's formed elements and, thanks to the hemoglobin it contains, ensures the transport and distribution of oxygen and iron to cells, as well as the elimination of carbon dioxide produced by these cells.

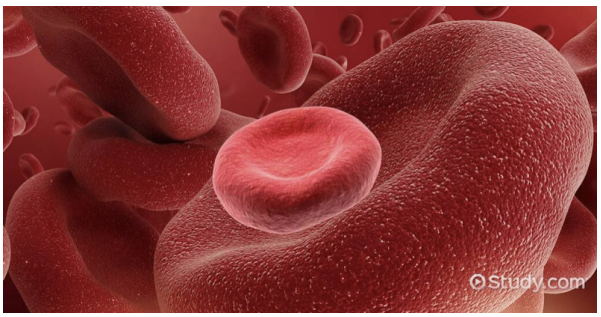
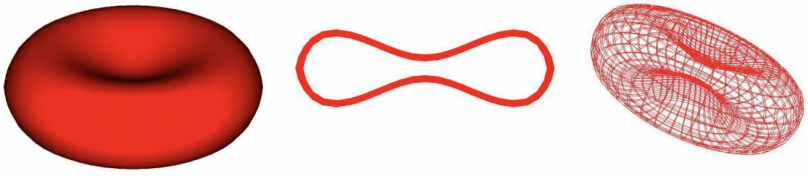


Figure 0.2: Red blood cells observed under an electron microscope, distinctly showing their characteristic biconcave shape [1].

When observed under an electron microscope, the red blood cell (RBC) reveals a very particular shape at rest: that of a biconcave disk, or discocyte (see Figure 0.2). This shape confers numerous properties, particularly significant elasticity, allowing it to optimally perform its function of transporting oxygen to the body's cells, capable of squeezing through capillaries with diameters up to half its resting diameter. As illustrated in Figure 0.3, understanding the structure of the RBC in detail is crucial. The 3D model of the RBC demonstrates its biconcave shape, which is essential for appreciating the cell's complex geometry and flexibility.

The cross-sectional view emphasizes the cell's unique geometry, particularly its thin central region, which enhances its deformability. Furthermore, the surface mesh depicted is vital for computational modeling and simulations, offering detailed insights into how the RBC interacts with its environment and deforms under various forces. These detailed visualizations are indispensable for accurate computational studies and for predicting RBC behavior in different physiological conditions. The cell membrane of the RBC, as shown in the magnified section



(**a**) 3D RBC model (**b**) Cross section (**c**) Surface mesh

Figure 0.3: (a) 3D model of a red blood cell (RBC), highlighting its biconcave shape. (b) Cross-sectional view of an RBC, emphasizing its geometry. (c) Surface mesh of an RBC, crucial for computational modeling and simulations [10].

of Figure 0.2, consists of a lipid bilayer interspersed with various protein molecules, which contribute to the cell's structural integrity and functionality. Erythrocytes' propensity to deform

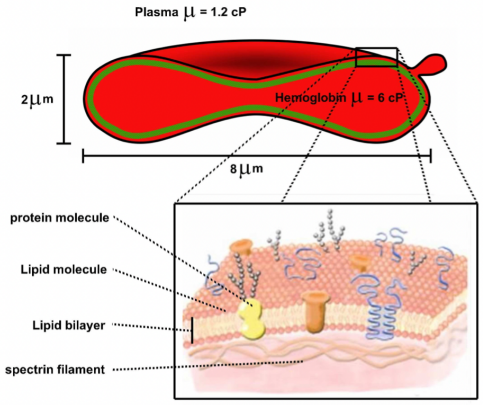


Figure 0.4: Diagram of a red blood cell (RBC) illustrating its dimensions along with the standard viscosities of hemoglobin and plasma. A section of the RBC is enlarged to highlight the composition of the lipid bilayer in the RBC membrane [93].

when passing through capillaries smaller than their own effectively identifies them, stressing the need to study their deformation; analysis of the deformation of healthy RBCs provides an insight into diseases characterized by RBC malformation, which can lead to a loss of elasticity properties and consequently inadequate oxygen transport in the body.

Vesicles

Vesicles, illustrated in Figures 0.5 and 0.6, are closed phospholipid membranes in an aqueous medium. They share the fundamental structural component of the lipid bilayer with RBCs. In Figure 0.5, the bilayer structure is clearly visible, showing how it encapsulates and separates the internal environment of the vesicle from the external environment. Figure 0.6 provides a

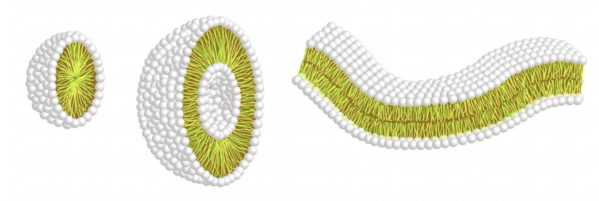


Figure 0.5: Illustration of vesicles showing the detailed structure of the lipid bilayer and its organization [43].

more detailed view of the vesicle membrane, highlighting the various proteins embedded in the lipid bilayer, which facilitate transport and communication processes. Understanding and

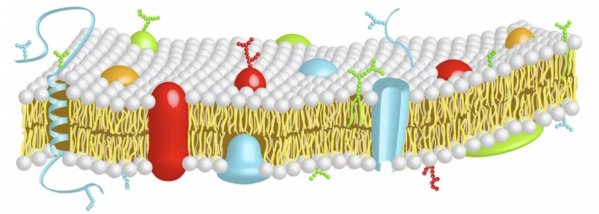


Figure 0.6: Detailed representation of a vesicle membrane, emphasizing the embedded proteins and their arrangement within the lipid bilayer [43].

analyzing their dynamical behaviors represents a watershed from several perspectives in non-equilibrium sciences due to their link to biological cells. The classical example is the Red blood cell (RBC). Furthermore, vesicles have been demonstrated to imitate some features of RBCs; hence, they are the focus of this thesis. In this context, an important challenge is to develop accurate mathematical models that can clearly explain vesicle motion in multiple dimensions, which will be discussed in the next section.

Dynamics of Red Blood Cells and Vesicles in Shear Flow

Throughout this thesis, we assume that the vesicle is exposed to a linear shear flow defined by $\mathbf{u}_0 = (\gamma y, 0, 0)$, where γ represents the shear rate. It is essential to highlight that the fluid dynamics, both inside and outside the vesicle, are the primary focus of our study and occur under conditions of low Reynolds number. Under these conditions, the hydrodynamics are effectively governed by the Stokes equations [64].

Structure and Properties of Deformable Particles

In shear flow, it has been discovered that vesicles exhibit three fundamental movement regimes [48, 64]: the tank-treading (TT) regime, where the vesicle maintains a constant angle relative to the flow direction while its membrane undergoes a tank-treading motion; the tumbling (TB) regime, characterized by the vesicle's membrane flipping back and forth like a rigid body; and the vacillating breathing (VB) regime, which acts as a transitional phase TT-mode and TB-mode [64]. In the VB regime, the vesicle's primary axis oscillates around the flow direction, and the vesicle's shape undergoes a breathlike motion. Figure 0.7 illustrates an insight into these regimes. Three

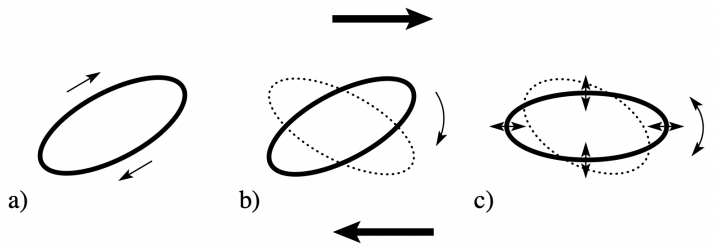


Figure 0.7: Tank-treading (a), tumbling (b), and vacillating-breathing (c) regimes of a vesicle in a shear flow, according to [26].

primary control parameters influence the presence of these regimes:

1. ****Excess Area**:** Given by $\Delta = \frac{A-4\pi R_0^2}{R_0^2}$, where A represents the vesicle's surface area and R_0 is the radius of a sphere with the same volume as the vesicle, calculated as $R_0 = \left(\frac{3V}{4\pi}\right)^{\frac{1}{3}}$.
2. ****Viscosity Ratio**:** The ratio of internal to external fluid viscosities, denoted as $\lambda = \frac{\eta_{\text{int}}}{\eta_{\text{ext}}}$.
3. ****Capillary Number**:** defined as $\mathscr{C}_\kappa = \frac{\eta_{\text{ext}}\gamma R_0^3}{k}$, where γ is the shear rate and k represents the membrane's bending rigidity.

The Keller-Skalak (KS) theory [48] explores the TT regime and the transition between TT and TB movements. It reveals that a high value of λ leads to the TB regime, whereas a low value results in the TT regime. Through three-dimensional numerical simulations, these findings were later corroborated by karaus in [51].

Misbah's research [64] introduced the VB mode, also known as trembling or swinging, by applying small deformation approximation theory to the most spherical vesicles. This extension of the KS model incorporated two dynamic variables: the shape deformation ($\mathscr{R}$) and the orientation angle (ψ). It demonstrated that the capillary number $\mathscr{C}_\kappa$ could be excluded from the evolution equation, leaving only λ and Δ as significant factors.

Additional studies showed that the vesicle problem in shear flow could be mapped to a rigid spherical problem in five dimensions [2]. This approach demonstrated that the governing equations for both rigid spherical particles and deformable vesicles [37] are analogous, enabling exact analytical solutions for the rigid sphere problem and extending these solutions to scenarios out-

side the shear plane. Figure 0.8 illustrates the out-of-plane angle ϑ orientation. Furthermore,

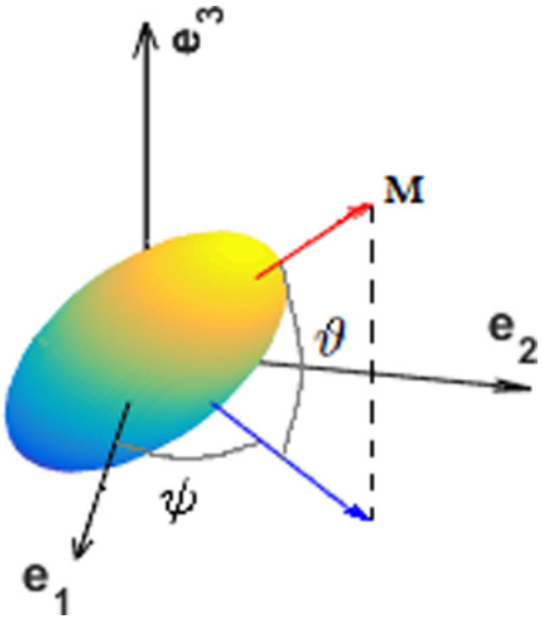


Figure 0.8: Diagram depicting the vesicle's configuration [2].

beyond the three primary modes of motion, an additional type of movement has been identified: kayaking (K), also known as spinning. In this regime, the vesicle's principal axis traces a cone outside the shear plane. Jeffery previously described this motion for rigid ellipsoids [42], where the principal axis forms a cone around the perpendicular to the shear plane. In [93], it is noted that the kayaking motion corresponds to a tumbling motion outside the shear plane.

The orientation equations for vesicles

For the convenience of the readers, we provide a brief explanation of the vesicle model in small deformation theory. The description that follows is based on the articles [2, 26, 64]. As highlighted above, vesicles exhibit similarities to real cells, particularly red blood cells. Thus, our investigation into vesicles serves as a means to understand the dynamic behavior of red cells and their deformation characteristics.

The vesicle deformation is described by the radial position r of the vesicle interface, which can be parametrized by

$$r = r_0[1 + f(\theta, \phi, t)], \tag{1}$$

where f is the deviation of the vesicle shape.

In the small deformation theory, the deviation of the shape from a sphere is parametrized by $r_0 = 1$

$$r = 1 + f(\theta, \phi, t). \tag{2}$$

One of the most powerful methods in investigating the vesicle deformation is the spherical harmonic parametrization.
The function f is expanded into series of scalar spherical harmonics

$$f = \sum_{n=0}^{\infty} \sum_{m=-n}^{m=n} F_{nm}(t) \mathscr{Y}_n^m(\theta, \phi), \tag{3}$$

where the function $\mathscr{Y}_n^m$ are the usual spherical harmonics and F_{nm} are unknown time-dependent amplitudes. The constraint on the fixed total area serves to relate the amplitude of the shape perturbation,

$$\Delta = \sum_{n} \sum_{m=-n}^{m=n} |F_{nm}(t)|^2 \frac{(n+2)(n-1)}{2}. \tag{4}$$

Under the linear shear flow only the second-order spherical harmonics functions survive, then we obtain,

$$f = \sum_{m=-2}^{m=2} F_{2m}(t) \mathscr{Y}_2^m(\theta, \phi), \tag{5}$$

and the area conservation constraint reads

$$\frac{\Delta}{2} = \sum_{|m| \leqslant 2} |F_{2m}|^2, \tag{6}$$

finally,

$$r = 1 + \sum_{|m| \leqslant 2} F_{2m} \mathscr{Y}_{2m}, \tag{7}$$

where $\mathscr{Y}_{2m}, |m| = 0, 1, 2$ are the usual spherical harmonics of order two. The evolution equations for F_{2m} are given by

$$\frac{dF_{2m}}{dt} = \gamma \left\{ -i \frac{m}{2} \delta_{2|m|} h + i \frac{m}{2} F_{2m} + \frac{4h}{\Delta} \operatorname{Im}(F_{22}) F_{2m} \right\}, \tag{8}$$

where $i^2 = -1, |m| = 0, 1, 2$, and $h = 60\sqrt{2\pi/15}/(32 + 23\lambda)$.
→ This evolution in time of the vesicle shape configuration in the shear plane is given by the dynamics of F_{22}.
→ $F_{2\mp1}$ and F_{20} modes describ deformations out of the shear plane.
→ The out-of-plane deformation along the vorticity direction is described by the F_{20} mode. Usually, $F_{2\mp1}$ modes are ignored for simplicity.
Misbah in [64] described the three classical regimes (TT, TB, and VB) using a two-dimensional model satisfied by the vesicle deformation amplitude $\mathscr{R}$ and the orientation angle ψ. Misbah [64] from

$$F_{22} = \mathscr{R}(t) e^{-2i\psi(t)}, \tag{9}$$

obtained the following coupled real non-linear ordinary differential equations,

$$\begin{aligned} \frac{d\mathscr{R}}{dt} &= h\left[1-4\frac{\mathscr{R}^2}{\Delta}\right]\sin(2\psi), \\ \frac{d\psi}{dt} &= -\frac{1}{2}+\frac{h}{2R}\cos(2\psi), \end{aligned} \tag{10}$$

where ψ coincides with the vesicle's orientation angle and verify $-\frac{\pi}{2} \leq \psi \leq \frac{\pi}{2}$ and $\mathscr{R}$ the amplitude of deformation of the vesicle, $0 \leq \mathscr{R} \leq 1$, the first equation describes the shape evolution, and the second one define the orientation of the vesicle in the flow.
Subsequently, the authors in [2] explored the mapping of vesicle equations onto those of a rigid sphere problem in five dimensions. To derive the mapped equations, they employed the method of splitting the complex amplitudes into their real and imaginary components.

$$F_{22} = f_{22} - i\tilde{f}_{22}, \quad F_{21} = f_{21} + i\tilde{f}_{21}, \quad F_{20} = \sqrt{2}f_{20}. \tag{11}$$

They obtained the following mapped equation

$$\gamma^{-1}\frac{d\boldsymbol{p}}{dt} = \Omega\cdot\boldsymbol{p} + \chi^{-1}(e_2 - e_2\cdot\boldsymbol{p}\boldsymbol{p}), \tag{12}$$

Where,

$$\boldsymbol{p} = \frac{2}{\sqrt{\Delta}}\left(f_{22}, \tilde{f}_{22}, f_{20}, f_{21}, \tilde{f}_{21}\right), \tag{13}$$

$e_2 = (0,1,0,0,0)$, $\chi = \sqrt{\Delta}/2h$ and a vorticity tensor Ω by,

$$\Omega = \begin{pmatrix} 0 & 1 & 0 & 0 & 0 \\ -1 & 0 & 0 & 0 & 0 \\ 0 & 0 & 0 & 0 & 0 \\ 0 & 0 & 0 & 0 & \frac{-1}{2} \\ 0 & 0 & 0 & \frac{1}{2} & 0 \end{pmatrix}. \tag{14}$$

Thus the vesicle dynamics are completely determined by that of the unit vector $\boldsymbol{p}$ in $\mathbb{R}^5$. Moreover, the system (10) represents the vesicle's orientation and deformability. It was proving that the dynamics of deformable vesicle was hiding in that of a rigid sphere [2]; the projection into the shear plane gives a system similar to (10),[2],

$$\mathbf{p}_\perp = \begin{pmatrix} \mathscr{R}\cos\varphi \\ \mathscr{R}\sin\varphi \end{pmatrix}. \tag{15}$$

For a rigid sphere, the angle φ is twice the angle between the vesicle's long axis and the shear direction. Thus, it provides the same information as ψ for a deformable vesicle, which explains the correspondence between the vesicle and the rigid sphere.
Equation (12) has also been utilized to model microswimmers [75] in the presence of an external

flow field. The orientation of the microswimmer is represented by a unit vector $\boldsymbol{p}$, which follows the same dynamics described by Eq. (12), with an appropriate value of χ. Additionally, the swimmer's motility is introduced by considering its position $\mathbf{x} \in \mathbb{R}^3$, governed by the equation

$$\frac{d\mathbf{x}}{dt} = \mathbf{u}_0(\mathbf{x}) + \mathbf{v_s}, \tag{16}$$

where $\mathbf{v_s} = v_s \boldsymbol{p}$ represents the swimmer's velocity relative to the fluid. The magnitude $v_s = |\mathbf{v_s}|$ is taken as constant. This equation (5.40) indicates that the velocity of the microswimmer is the sum of the fluid velocity at its position, $\mathbf{u}_0$, and the swimming velocity $v_s \boldsymbol{p}$, where the direction of swimming, $\boldsymbol{p}$, is governed by Eq. (12).

The dynamics of the swimming direction closely resemble those of vesicle orientation, as both systems are described by similar equations. Based on established results for vesicles [2, 37], if $\chi > 1$, the swimmer's projection in the xyz-space (i.e., the vector $\boldsymbol{p}$) undergoes tumbling motion, which corresponds to periodic solutions. In contrast, when $\chi < 1$, the vector $\boldsymbol{p}$ stabilizes at a fixed orientation, meaning the swimmer aligns along this final orientation. Thus, Eqs. (12) and (5.40) capture the run-and-tumble behavior of the swimming particle, depending on the value of the parameter χ.

Historically, run-and-tumble dynamics were introduced to describe the motion of certain self-propelled particles, such as *E. coli* bacteria [18], which alternate between straight-line runs and reorientation events, known as tumbles, where the bacterium momentarily stops moving. Interestingly, Eq. (12) inherently models run-and-tumble dynamics via the parameter χ. Consequently, an alternative way to reproduce this behavior would be to randomly assign values greater than or less than unity to χ.

Microorganisms often exhibit responses to both fluid flow and various external stimuli, such as gravity (gyrotaxis), magnetic fields (magnetotaxis), and light (phototaxis). The interplay between fluid flow and these external forces results in a range of complex movements. To date, most trajectories of these microswimmers have been determined through numerical methods, in the presence of both flow and an external field [19, 19, 39]. However, none of these studies presented analytical solutions for the orientation angle in the tumbling regime or the trajectory of the particle. Nevertheless, in [38], several cases involving linear flows and external fields with varying orientations were investigated. It was demonstrated that explicit analytical solutions can be derived for both the particle orientation and trajectories in nearly all the cases considered.

Epidemiologic Modeling of Drug Transmission with Memory Effects

In recent years, drug addiction has emerged as a significant public health crisis, akin to an epidemic, affecting millions of individuals and communities worldwide. The complexities surround-

ing drug abuse are multifaceted, involving health, social, economic, and political dimensions. As drug dependence continues to escalate, understanding its dynamics becomes crucial for developing effective intervention strategies. Epidemiology, the study of how diseases spread and impact populations, plays a pivotal role in addressing this issue by identifying patterns, causes, and effects of drug-related health conditions within communities. Drug abuse is considered as a new epidemic, it has similar features with classical epidemics (SIR, SEIR,...) [22, 34, 35]. Epidemiological models serve as essential tools in this endeavor, providing insights into the transmission and control of drug abuse.

Historical Development of Epidemiologic Models

In 1911, Sir Ronald Ross (Nobel Prize in Medicine 1902, 1857-1932) [79] introduced the first mathematical model of malaria transmission, which revealed a threshold phenomenon. This model is one of the earliest examples of compartmental models and established Ross as a pioneering figure in mathematical epidemiology. In 1927, W.O. Kermack and A.G. McKendrick [49] built upon Ross's ideas and proposed the SIR model to study the transmission of infectious diseases among humans.

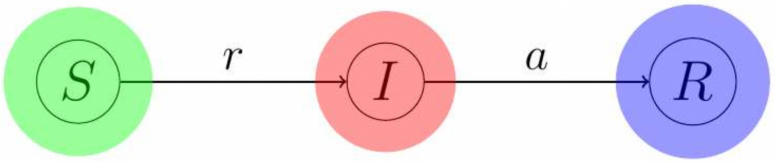


Figure 0.9: Schematic diagram for SIR model.

The SIR model, for example, divides the population into three compartments: susceptible individuals who can contact the disease, infected individuals who are currently ill, and recovered individuals who have overcome the illness. This model helps in understanding how individuals transition between these states and the factors influencing these transitions. The SIR model is described by the following system of differential equations

$$\begin{cases} S' = -r\dfrac{SI}{N}, \\ I' = r\dfrac{SI}{N} - aI, \\ R' = aI, \\ N = S + I + R, \end{cases}$$

with initial conditions:

$$S(0) = S_0, \quad I(0) = I_0, \quad R(0) = R_0.$$

We observe that the total population $N = S + I + R$ remains constant. This is confirmed by the fact that $S' + I' + R' = 0$. Furthermore, to find the equilibrium points, we solve the following system

$$\begin{cases} 0 = -r\dfrac{\bar{S}\bar{I}}{N}, \\ 0 = r\dfrac{\bar{S}\bar{I}}{N} - a\bar{I}, \\ 0 = a\bar{I}. \end{cases}$$

From the third equation, we get $\bar{I} = 0$, which is the only solution. Thus, we expect that the number of infected individuals should approach zero to achieve equilibrium. However, this does not provide information about the total number of individuals who have been infected, which corresponds to the final number in the R compartment.

$$\begin{cases} S' = -r\dfrac{SI}{N}, \\ I' = r\dfrac{SI}{N} - aI, \\ R' = aI. \end{cases}$$

The question posed here is : Given r, a, S_0, and I_0, can we determine if an epidemic will occur? We evaluate $I'(0)$ as follows:

$$I'(0) = I_0\left(r\frac{S_0}{N} - a\right).$$

1. If $rS_0 < aN$, then $I'(0) < 0$. Since $S' \leq 0$, it follows that $I'(t) < 0$ for all t. Hence, the number of infected individuals I will decrease until it reaches extinction.

2. If $rS_0 > aN$, then $I'(0) > 0$. The number of infected individuals will start to increase.

This threshold phenomenon was first identified by Sir Ronald Ross [79], who was awarded the Nobel Prize in Medicine in 1902. We define the basic reproduction number as:

$$R_0 = \frac{rS_0}{aN}.$$

Similarly, the SEIR model introduces an additional compartment for exposed individuals, who have been in contact with the disease but are not yet infected. This distinction is particularly relevant in the context of understanding how exposure to a disease can lead to subsequent infection, mirroring the dynamics of infectious diseases [52, 61].

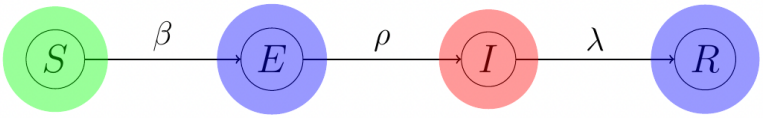


Figure 0.10: Schematic diagram for SEIR model.

Where the parameters are β rate of infection, ρ transition rate from exposed to infected, and λ recovery rate.

These models categorize the population into distinct compartments based on their disease status, allowing researchers to quantify the dynamics of disease transmission and evaluate the impact of various public health interventions. Mathematics serves as a fundamental tool in epidemiology, offering a systematic approach to analyze and predict the behavior of disease spread. Mathematical models can range from simple compartmental models to complex stochastic simulations, each providing valuable insights into how diseases propagate through populations. These models often incorporate variables such as transmission rates, recovery rates, and population demographics to simulate disease dynamics and forecast potential outcomes [24, 84].

However, traditional compartmental models may not fully capture the complexities of disease transmission, particularly the memory effects associated with past infections and the delayed responses to interventions. This is where fractional calculus comes into play. Fractional calculus, an advanced branch of mathematics dealing with non-integer order derivatives and integrals, has gained attention in epidemiology for its ability to model complex systems with memory effects. By incorporating fractional derivatives into epidemiological models, researchers can more accurately represent the dynamics of disease transmission, capturing the nuanced behavior of infections and the impact of public health measures.

The integration of fractional calculus into transmission models allows for a more comprehensive understanding of how past infections influence current behavior and how educational efforts can shape future trends. For instance, the effects of public health campaigns and educational programs can be modeled to assess their impact on reducing disease transmission. This approach not only enhances the understanding of transmission dynamics but also informs public health policy and intervention strategies.

Moreover, the application of sophisticated mathematical techniques, such as the modified trapezoidal rule [72] and the fractional Euler method [5], can provide numerical support for analytical findings, demonstrating the effectiveness of interventions over time. By analyzing the basic reproduction number $\mathscr{R}_0$, which serves as a threshold quantity for the extinction or spread of a disease, researchers can evaluate the potential success of various public health strategies. In this thesis, we have chosen to focus on the specific case of drug addiction within the broader context of epidemiology. The reason for this choice will be explored in detail in the following section, where we will discuss the historical development of epidemiological models and their relevance to understanding drug addiction. By examining the evolution of these models and their applications, we aim to highlight the importance of sophisticated mathematical techniques, such as fractional calculus, in addressing the complexities of drug addiction as an epidemic.

Fractional Derivatives in Drug Abuse Modeling

Several mathematical models for drugs have been developed and studied as well as many studies mentioned how drug use spreads as an infectious disease [21, 40, 62, 66, 70]. Different mathematical models enable us to better understanding of drug transmission mechanisms and the presentation of effective countermeasures. See for example [67, 88], as well as a recent article [3, 30, 87]. A heroin model was presented in [88], along with the basic reproduction number $\mathscr{R}_0$. They concluded that prevention was preferable to treatment. In [60], they used distributed delays to develop a heroin model. The authors showed that the stability of equilibrium is related to $\mathscr{R}_0$. The authors in [67], presented a SIRS model taking into account both light and heavy drugs, and they analysed the global stability using the Lyapunov function method. A large part of the epidemic models includes classical treatments such as vaccination, isolation, treatment, and so on, but some models also include public health education. In [65], they examined the impact of health education initiatives on the spread of HIV/AIDS. They showed that these campaigns might reduce the epidemic's spread. The authors in [89], found that educating the public about the dangers of drinking was one of the most efficient methods for reducing excessive drinking; they investigated a drinking model with public health educational campaigns and discovered that these campaigns can reveal drinking dynamics by comparing the basic reproductive number $\mathscr{R}_0$ for the model with the basic reproductive number $\mathscr{R}_1$ in the absence of public health educational campaigns. Motivated by this work, in [54], they introduced a six-dimensional drug model of family and public health education for controlling drug transmission. They found that family and public health education have a considerable impact on the spread of drug transmission. Recently, the authors in [78] showed that increasing the rate of education may reduce the rate of spread of drug addicts, resulting in a slower spread of drug addicts who will eventually disappear from society. Very recently, the authors in [6] used a fractional SIR epidemic model with the Caputo fractional derivative (as defined in Chapter 1) and an awareness campaign strategy to demonstrate the role of awareness programmes in presenting disease spread during an outbreak, epidemic, or pandemic.

In the literature, several epidemiological models have evolved a fractional derivative instead of a classical derivative. The fractional order derivative is a non-local operator that takes into account the memory effect (all the history) [76, 80]. [27] has examined integer order model and the numerical solutions of fractional-order model and found that the fractional order system model provides more relevant interpretation than integer order model. In fact, there are many phenomena which are related to memory and affected by heredity cannot be represented by integer order model [31].

Understanding drug addiction through the lens of epidemiological models offers valuable insights into the dynamics of substance abuse and the effectiveness of intervention strategies. The integration of fractional calculus into these models provides a more nuanced perspective on how past drug use influences current behavior and how public health education can shape future

trends. This approach contributes to a deeper understanding of drug addiction and informs the development of targeted and effective public health policies.
In conclusion, the intersection of epidemiology, mathematical modeling, and fractional calculus presents a promising avenue for addressing the challenges posed by drug addiction. By leveraging these tools, researchers and policymakers can develop more effective measures to control and prevent substance abuse, ultimately contributing to better health outcomes and more resilient healthcare systems. The fight against drug addiction requires a multifaceted approach, and the insights gained from mathematical modeling can play a crucial role in shaping effective public health strategies.
In this Thesis, motivated by previous research we examine the six-dimensional drug model that incorporates family education and public health education introduced by [54].

Thesis Objectives and Scope

This thesis aims to explore and advance the application of fractional calculus across a range of dynamic systems, with a particular focus on the interplay between memory effects and particle dynamics. The primary objective is to provide a comprehensive analysis of how fractional calculus can enhance our understanding of complex behaviors in various contexts.
The structure of this thesis is organized as follows:

chapter 1: In this chapter, we will present some fundamental tools used throughout this thesis, including: special functions (namely, the Gamma function, the Beta function, and the Mittag-Leffler function), the Laplace transform, fractional integrals and derivatives, as well as foundational theorems and lemmas for fractional differential equations.

Chapter 2: In this chapter, we explore the dynamics of vesicles and red blood cells in shear flow through the application of fractional calculus. We begin by presenting a fractional ordinary differential system that investigates vesicle motion and deformation, revealing three distinct states: the classical Tank Treading (TT), an over-damped tank-treading (OD-TT) mode, and an under-damped tank-treading (UD-TT) mode. The chapter further bridges the gap between analytical and numerical approaches by comparing the insights gained from the Caputo derivative with those obtained using the Jumarie fractional derivative, enhancing our understanding of vesicle behavior in complex fluid systems. Finally, we extend the Keller and Skalak (KS) theory by incorporating the modified Riemann-Liouville fractional derivative to investigate the transition of red blood cells from flipping to stationary motion, highlighting the importance of memory effects in capturing the intricate dynamics of these particles. Collectively, these studies underscore the significance of fractional derivatives in advancing mathematical modeling and our comprehension of fluid dynamics.

Chapter 3: In this chapter, we investigate a fractional rigid sphere model in five dimensions that utilizes the Caputo operator to map the dynamics of a vesicle. This model provides new in-

sights into the mechanisms behind the memory effect, revealing the emergence of two additional motion types in addition to the classical tank-treading mode, where the vesicle rotates about its axis while maintaining a constant shape.

Chapter 4: In this chapter, we explore the solution of fractional differential equations. This study presents an innovative exploration of vesicle dynamics using Jumarie's modified Riemann–Liouville fractional derivative within a five-dimensional fractional rigid sphere model. We reveal an exact solution through the Mittag-Leffler function, which provides a deeper understanding of intricate vesicle dynamics. Additionally, a comparative analysis with Caputo's derivative emphasizes the effectiveness of these fractional derivatives, contributing not only to theoretical insights but also to practical implications in applied mathematics and biophysical systems. The findings advance our understanding of complex vesicle behaviors, particularly in mimicking real cell-like dynamics, and pave the way for further research and applications in the field.

Chapter 5: In this chapter, we investigate the captivating dynamics of spherical microswimmers in a 1D shear flow, revealing the intricate interplay between memory effects and fluid mechanics through the lens of fractional calculus. By deriving exact solutions for the orientation and trajectory of these microswimmers, we uncover a rich tapestry of motion patterns that challenge traditional models. Our findings not only enhance the theoretical understanding of microswimmer behavior but also hold significant implications for practical applications in biophysics and targeted drug delivery. This research underscores the power of fractional calculus as a transformative tool in unraveling the complexities of biological systems, paving the way for innovative approaches in the study of fluid dynamics.

Chapter 6: In this chapter, we examine a critical problem of both theoretical and numerical significance within standard epidemiological models. Our investigation focuses on a drug transmission model grounded in compartmental dynamic frameworks, paralleling those used in infectious disease epidemiology. To facilitate a thorough analysis and obtain a comprehensive range of results, we utilize a fractional time-Caputo derivative in place of the classical time derivative. Our analytical and numerical results including the existence and uniqueness of solutions, stability analysis of equilibrium points, sensitivity of parameters, trapezoidal rule, and fractional Euler method demonstrate that the interplay between family education and public health efforts significantly influences the dynamics of drug transmission.

Overall, this thesis concludes with a comprehensive synthesis of the key contributions made throughout the research, highlighting their significance in the broader context of scientific inquiry. Additionally, it presents a discussion of potential avenues for future research, offering suggestions for extending and building upon the work presented.

CHAPTER 1

PRELIMINARY CONCEPTS AND INSIGHTS

Contents

1.1 Background of non-integer calculus **19**

1.1.1 Introduction 19

1.1.2 Special Functions 19

1.1.3 Elements on Laplace Transform 21

1.1.4 Fractional Integrals and Derivatives 22

1.2 Foundational Theorems and Lemmas for Fractional Differential Equations . . **26**

1.1 Background of non-integer calculus

1.1.1 Introduction

Fractional derivatives represent an innovative extension of the classical concept of differentiation, introducing a continuous generalization of the derivative operation to non-integer orders. The introduction of fractional derivatives has been motivated by the need to accurately model complex and non-stationary phenomena, including anomalous diffusion, stochastic processes, and fractal dynamical systems.
Here, we will explore the theoretical aspects of fractional derivatives, their remarkable properties, and their implications in specific domains of our study.
The ultimate goal is to provide an in-depth understanding of this extension of classical differentiation and to investigate its potential applications for solving complex, and interdisciplinary problems.

1.1.2 Special Functions

In this part, we present fundamental concepts related to special functions, which find application in subsequent chapters. Specifically, we provide insights into the Gamma, Beta, and Mittag-Leffler functions, all pivotal roles in the realms, and the theory of fractional differential equations. These special functions, enriched by their intricate properties, lay the groundwork for a deeper understanding of advanced Mathematical concepts.

1.1.2.1 The Gamma-Function

The Gamma Function was introduced by the Swiss mathematician Leonard Euler (1707-1783) to generalize the factorial for non-integer values. Later, due to its importance, it was studied by other mathematicians.

Definition 1.1.1. *[76] The Gamma function, denoted as* $\Gamma(z)$*, is one of the fundamental functions in fractional calculus. It is defined by the following integral*

$$\Gamma(z) = \int_0^{+\infty} t^{z-1} e^{-t} dt. \tag{1.1}$$

Properties 1.1.1.
• *An important property of the Gamma function, is the following recurrence relation*

$$\Gamma(z+1) = z\Gamma(z), \tag{1.2}$$

which can be demonstrated by through integration by parts.
• *The Euler Gamma function generalizes the factorial, as*

$$\Gamma(n+1) = n!. \tag{1.3}$$

1.1.2.2 The Beta-Function

In many cases, it is more convenient to use the Beta function instead of a specific combination of values of the Gamma function.

Definition 1.1.2. *The Beta function, which is a type of Euler integral similar to the Gamma function is a function defined by*

$$\beta(p,q) = \int_0^1 \tau^{p-1}(1-\tau)^{q-1} d\tau, \tag{1.4}$$

such that $p > 0$ *and* $q > 0$.

Properties 1.1.2.

• *In its integral definition, the change of variable* $S = 1 - \tau$ *demonstrates that this function is symetric,*

$$\beta(p,q) = \beta(q,p). \tag{1.5}$$

• *It is sufficient to perform integration by parts to prove that*

$$p\beta(p,q+1) = q\beta(p+1,q). \tag{1.6}$$

1.1.2.3 The relationship between the Gamma function and the Beta function

The Beta function is connected to the Gamma function by the following equation

$$\beta(p,q) = \frac{\Gamma(p)\Gamma(q)}{\Gamma(p+q)}. \tag{1.7}$$

Remark 1.1.1. *If p and q are integers, we obtain*

$$\beta(p,q) = \frac{(p-1)!(q-1)!}{(p+q-1)!}. \tag{1.8}$$

1.1.2.4 The Mittag-Leffler Function

The Mittag-Leffler function, is a special function that generalizes the exponential function. It was introduced by the swedish mathematician Gosta Mittag-Leffler in 1903.

Definition 1.1.3. *[76] The function is defined as an infinite series as follows*

$$E_\alpha(z) = \sum_{k=0}^{+\infty} \frac{z^k}{\Gamma(\alpha k + 1)}, \tag{1.9}$$

where z is the variable, α *is the parameter, and* Γ *represents the Gamma function.*

In order to express some solutions obtained in this thesis, we need to introduce the following generalized trigonometry functions defined by the Mittag-Leffler function

$$\begin{aligned} \cos_\alpha(t) &= \frac{E_\alpha(it^\alpha)+E_\alpha(-it^\alpha)}{2}, \\ \sin_\alpha(t) &= \frac{E_\alpha(it^\alpha)-E_\alpha(-it^\alpha)}{2i}, \\ \tan_\alpha(t) &= \frac{\sin_\alpha(t)}{\cos_\alpha(t)}. \end{aligned} \tag{1.10}$$

The Mittag-Leffler function has various applications in different branches of mathematics, physics, and engineering. It is particularly useful in fractional calculus, a field that extends the concepts of differentiation and integration to non-integer orders.

Definition 1.1.4. *[76] The two-parameter Mittag-Leffler function plays a very important role in the theory of fractional calculus. This function was introduced by Agrawal and Endelyi in 1953-1954 and is defined by a series expansion as follows*

$$E_{\alpha_1,\alpha_2}(z) = \sum_{k=0}^{+\infty} \frac{z^k}{\Gamma(\alpha_1 k+\alpha_2)}, \tag{1.11}$$

from formula (1.11)*, it follows that,*

$$E_{\alpha_1,\alpha_2}(z) = \frac{1}{\Gamma(\alpha_2)} + zE_{\alpha_1,\alpha_2}(z). \tag{1.12}$$

1.1.3 Elements on Laplace Transform

Operational calculus is a tool often used for solving engineering problems. It proves powerful and indispensable, especially in the study of fractional systems. Therefore, in this paragraph, we will review some basic elements of Laplace transform in the integer case before extending it to the fractional case.

Definition 1.1.5. *[17] Let $f:\mathbb{R}_+ \longrightarrow \mathbb{R}$. If the integral $\int_0^{+\infty} e^{-st} f(t)dt$ exists, then it is called the Laplace transform of the function f, denoted as*

$$F(s) = \mathscr{L}\{f(t):s\} = \mathscr{L}[f](s) = \int_0^{+\infty} e^{-st} f(t)dt. \tag{1.13}$$

The function $f(t)$ is called the original function.

Definition 1.1.6. *[17] The original function $f(t)$ can be reconstructed from the Laplace transform $F(s)$ using the inverse Laplace transform*

$$f(t) = \mathscr{L}^{-1}\{F(s):t\} = \frac{1}{2\pi i}\int_{c-i\infty}^{c+i\infty} e^{st}F(s)ds, \qquad c = \mathscr{R}e(s). \tag{1.14}$$

- **Essential Laplace Transforms: A Quick Summary**

$Y(s)=\mathscr{L}\{y(t)\}$	$y(t)=\mathscr{L}^{-1}\{Y(s)\}$
$\frac{1}{s^{\alpha}}$	$\frac{t^{\alpha}-1}{\Gamma(\alpha)}$
$\frac{1}{(s+a)^{\alpha}}$	$\frac{t^{\alpha-1}}{\Gamma(\alpha)}e^{-at}$
$\frac{1}{s^{\alpha}-a}$	$t^{\alpha-1}E_{\alpha,\alpha}(at^{\alpha})$
$\frac{s^{\alpha}}{s(s^{\alpha}-a)}$	$E_{\alpha}(-at^{\alpha})$
$\frac{a}{s(s^{\alpha}+a)}$	$1-E_{\alpha}(-at^{\alpha})$
$\frac{1}{s^{\alpha}(s-a)}$	$t^{\alpha}E_{1,\alpha+1}(at)$
$\frac{s^{\alpha-\beta}}{s^{\alpha}-a}$	$t^{\beta-1}E_{\alpha,\beta}(at^{\alpha})$

Definition 1.1.7. *[76] When the product $f(x-t)g(t)$ is integrable over $\mathbb{R}$, the convolution of f and g is defined as*

$$(f\star g)(x):=\int_{-\infty}^{+\infty}f(x-t)g(t)dt. \tag{1.15}$$

Properties 1.1.3.

• *The Laplace Transform of an n-th order derivative of the function f is given by*

$$\mathscr{L}\{f^{(n)}(t)\}(s)=s^{n}F(s)-\sum_{k=0}^{n-1}s^{n-k-1}f^{(}k)(0). \tag{1.16}$$

This can be obtained from Definition 1.1.5 by integration by parts under the assumption that the corresponding integrals exist.

• *If the Laplace transforms of f and g exist, then the Laplace transform of the convolution product satisfies*

$$\mathscr{L}\{f\star g\}(s)=\mathscr{L}\{f\}(s)\mathscr{L}\{g\}(s). \tag{1.17}$$

1.1.4 Fractional Integrals and Derivatives

In this part, we mention some definitions and results of fractional calculus. Fractional calculus was initially explored by great mathematicians such as Fourier, Euler, and Laplace, each with their own notation and methodology for defining non-integer order derivatives or integrals. However, the most well-known definitions today are those of Riemann-Liouville, Caputo, and Jumarie.

A few years earlier, S.F. Lacroix succeeded in introducing the non-integer order derivative for the function $f(x)=x^{\beta}$. The idea is as follows: We know that the n^{th} derivative of the function $f(x)=x^{m}$, where $n,m\in\mathbb{N}$ and $n\leqslant m$, is given by:

$$D^{n}x^{m}=\frac{m!}{(m-n)!}x^{m-n}.$$

By using the Gamma function (see Section 1.1), we can generalize the result for $n \in \mathbb{R}_+$. So Lacroix defined the non-integer order derivative as

$$D^{\alpha}x^{\beta} = \frac{\Gamma(\beta+1)}{\Gamma(\beta-\alpha+1)}x^{\beta-\alpha},$$

where $\alpha < \beta+1$ and $\beta > -1$.

Examples 1.1.1.

$$\bullet\, D^{\frac{1}{2}}x = \frac{\Gamma(2)}{\Gamma\left(\frac{3}{2}\right)}x^{\frac{1}{2}} = \frac{x^{\frac{1}{2}}}{\frac{1}{2}\sqrt{\pi}} = 2\sqrt{\frac{x}{\pi}}$$

$$\bullet\, D^{\frac{1}{2}}x^2 = \frac{\Gamma(3)}{\Gamma\left(\frac{5}{2}\right)}x^{\frac{3}{2}} = 2\frac{x^{\frac{3}{2}}}{\frac{3}{4}\sqrt{\pi}} = \frac{8x}{3}\sqrt{\frac{x}{\pi}}$$

$$\bullet\, D^{\alpha}1 = \frac{\Gamma(1)}{\Gamma(1-\alpha)}x^{-\alpha} = \frac{x^{-\alpha}}{\Gamma(1-\alpha)}.$$

$$D^{-1}1 = \frac{\Gamma(1)}{\Gamma(2)}x = \frac{x}{\Gamma(2)} = x, \quad D^{0}1 = 1.$$

$$\bullet\, D^{\frac{1}{2}}1 = \frac{1}{\sqrt{\pi x}}.$$

1.1.4.1 Riemann-Liouville Fractional Integral

Let f be a continuous function on the interval $[a,b]$. A primitive of f is given by the expression:

$$I^{(1)}f(x) = \int_a^x f(t)dt$$

For a second primitive, we have:

$$I^{(2)}f(x) = \int_a^x dt \int_a^t f(u)du$$

By using Fubini's theorem, we can write:

$$I^{(2)}f(x) = \int_a^x (x-t)f(t)dt$$

More generally, the n^{th} iterate of the operator I can be written as:

$$I^{(n)}f(x) = \int_a^x dx_1 \int_a^{x_1} dx_2 \ldots \int_a^{x_{n-1}} f(x_n)dx_n = \frac{1}{(n-1)!}\int_a^x (x-t)^{n-1}f(t)dt, \tag{1.18}$$

for any integer n [76].

This formula is called the Cauchy formula, and since the generalization of factorial by the Gamma function: $(n-1)! = \Gamma(n)$, Riemann realized that the second term of (2.3) could have meaning even when n takes a non-integer value. So it was natural to define the fractional integration operator as follows

Definition 1.1.8. *[76] Let $f \in C([a,b])$, $\alpha \in \mathbb{R}_+$. The Riemann-Liouville integral of f is defined by the following formula*

$$\left(I_a^{\alpha}f\right)(t) = \frac{1}{\Gamma(\alpha)}\int_a^t (t-\tau)^{\alpha-1}f(\tau)d\tau. \tag{1.19}$$

Remark 1.1.2. *The formula* (1.19) *is a generalization of the* n^{th} *primitive with a non-integer order of primitive* α.

Remark 1.1.3. *The fractional Riemann-Liouville integral can notably be written as a convolution product of the power function* $h_\alpha(t) = \frac{t^{\alpha-1}}{\Gamma(\alpha)}$ *and* $f(t)$ *as follows*

$$I_a^\alpha f(t) = \int_a^t h_\alpha(t-\tau) f(\tau) d\tau = (h_\alpha \star f)(t). \tag{1.20}$$

Properties 1.1.4. *The Laplace Transform of the Riemann-Liouville fractional integral for* $a = 0$ *of a function* f *is formulated as follows*

$$\mathscr{L}\left(I_0^\alpha f\right)(s) = s^{-\alpha}\mathscr{L}(f)(s). \tag{1.21}$$

1.1.4.2 Riemann-Liouville Fractional Derivatives

Definition 1.1.9. *[76] The Riemann-Liouville fractional derivative of order* α *of the function* f *is given by*

$${}^{\mathscr{RL}}D_a^\alpha f(t) = \frac{d^n}{dt^n}\left(I_a^{n-\alpha}(f(t))\right). \tag{1.22}$$

In other words

$${}^{\mathscr{RL}}D_a^\alpha f(t) = \frac{d^n}{dt^n}\left[\frac{1}{\Gamma(n-\alpha)}\int_a^t (t-\tau)^{n-\alpha-1} f(\tau) d\tau\right], \tag{1.23}$$

where, $\frac{d^n}{dt^n}$ *is an integer order derivative* $n = [\alpha] + 1$.

Properties 1.1.5. *If* $f \in L^1[a,b]$ *where* $b > 0$*, the Laplace transform of the Riemann-Liouville fractional derivative of* f *is given by*

$$\mathscr{L}\left({}^{\mathscr{RL}}D_0^\alpha f\right)(s) = s^\alpha(\mathscr{L}f)(s) - \sum_{k=0}^{n-1} s^k \left[{}^{\mathscr{RL}}D_0^{\alpha-k-1} f(t)\right]_{t=0}, \tag{1.24}$$

where $n-1 < \alpha < n$.

1.1.4.3 Caputo Fractional Derivatives

In the realm of fractional calculus and its applications in both theoretical and applied mathematics, the Caputo derivative has emerged as a pivotal concept. Much like the Riemann-Liouville definition, the Caputo derivative plays a crucial role in extending classical calculus to non-integer orders. Its significance lies in its ability to capture and represent fractional-order dynamics in various mathematical models, making it an indispensable tool in the study of complex phenomena. However, as with any mathematical framework, its applications and implications evolve, prompting ongoing exploration and refinement, particularly in areas such as physics, engineering, and other scientific disciplines where the Caputo derivative proves instrumental in enhancing our understanding of intricate physical systems.

Definition 1.1.10. *[46, 76] The fractional derivative in the Caputo sense of a given function $f(t)$ on the interval $[a,b]$ is defined by the following relation:*

$$ {}^{C}D_a^{\alpha} f(t) = I_a^{n-\alpha} \frac{d^n}{dt^n} f(t) = \frac{1}{\Gamma(n-\alpha)} \int_a^t (t-s)^{n-\alpha-1} f^{(n)}(s) ds. \tag{1.25} $$

with $n \in \mathbb{N}$ et $n = [\alpha] + 1$, where $[\alpha]$ is the integer part of α.

Properties 1.1.6. *Suppose that $F(s)$ is the Laplace transform of $f(t)$. Then, the Laplace transform of the Caputo fractional derivative operator of order α, where $n-1 < \alpha < n$, is given by*

$$ \mathscr{L}\left\{ {}^{C}D_a^{\alpha} f \right\}(s) = s^{\alpha} F(s) - \sum_{k=0}^{n-1} s^{\alpha-k-1} f^{(k)}(0). \tag{1.26} $$

Remark 1.1.4. *Let $a > 0$ with $n-1 < \alpha < n$ where $n \in \mathbb{N}^*$. Suppose that f is a function such that both ${}^{C}D_a^{\alpha} f(t)$ and ${}^{\mathscr{RL}}D_a^{\alpha} f(t)$ exist. Then, the relation between the Riemann-Liouville fractional derivative ${}^{C}D_a^{\alpha} f(t)$ and the Caputo fractional derivative $D_a^{\alpha} f(t)$ is given by*

$$ {}^{C}D_a^{\alpha} f(t) = {}^{\mathscr{RL}}D_a^{\alpha} f(t) - \sum_{k=0}^{n-1} \frac{(t-a)^{k-\alpha}}{\Gamma(k-\alpha+1)} f^{(k)}(a). $$

•The main advantage of the Caputo approach is that the initial conditions of fractional differential equations with Caputo derivatives take the same form as those for integer-order differential equations.

• Graphically, it can be said that the path followed to arrive at the Caputo fractional derivative is also the reverse when following the other approach (Riemann-Liouville). That is, to find the fractional derivative of order a where $n-1 < a < n$ through the Riemann-Liouville approach, one starts by first fractionally integrating of order $(n-a)$ for the function $f(x)$, and then differentiating the obtained result to the integer order n*. However, to find the fractional derivative of order a where* $\mathrm{n}-1 < \mathrm{a} < \mathrm{n}$ *through the Caputo approach, one begins by taking the integer-order derivative n of the function $f(x)$ and then fractionally integrates of order $(n-a)$.*

1.1.4.4 Modified Riemann-Liouville Fractional Derivatives

In the realm of fractional calculus, Jumarie's modified Riemann-Liouville fractional derivative has also gained significant importance. Similar to the Caputo derivative, Jumarie's derivative extends the classical calculus to non-integer orders, providing a powerful tool for describing fractional-order dynamics in various mathematical models.

Just like the Caputo, Jumarie's modified Riemann-Liouville fractional derivative finds applications in diverse fields such as physics, engineering, and other scientific disciplines. Its versatility and effectiveness make it an indispensable tool for understanding and modeling complex phenomena.

Definition 1.1.11. *[44, 45] Let f and g be continuous and differentiable functions, Jumarie derivative of order α of the function g is expressed as*

$$
\begin{aligned}
&{}^{\mathcal{J}}D_t^{\alpha} g(t) = \frac{1}{\Gamma(1-\alpha)} \frac{d}{dt} \int_0^t (t-\tau)^{-\alpha} [g(\tau) - g(0)] d\tau, && 0 < \alpha < 1, \\
&{}^{\mathcal{J}}D_t^{\alpha} g(t) = \left(g^{(\alpha-n)}\right)^{(n)}, && n \leq \alpha < n+1, \ \ n \geq 1.
\end{aligned}
\tag{1.27}
$$

As a result, the following properties hold

Properties 1.1.7.

$$
{}^{\mathcal{J}}D_t^{\alpha_1} t^{\alpha_2} = \frac{\Gamma(\alpha_2+1)}{\Gamma(\alpha_2+1-\alpha_1)} t^{\alpha_2-\alpha_1}, \alpha_2 > 0, \alpha_2 \geq \alpha_1, \quad {}^{\mathcal{J}}D_t^{\alpha} C = 0, \tag{1.28}
$$

$$
{}^{\mathcal{J}}D_t^{\alpha}[f(t)g(t)] = g(t)\,{}^{\mathcal{J}}D_t^{\alpha} f(t) + f(t)\,{}^{\mathcal{J}}D_t^{\alpha} g(t) \tag{1.29}
$$

$$
{}^{\mathcal{J}}D_t^{\alpha} f[g(t)] = \left(\frac{d}{dg} f[g(t)]\right) {}^{\mathcal{J}}D_t^{\alpha} g(t) = {}^{\mathcal{J}}D^{\alpha} f[g(t)] \left(\frac{d}{dt} g(t)\right)^{\alpha}, \tag{1.30}
$$

with C is constant and $\frac{d}{dt}$ is the ordinary derivative with respect to the variable t.

This derivative provides a robust framework for accurately capturing the intricate dynamics of systems displaying fractional-order behaviour by addressing challenges such as defining derivatives of constants and handling the product or composition of two functions. This new tool has many interesting properties when compared with other definitions and has proven instrumental in computing exact solutions for some fractional equations [44]. However, the quest for exact solutions of fractional differential equations remains challenging, requiring significant effort and further research to advance in this field. While several questions have been raised in the literature, it has been noted that there are counterexamples to Jumarie's basic formulae for non-differentiable functions [57, 58]. However, in other works, the use of the Jumarie derivative for differentiable functions has yielded pertinent results [33, 81]. Since our study specifically focuses on differentiable functions, the concerns raised regarding non-differentiable functions do not apply to our investigation. This further motivated our decision to employ the basic properties of the modified Riemann-Liouville derivative for determining an exact analytical solution.

1.2 Foundational Theorems and Lemmas for Fractional Differential Equations

In this section, we present several fundamental results that underpin our study of fractional differential equations and their applications in various contexts, including epidemiology. These results, based on existing literature, will serve as a foundation for the subsequent analysis and

discussion.
Let $f:\mathbb{R}^n \to \mathbb{R}^n$ where $n \geq 1$, consider the following fractional order system

$$\begin{cases} {}^{C}D_t^{\alpha} X(t) &= f(X(t)), \\ X(0) &= X_0, \end{cases} \tag{1.31}$$

with ${}^{C}D_t^{\alpha}$ is the Caputo fractional derivative, $0 < \alpha \leq 1$, and $X_0 \in \mathbb{R}^n$.
To verify the positivity of the fractional model solutions (1.31), we will first recall some of the prerequisites for this suggested study.

Lemma 1.2.1. *[74]*
Suppose that $f(t) \in C[a,b]$ and ${}^{C}D_t^{\alpha} f(t) \in C(a,b]$, for $0 < \alpha \leqslant 1$, where ${}^{C}D_t^{\alpha}$ represents the Caputo derivative, then we have

$$f(t) = f(a) + \frac{1}{\Gamma(\alpha)} \left({}^{C}D_a^{\alpha} f\right)(\zeta) \cdot (t-a)^{\alpha}, \tag{1.32}$$

with $a \leqslant \zeta \leqslant t, \forall t \in (a,b]$.

Lemma 1.2.2. *[74]*
Suppose that $f(t) \in C[a,b]$ and ${}^{C}D_t^{\alpha} f(t) \in C(a,b]$, for $0 < \alpha \leq 1$. The following requirements are then verified:
If ${}^{C}D_t^{\alpha} f(t) \geq 0, \forall t \in (a,b)$ then $f(t)$ is non-decreasing $\forall t \in [a,b]$.
If ${}^{C}D_t^{\alpha} f(t) \leq 0, \forall t \in (a,b)$, then $f(t)$ is non-increasing $\forall t \in [a,b]$.

Lemma 1.2.3. *[56]*
Assume that f fulfills the following criteria:
(i) $f(t)$ and $\frac{\partial f}{\partial t}$ are continuous for all $t \in \mathbb{R}^n$.
(ii) $\|f(t)\| \leq \tau + \|\nu t\| \quad \forall t \in \mathbb{R}^n$, where τ and ν are two positive constants.
Then, the initial value problem (1.31) *has a unique solution on* $[0, +\infty)$.

The following theorems ensure the existence and the uniqueness of the solution to the initial value problem (1.31), provided that the function f satisfies the Lipschitz condition.

Theorem 1.2.1. *(Existence[28]).*
Assume that $G := [0,T] \times \left[x_0^{(0)} - \epsilon, x_0^{(0)} + \epsilon\right]$ with some $T > 0$ and some $\epsilon > 0$, and let the function $f : G \to \mathbb{R}$ be continuous. In addition, let $h := \min\left\{T, \to (\epsilon\Gamma(\alpha+1)/\|f\|_{\infty})^{\frac{1}{\alpha}}\right\}$. Then, there exists a function $x : [0,h] \to \mathbb{R}$ solving the initial value problem (1.31).

Theorem 1.2.2. *(Uniqueness[28]).*
Assume that $G := [0,T] \times \left[x_0^{(0)} - \epsilon, x_0^{(0)} + \epsilon\right]$ with some $T > 0$ and some $\epsilon > 0$. Moreover, let the function $f : G \to \mathbb{R}$ be bounded on G and satisfy a Lipschitz condition with respect to the second variable i.e $|f(t,x) - f(t,y)| \leq A|x-y|$, with some constant $A > 0$ independent of t, x and y. Then, denoting h as in theorem 2.1, there exists at most one function $x : [0,h] \to \mathbb{R}$ solving (1.31).

Furthermore, this theorem now provides criteria for stability and asymptotic stability of the equilibrium points of the system (1.31), which is essential for understanding the long-term behavior of the solutions.

Theorem 1.2.3. *[63, 91].*

• *The equilibrium of the system* (1.31) *is stable if and only if all eigenvalues* $\tilde{\lambda}_j$, $j = 1,\ldots,n$ *of the Jacobian matrix calculated at the equilibrium point fulfill the requirement* $|\arg(\tilde{\lambda}_j)| \geq \frac{\alpha\pi}{2}$, $\forall j$.

• *The equilibrium of the system* (1.31) *is asymptotically stable if and only if* $|\arg(\tilde{\lambda}_j)| > \frac{\alpha\pi}{2}$, $\forall j$.

CHAPTER 2

FRACTIONAL DYNAMICS AND MEMORY EFFECTS: INSIGHTS INTO VESICLE AND ELLIPSOIDAL PARTICLE BEHAVIOR IN SHEAR FLOW

Contents

2.1 Introduction **31**

2.2 Analytical solutions and classification of vesicle motion and deformation in shear flow: Uncovering new tank-treading modes **32**

2.2.1 The vesicle model formulation and Fractional vesicle model 32

2.2.2 Stability analysis 33

2.2.3 Exact solutions and vesicle dynamics 35

2.2.4 Tank-treading mode ($h > h_c$) 36

2.2.5 The damped oscillatory modes ($h < h_c$) 36

2.3 Dynamic Insights on the Caputo Derivative's Impact in Unraveling Vesicle Behavior **43**

2.3.1 Formulation of the Vesicle Model and the Caputo Fractional Vesicle Model 43

2.3.2 Analysis of Existence and Uniqueness of Solutions in Caputo-Fractional Equations 44

2.3.3 Equilibrium and Local Stability Analysis of the Fractional Model 45

2.3.4 Numerical Computation Method 45

2.3.5 Tank-treading mode ($h > h_c$) 46

2.3.6 Damping tank-treading mode ($h < h_c$) 46

2.4 Comparison of Caputo and the Modified Riemann–Liouville Fractional Derivatives in Vesicle Dynamics **52**

2.5 Motion of an Ellipsoidal Particle in Shear Flow: Analyzing Memory Effect Influence Through Exact Solutions Investigation **58**

2.5.1 TT-mode 59

2.5.2 TB-mode 60

2.6 Conclusion **62**

2.1 Introduction

From a biological viewpoint [32], at the molecular level, red blood cell dynamics, specifically their deformation and orientation, affect blood fluidity and mass transport. Which motivates us to further analyse the behaviour of the vesicle as a simplified model of the red blood cell. In this chapter, we delve into the intricate dynamics of vesicles, red blood cells, and ellipsoidal particles in shear flows, using the advanced mathematical tools of fractional calculus, as introduced in Chapter 1, to gain deeper insights into their motion and deformation. The application of fractional derivatives, specifically the Jumarie and Caputo formulations, enables us to model and investigate the complex, memory-driven behaviors of these entities in ways that classical methods cannot fully capture. By providing both exact analytical and numerical solutions and through a detailed comparative analysis of the Jumarie and Caputo derivatives, we uncover new, previously unobserved phenomena.

The integration of fractional calculus into our modeling framework reveals subtle transitions between various dynamic states, such as classical behaviors like tank-treading, vacillating breathing, and tumbling, alongside new motions driven by fractional order effects. These transitions are strongly influenced by memory effects and non-local interactions, which are uniquely captured by fractional derivatives, highlighting their significance in fluid-structure interactions. Moreover, we expand upon the theoretical work of Keller and Skalak [48], who predicted an increase in the period of flipping and eventual alignment with the flow, resulting in a stationary orientation. Despite these predictions, the finer details of this transition remain elusive and largely unexplored. By incorporating fractional derivatives into their framework, we aim to shed light on this process, examining how memory effects influence the flipping period and the red blood cell's alignment with the flow a phenomenon yet to be fully understood.

Overall, this chapter advances our understanding of vesicles, red blood cells, and ellipsoidal particles under shear flow, bridging the gap between classical fluid dynamics and modern fractional calculus approaches. The insights gained not only enhance our comprehension of fluid-structure interactions but also open new avenues for future research and practical applications in biophysics, biomedical engineering, and the study of complex fluid systems. Te chapter is organized as follows: Section 2.2 presents analytical solutions for vesicle motion and deformation, highlighting the discovery of new tank-treading modes in shear flow. Section 2.3 investigates how the Caputo fractional derivative impacts vesicle dynamics, providing deeper insights into the time-dependent behavior of vesicles. Section 2.4 offers a comparison between the Caputo and Modified Riemann–Liouville fractional derivatives, analyzing their effects on vesicle motion. Section 2.5 focuses on the motion of an ellipsoidal particle in shear flow, examining how memory effects influence its orientation and trajectory through exact solutions. The chapter concludes by summarizing key findings and their implications for future research in fractional vesicle and particle dynamics. The results of this chapter are based on the papers [11, 13, 14].

2.2 Analytical solutions and classification of vesicle motion and deformation in shear flow: Uncovering new tank-treading modes

In this section, we examine the dynamics of vesicles in shear flow using Jumarie's fractional derivative to capture memory effects. The study focuses on the classical regimes of vesicle motion, such as tank-treading, tumbling, and vacillating-breathing, while incorporating this fractional derivative to extend traditional models. By leveraging the properties of Jumarie's derivative, as described in Chapter 1, we were able to find exact solutions something not achievable with other types of fractional derivatives. We will present the exact analytical solutions for vesicle shape deformation and orientation, highlighting how the fractional derivative influences these regimes. Important factors, such as the evolution of vesicle shape and the memory effect on vesicle behavior, will be thoroughly analyzed.

2.2.1 The vesicle model formulation and Fractional vesicle model

As indicated in the introduction, the evolution dynamics in linear shear flow are determined by the three amplitudes $F_{2\pm2}$ and F_{20}. The evolution of the amplitude F_{22} gives the evolution in time of the vesicle shape deformation in the shear plane. F_{20} mode describes the deformation out of the shear plane.

The implementation of (9), clarifies the role of the amplitude F_{22}, where $\psi(t)$ represents the vesicle's orientation angle and $\mathscr{R}$ is the vesicle's amplitude of deformation, then we get the following system

$$\begin{aligned} {}^{\mathscr{J}}D_t^{\alpha}\mathscr{R} &= h\left[1-4\frac{\mathscr{R}^2}{\Delta}\right]\sin(2\psi),\\ {}^{\mathscr{J}}D_t^{\alpha}\psi &= -\frac{1}{2}+\frac{h}{2\mathscr{R}}\cos(2\psi), \end{aligned} \tag{2.1}$$

In the classical case (i.e, when $\alpha = 1$), it is demonstrated in [64], that the above system qualitatively describes the three classical regimes (TT,TB and VB).

The system (2.1) seems difficult at first sight. Therefore, the basic principle for finding exact analytical solutions is to introduce new coordinates in which the system (2.1) simplifies. The authors of [37] discover that the real and imaginary parts of $F_{22} = \xi - i\zeta$ can be used to describe vesicle motion alternatively to ψ and $\mathscr{R}$, where ξ and ζ are related to the orientation angle ψ and the shape deviation $\mathscr{R}$ by the following relations obtained using (9)

$$\xi(t) = \mathscr{R}(t)\cos[2\psi(t)], \quad \zeta(t) = \mathscr{R}(t)\sin[2\psi(t)]. \tag{2.2}$$

Consequently, the shape deformation $\mathscr{R}$ and the orientation angle ψ are defined with respect to the coordinates (ξ,ζ) as follows

$$\mathscr{R}(t) = \sqrt{\xi^2+\zeta^2}, \quad \psi(t) = \frac{1}{2}tan^{-1}\left(\frac{\zeta}{\xi}\right), \tag{2.3}$$

where tan^{-1} is the inverse Tangent function.

We obtain the fractional vesicle model by applying the modified Riemann-Liouville fractional derivative to equation (2.3) and employing system (2.1). The resulting model is described as follows

$$\begin{aligned} {}^{\mathcal{J}}D_t^{\alpha}\xi &= \zeta\left(1-\frac{4h}{\Delta}\xi\right), \\ {}^{\mathcal{J}}D_t^{\alpha}\zeta &= h-\xi-\frac{4h}{\Delta}\zeta^2, \end{aligned} \tag{2.4}$$

where ${}^{\mathcal{J}}D_t^{\alpha}$, denotes the modified Riemann-Liouville fractional operator of order $0 < \alpha \leq 1$. The classical vesicle system have been analytically [37] and numerically [64] studied.

Clearly, from (9) and by considering $F_{2\pm1} = 0$ for simplicity the constraint area (6) is formulated as,

$$4\mathscr{R}^2 + 2F_{20}^2 = \Delta, \tag{2.5}$$

where Δ is the excess area relative to a sphere.

Moreover, we can determine the dynamics of F_{20} using the evolution equation (8), and applying the Jumarie fractional derivative we get

$${}^{\mathcal{J}}D_t^{\alpha}F_{20}(t) = \frac{-4h}{\Delta}\zeta F_{20}. \tag{2.6}$$

Using the system (2.4), when $\alpha = 1$, the authors in [37] were able to describe the different motions of vesicles in the shear plane. In addition, they examined the TB and VB modes, as well as the transition between them, which are affected by the initial conditions as functions of a control parameter that may be designated as a TB-VB parameter.

The main objective of this research is to first employ the modified Riemann-Liouville fractional derivative [44], which was described above, in order to illustrate the shape of the vesicle and explore its deformation in a thoughtful way. It is well known that fractional calculus shines when dealing with non-integer order differential equations, which permits a more precise representation of reality to be obtained.

2.2.2 Stability analysis

As in the theory of integer order differential systems, the study on stability of equilibrium states of fractional differential systems is a central work. In the literature, some stability theorems has been investigated and developed for a rang of non-integer order systems [77]. In this section we discuss the equilibrium's local asymptotic stability of system (2.4) with the help of a fractional process.

System (2.4) has three real equilibrium, $(\xi_1,\zeta_1) = (h,0)$ and $(\xi_2,\zeta_2) = \left(\frac{\Delta}{4h}, \pm\frac{\Delta}{4h}\sqrt{\omega-1}\right)$ if $\omega > 1$, with $\omega = \frac{4h^2}{\Delta}$.

Remark 2.2.1. *When $\omega = 1$, the equilibrium points coincide $(\xi, \zeta) = (h, 0)$.*

The Jacobian matrix associated to system (2.4) is given by

$$J(\xi,\zeta) = \begin{pmatrix} -\frac{4h}{\Delta}\zeta & 1-\frac{4h}{\Delta}\xi \\ -1 & -\frac{8h}{\Delta}\zeta \end{pmatrix}. \tag{2.7}$$

For $(\xi_1, \zeta_1) = (h, 0)$ we obtain,

$$J_1(\xi_1,\zeta_1) = \begin{pmatrix} 0 & 1-\omega \\ -1 & 0 \end{pmatrix}, \tag{2.8}$$

this implies,

$$P(\tilde{\lambda}) = \tilde{\lambda}^2 + 1 - \omega, \tag{2.9}$$

subsequently, we have

1. $\omega > 1$

$$P(\lambda) = 0 \text{ gives } \tilde{\lambda}_{\pm} = \pm\sqrt{\omega - 1}, \tag{2.10}$$

one can see $\left|\arg(\tilde{\lambda}_+)\right| = 0 < \frac{\alpha\pi}{2}$, for all $\alpha > 0$ and $\left|\arg(\tilde{\lambda}_-)\right| = \pi > \frac{\alpha\pi}{2}$ for $0 < \alpha < 1$.

2. $\omega < 1$

$$P(\tilde{\lambda}) = 0 \text{ gives } \tilde{\lambda}_{\pm} = \pm i\sqrt{1 - \omega}, \tag{2.11}$$

in this case we have $\left|\arg(\tilde{\lambda}_+)\right| = \frac{\pi}{2} > \frac{\alpha\pi}{2}$ and $\left|\arg(\tilde{\lambda}_-)\right| = \frac{3\pi}{2} > \frac{\alpha\pi}{2}$ for $0 < \alpha < 1$.

Using theorem 1.2.3 we deduce that the equilibrium state $(h, 0)$ is unstable for $\omega > 1$ and asymptotically stable for $\omega < 1$.
It is worth noting that; in the classical system, when $\omega < 1$ the eigenvalues are purely imaginary, no conclusion can be drawn about the stability of $(h, 0)$. However, the fractional approach removed the doubt about this case and we have deduced the asymptotic stability.
For $(\xi_2, \zeta_2) = \left(\frac{\Delta}{4h}, \pm\frac{\Delta}{4h}\sqrt{\omega - 1}\right)$ we have,

$$J_2(\xi_2,\zeta_2) = \begin{pmatrix} -\left(\pm\sqrt{\omega - 1}\right) & 0 \\ -1 & -\left(\pm 2\sqrt{\omega - 1}\right) \end{pmatrix}, \tag{2.12}$$

which result in
$\tilde{\lambda}_1 = \sqrt{\omega - 1}$ and $\tilde{\lambda}_2 = 2\sqrt{\omega - 1}$ with respect to $\left(\frac{\Delta}{4h}, -\frac{\Delta}{4h}\sqrt{\omega - 1}\right)$, then

$|\arg(\tilde{\lambda}_j)| = 0, j = \{1,2\}$.

$\tilde{\lambda}_1 = -\sqrt{\omega-1}$ and $\tilde{\lambda}_2 = -2\sqrt{\omega-1}$ with respect to $\left(\frac{\Delta}{4h}, \frac{\Delta}{4h}\sqrt{\omega-1}\right)$, then

$|\arg(\tilde{\lambda}_j)| = \pi, j = \{1,2\}$.

We conclude from theorem (1.2.3) that $\left(\frac{\Delta}{4h}, \frac{\Delta}{4h}\sqrt{\omega-1}\right)$ is asymptotically stable but $\left(\frac{\Delta}{4h}, -\frac{\Delta}{4h}\sqrt{\omega-1}\right)$ is unstable.

2.2.3 Exact solutions and vesicle dynamics

This part's objective is to find all physical solutions so that the constraint area (2.5) holds.
For that, we introduce the function φ, which verifies

$$\xi = \zeta\varphi + h. \tag{2.13}$$

Finding explicit formulas for φ allows one to solve system (2.4) and perform an analytical analysis of the previously described various regimes.
Using system (2.4), we get the following fractional Riccati equation

$$^{\mathcal{J}}D_t^{\alpha}\varphi = \varphi^2 + 1 - \omega, \tag{2.14}$$

with $^{\mathcal{J}}D_t^{\alpha}$, denotes the the modified Riemann-Liouville fractional operator of order $0 < \alpha \leq 1$, and $\omega = \frac{4h^2}{\Delta}$.
Five solutions to equation (2.14) were first proposed by Zang and al. in [92] witch depend on the sign of $1-\omega$, the following expressions on the solution are specially interesting to our investigation

$$\varphi(t) = -\Lambda\frac{E_{\alpha}(\Lambda t^{\alpha}) + K_1 E_{\alpha}(-\Lambda t^{\alpha})}{E_{\alpha}(\Lambda t^{\alpha}) - K_1 E_{\alpha}(-\Lambda t^{\alpha})}, \tag{2.15}$$

for $\omega > 1$ (i.e., $h > h_c$), and for $\omega < 1$ (i.e.,$h < h_c$) with $h_c = \frac{\sqrt{\Delta}}{2}$,

$$\varphi(t) = \Lambda tan_{\alpha}(\Lambda^{\frac{1}{\alpha}} + K_1'), \tag{2.16}$$

where K_1 and K_1' are constants that depend on initial conditions , and $\Lambda = \sqrt{|1-\omega|}$.
We now have explicit expressions for φ, which we can use to solve system (2.4), to compare and contrast the several regimes mentioned.
From (2.13) and system (2.4), we get the following fractional equation that can be solved exactly

$$^{\mathcal{J}}D_t^{\alpha}\zeta = -\varphi\zeta - \frac{4h}{\Delta}\zeta^2. \tag{2.17}$$

Next, by employing (2.17) and the properties of the Jumarie derivative, we will unveil the analytical solutions for ξ and ζ to investigate the exact expressions of $\mathbb{R}$ and ψ. We will further illustrate their behavior using the MATLAB software.

2.2.4 Tank-treading mode ($h > h_c$)

In [37], the authors have presented exact solutions to the classical model (2.1). Now, the goal of our research is to find exact analytical solutions for the fractional model (2.4), which is an extension of system (2.1).
In this case, the expression of ζ using (2.17), (2.15) and the properties mentioned in section 1, as well as calculating techniques for solving fractional equations, is found to be

$$\zeta(t) = \Lambda h \omega^{-1} \frac{E_\alpha(\Lambda t^\alpha) - K_1 E_\alpha(-\Lambda t^\alpha)}{K_2 + E_\alpha(\Lambda t^\alpha) + K_1 E_\alpha(-\Lambda t^\alpha)}, \tag{2.18}$$

this leads to the expression of ξ in the following form by combining (2.13) and (2.15)

$$\xi(t) = h\omega^{-1} + h\omega \frac{K_2}{K_2 + E_\alpha(\Lambda t^\alpha) + K_1 E_\alpha(-\Lambda t^\alpha)}. \tag{2.19}$$

From (2.6) and (2.18) we can determine the expression of F_{20}

$$F_{20}(t) = \frac{K_3}{K_2 + E_\alpha(\Lambda t^\alpha) + K_1 E_\alpha(-\Lambda t^\alpha)}, \tag{2.20}$$

where the constants K_2 and K_3 depend on initial conditions.

Consequently, the inclination angle and the shape deformation in this case employing (2.3) are defined by

$$\psi(t) = \frac{1}{2} \arctan\left(\Lambda \frac{E_\alpha(\Lambda t^\alpha) - K_1 E_\alpha(-\Lambda t^\alpha)}{\omega K_2 + E_\alpha(\Lambda t^\alpha) + K_1 E_\alpha(-\Lambda t^\alpha)} \right), \tag{2.21}$$

and

$$\mathscr{R}^2(t) = \omega^{-2} h^2 \frac{\Lambda^2 (E_\alpha(\Lambda t^\alpha) - K_1 E_\alpha(-\Lambda t^\alpha))^2 + (\omega K_2 + E_\alpha(\Lambda t^\alpha) + K_1 E_\alpha(-\Lambda t^\alpha))^2}{(K_2 + E_\alpha(\Lambda t^\alpha) + K_1 E_\alpha(-\Lambda t^\alpha))^2}. \tag{2.22}$$

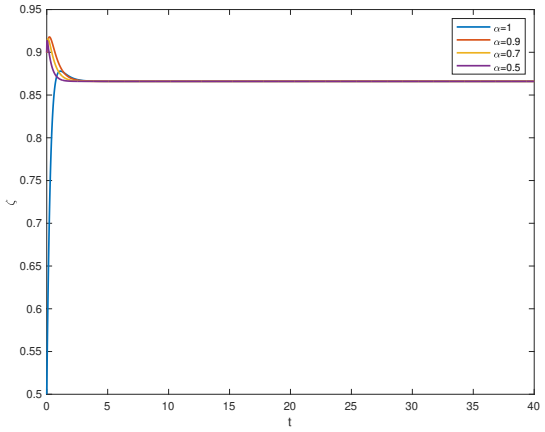
Figure 2.1 depicts the dynamics of ξ, ζ and F_{20} that tend toward a stable point. We also notice that as t approaches infinity, $\mathscr{R}$ tends to $\frac{\sqrt{\Delta}}{2}$ and the orientation angle, ψ, tends monotonically to

$$\psi(\infty) = \frac{1}{2} tan^{-1}(\Lambda), \tag{2.23}$$

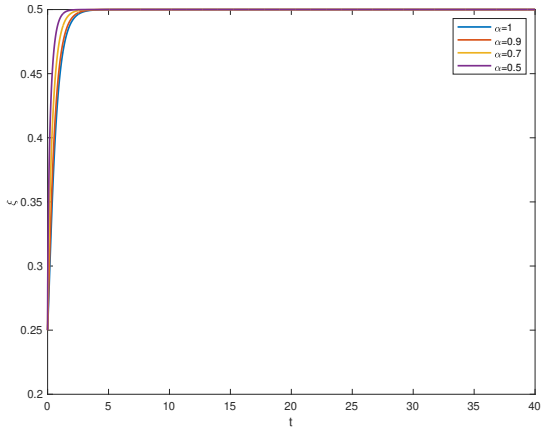
which means that the orientation angle is always less than $\pi/4$. Figure 2.2 shows an instance of shape deviation and orientation angle for various values of α to support the theoretical results. Furthermore, the solutions reveal that the ψ orientation angle of the vesicle remains constant for different values of α. This means that the vesicle in this case predicts a pure TT mode.

2.2.5 The damped oscillatory modes ($h < h_c$)

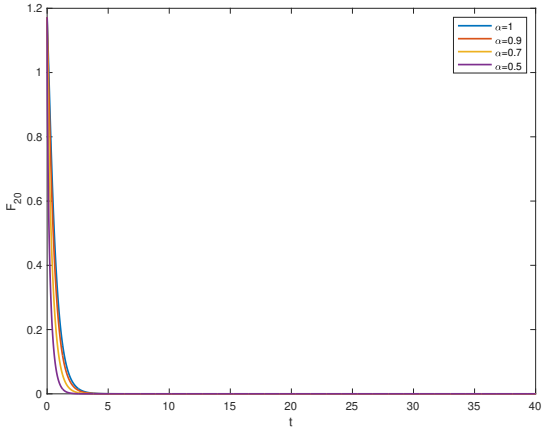
Now, we will concentrate on time-dependent solutions (which exist when $\omega < 1$). Misbah [64] provided numerical solutions to system (2.1), indicating that the VB mode coexists with the TB



((a)) The time evolution of ζ for Jumarie operator.



((b)) The time evolution of ξ for Jumarie operator.



((c)) The time evolution of F_{20} for Jumarie operator.

Figure 2.1: The representation of the solutions of the fractional model obtained for the components ζ, ξ and F_{20} for four arbitrary values of fractional order. Parameters are : $\Delta = 4$ and $h = 2$.

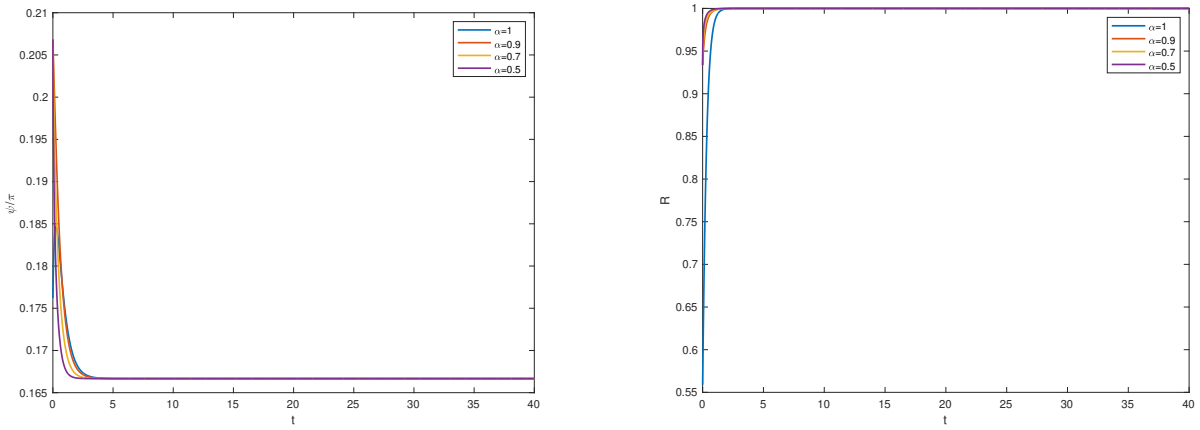
mode, and the mode selection is dependent on initial conditions, as described previously. The authors of [37] used this information to identify the specific initial conditions and parameters that correspond to the TB or VB regime.

As before, we only need to solve the fractional differential equation below

$$ {}^{\mathcal{J}}D_t^{\alpha}\zeta = -\varphi\zeta - \frac{4h}{\Delta}\zeta^2. \tag{2.24} $$

Using the exact expression (2.16) of φ and several features of the Mittag-Leffler function as well as the Jumarie fractional derivative's properties, we have found that coordinates ζ, ξ, and F_{20} are determined by

$$ \zeta(t) = \Lambda h \omega^{-1} \frac{\cos_{\alpha}(\Lambda^{\frac{1}{\alpha}} t + K_1')}{K_2' + \sin_{\alpha}(\Lambda^{\frac{1}{\alpha}} t + K_1')}, \tag{2.25} $$



((a)) Dynamics of the orientation angle. ((b)) The amplitude $\mathscr{R}$.

Figure 2.2: The behaviour of the orientation angle ψ and the amplitude $\mathscr{R}$ for four arbitrary values of fractional order. Parameters are : $\Delta = 4$ and $h = 2$.

$$\xi(t) = h\omega^{-1}\frac{\Gamma + \sin_\alpha(\Lambda^{\frac{1}{\alpha}}t + K_1')}{K_2' + \sin_\alpha(\Lambda^{\frac{1}{\alpha}}t + K_1')}, \tag{2.26}$$

and, from (2.6) and (2.25) we get

$$F_{20}(t) = \frac{K_3'}{K_2' + \sin_\alpha(\Lambda^{\frac{1}{\alpha}}t + K_1')}. \tag{2.27}$$

The expression of the constant K_2' is given by

$$K_2' = \pm\frac{h\omega^{-1} - \xi(0)}{\sqrt{\zeta^2(0)\Lambda^2 + [\xi(0) - h]^2}}, \tag{2.28}$$

it results from (6) that $|K_2'| \geq \sqrt{\omega^{-1}}$, and subsequently $|K_2'| > 1$ since $\omega < 1$. Therefore the above solutions exist for all times.

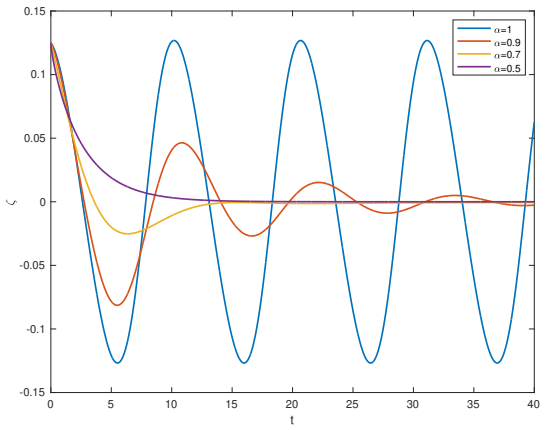
Figure 2.3 illustrates a cosine form that varies depending on the order of the fractional derivative α, which is shown by Equations (2.25) and (2.26). The amplitude is seen to decrease as α decreases. Let us examine this more thoroughly to explain how the order of fractional derivative affects the dynamics of a deformable particle.

Using equation (2.3), we get that the shape deformation is represented by

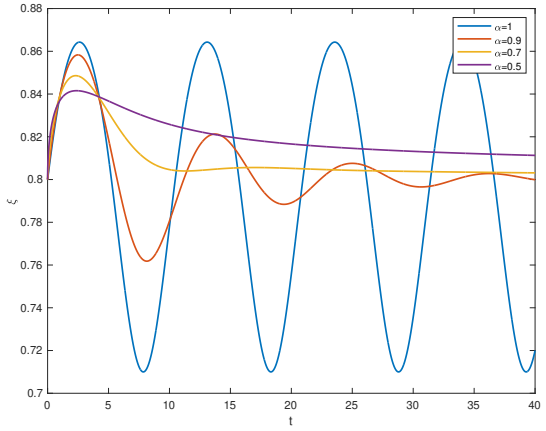
$$\mathscr{R}^2(t) = h^2\omega^{-2}\frac{\left\{\Lambda^2\cos_\alpha^2\left(\Lambda^{\frac{1}{\alpha}}t + K_1'\right) + \left[\Gamma + \sin_\alpha\left(\Lambda^{\frac{1}{\alpha}}t + K_1'\right)\right]^2\right\}}{\left[K_2' + \sin_\alpha\left(\Lambda^{\frac{1}{\alpha}}t + K_1'\right)\right]^2}, \tag{2.29}$$

and the angle of inclination by

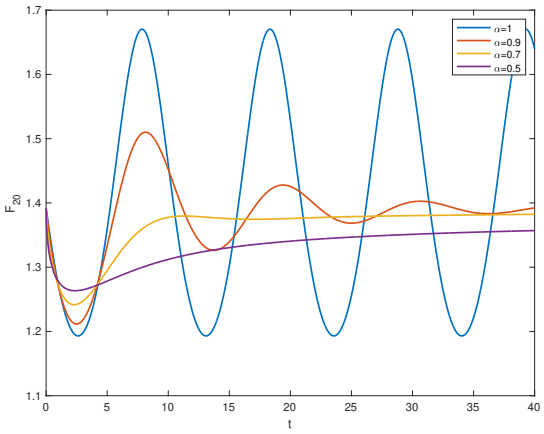
$$\psi(t) = \frac{1}{2}\arctan\left(\Lambda\frac{\cos_\alpha\left(\Lambda^{\frac{1}{\alpha}}t + K_1'\right)}{\Gamma + \sin_\alpha\left(\Lambda^{\frac{1}{\alpha}}t + K_1'\right)}\right), \tag{2.30}$$



((a)) The time evolution of ζ for Jumarie operator.



((b)) The time evolution of ξ for Jumarie operator.



((c)) The time evolution of F_{20} for Jumarie operator.

Figure 2.3: The representation of the solutions of the fractional model obtained for the classical components ζ, ξ and F_{20} for four arbitrary values of fractional order. Parameters are : $\Delta = 4$ and $h = 0.8$.

where, $\Gamma = \omega K_2'$.

The expression of ψ shows that the vesicle can describe a Vacillating-Breathing motion and no Tumbling motion can pointed out. Indeed, we have

$$\frac{-\pi}{4} \leq \psi(t) \leq \frac{\pi}{4}, \quad \forall\ t, \tag{2.31}$$

therefore, the expression of ψ can be sophisticated once see that $\psi \pm \frac{\pi}{2}$ is also a solution.

Thus, for a valid mathematical and physical argument, we can express ψ as follows

$$\psi(t)=\begin{cases}\frac{1}{2}\arctan\left(\Lambda\frac{\cos_\alpha\left(\Lambda^{\frac{1}{\alpha}}t+K_1'\right)}{\Gamma+\sin_\alpha\left(\Lambda^{\frac{1}{\alpha}}t+K_1'\right)}\right), & \text{if} \quad \xi>0,\\ -\frac{\pi}{2}+\frac{1}{2}\arctan\left(\Lambda\frac{\cos_\alpha\left(\Lambda^{\frac{1}{\alpha}}t+K_1'\right)}{\Gamma+\sin_\alpha\left(\Lambda^{\frac{1}{\alpha}}t+K_1'\right)}\right), & \text{if} \quad \xi<0,\zeta<0,\\ +\frac{\pi}{2}+\frac{1}{2}\arctan\left(\Lambda\frac{\cos_\alpha\left(\Lambda^{\frac{1}{\alpha}}t+K_1'\right)}{\Gamma+\sin_\alpha\left(\Lambda^{\frac{1}{\alpha}}t+K_1'\right)}\right), & \text{if} \quad \xi<0,\zeta>0.\end{cases} \tag{2.32}$$

As of system (2.32), we can have more than one trajectory. In [37] the authors has shown that the evolution of ψ is affected by the value of Γ.

We get oscillatory solutions for the classical case (i.e, $\alpha = 1$). In this case, it is known that the system (2.4) provides a description of the two regimes, TB and VB. Furthermore, the TB and VB regimes do not distinguish from the equations (2.25) and (2.26). The parameter Γ has a significant impact on both the inclination angle and the shape deviation, which allows us to differentiate between the two regimes. It was explored as a control parameter for the VB and TB regimes in [37], where it was discovered that if $\Gamma < 1$, the inclination angle ψ would oscillate between $\pm\frac{\pi}{2}$, which is indicative of a TB mode. If $\Gamma > 1$, the inclination angle predicts a periodic VB regime, and the transition between TB and VB modes occurs when $\Gamma = 1$.

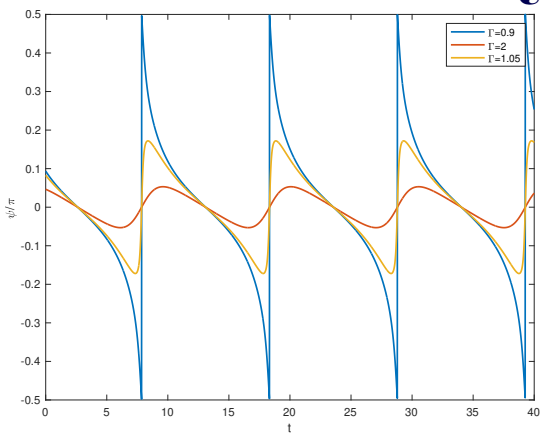
Therefore, we have framed the following question: while utilizing a variety of values for α, does the control parameter TB-VB still impact the behavior of the vesicle? In order to provide an answer to this question, we have plotted in figures 2.4 and 2.5 the time evolution of the angle between the main axis and the direction of the shear plane, as well as, the shape deviation for each value of α and different values of Γ.

To investigate the effect of Γ on mode selection, we fixed ω and plotted in Figure 2.4 an example of the time evolution of the inclination angle ψ for the same parameters h and Δ with three different values of Γ for each α. Herein we have considered four arbitrary values of fractional order.

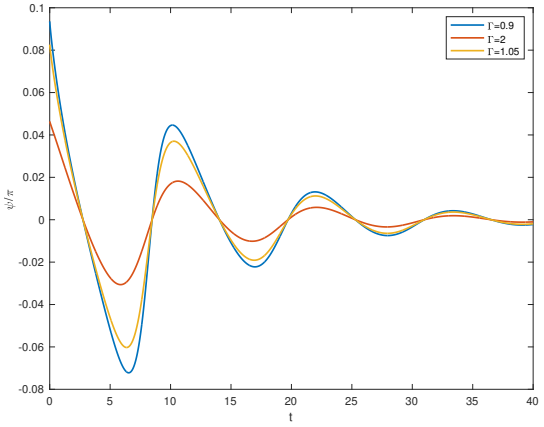
Figure 2.4(a) depicts that for the classical derivative (that is, $\alpha = 1$), we have a TB mode in which the orientation angle jumps discontinuously from $-\pi/2$ to $\pi/2$ for $\Gamma < 1$. However, for $\Gamma > 1$, the evolution is continuous and this represents a VB mode. Consequently, the parameter Γ, which depends on the initial shape, may be defined here as the TB or VB parameter, as was previously highlighted in [37]. Consequently, when $\alpha = 1$, the fractional and classical results are identical.

We now turn to the crux of this chapter, when $0 < \alpha < 1$. The graphical representation above shows that we have oscillations with decreasing amplitudes regardless of the value of Γ, which means that as α decreases, the initial conditions (the Γ parameter) has entirely lost its influence on types of movements selected.

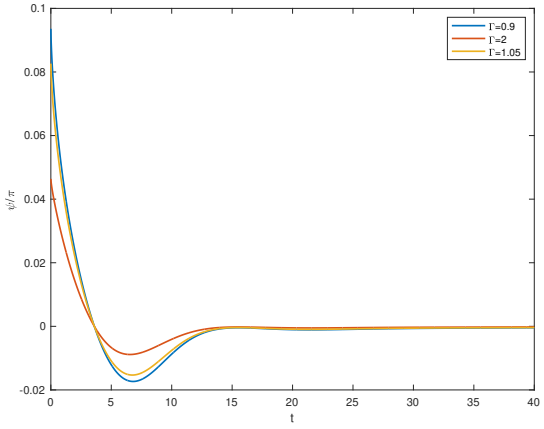
In fact, it is obvious from the definition of the modified Riemann-Liouville derivative given in section 1 that the values of the fractional derivative in t are affected by the historical values of ψ (at each time before t). As a result, the fractional derivative takes into account not only the initial shape but also the entirety of the instant τ between 0 and t, during which it is expected



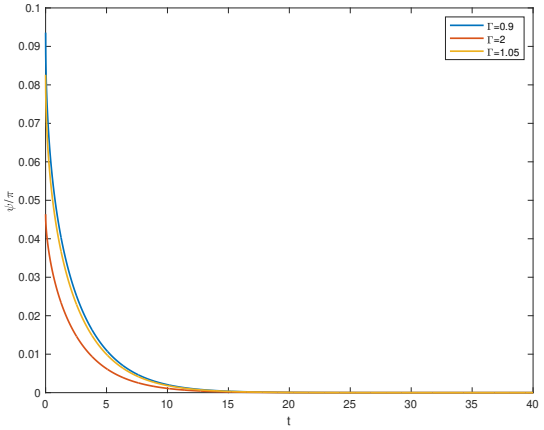
((a)) Dynamics of the orientation angle ψ when $\alpha = 1$.



((b)) Dynamics of the orientation angle ψ when $\alpha = 0.9$.



((c)) Dynamics of the orientation angle ψ when $\alpha = 0.7$.



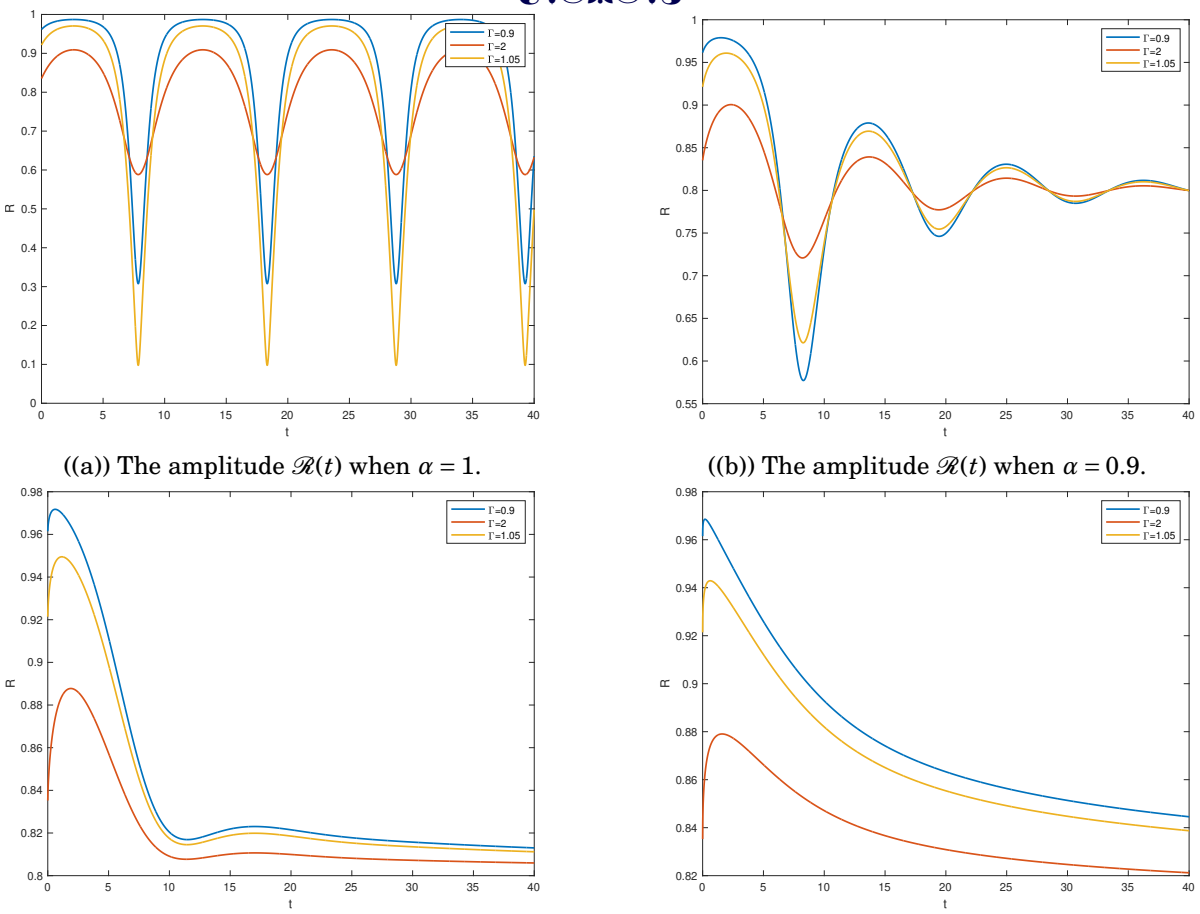
((d)) Dynamics of the orientation angle ψ when $\alpha = 0.5$.

Figure 2.4: The behaviour of the orientation angle ψ for four arbitrary values of fractional order. Parameters are : $\Delta = 4$ and $h = 0.8$ with $\Gamma = 0.9$, $\Gamma = 2$ and $\Gamma = 1.05$.

that some degree of memory would be preserved. In Figure 2.5, we show how the amplitude $\mathscr{R}$ behaves for three different values of Γ for each of the four different values of α. We observe that in figure 2.5(a), when $\alpha = 1$, the regime is accompanied by an oscillation of $\mathscr{R}$.
Furthermore, the figure 2.5 reveals that $\mathscr{R}$ remains constant over time and tends to h when $0 < \alpha < 1$, implying that $\mathscr{R}$ never reaches its maximum value $\sqrt{\Delta}/2$, involves that $F_{20}(t) \neq 0$ at all times due to the area conservation constraint. In fact,

$$F_{20}(t) = \pm\sqrt{\frac{\Delta}{2} - 2\mathscr{R}^2(t)}\,. \tag{2.33}$$

It is evident that $F_{20}(t) = 0$ only if $F_{20}(0) = 0$, which indicates the suppression of deformation in the vorticity's direction, according to equation (2.27). In this case, (2.33) implies that $\mathscr{R}$ is equal to its maximum value $\sqrt{\Delta}/2$, which reflects the shape preservation behavior, that Keller and Skalak (KS) used in their theory, in which the vesicle is assumed to have a fixed shape (rigid



((a)) The amplitude $\mathscr{R}(t)$ when $\alpha = 1$.

((b)) The amplitude $\mathscr{R}(t)$ when $\alpha = 0.9$.

((c)) The amplitude $\mathscr{R}(t)$ when $\alpha = 0.7$.

((d)) The amplitude $\mathscr{R}(t)$ when $\alpha = 0.5$.

Figure 2.5: The dynamic of the amplitude $\mathscr{R}$ for four arbitrary values of fractional order. Parameters are : $\Delta = 4$ and $h = 0.8$ with $\Gamma = 0.9$, $\Gamma = 2$ and $\Gamma = 1.05$.

particles) and in this case the TT and TB regimes and their transition are described in [48]. However, in this case, it is clear that when $0 < \alpha < 1$, the influence of Γ is removed due to the stability of the equilibrium point, which was not the case in the classical derivative system (2.4), where nothing can be deduced, and these results can be considered one of the most essential results of this investigation. Therefore, for a given value of Δ, the regimes will depend on the parameter h, moreover our TB regime solution corresponds with the KS one only when $h = \sqrt{\Delta}/2$ (i.e, if $\omega = 1$, shape-preservation regime). This indicates that when $\omega < 1$, the deformation along the vorticity direction will always occur.

As a result of using the fractional Jumarie derivative, the vesicle exhibits small oscillations rather than the pure TT, TB, or VB motion. Figure 2.4(d) and figure 2.4(c) indicate that as α increases, we tend more slowly toward equilibrium, in other meaning the orientation angle ψ aligns along the flow, by executing non-asymmetric oscillations, which decreases over time and tends towards the attractive angle $(\psi = 0)$, this motion can be represented by TT with over-damped (OD-TT) vesicle oscillations. Moreover, figure 2.4(b) and figure 2.4(a) demonstrate that when α approaches

1, there are oscillations about the equilibrium state with increasing amplitudes, giving birth to the VB and TB modes. These can be identified as under-damped TT oscillations (UD-TT). This means that the TT regime is on the verge of losing stability to the VB and TB modes with respect to the parameter Γ.

2.3 Dynamic Insights on the Caputo Derivative's Impact in Unraveling Vesicle Behavior

Now, we turn our attention to the Caputo fractional derivative. This section will focus on how the Caputo derivative enhances our modeling of vesicle behavior in shear flow by incorporating a different perspective on memory effects. We will discuss the formulation of the vesicle model using the Caputo derivative, and how this approach offers a refined understanding of vesicle dynamics, including deformation and orientation under various conditions.

2.3.1 Formulation of the Vesicle Model and the Caputo Fractional Vesicle Model

We incorporate the memory effect into the system of $\mathscr{R}$ and ψ by substituting the classical derivative in (10) with the Caputo operator, as discussed in Section 1, to derive a generalized model. The resulting system of Caputo-fractional differential equations is then defined as follows

$$\begin{aligned} {}^{C}D_t^{\alpha}\mathscr{R} &= h\left[1-4\frac{\mathscr{R}^2}{\Delta}\right]\sin(2\psi),\\ {}^{C}D_t^{\alpha}\psi &= -\frac{1}{2}+\frac{h}{2\mathscr{R}}\cos(2\psi), \end{aligned} \tag{2.34}$$

where ${}^{C}D_t^{\alpha}$ represents the Caputo fractional derivative of order α. In the classical case (i.e., when $\alpha = 1$), it is demonstrated in [64] that this system qualitatively describes the three classical regimes: tank-treading (TT), tumbling (TB), and vacillating-breathing (VB).

To derive the fractional vesicle model, we substitute the classical derivative with the Caputo operator in the system governing ξ, ζ, and F_{20}, analogous to the use of the Jumarie derivative in 2.2.1. The resulting model is described as follows

$$\begin{aligned} {}^{C}D_t^{\alpha}\xi &= \zeta\left(1-\frac{4h}{\Delta}\xi\right),\\ {}^{C}D_t^{\alpha}\zeta &= h-\xi-\frac{4h}{\Delta}\zeta^2,\\ {}^{C}D_t^{\alpha}F_{20} &= -\frac{4h}{\Delta}\zeta F_{20}, \end{aligned} \tag{2.35}$$

where ${}^{C}D_t^{\alpha}$ represents the Caputo fractional operator of order $0 < \alpha \leq 1$. The classical vesicle system has been studied both analytically [37] and numerically [64].

2.3.2 Analysis of Existence and Uniqueness of Solutions in Caputo-Fractional Equations

In this section, we study the existence of solutions for the system by applying Theorems 1.2.1 and 1.2.2. We define the right-hand side functions of the fractional system (2.35) as:

$$g_1(t,\xi(t)) = \zeta - \frac{4h}{\Delta}\zeta\xi,$$
$$g_2(t,\zeta(t)) = h - \xi - \frac{4h}{\Delta}\zeta^2,$$
$$g_3(t,F_{20}(t)) = -\frac{4h}{\Delta}\zeta F_{20}.$$

Theorem 2.3.1. *The initial value problem for the Caputo-fractional system* (2.35) *can be formulated as:*

$$^{C}D_t^{\alpha}x(t) = V + \mathscr{M}_1 x(t) + \zeta(t)\mathscr{M}_2 x(t), \quad x(0) = x_0,$$

where $0 < t \le T$, $x = (\xi,\zeta,F_{20})^T \in \mathbb{R}^3$, $x_0 = \left(\xi_0,\zeta_0,F_{20_0}\right)^T$, $\mathscr{M}_1 = \begin{pmatrix} 0 & 1 & 0 \\ -1 & 0 & 0 \\ 0 & 0 & 0 \end{pmatrix}$, $V = (0,\frac{4h}{\Delta},0)^T$, *and* $\mathscr{M}_2 = -\frac{4h}{\Delta} \times I_3$, *for some constant* $T > 0$. *The system has a unique solution.*

Proof. Consider $G(t,x(t)) = \begin{pmatrix} g_1(t,\xi(t)) \\ g_2(t,\zeta(t)) \\ g_3(t,F_{20}(t)) \end{pmatrix}$, which is continuous and bounded over the interval $[x_0-\epsilon, x_0+\epsilon]$ for any $\epsilon > 0$. Moreover, we have:

$$\begin{aligned}\left|G(t,x(t)) - G\left(t,x'(t)\right)\right| &= \left|\mathscr{M}_1\left(x(t)-x'(t)\right) + \zeta(t)\mathscr{M}_2 x(t) - \zeta'(t)\mathscr{M}_2 x x'(t)\right| \\ &\le \left|\left(\mathscr{M}_1 + \zeta'(t)\mathscr{M}_2\right)\left(x(t)-x'(t)\right) + \mathscr{M}_2 x(t)\left(\zeta(t)-\zeta'(t)\right)\right|.\end{aligned}$$

Since $\left|\zeta(t)-\zeta'(t)\right| \le \left|x(t)-x'(t)\right|$, we obtain:

$$\left|G(t,x(t)) - G\left(t,x'(t)\right)\right| \le \left(\|\mathscr{M}_1\| + \|\mathscr{M}_2\|\left(|x(t)| + \left|x_2'(t)\right|\right)\right)\left|x(t)-x'(t)\right|,$$

which simplifies to:

$$\left|G(t,x(t)) - G\left(t,x'(t)\right)\right| \le \left(\|\mathscr{M}_1\| + \|\mathscr{M}_2\|\left(2|x_0| + \epsilon\right)\right)\left|x(t)-x'(t)\right|,$$

and finally:

$$\left|G(t,x(t)) - G\left(t,x'(t)\right)\right| \le \mathscr{M}\left|x(t)-x'(t)\right|,$$

where $\mathscr{M} = \|\mathscr{M}_1\| + \|\mathscr{M}_2\|(2|x_0|+\epsilon) > 0$, and $\|.\|$ and $|.|$ denote the matrix and vector norms, respectively.

Therefore, the Lipschitz condition is satisfied, and by Theorems 1.2.1 and 1.2.2, the Caputo-fractional system (2.35) has a unique solution. ■

2.3.3 Equilibrium and Local Stability Analysis of the Fractional Model

In fractional differential systems, analyzing the stability of equilibrium points is a fundamental aspect, similar to the analysis performed in integer-order differential systems. The literature has established various stability theorems for non-integer order systems [23]. Considering that F_{20} does not appear in the first and second equations, we can simplify system (2.36) as follows:

$$\begin{aligned} {}^{C}D_t^{\alpha}\xi &= \zeta - \frac{4h}{\Delta}\zeta\xi, \\ {}^{C}D_t^{\alpha}\zeta &= \frac{4h}{\Delta} - \xi - \frac{4h}{\Delta}\zeta^2. \end{aligned} \tag{2.36}$$

To study the stability of this fractional system, we examine the equilibrium points and the corresponding eigenvalues of the Jacobian matrix, as detailed in 2.2.1. For $h < \sqrt{\Delta}/2$, the equilibrium point $(h,0)$ is stable. In contrast, when $h > \sqrt{\Delta}/2$, this point becomes unstable. It is important to highlight that in the classical case, when $h < \sqrt{\Delta}/2$, the eigenvalues are purely imaginary, making it impossible to draw any definitive conclusions about the stability of the point $(h,0)$. However, by employing the fractional approach, this ambiguity is resolved, and we are able to deduce the stability.

Moreover, for $h > \sqrt{\Delta}/2$, the equilibrium points are $\left(\frac{\Delta}{4h}, \pm\frac{\Delta}{4h}\sqrt{\frac{4h^2}{\Delta}-1}\right)$, where $\left(\frac{\Delta}{4h}, \frac{\Delta}{4h}\sqrt{\frac{4h^2}{\Delta}-1}\right)$, is asymptotically stable and $\left(\frac{\Delta}{4h}, -\frac{\Delta}{4h}\sqrt{\frac{4h^2}{\Delta}-1}\right)$, is completely unstable. The local stability of the fractional system solutions, as analyzed using Theorem 1.2.3, indicates that stability can be conclusively determined in this context, unlike classical derivatives where such determinations are not feasible.

2.3.4 Numerical Computation Method

In this part, we apply an algorithm based on the Adams-Bashforth-Moulton predictor-corrector scheme, commonly referred to as the fractional Adams method [29], to compute the numerical solution of the fractional differential equation. We use the same notation as in Section 2.3.2. Consider the Caputo fractional differential equation:

$$\begin{cases} {}^{C}D_0^{\alpha}x(t) = G(t,x(t)), \quad 0 < \alpha \leq 1, \\ x(0) = x_0, \end{cases} \tag{2.37}$$

where $x_0 = \left(\xi_0, \zeta_0, F_{20_0}\right)$ represents the initial condition vector. Using the Riemann-Liouville integral, we obtain

$$x(t) = x(0) + I_0^{\alpha}(G(t,x(t))), \tag{2.38}$$

which simplifies to

$$x(t) = x(0) + \frac{1}{\Gamma(\alpha)}\int_0^t (t-\tau)^{\alpha-1} g(\tau)\, d\tau. \tag{2.39}$$

We discretize the interval $[0,T]$ uniformly into $N+1$ points, denoted by $t_0 = 0 < t_1 < \ldots < t_k < \ldots < t_N = T$, with $\Delta t = \frac{T}{N}$ as the step size.

To approximate the fractional integral, we use the fractional Adams method [29]. At the point $t_{n+1} = (n+1)\Delta t$ with $\Delta t = t_{n+1} - t_n$, the Caputo-fractional model is approximated by

$$\begin{aligned} x(t_{n+1}) = x(0) &+ \frac{(\Delta t)^\alpha}{\Gamma(\alpha+2)} G\left(t_{n+1}, x^P(t_{n+1})\right) \\ &+ \frac{(\Delta t)^\alpha}{\Gamma(\alpha+2)} \sum_{k=0}^{n} a_{k,n+1} G(t_k, x(t_k)), \end{aligned} \tag{2.40}$$

where

$$a_{k,n+1} = \begin{cases} n^{\alpha+1} - (n-\alpha)(n+1)^\alpha, & \text{if } k = 0, \\ (n-k+2)^{\alpha+1} + (n-k)^{\alpha+1} - 2(n-k+1)^{\alpha+1}, & \text{if } 1 \le k \le n, \\ 1, & \text{if } k = n+1. \end{cases} \tag{2.41}$$

The predictor approximation $x^P(t_{n+1})$ is defined by:

$$x^P(t_{n+1}) = x(0) + \frac{1}{\Gamma(\alpha)} \sum_{k=0}^{n} b_{k,n+1} G(t_k, x(t_k)), \tag{2.42}$$

where

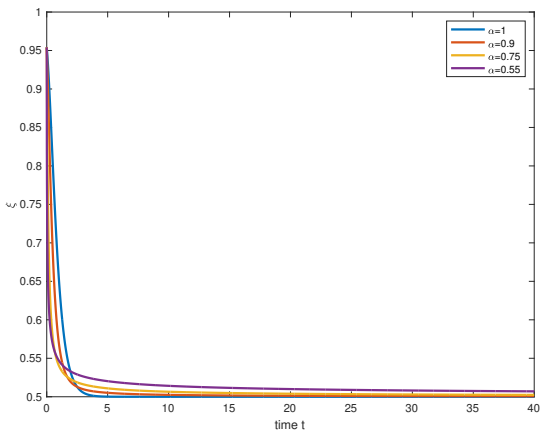
$$b_{k,n+1} = \frac{(\Delta t)^\alpha}{\alpha} \left((n+1-k)^\alpha - (n-k)^\alpha\right). \tag{2.43}$$

2.3.5 Tank-treading mode ($h > h_c$)

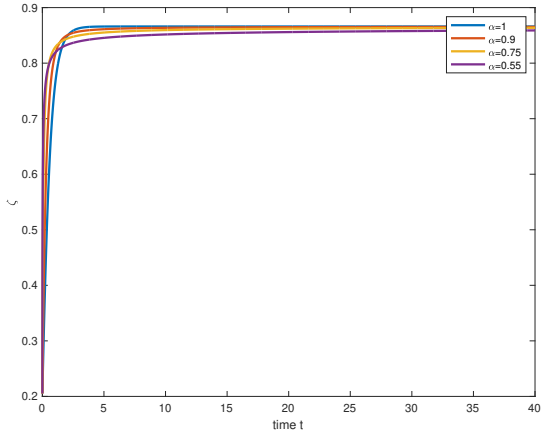
Figure 2.6 illustrates the behavior of ξ, ζ, and F_{20} as they converge towards a stable point. Additionally, it is observed that as t approaches infinity, $\mathscr{R}$ tends towards $\sqrt{\Delta}/2$, and the orientation angle ψ steadily approaches a constant value, remaining consistently below $\pi/4$. Figure 2.7 presents examples of shape deviations and orientation angles for various values of α, providing empirical support for the theoretical predictions. The solutions further indicate that the orientation angle ψ of the vesicle stabilizes across different α values, suggesting that the vesicle predominantly exhibits a pure tank-treading (TT) mode.

2.3.6 Damping tank-treading mode ($h < h_c$)

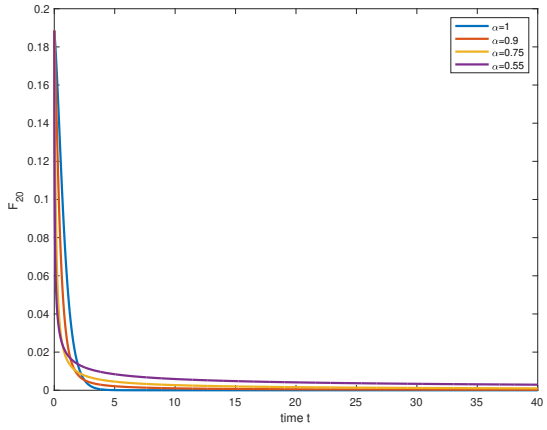
We now turn our attention to time-dependent solutions, which are central to our research, especially in the scenario where $h < \sqrt{\Delta}/2$. In previous work [11], we provided analytical solutions to system (2.36), revealing the emergence of a novel motion termed the damped tank-treading mode using the Jumarie derivative. In this study, we propose utilizing the Caputo derivative to explore whether it yields similar results and to assess its effectiveness in capturing the dynamics of mode selection influenced by initial conditions, as previously discussed.



((a)) The time evolution of ξ for the Caputo operator.



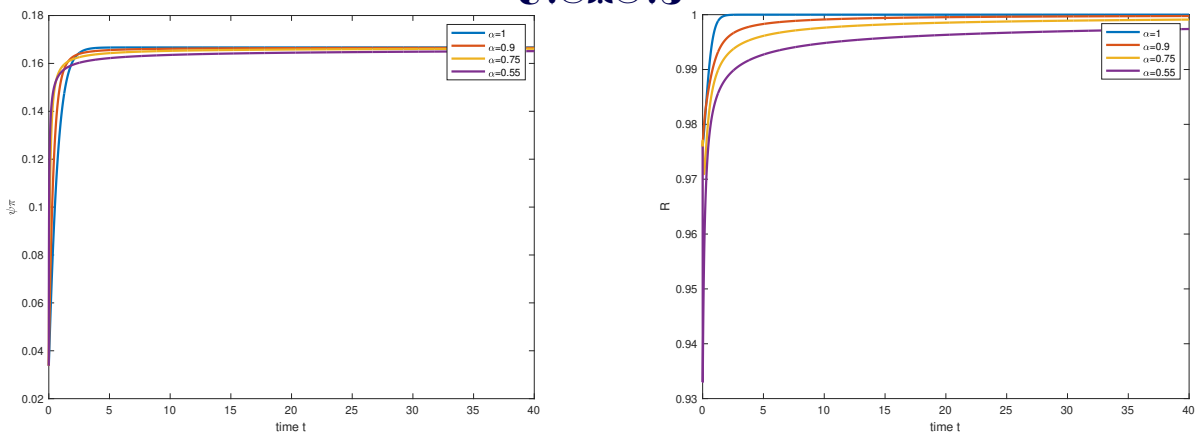
((b)) The time evolution of ζ for the Caputo operator.



((c)) The time evolution of F_{20} for the Caputo operator.

Figure 2.6: The representation of the solutions of the fractional model obtained for the classical components ζ, ξ and F_{20} for four arbitrary values of fractional order. Parameters are : $\Delta = 4$ and $h = 2$.

This approach is particularly valuable because the Caputo derivative offers a different perspective on the system's memory effects and can potentially provide deeper insights into the behavior of deformable particles. The comparison between the two derivatives could reveal the extent to which the Caputo derivative enhances our understanding of the transition dynamics and stability of these modes. Figure 2.8 illustrates a cosine function that varies with the order of the fractional derivative α. Notably, the amplitude decreases as α decreases. We will delve into this further to clarify how the order of the fractional derivative impacts the dynamics of a deformable particle, highlighting the unique contributions of the Caputo derivative to this analysis.
To examine the impact of α on mode selection, we fixed h and Δ, then we plotted the time evolution of the inclination angle ψ for three different values of Γ in Figure 2.9, considering four arbitrary values of fractional order α.



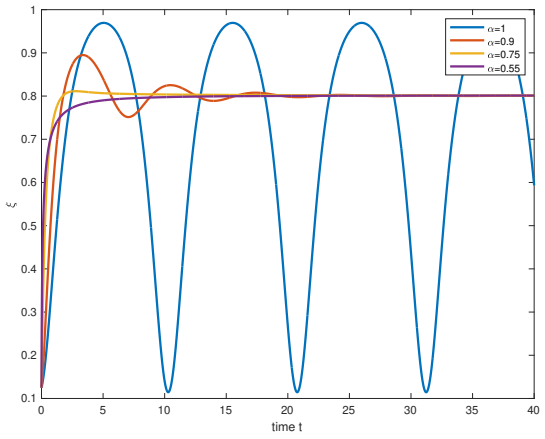
((a)) Dynamics of the orientation angle.

((b)) The amplitude $\mathscr{R}$.

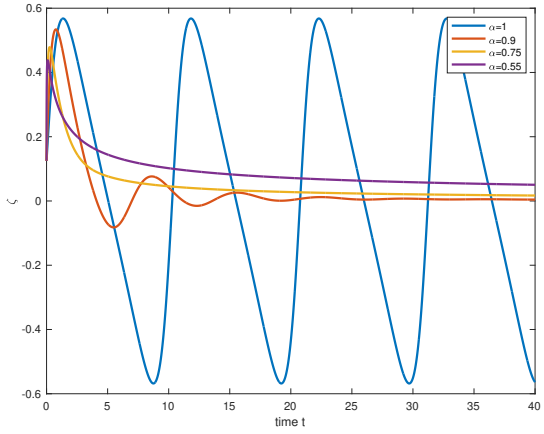
Figure 2.7: The behaviour of the orientation angle ψ and the amplitude $\mathscr{R}$ for four arbitrary values of fractional order. Parameters are : $\Delta = 4$ and $h = 2$.

Figure 2.9(a) illustrates that with the classical derivative (i.e., $\alpha = 1$), the system exhibits a tumbling (TB) mode, where the orientation angle undergoes a discontinuous jump from $-\pi/2$ to $\pi/2$ for $\Gamma < 1$. For $\Gamma > 1$, the evolution becomes continuous, representing a vacillating-bending (VB) mode. Thus, the parameter Γ, which depends on the initial shape, can be defined here as the TB or VB parameter, as previously discussed in [37]. Consequently, when $\alpha = 1$, the results for the fractional and classical derivatives are identical. Turning to the core of this study, when $0 < \alpha < 1$, the graphical representation reveals oscillations with decreasing amplitudes regardless of the value of Γ. This indicates that as α decreases, the influence of initial conditions (represented by Λ) on the selected modes decreases.

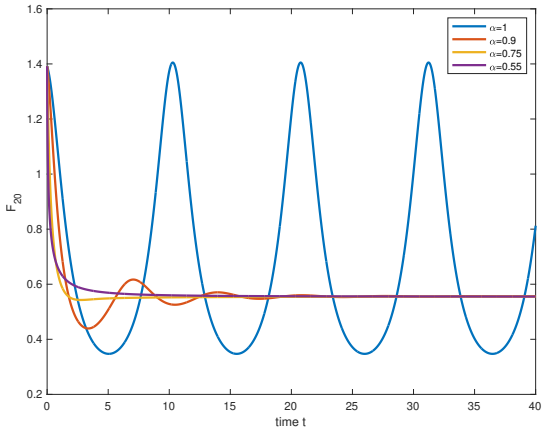
This observation aligns with the definition of the modified Riemann–Liouville derivative discussed in Section 1 which indicates that the fractional derivative in time is influenced by historical values of ψ (at each moment before t). As a result, the fractional derivative accounts not only for the initial shape but also for the entire interval during which some degree of memory is preserved. Figure 2.10 shows the behavior of the amplitude $\mathscr{R}$ for three different values of Γ across the four fractional orders α. In Figure 2.10(a), when $\alpha = 1$, the regime is characterized by oscillations in $\mathscr{R}$. Conversely, Figure 2.10(c) reveals that when $0 < \alpha < 1$, $\mathscr{R}$ remains constant over time and approaches h, suggesting that $\mathscr{R}$ does not reach its maximum value of $\sqrt{\Lambda}/2$. This behavior indicates that $F_{20}(t) \neq 0$ at all times due to the conservation of area constraint (6).



((a)) The time evolution of ξ for the Caputo operator.

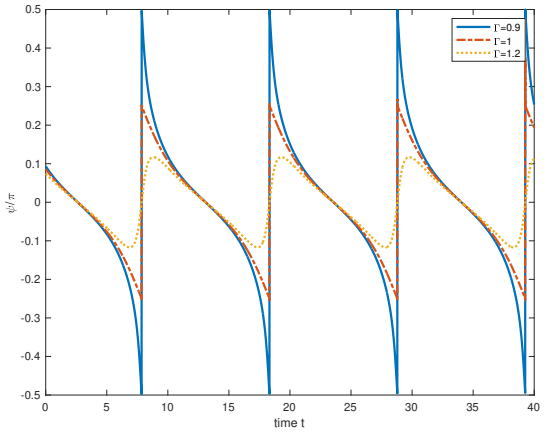


((b)) The time evolution of ζ for the Caputpo operator.

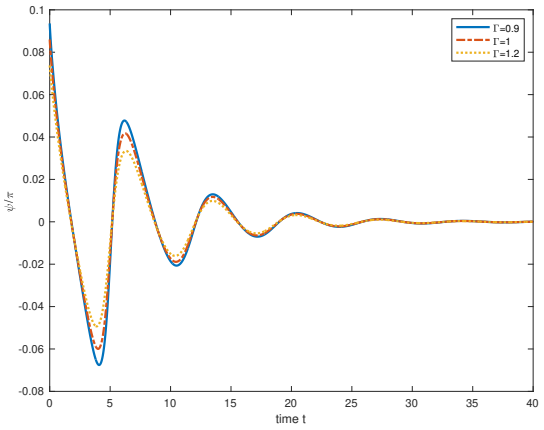


((c)) The time evolution of F_{20} for the Caputo operator.

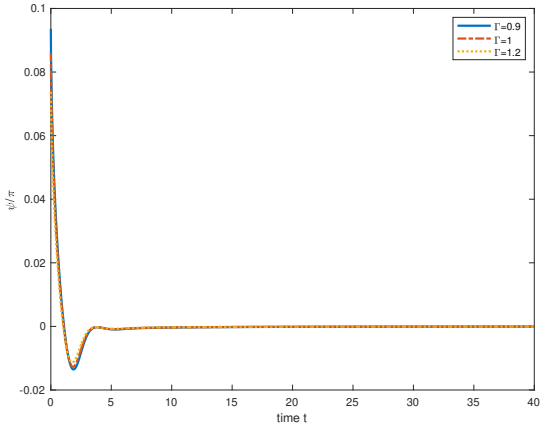
Figure 2.8: The representation of the solutions of the fractional model obtained for the classical components ζ, ξ and F_{20} for four arbitrary values of fractional order. Parameters are : $\Delta = 4$ and $h = 0.8$.



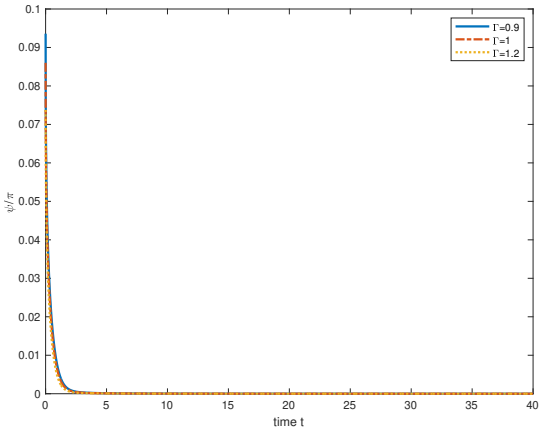
((a)) Dynamics of the orientation angle ψ when $\alpha = 1$.



((b)) Dynamics of the orientation angle ψ when $\alpha = 0.9$.

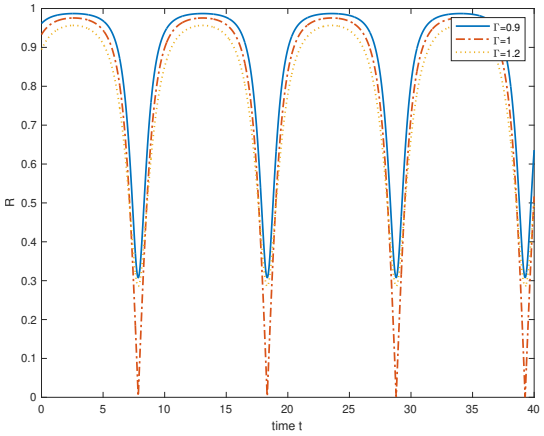


((c)) Dynamics of the orientation angle ψ when $\alpha = 0.7$.

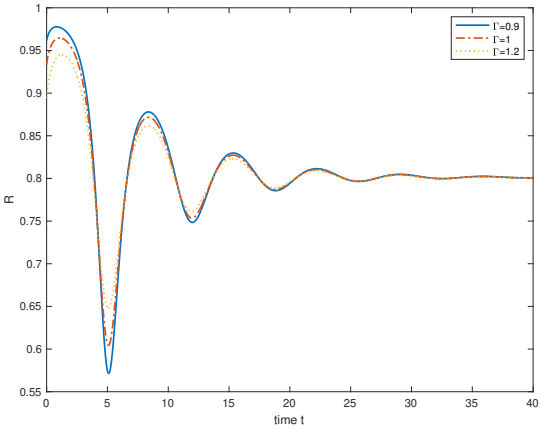


((d)) Dynamics of the orientation angle ψ when $\alpha = 0.5$.

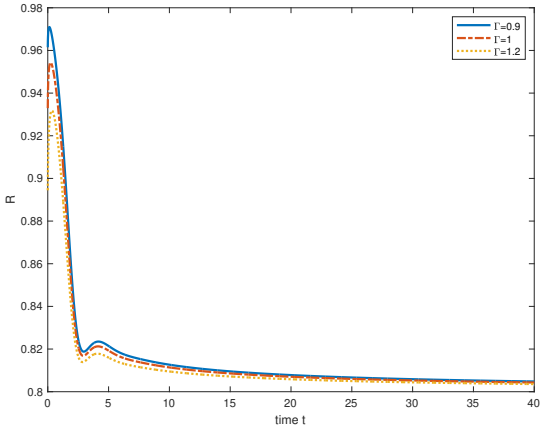
Figure 2.9: The behaviour of the orientation angle ψ for four arbitrary values of fractional order. Parameters are : $\Delta = 4$ and $h = 0.8$ with $\Gamma = 0.9$, $\Gamma = 1$ and $\Gamma = 1.2$.



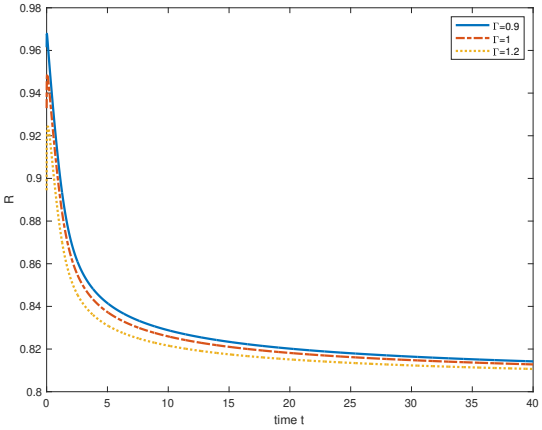
((a)) The amplitude $\mathscr{R}(t)$ when $\alpha = 1$.



((b)) The amplitude $\mathscr{R}(t)$ when $\alpha = 0.9$.



((c)) The amplitude $\mathscr{R}(t)$ when $\alpha = 0.7$.

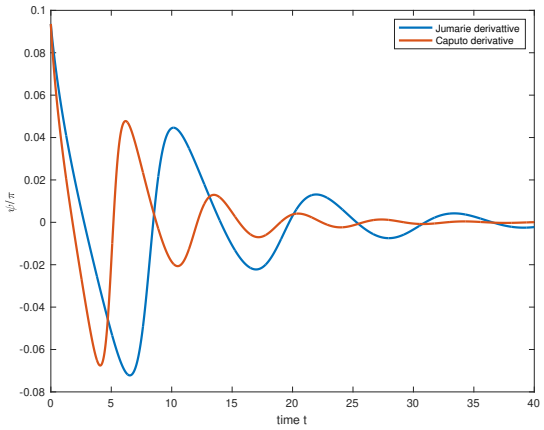


((d)) The amplitude $\mathscr{R}(t)$ when $\alpha = 0.5$.

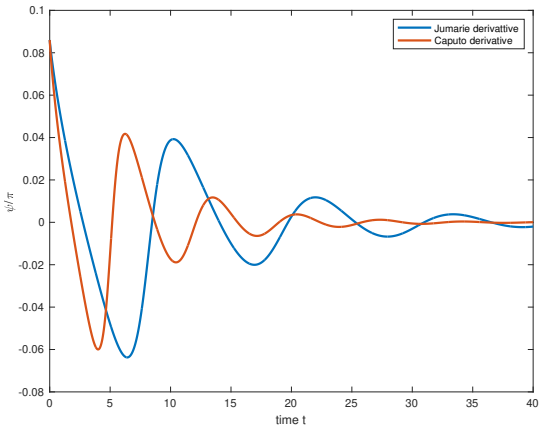
Figure 2.10: The dynamic of the amplitude $\mathscr{R}$ for four arbitrary values of fractional order. Parameters are : $\Delta = 4$ and $h = 0.8$ with $\Gamma = 0.9$, $\Gamma = 1$ and $\Gamma = 1.2$.

2.4 Comparison of Caputo and the Modified Riemann–Liouville Fractional Derivatives in Vesicle Dynamics

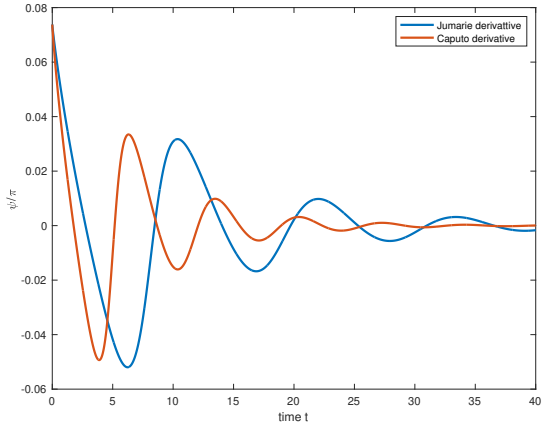
To address the ongoing question of selecting the appropriate fractional derivative, this section conducts a comparative analysis between the Jumarie and Caputo fractional derivatives within the context of vesicle dynamics, particularly in the intriguing case where $h < \sqrt{\Delta}/2$ (Damping mode). The goal is to determine which derivative is more suitable for this specific study. Notably, the Caputo derivative was approximated using the Adams–Bashforth method due to its inherent limitations as detailed in 2.3. In contrast, the Jumarie derivative was selected for its potential to facilitate the derivation of exact solutions, as demonstrated in 2.2.



((a)) The orientation angle φ when $\alpha = 0.9$ and $\Gamma = 0.9$.



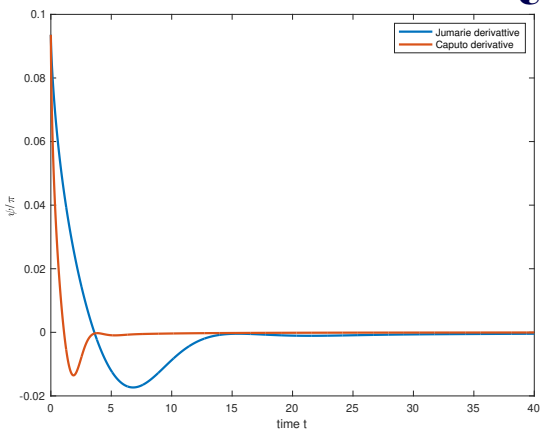
((b)) The orientation angle φ when $\alpha = 0.9$ and $\Gamma = 1$.



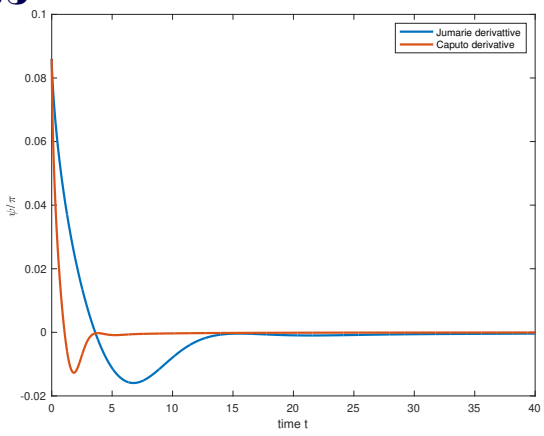
((c)) The orientation angle φ when $\alpha = 0.9$ and $\Gamma = 1.2$.

Figure 2.11: The orientation angle dynamics ψ for $\alpha = 0.9$ with Caputo and Modified Riemann-Liouville Fractional Derivatives and Three Different Γ Values at $\Delta = 4$ and $h = 0.8$.

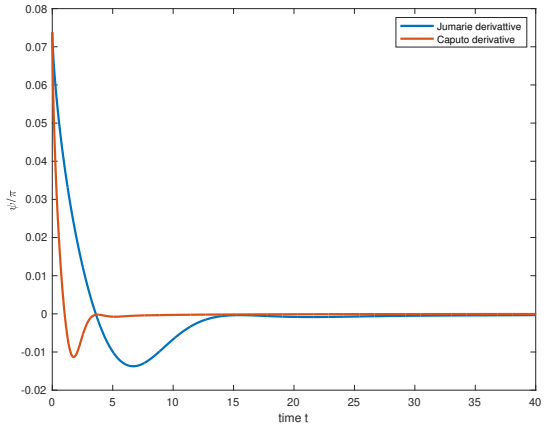
To further explore this observation, we have illustrated the dynamics of the orientation angle in Figures 2.11, 2.12, and 2.13 for three distinct initial conditions (different Γ values) and various



((a)) The orientation angle φ when $\alpha = 0.7$ and $\Gamma = 0.9$.



((b)) The orientation angle φ when $\alpha = 0.7$ and $\Gamma = 1$.



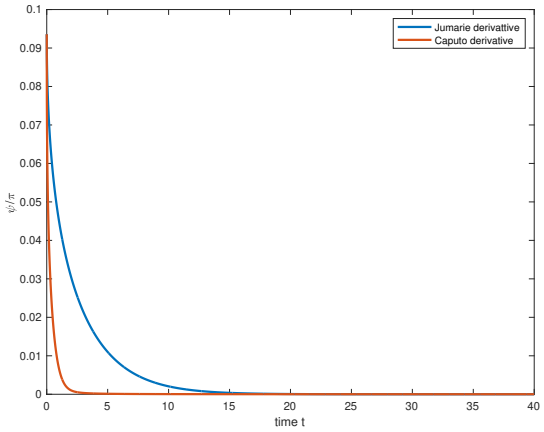
((c)) The orientation angle φ when $\alpha = 0.7$ and $\Gamma = 1.2$.

Figure 2.12: The orientation angle dynamics φ for $\alpha = 0.7$ with Caputo and Modified Riemann-Liouville Fractional Derivatives and Three Different Γ Values at $\Delta = 4$ and $h = 0.8$.

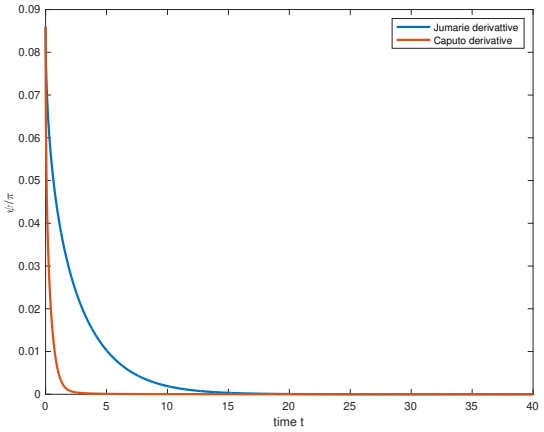
α values, with h consistently set at $h < \sqrt{\Delta}/2$. The corresponding shape deformation is shown in Figures 2.14, 2.15, and 2.16.

Upon closer examination, it becomes apparent that as α decreases, the Caputo derivative yields more pertinent results, with faster convergence in this scenario. The oscillations quickly diminish, leading to stabilization at the equilibrium point and the development of a new damping motion.

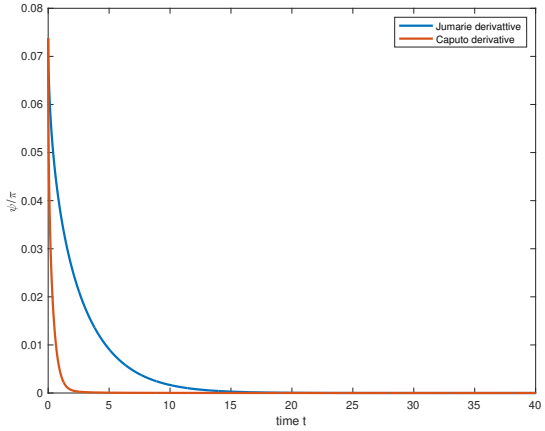
This comparison highlights the difference between the speed of convergence and the relevance of results, emphasizing the sensitivity of the vesicle's behavior to the choice of fractional derivative. In this case, as α moves further from 1, the vesicle's behavior predicts damping-TT for both types of derivatives. However, the Caputo derivative converges more swiftly, allowing us to discern the time difference in achieving convergence or stability between the two derivatives. This phenomenon demonstrates the Caputo derivative's ability to capture and highlight the



((a)) The orientation angle φ when $\alpha = 0.5$ and $\Gamma = 0.9$.



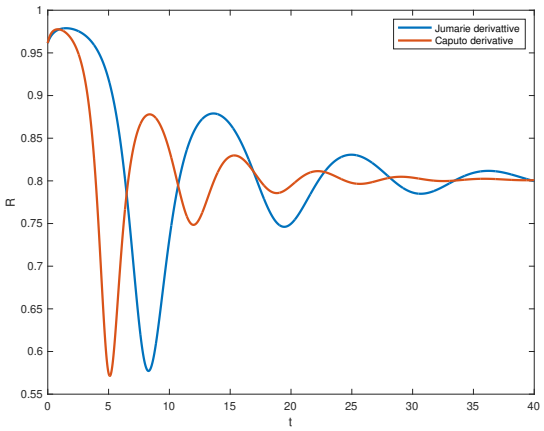
((b)) The orientation angle φ when $\alpha = 0.5$ and $\Gamma = 1$.



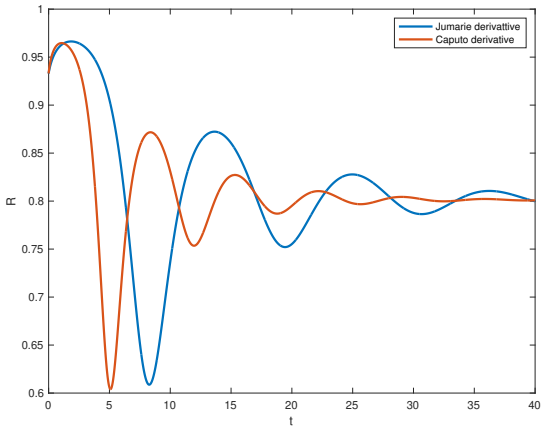
((c)) The orientation angle φ when $\alpha = 0.5$ and $\Gamma = 1.2$.

Figure 2.13: The orientation angle dynamics φ for $\alpha = 0.5$ with Caputo and Modified Riemann-Liouville Fractional Derivatives and Three Different Γ Values at $\Delta = 4$ and $h = 0.8$.

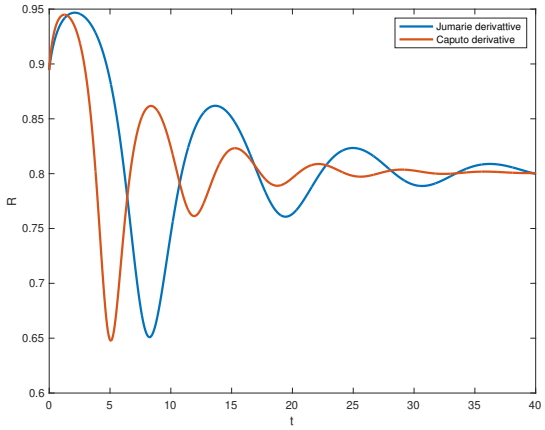
system's intrinsic characteristics, particularly during the transition from oscillatory behavior to stabilization. These observations emphasize the difficulty in determining which derivative is better suited for this type of system.



((a)) The amplitude $\mathscr{R}(t)$ when $\alpha = 0.9$ and $\Gamma = 0.9$.

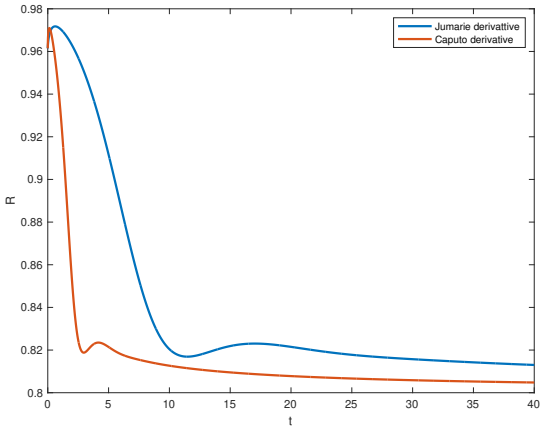


((b)) The amplitude $\mathscr{R}(t)$ when $\alpha = 0.9$ and $\Gamma = 1$.

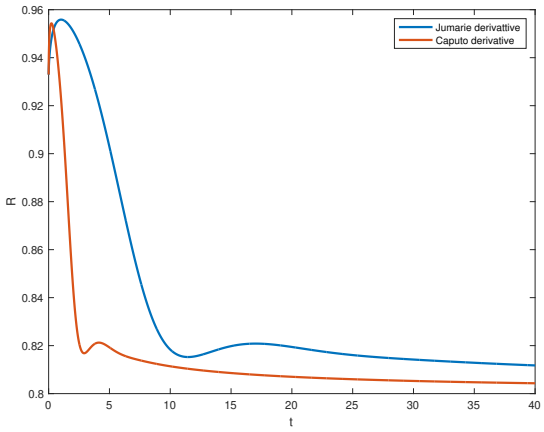


((c)) The amplitude $\mathscr{R}(t)$ when $\alpha = 0.9$ and $\Gamma = 1.2$.

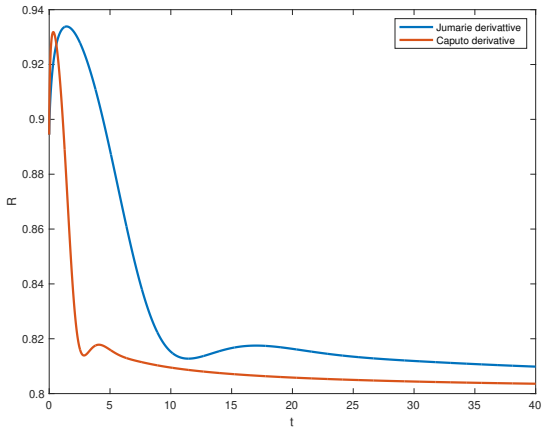
Figure 2.14: The dynamics of the shape deformation $\mathscr{R}$ for $\alpha = 0.9$ with Caputo and Modified Riemann-Liouville Fractional Derivatives and Three Different Γ Values at $\Delta = 4$ and $h = 0.8$.



((a)) The amplitude $\mathscr{R}(t)$ when $\alpha = 0.7$ and $\Gamma = 0.9$.

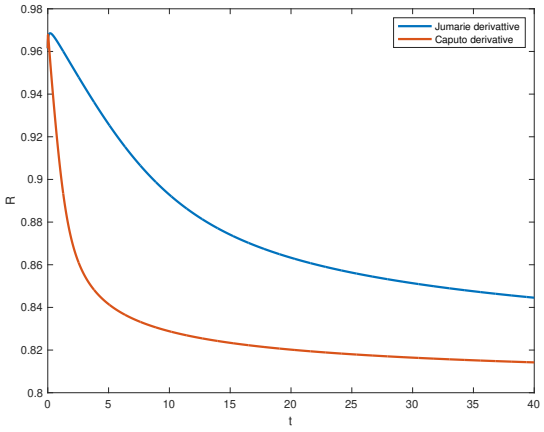


((b)) The amplitude $\mathscr{R}(t)$ when $\alpha = 0.7$ and $\Gamma = 1$.

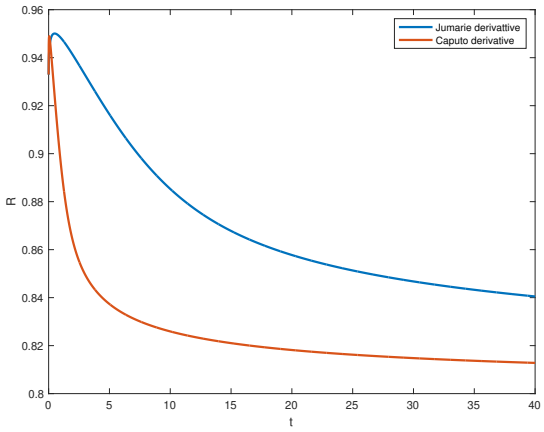


((c)) The amplitude $\mathscr{R}(t)$ when $\alpha = 0.7$ and $\Gamma = 1.2$.

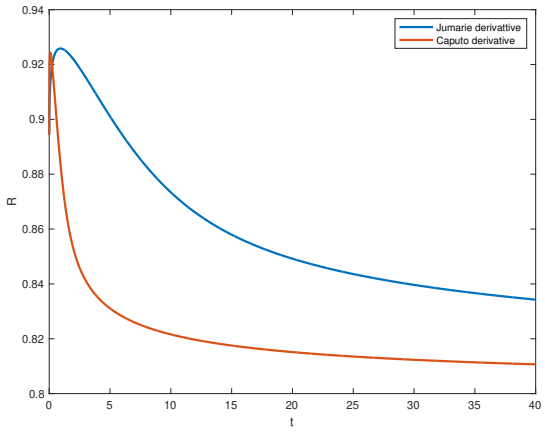
Figure 2.15: The dynamics of the shape deformation $\mathscr{R}$ for $\alpha = 0.7$ with Caputo and Modified Riemann-Liouville Fractional Derivatives and Three Different Γ Values at $\Delta = 4$ and $h = 0.8$.



((a)) The amplitude $\mathscr{R}(t)$ when $\alpha = 0.5$ and $\Gamma = 0.9$.



((b)) The amplitude $\mathscr{R}(t)$ when $\alpha = 0.5$ and $\Gamma = 1$.



((c)) The amplitude $\mathscr{R}(t)$ when $\alpha = 0.5$ and $\Gamma = 1.2$.

Figure 2.16: The dynamics of the shape deformation $\mathscr{R}$ for $\alpha = 0.5$ with Caputo and Modified Riemann-Liouville Fractional Derivatives and Three Different Γ Values at $\Delta = 4$ and $h = 0.8$.

2.5 Motion of an Ellipsoidal Particle in Shear Flow: Analyzing Memory Effect Influence Through Exact Solutions Investigation

Here we extend Keller and Skalak's foundational KS theory, which initially focused on the motion of ellipsoidal particles under shear flow conditions. The following section will delve into the specific contributions of this study, outlining the objectives, methodology, results, and implications in further detail. This investigation aims to reveal the extent of the memory effect's impact on the mobility of ellipsoidal particles.

The incorporation of fractional calculus, specifically the modified Riemann-Liouville fractional derivative, promises a more nuanced modeling framework for complex particle dynamics. This approach not only enhances our understanding of particle motion but also explores how temporal memory effects influence the transition from flipping to stationary motion in shear flows.

Based on the theoretical framework laid down by Keller and Skalak, and the subsequent expansion using fractional derivatives, this study seeks to address a pivotal question: How does the incorporation of fractional calculus, specifically the modified Riemann-Liouville fractional derivative, offer insights into the transition from flipping to stationary motion in red blood cells under varying viscosity ratios in shear flows? By disregarding the memory effect inherent in classical derivatives, there is a risk of overlooking the true dynamics of this transition. Therefore, the adoption of fractional derivatives holds the potential to enable us to observe and verify Keller and Skalak's prediction regarding the increased period of motion during this critical transition phase.

In this study, our aim is to specifically focus on the dynamics of ellipsoidal particles using the shape-preserving theory ($\mathscr{R} \equiv \frac{\sqrt{\Delta}}{2}$) and incorporating fractional derivatives. In the classical case, subsequent research by Misbah [64] explored deformable vesicles and introduced the vacillating-breathing (VB) mode as a transitional state between tank-treading and tumbling as mentioned in the Introduction . However, following this study, researchers have primarily considered the case where the particle is deformable (i.e., vesicle) [2, 37] and have neglected the scenario where it could be a rigid particle. This has prompted us to explore this case, given that fractional calculus has already been utilized in the vesicle scenario in 2.2 and 2.3, as mentioned in the introduction, where another motion was identified, considered as the transition between TT and VB. Here, we aim to investigate if we can approach the prediction given by KS, where they studied an ellipsoidal particle while preserving its shape, providing a deeper understanding of ellipsoidal particle motion in shear flows. Then, the system (2.1) is reduced to the generalization of the Jeffery equation [42]

$$ {}^{\mathscr{J}}D_t^{\alpha}\psi = \frac{-1}{2} + \frac{h}{\sqrt{\Delta}} cos(2\psi), \tag{2.44}$$

the particle dynamic is exclusively characterised by the variation of the angle ψ, this simplifies the dynamics. Keller and Skalak [48] thoroughly explored equation (2.44) in the classical case (i.e., $\alpha = 1$) and the purpose of this section is to derive exact solutions for the fractional equation (2.44) by using the properties of the modified Riemann-Liouville fractional derivative describe above in Chapter 1, aiming to quantify the influence of both the parameters h and Δ and the fractional derivative α on the mobility of the ellipsoidal particle. This choice enabled us to delve deeper into the influence of fractional-order derivatives on the dynamics of ellipsoidal particles and their associated memory effects. Moreover, our utilization of Jumarie's modified Riemann-Liouville derivative unveiled a spectrum of behaviors consistent with the predictions of Keller and Skalak, including an increase in period duration that was not evident in their theory when employing classical derivatives. To provide a more comprehensive analysis of our findings and their practical implications, we will now examine these aspects through a set of subsections.

2.5.1 TT-mode

In this section, we investigate the tank-treading mode (TT-mode), a distinct behavior observed in specific fluid dynamics scenarios. This behavior is analyzed using Jumarie's modified Riemann-Liouville fractional derivative and its properties to determine the expression of ψ. The resulting expression reveals the manifestation of the tank-treading mode.

$$\psi(t) = \arctan\Big[-\frac{\chi-1}{\sqrt{\chi^2-1}}.\frac{1-K\exp\Big(\frac{\sqrt{\chi^2-1}}{\Gamma(\alpha+1)}(t-t_0)^\alpha\Big)}{1+K\exp\Big(\frac{\sqrt{chi^2-1}}{\Gamma(\alpha+1)}(t-t_0)^\alpha\Big)}\Big], \tag{2.45}$$

where $\chi = \dfrac{2h}{\sqrt{\Delta}}$, $K = \dfrac{tan(\psi_0) + \frac{\chi-1}{\sqrt{\chi^2-1}}}{tan(\psi_0) - \frac{\chi-1}{\sqrt{\chi^2-1}}}$ and $\psi_0 = \psi(t_0)$, where t_0 is the initial value.

Figures 2.17 illustrate the orientation angle ψ for different values of α. The solutions demonstrate that ψ remains constant for various α values, indicating that the solution tends to a stable equilibrium independently of the initial orientation. This observation confirms that the particle exhibits tank-treading (TT) motion. Additionally, the orientation lies in the shear plane, corresponding to the TT motion for the vesicle.

From the above figure, it is evident that the order of the fractional derivative has no impact on the stability of the equilibrium. Therefore, increasing the value of α enables the solutions to converge to the steady state more rapidly. The strength of memory effects, governed by α, significantly influences the dynamics of rigid particles. Consequently, the dynamics of the ellipsoidal particle are influenced by both the current time and the time history, which can be effectively captured using fractional calculus concepts.

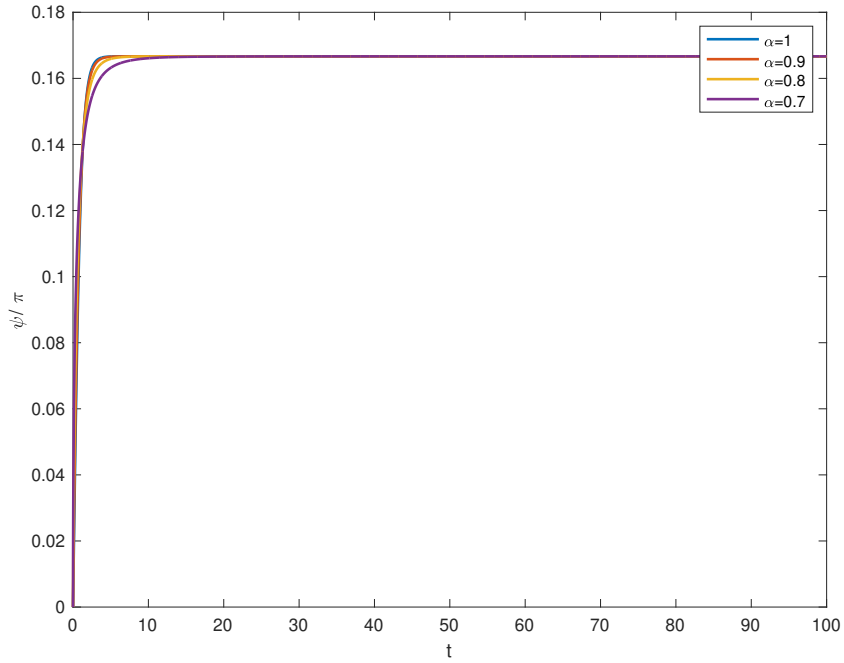


Figure 2.17: The orientation angle ψ of the ellipsoidal particle for four different fractional order values when the parameter $\chi > 1$.

2.5.2 TB-mode

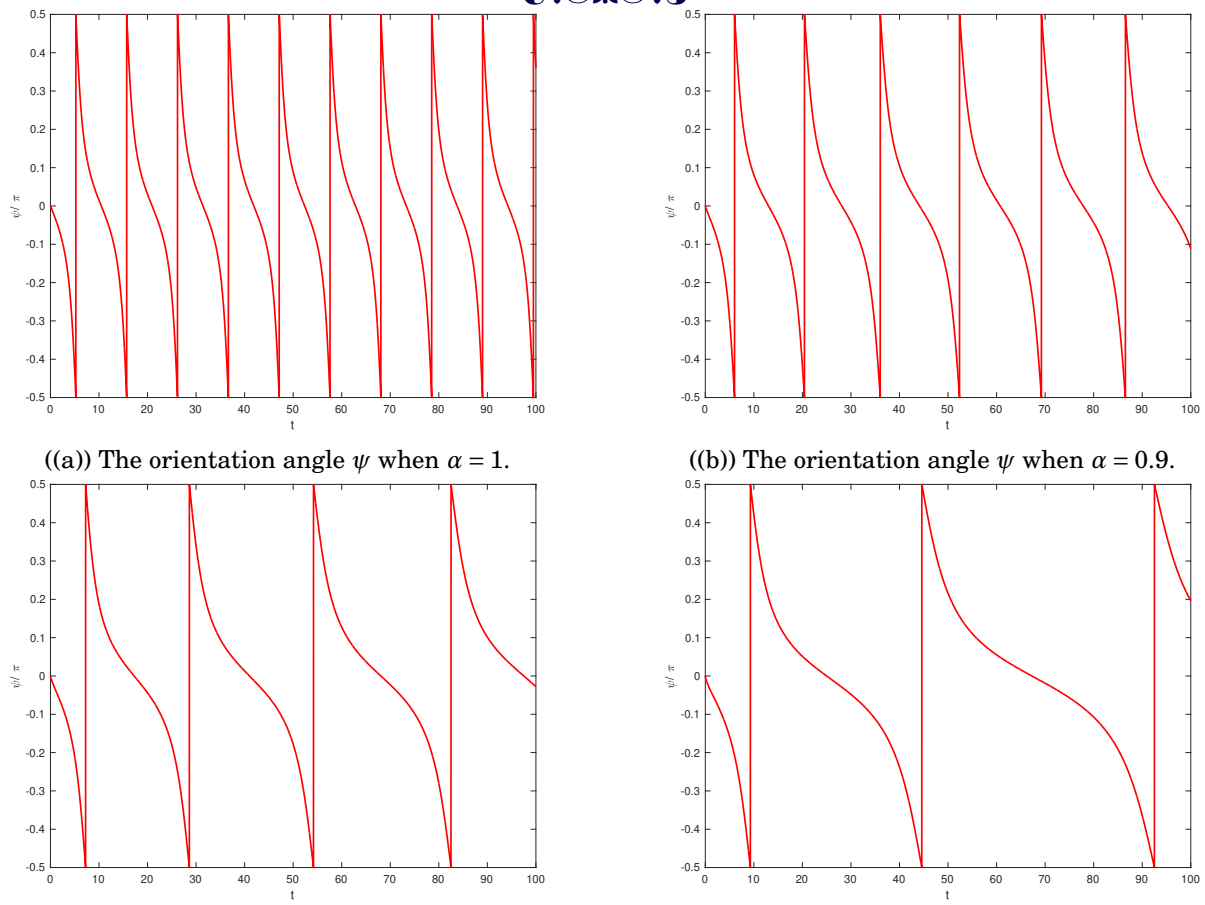
Embarking on the pivotal segment of our research, we now pivot our attention to the oscillatory solution where $\chi < 1$, previously elucidated and explored in the classical context by the authors in [42, 48]. They noted that the details of the transition from flipping motion to stationary orientation have not yet been experimentally investigated [48].

This prompted us to consider that neglecting the memory effect might have prevented us from theoretically observing it, hence the idea of taking the memory effect into account, which led us to add the Jumarie fractional derivative. Advancing our inquiry in the present chapter, we delve into the computation of exact solutions, considering the memory effect exemplified by the fractional derivative of Jumarie. Similarly to the case where $\chi > 1$, our aim is to solve equation (2.44) utilizing the fundamental properties of the Jumarie derivative delineated in section 1. Following meticulous calculations, we unveil the subsequent expressions.

$$\psi(t) = \arctan\left[-\frac{1-\chi}{\sqrt{1-\chi^2}}\tan\left(\frac{\sqrt{1-\chi^2}}{2\Gamma(\alpha+1)}(t-t_0)^{\alpha} + \arctan\left(\frac{-\sqrt{1-\chi^2}}{1-\chi}\tan(\psi_0)\right)\right)\right], \tag{2.46}$$

where $\psi_0 = \psi(t_0)$, where t_0 is the initial value.

Figure 2.18 illustrates the orientation angle ψ for four different α values when $\chi < 1$. In the classical case ($\alpha = 1$), we observed that the particle flips increasingly like a rigid ellipsoid, as shown in [48], where the authors noted that as the viscosity ratio increases, the particle's motion converges towards Jeffery's solution [42]. However, the prediction made by K-S indicates that an increased viscosity ratio results in a longer flipping period and greater alignment with the



((a)) The orientation angle ψ when $\alpha = 1$.

((b)) The orientation angle ψ when $\alpha = 0.9$.

((c)) The orientation angle ψ when $\alpha = 0.8$.

((d)) The orientation angle ψ when $\alpha = 0.7$.

Figure 2.18: The particle's orientation angle psi for four different fractional order values when the parameter $\chi < 1$.

flow, ultimately leading to a stationary orientation. This highlights the significant impact of the viscosity ratio on red blood cell dynamics in shear flow. Additionally, we show that the memory effect also influences the flipping period.

Notably, in the case where $0 < \alpha < 1$, the introduction of the modified Riemann-Liouville fractional derivatives increases the period of the ψ angle, leading to several important conclusions. Understanding these observations becomes critical, particularly in the context of introducing the memory effect to substantiate Keller and Skalak's predictions, which represent unexplored aspects.

The memory effect is crucial for how particles react and orient over time. Fractional-order derivatives allow particles to respond based on recent history, influencing current orientation and dynamically adapting to environmental changes. The increase in motion period as the fractional derivative order decreases suggests that lower-order derivatives introduce more pronounced memory effects into the system, where motion is influenced by a wider range of historical information or past states, resulting in slower motion evolution. The relationship between fractional

derivative order of the modified Riemann-Liouville fractional derivative and motion period underscores the complexity of system dynamics.

Our utilization of the Jumarie derivative unveild a spectrum of behaviors consistent with the predictions of KS, including an increase in period duration that was not evident in the KS-theory when employing classical derivative.

The flipping period significantly affects particle dynamics, with variations impacting motion types. Changes in the flipping period due to alterations in the viscosity ratio between inner and outer liquids can shift the particle's behaviour between steady stationary-orientation and unsteady flipping motion. Moreover, the flipping period can indicate transitions between different motion modes exhibited by the ellipsoidal particle, particularly as the viscosity ratio approaches critical threshold values. By studying the flipping period and its correlation with viscosity ratio, researchers gain insights into ellipsoidal particle dynamics in shear flows, emphasizing the parameter's importance in understanding particle motion in complex fluid environments.

This can be explained by the fact that, when considering the memory effect (the entire time history), the period of the flipping motion and the time spent aligned with the flow will increase, eventually leading the particle to assume a stationary orientation. In summary, the increase in the ψ angle period with the introduction of fractional-order derivatives signifies more complex and adaptive system dynamics, with notable memory effects and emergent properties. Understanding and interpreting these changes are vital for accurately modeling and predicting system behavior. By incorporating Jumarie's modified Riemann-Liouville derivative, we present a more realistic and comprehensive model.

2.6 Conclusion

In conclusion, this chapter demonstrates the substantial advancements made by applying fractional calculus to the study of vesicles, red blood cells, and ellipsoidal particles in shear flows. Utilizing both the Jumarie and Caputo fractional derivatives has deepened our understanding of the complex behaviors and memory effects in these systems.

The Caputo fractional derivative, in particular, has proven effective in capturing the intricate dynamics of vesicles, offering a more accurate depiction of their behavior over time compared to traditional methods. This approach has shown improved stability and convergence, especially in scenarios with significant memory effects. The comparative analysis with the Jumarie derivative further underscores the Caputo approach's strengths in modeling long-term memory and stability.

Additionally, our study has introduced new motion modes, such as over-damped and under-damped tank-treading, which enhance our understanding of vesicle dynamics. These findings reveal novel behaviors and transitions that were previously unexplored, providing valuable insights into complex fluid dynamics.

By extending Keller and Skalak's theory with fractional derivatives, we have also shed light on the transition from flipping to stationary motion in red blood cells, offering a more detailed understanding of particle behavior in fluid environments. This work highlights the relevance of fractional calculus in modeling real-world complexities and opens avenues for future research and practical applications in biomedical and fluid dynamics.

CHAPTER 3

EXPLORING THE INTERPLAY BETWEEN MEMORY EFFECTS AND VESICLE DYNAMICS: A FIVE-DIMENSIONAL NUMERICAL ANALYSIS USING RIGID SPHERE MODELS AND MAPPING TECHNIQUES

Contents

3.1 Introduction **65**
3.2 Fractional model **65**
3.3 Results **66**
3.3.1 Existence and uniqueness of solutions of the Caputo-fractional model . 66
3.3.2 Existence of equilibrium and Stability analysis 68
3.3.3 Numerical method 70
3.4 Discussion **71**
3.4.1 Tank-treading mode 71
3.4.2 Tumbling and Vacillating-breathing modes 74
3.4.3 The effect of initial conditions and fractional order on dynamics 76
3.5 Conclusion **78**

3.1 Introduction

In this chapter, we delve into the intricate dynamics of vesicles, particularly focusing on the memory effects observed in these systems. This study employs a fractional rigid sphere model in five dimensions, utilizing the Caputo operator to map the dynamics of vesicles. By exploring this model, we gain a deeper understanding of the mechanisms behind the memory effect and identify three distinct modes of vesicle motion: tank-treading with underdamped oscillations, tank-treading with overdamped oscillations, and the standard tank-treading mode where the vesicle rotates while maintaining its shape.

The findings presented in this chapter represent a significant advancement in the field of vesicle dynamics and have important implications for our understanding of RBC behavior. Through this exploration, we aim to shed light on the complex interplay between memory effects and vesicle dynamics, contributing to the broader knowledge in the field of biophysics and applied mathematics.

The present chapter is structured as follows: In the following section, we begin by presenting the fractional differential equations. Section 3.3 details the main outcomes of this work, including proofs of existence and uniqueness of the solution for these equations, as well as an analysis of the local stability of the equilibrium points. Additionally, we support our analytical findings using the Adams–Bashforth–Moulton predictor–corrector scheme. Section 3.4 illustrates our principal results with graphs and discusses the memory effect and the various regimes observed. Finally, Section 3.5 provides the conclusions of the study. The results of this chapter are based on the paper [15].

3.2 Fractional model

The mapped equation (12) whose corresponds to dynamics out and in the shear plane has been solved analytically [2]. Its solutions do not depend on the previous instant due to the no memory of the classical models of ordinary differential equations. Fractional calculus is a great way to describe real-life, as well as, phenomena with the memory effect [16]. The mapped equation (12) can be described as:

$$\begin{aligned} \frac{d\boldsymbol{p}_1}{dt} &= \gamma\left(\boldsymbol{p}_2 - \chi^{-1}\boldsymbol{p}_2\boldsymbol{p}_1\right), \\ \frac{d\boldsymbol{p}_2}{dt} &= \gamma\left(\chi^{-1} - \boldsymbol{p}_1 - \chi^{-1}\boldsymbol{p}_2^2\right), \\ \frac{d\boldsymbol{p}_3}{dt} &= \gamma\left(-\chi^{-1}\boldsymbol{p}_2\boldsymbol{p}_3\right), \end{aligned} \tag{3.1}$$

$$\begin{aligned} \frac{d\boldsymbol{p}_4}{dt} &= \gamma\left(-\chi^{-1}\boldsymbol{p}_2\boldsymbol{p}_4 - \frac{1}{2}\boldsymbol{p}_5\right), \\ \frac{d\boldsymbol{p}_5}{dt} &= \gamma\left(\frac{1}{2}\boldsymbol{p}_4 - \chi^{-1}\boldsymbol{p}_2\boldsymbol{p}_5\right) \quad . \end{aligned} \tag{3.2}$$

The system (3.1) corresponds for the vesicles, to the dynamics in the shear plane (i.eF $_{2\mp1} = 0$), and the system (3.2) corresponds to the dynamics out of the plane (i.e $F_{2\mp1} \neq 0$).
We introduce the memory effect [16] into the mapped equation by replacing the order of the derivative of the classical model with the Caputo operator mentioned in Chapter 1 to obtain a generalized model. Finally, the system of Caputo-fractional ODEs is defined as follows

$$\begin{aligned} {}^{C}D_t^{\alpha}\boldsymbol{p}_1 &= \gamma\left(\boldsymbol{p}_2 - \chi^{-1}\boldsymbol{p}_2\boldsymbol{p}_1\right), \\ {}^{C}D_t^{\alpha}\boldsymbol{p}_2 &= \gamma\left(\chi^{-1} - \boldsymbol{p}_1 - \chi^{-1}\boldsymbol{p}_2^2\right), \\ {}^{C}D_t^{\alpha}\boldsymbol{p}_3 &= \gamma\left(-\chi^{-1}\boldsymbol{p}_2\boldsymbol{p}_3\right), \end{aligned} \tag{3.3}$$

$$\begin{aligned} {}^{C}D_t^{\alpha}\boldsymbol{p}_4 &= \gamma\left(-\chi^{-1}\boldsymbol{p}_2\boldsymbol{p}_4 - \frac{1}{2}\boldsymbol{p}_5\right), \\ {}^{C}D_t^{\alpha}\boldsymbol{p}_5 &= \gamma\left(\frac{1}{2}\boldsymbol{p}_4 - \chi^{-1}\boldsymbol{p}_2\boldsymbol{p}_5\right). \end{aligned} \tag{3.4}$$

The system (3.3) corresponds for the vesicles, to the dynamics in the shear plane (i.e $F_{2\mp1} = 0$), and the system (3.4) corresponds to the dynamics out of the plane (i.eF $_{2\mp1} \neq 0$). The mapped equation (12) has been solved exactly in [2].
Thus, the fractional mapped equation is given by,

$$\gamma^{-1C}D_t^{\alpha}\boldsymbol{p} = \Omega\cdot\boldsymbol{p} + \chi^{-1}(e_2 - e_2\cdot\boldsymbol{p}\boldsymbol{p}), \tag{3.5}$$

where, $\boldsymbol{p} = \left(\boldsymbol{p}_1, \boldsymbol{p}_2, \boldsymbol{p}_3, \boldsymbol{p}_4, \boldsymbol{p}_5\right)^T$, ${}^{C}D_t^{\alpha}$ is the Caputo fractional operator of order $0 < \alpha < 1$.

3.3 Results

3.3.1 Existence and uniqueness of solutions of the Caputo-fractional model

In this section, we prove the existence of the system of solutions by applying theorem 2.1 and theorem 2.2. We prove the existence of the case when the vesicle is allowed to move outside the shear plane $F_{2\mp1} \neq 0$ (i.e $\boldsymbol{p}_4 \neq 0$ and $\boldsymbol{p}_5 \neq 0$).
We have,

$$\begin{aligned} {}^{C}D_t^{\alpha}\boldsymbol{p}_1 &= \gamma\boldsymbol{p}_2 - \beta\boldsymbol{p}_2\boldsymbol{p}_1, \\ {}^{C}D_t^{\alpha}\boldsymbol{p}_2 &= \beta - \gamma\boldsymbol{p}_1 - \beta\boldsymbol{p}_2^2, \\ {}^{C}D_t^{\alpha}\boldsymbol{p}_3 &= -\beta\boldsymbol{p}_2\boldsymbol{p}_3, \\ {}^{C}D_t^{\alpha}\boldsymbol{p}_4 &= -\beta\boldsymbol{p}_2\boldsymbol{p}_4 - \frac{\gamma}{2}\boldsymbol{p}_5, \\ {}^{C}D_t^{\alpha}\boldsymbol{p}_5 &= \frac{\gamma}{2}\boldsymbol{p}_4 - \beta\boldsymbol{p}_2\boldsymbol{p}_5. \end{aligned} \tag{3.6}$$

where ${}^{C}D_t^{\alpha}$ is the Caputo-fractional operator of order $0 < \alpha < 1$ and $\beta = \gamma\chi^{-1}$.
We use the following notations for the right side of the fractional system (3.6),

$$\begin{aligned}
f_1\left(t,\boldsymbol{p}_1(t)\right) &= \gamma\boldsymbol{p}_2 - \beta\boldsymbol{p}_2\boldsymbol{p}_1,\\
f_2\left(t,\boldsymbol{p}_2(t)\right) &= \beta - \gamma\boldsymbol{p}_1 - \beta\boldsymbol{p}_2^2,\\
f_3\left(t,\boldsymbol{p}_3(t)\right) &= -\beta\boldsymbol{p}_2\boldsymbol{p}_3,\\
f_4\left(t,\boldsymbol{p}_4(t)\right) &= -\beta\boldsymbol{p}_2\boldsymbol{p}_4 - \frac{\gamma}{2}\boldsymbol{p}_5,\\
f_5\left(t,\boldsymbol{p}_5(t)\right) &= \frac{\gamma}{2}\boldsymbol{p}_4 - \beta\boldsymbol{p}_2\boldsymbol{p}_5.
\end{aligned}$$

Theorem 3.3.1. *The initial value problem of Caputo-fractional order system* (3.6) *can be given as follows:*

$${}^{C}D_t^{\alpha}\boldsymbol{p}(t) = V + A_1 p(t) + \boldsymbol{p}_2(t)A_2\boldsymbol{p}(t), \quad p(0) = \boldsymbol{p}_0,$$

where
$0 < t \leq T, \boldsymbol{p} = \left(\boldsymbol{p}_1,\boldsymbol{p}_2,\boldsymbol{p}_3,\boldsymbol{p}_4,\boldsymbol{p}_5\right)^T \in \mathbb{R}^5$, $\boldsymbol{p}_0 = \left(\boldsymbol{p}_1(0),\boldsymbol{p}_2(0),\boldsymbol{p}_3(0),\boldsymbol{p}_4(0),\boldsymbol{p}_5(0)\right)^T$, $V = (0,\beta,0,0,0)^T$, $A_1 = \gamma \times \Omega$, $A_2 = -\beta \times I_5$, *for some constant* $T > 0$, *then it has a unique solution.*

Proof. Consider $F(t,\boldsymbol{p}(t)) = \begin{pmatrix} f_1\left(t,\boldsymbol{p}_1(t)\right), \\ f_2\left(t,\boldsymbol{p}_2(t)\right) \\ f_3\left(t,\boldsymbol{p}_3(t)\right) \\ f_4\left(t,\boldsymbol{p}_4(t)\right) \\ f_5\left(t,\boldsymbol{p}_5(t)\right) \end{pmatrix}$ which is continuous and bounded on the interval $\left[\boldsymbol{p}_0 - \epsilon, \boldsymbol{p}_0 + \epsilon\right]$ for any $\epsilon > 0$. Moreover, we have

$$\begin{aligned}
|F(t,\boldsymbol{p}(t)) - F\left(t,\boldsymbol{p}'(t)\right)| &= |A_1\left(\boldsymbol{p}(t) - \boldsymbol{p}'(t)\right) + \boldsymbol{p}_2(t)A_2 p(t) - \boldsymbol{p}_2'(t)A_2 p'(t)|\\
&\leq |\left(A_1 + \boldsymbol{p}_2'(t)A_2\right)\left(\boldsymbol{p}(t) - \boldsymbol{p}'(t)\right) + A_2\boldsymbol{p}(t)\left(\boldsymbol{p}_2(t) - \boldsymbol{p}_2'(t)\right)|.
\end{aligned}$$

Since, $|\boldsymbol{p}_2(t) - \boldsymbol{p}_2'(t)| \leq |\boldsymbol{p}(t) - \boldsymbol{p}'(t)|$,
we get,

$$|F(t,\boldsymbol{p}(t)) - F\left(t,\boldsymbol{p}'(t)\right)| \leq \left(\|A_1\| + \|A_2\|\left(|\boldsymbol{p}(t)| + |\boldsymbol{p}_2'(t)|\right)\right)|\boldsymbol{p}(t) - \boldsymbol{p}'(t)|,$$

thus,

$$|F(t,\boldsymbol{p}(t)) - F\left(t,\boldsymbol{p}'(t)\right)| \leq \left(\|A_1\| + \|A_2\|\left(2|\boldsymbol{p}_0| + \epsilon\right)\right)|\boldsymbol{p}(t) - \boldsymbol{p}'(t)|,$$

finally,

$$|F(t,\boldsymbol{p}(t)) - F\left(t,\boldsymbol{p}'(t)\right)| \leq A|\boldsymbol{p}(t) - \boldsymbol{p}'(t)|,$$

where we set $A = \|A_1\| + \|A_2\|\left(2|\boldsymbol{p}_0| + \epsilon\right) > 0$, $\|.\|$ and $|.|$ represent matrix and vector norm respectively.
Hence, the Lipschitz condition is satisfied, and according to Theorems 1.2.1 and 1.2.2 the Caputo-fractional system (3.6) has a unique solution. ■

3.3.2 Existence of equilibrium and Stability analysis

In this section, we will determine the equilibrium points of the system of Caputo-fractional ODEs and we will study the local asymptotic stability of the equilibrium.

First, we determine the equilibria of the case when the vesicle is allowed to move outside the shear plane (i.e $F_{2\mp1} \neq 0$) models.

We have in this case $\boldsymbol{p}_4 \neq 0$ and $\boldsymbol{p}_5 \neq 0$ then we solve:

$$\begin{aligned} \boldsymbol{p}_2 - \chi^{-1}\boldsymbol{p}_2\boldsymbol{p}_1 &= 0, \\ \chi^{-1} - \boldsymbol{p}_1 - \chi^{-1}\boldsymbol{p}_2^2 &= 0, \\ -\chi^{-1}\boldsymbol{p}_2\boldsymbol{p}_3 &= 0, \\ -\chi^{-1}\boldsymbol{p}_2\boldsymbol{p}_4 - \frac{1}{2}\boldsymbol{p}_5 &= 0, \\ \frac{1}{2}\boldsymbol{p}_4 - \chi^{-1}\boldsymbol{p}_2\boldsymbol{p}_5 &= 0. \end{aligned} \tag{3.7}$$

The first and second equilibriums are: $\left(\chi, \pm\sqrt{1-\chi^2}, 0, 0, 0\right)$ if $\chi < 1$.
The third and forth equilibriums are : $\left(\chi^{-1}, 0, \pm\sqrt{1-\chi^{-2}}, 0, 0\right)$ if $\chi > 1$.

Remark 3.3.1. *If* $\chi = 1$ *the equilibrium points coincide in* $(1,0,0,0,0)$.

To study the local asymptotic stability of the equilibrium when the vesicle is allowed to move outside the shear plane (i.e $F_{2\mp1} \neq 0$) we write the fractional mapped equation (3.5) as

$$\begin{aligned} {}^{C}D_t^{\alpha}\boldsymbol{p}_1 &= \boldsymbol{p}_2 - \chi^{-1}\boldsymbol{p}_2\boldsymbol{p}_1, \\ {}^{C}D_t^{\alpha}\boldsymbol{p}_2 &= \chi^{-1} - \boldsymbol{p}_1 - \chi^{-1}\boldsymbol{p}_2^2, \\ {}^{C}D_t^{\alpha}\boldsymbol{p}_3 &= -\chi^{-1}\boldsymbol{p}_2\boldsymbol{p}_3, \\ {}^{C}D_t^{\alpha}\boldsymbol{p}_4 &= -\chi^{-1}\boldsymbol{p}_2\boldsymbol{p}_4 - \frac{1}{2}\boldsymbol{p}_5, \\ {}^{C}D_t^{\alpha}\boldsymbol{p}_5 &= \frac{1}{2}\boldsymbol{p}_4 - \chi^{-1}\boldsymbol{p}_2\boldsymbol{p}_5. \end{aligned} \tag{3.8}$$

We can linearise the system and apply the theorem 1.2.3 to study the local stability of the solutions of the fractional system. The Jacobian Matrix:

$$J\left(\boldsymbol{p}_1,\boldsymbol{p}_2,\boldsymbol{p}_3,\boldsymbol{p}_4,\boldsymbol{p}_5\right) = \begin{pmatrix} -\chi^{-1}\boldsymbol{p}_2 & 1-\chi^{-1}\boldsymbol{p}_1 & 0 & 0 & 0 \\ -1 & -2\chi^{-1}\boldsymbol{p}_2 & 0 & 0 & 0 \\ 0 & -\chi^{-1}\boldsymbol{p}_3 & -\chi^{-1}\boldsymbol{p}_2 & 0 & 0 \\ 0 & -\chi^{-1}\boldsymbol{p}_4 & 0 & -\chi^{-1}\boldsymbol{p}_2 & -\frac{1}{2} \\ 0 & -\chi^{-1}\boldsymbol{p}_5 & 0 & \frac{1}{2} & -\chi^{-1}\boldsymbol{p}_2 \end{pmatrix}. \tag{3.9}$$

For the first and second equilibrium: $\chi < 1$,

(3.10)
$$J\left(\chi,\pm\sqrt{1-\chi^2},0,0,0\right)=\begin{pmatrix} \mp\sqrt{\chi^{-2}-1} & 0 & 0 & 0 & 0\\ -1 & \mp 2\sqrt{\chi^{-2}-1} & 0 & 0 & 0\\ 0 & 0 & \mp\sqrt{\chi^{-2}-1} & 0 & 0\\ 0 & 0 & 0 & \mp\sqrt{\chi^{-2}-1} & -\frac{1}{2}\\ 0 & 0 & 0 & \frac{1}{2} & \mp\sqrt{\chi^{-2}-1} \end{pmatrix}.$$

We find the eigenvalues by solving the following characteristic equation

$$\det\left(J\left(\chi,\pm\sqrt{1-\chi^2},0,0,0\right)-\tilde{\lambda}I_5\right)=0.$$

Hence, the eigenvalues associated to the first equilibrium are :

$$\tilde{\lambda}_{1_\pm}=\mp\sqrt{\chi^{-2}-1},\quad \tilde{\lambda}_{2_\pm}=\mp 2\sqrt{\chi^{-2}-1},$$

$$\tilde{\lambda}_{3_\pm}=\mp\sqrt{\chi^{-2}-1}+\frac{1}{2}i,\quad \tilde{\lambda}_{4_\pm}=\mp\sqrt{\chi^{-2}-1}-\frac{1}{2}i.$$

It is clear that for the eigenvalues

$$\tilde{\lambda}_{1_+}=-\sqrt{\chi^{-2}-1}\quad\text{and}\quad \tilde{\lambda}_{2_+}=-2\sqrt{\chi^{-2}-1},$$

we have

$$|\arg(\tilde{\lambda}_{j_+})|=\pi>\frac{\pi}{2}>\frac{\alpha\pi}{2},\quad j=1,2.$$

We have also

$$\tilde{\lambda}_{3_+}=-\sqrt{\chi^{-2}-1}+\frac{1}{2}i,\quad {}_{4_+}=-\sqrt{\chi^{-2}-1}-\frac{1}{2}i,$$

that means;

$$|\arg(\tilde{\lambda}_{j_+})|=|\arctan\left(\frac{1}{2\sqrt{\chi^{-2}-1}}\right)-\pi|>\frac{\pi}{2}>\frac{\alpha\pi}{2},\quad j=3,4.$$

Then, from the theorem 1.2.3 one can easily see that the equilibrium $\left(\chi,+\sqrt{1-\chi^2},0,0,0\right)$ is asymptotically stable. Thus the equilibrium $\left(\chi,-\sqrt{1-\chi^2},0,0,0\right)$ incompletely unstable for the reason that,

$$\tilde{\lambda}_{1_-}=\sqrt{\chi^{-2}-1},\qquad \tilde{\lambda}_{2_-}=2\sqrt{\chi^{-2}-1},$$
$$|\arg(\tilde{\lambda}_{j_-})|=0<\tfrac{\alpha\pi}{2},\quad \text{for}\quad 0<\alpha<1,\quad j=1,2.$$

For the third and forth equilibrium:

(3.11)
$$J\left(\chi^{-1},0,\pm\sqrt{1-\chi^{-2}},0,0\right)=\begin{pmatrix} 0 & 1-\chi^{-2} & 0 & 0 & 0\\ -1 & 0 & 0 & 0 & 0\\ 0 & \mp\chi^{-1}\sqrt{\chi^{-2}-1} & 0 & 0 & 0\\ 0 & 0 & 0 & 0 & -\frac{1}{2}\\ 0 & 0 & 0 & \frac{1}{2} & 0 \end{pmatrix}.$$

By solving the following characteristic equation

$$\det\left(J\left(\chi^{-1},0,\pm\sqrt{1-\chi^{-2}},0,0\right)-\tilde{\lambda}I_5\right)=0,$$

we obtain the following eigenvalues

$$\tilde{\lambda}_1=0,\quad \tilde{\lambda}_{2_\pm}=\pm i\sqrt{1-\chi^{-2}},\quad \tilde{\lambda}_{3_\pm}=\pm i\frac{1}{2},$$
$$|\arg(\tilde{\lambda}_{j_\pm})|=\frac{\pi}{2}>\frac{\alpha\pi}{2},\quad j=2,3\quad \text{for}\quad 0<\alpha<1.$$

Consequently, the third and forth equilibrium $\left(\chi^{-1},0,\pm\sqrt{1-\chi^{-2}},0,0\right)$ are stable but not asymptotically stable [77].

3.3.3 Numerical method

In this section, we will use an algorithm based on the Adams-Bashforth-Moulton predictor-corrector scheme (often called the fractional Adams method) [29], to present numerical solution of the fractional mapped equation.

For this purpose we use the same notation of section 3.3.1. Consider the Caputo fractional differential equation :

$$\begin{cases} {}^{C}D_0^{\alpha}\boldsymbol{p}(t)=F(t,\boldsymbol{p}(t)),\quad 0<\alpha<1,\\ \boldsymbol{p}(0)=\boldsymbol{p}_0, \end{cases} \tag{3.12}$$

where $\boldsymbol{p}_0=(\boldsymbol{p}_{10},\boldsymbol{p}_{20},\boldsymbol{p}_{30},\boldsymbol{p}_{40},\boldsymbol{p}_{50})$ is the initial condition vector.

Using the Riemann-Liouville integral, we get,

$$\boldsymbol{p}(t)=\boldsymbol{p}(0)+I_0^{\alpha}(F(t,\boldsymbol{p}(t))),$$

this implies,

$$\boldsymbol{p}(t)=\boldsymbol{p}(0)+\frac{1}{\Gamma(\alpha)}\int_0^t(t-\tau)^{\alpha-1}f(\tau)d\tau,$$

we consider $t_0=0<t_1<\ldots t_k\ldots<t_N=T$ an uniform discretization of interval $[0,T]$ in $N+1$ points. Let $h=\frac{T}{N}$ be the step size.

We will use the fractional Adams method [29] to approximate the fractional integral.

Thus, at the point $t_{n+1}=(n+1)h$ with $h=t_{n+1}-t_n$, we obtain the desired approach for the Caputo-fractional model,

$$\boldsymbol{p}(t_{n+1})=\boldsymbol{p}(0)+\frac{h^{\alpha}}{\Gamma(\alpha+2)}F\left(t_{n+1},\boldsymbol{p}^{p}(t_{n+1})\right)+\frac{h^{\alpha}}{\Gamma(\alpha+2)}\sum_{k=0}^{n}a_{k,n+1}F(t_k,\boldsymbol{p}(t_k)), \tag{3.13}$$

where,

$$a_{k,n+1}=\begin{cases} n^{\alpha+1}-(n-\alpha)(n+1)^{\alpha}, & \text{if } k=0,\\ (n-k+2)^{\alpha+1}+(n-k)^{\alpha+1}-2(n-k+1)^{\alpha+1}, & \text{if } 1\le k\le n,\\ 1, & \text{if } k=n+1. \end{cases}$$

The approximation $p^P(t_{n+1})$ is called predictor and is defined by,

$$\boldsymbol{p}^P(t_{n+1}) = \boldsymbol{p}(0) + \frac{1}{\Gamma(\alpha)} \sum_{k=0}^{n} b_{k,n+1} F(t_k, \boldsymbol{p}(t_k)), \tag{3.14}$$

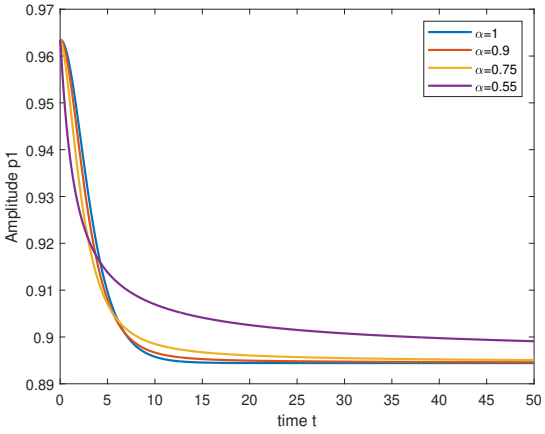
where,

$$b_{k,n+1} = \frac{h^\alpha}{\alpha} \left((n+1-k)^\alpha - (n-k)^\alpha \right). \tag{3.15}$$

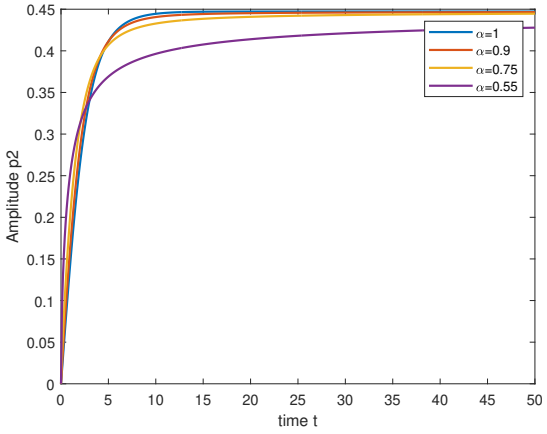
3.4 Discussion

3.4.1 Tank-treading mode

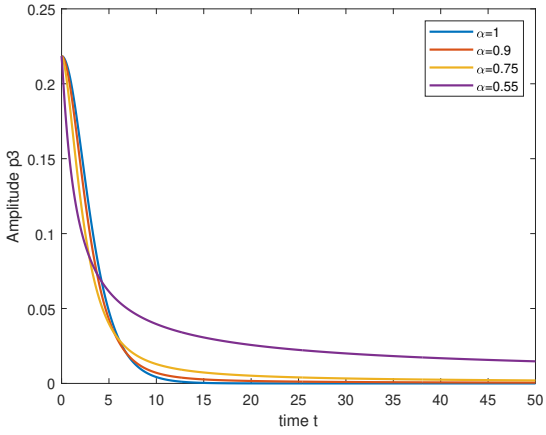
Figure 3.2 shows an instance of the dynamics of $F_{2\pm1}$ modes (components $\boldsymbol{p}_4$ and $\boldsymbol{p}_5$), which oscillate and reach 0 asymptotically for $t \to \infty$.
The outcome acquired from Figure 3.1 and Figure 3.2 reveals that the approximation of $\boldsymbol{p}$ for Caputo operator predicts a run motion equivalent to the tank-treading mode for vesicles [2].



((a)) The time evolution of $\boldsymbol{p}_1$ for Caputo operator.



((b)) The time evolution of $\boldsymbol{p}_2$ for Caputo operator.

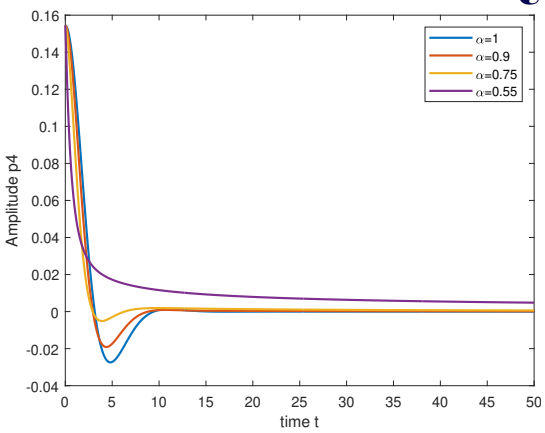


((c)) The time evolution of $\boldsymbol{p}_3$ for Caputo operator.

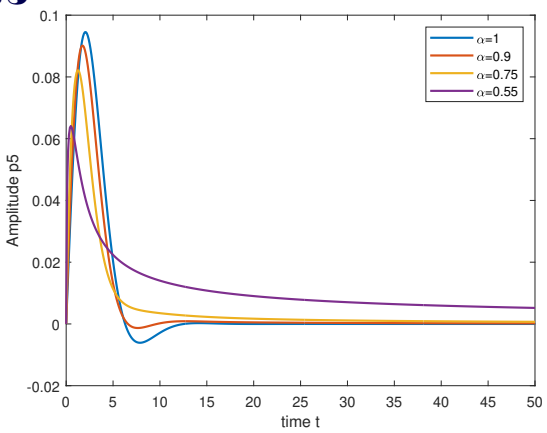
Figure 3.1: The representation of the numerical solutions of the fractional model obtained for the classical components $\boldsymbol{p}_1, \boldsymbol{p}_2$ and $\boldsymbol{p}_3$ for four arbitrary values of fractional order. Parameters are : $\chi = 0.4\sqrt{5}, \gamma = 1, a = c = 0.2\sqrt{5}$ and $b = 2\sqrt{0.1}$.

Since $\boldsymbol{p}_1$ and $\boldsymbol{p}_2$ are connected to the shape deformation and the orientation angle for a rigid sphere, respectively, $\mathscr{R}$ and φ (10), thus at the point $t_{n+1} = (n+1)h$ with $h = t_{n+1} - t_n$, we get the following approximations,

$$\mathscr{R}(t_{n+1}) = \sqrt{\boldsymbol{p}_1^2(t_{n+1}) + \boldsymbol{p}_2^2(t_{n+1})}, \quad \varphi(t_{n+1}) = \tan^{-1}\left(\frac{\boldsymbol{p}_2(t_{n+1})}{\boldsymbol{p}_1(t_{n+1})}\right). \tag{3.16}$$



((a)) The time evolution of $\boldsymbol{p}_4$ for Caputo operator.



((b)) The time evolution of $\boldsymbol{p}_5$ for Caputo operator.

Figure 3.2: The representation of the numerical solutions of the fractional model obtained for the dynamics of the components of F_{21} for four arbitrary values of fractional order. Parameters are : $\chi = 0.4\sqrt{5}, \gamma = 1, a = c = 0.2\sqrt{5}$ and $b = 2\sqrt{0.1}$.

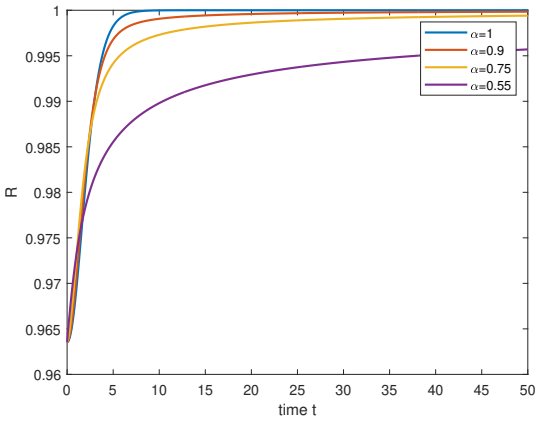


Figure 3.3: The shape deformation $\mathscr{R}$ of the particle for four arbitrary values of fractional order. Parameters are : $\chi = 0.4\sqrt{5}, \gamma = 1, a = c = 0.2\sqrt{5}$ and $b = 2\sqrt{0.1}$.

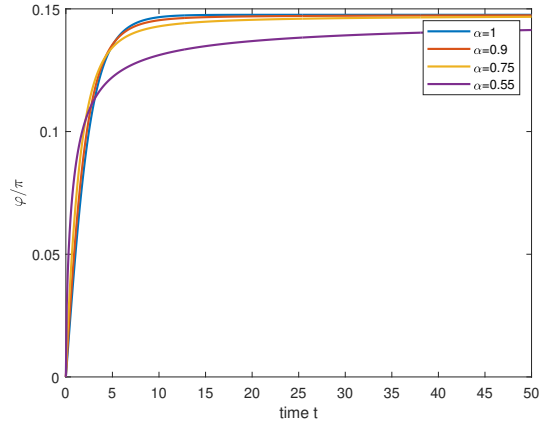


Figure 3.4: The orientation angle φ of the particle for four arbitrary values of fractional order. Parameters are : $\chi = 0.4\sqrt{5}, \gamma = 1, a = c = 0.2\sqrt{5}$ and $b = 2\sqrt{0.1}$

Figures 3.3 and 3.4 depict an instance of the shape deviation $\mathscr{R}$ and the orientation angle ψ for different values of α. Moreover, the solutions show that $\mathscr{R}$ tends to 1 and ψ remains constant for various α values, demonstrating that the unit vector p, which represents the projection of a rigid sphere [2], exhibits run motion.

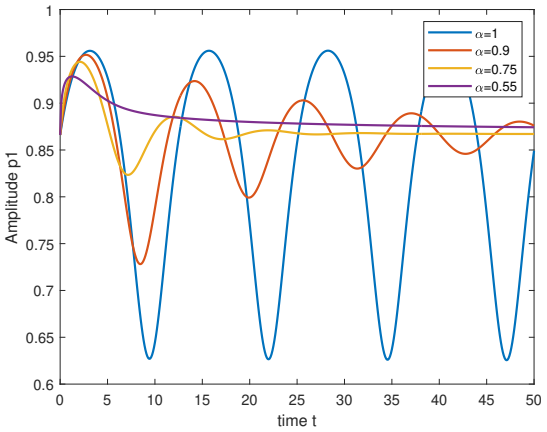
Figure 3.1 and 3.2 confirm that p tends to $\left(\chi, +\sqrt{1-\chi^2}, 0, 0, 0\right)$ independently of the initial orientation, which is in perfect accord with our theoretical finding about the stability of this equilibrium. Further, the terminal vector lies in the shear plane, which corresponds to the tank-treading for the vesicle.

In this case, it is apparent from the above figures that the order of the fractional derivative

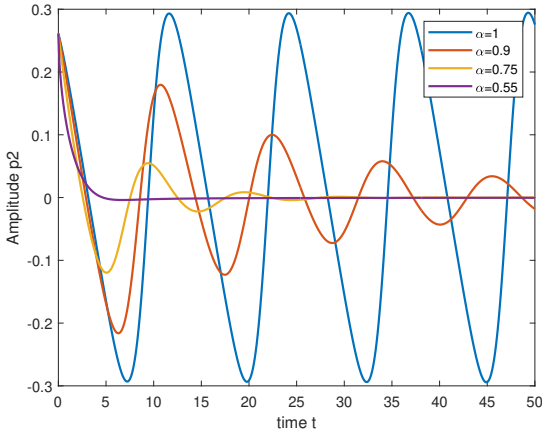
has no influence on the stability of the equilibrium. Therefore, increasing the value of α, which represents the longer memory time, allows the solutions to converge to the steady state more quickly. That is, the strength of memory effects, which are controlled by α, has a strong influence on the dynamics of rigid particles. As an outcome, the dynamics of the vesicle depends on the current time as well as the time history, which may be efficiently represented using the notions of fractional calculus. By incorporating the Caputo fractional derivative, we present a much more realistic model.

3.4.2 Tumbling and Vacillating-breathing modes

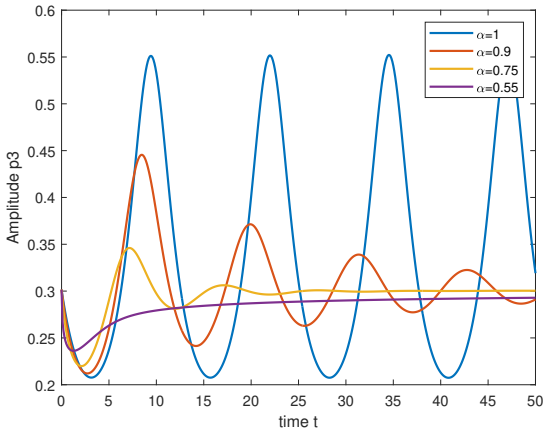
Now, we move to the most interesting case $\chi > 1$.
Let us see how the fractional-order parameter α when $\chi > 1$ can affect the dynamics of the vector p of the rigid particle problem and how it influences the three modes (TT,VB, and TB).
In this case, our theoretical findings reveal that the fractional order derivative α has a strong influence on the stability of the equilibrium, while in the classical order (that is, $\alpha = 1$), nothing can be deduced concerning the stability. Further, the following graphical representations are in agreement with our theoretical results.



((a)) The time evolution of $\boldsymbol{p}_1$ for Caputo operator.



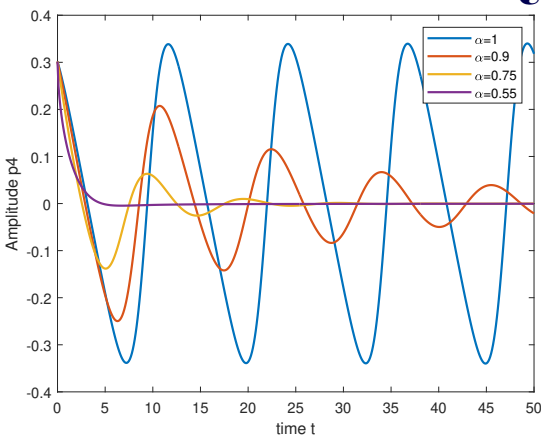
((b)) The time evolution of $\boldsymbol{p}_2$ for Caputo operator.



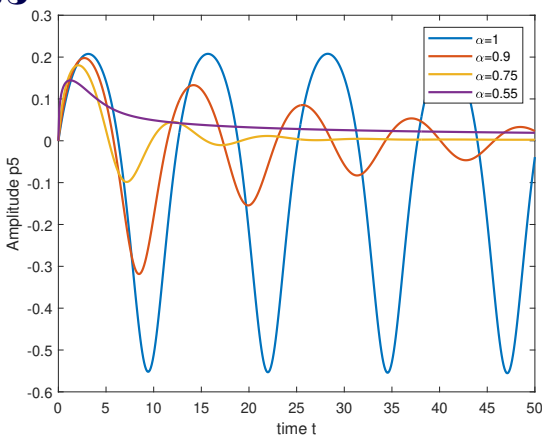
((c)) The time evolution of $\boldsymbol{p}_3$ for Caputo operator.

Figure 3.5: The representation of the numerical solutions of the fractional model obtained for the classical components $\boldsymbol{p}_1, \boldsymbol{p}_2$ and $\boldsymbol{p}_3$ for four arbitrary values of fractional order. Parameters are : $\chi = 2/\sqrt{3}, \gamma = 1, a = 2\sqrt{(}11)/3$, $\Gamma = \sqrt{(11)/3}$ and $b = c = 1$.

In Figure 3.5, we have plotted the time evolution of the $\boldsymbol{p}_1$, $\boldsymbol{p}_2$, and $\boldsymbol{p}_3$ amplitudes for the Caputo operator for $\chi = 2/\sqrt{3}$ and with four different values of α.
Moreover, these graphics depict a cosine form that varies depending on the order of the fractional derivative α. We can clearly observe that when $\alpha = 1$, we have oscillations of the F_{22} and F_{20} modes (equivalently $\boldsymbol{p}_1, \boldsymbol{p}_2$, and $\boldsymbol{p}_3$). However, for $0 < \alpha < 1$, which is the crux of this investigation, the amplitude is seen to decrease as α decreases.



((a)) The time evolution of $\boldsymbol{p}_4$ for Caputo operator.



((b)) The time evolution of $\boldsymbol{p}_5$ for Caputo operator.

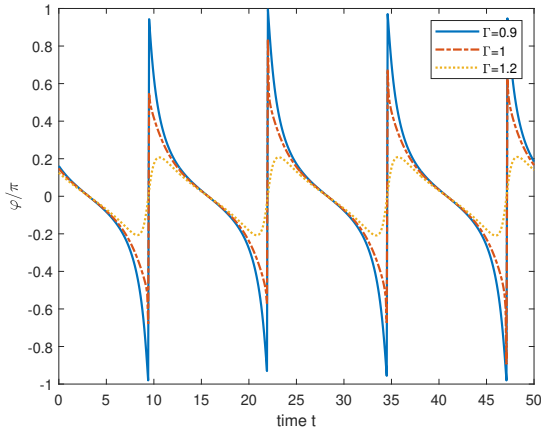
Figure 3.6: The representation of the numerical solutions of the fractional model obtained for the dynamics of the components of F_{21} for four arbitrary values of fractional order. Parameters are : $\chi = 2/\sqrt{3}, \gamma = 1, a = 2\sqrt{(}11)/3$, $\Gamma = \sqrt{(11)/3}$ and $b = c = 1$.

Let's move to the case where the main axis of the vesicle does not go back to the shear plane (*i.e* $F_{2\pm1} \neq 0$). Figure 3.6 depicts the behaviour of $F_{2\pm1}$ modes for four different α values. When $\alpha = 1$, the components $\boldsymbol{p}_4$ and $\boldsymbol{p}_5$ predict an oscillation mode that can be represented by TB or VB; however, when $0 < \alpha < 1$, the amplitudes decrease, indicating that the rigid particles predict another regime instead of the pure TB or VB.
[2] demonstrated that for $\chi < 1$, each initial condition tends to the same end point, as opposed to the case where $\chi > 1$ where the choice of initial conditions, particularly Γ, has an effect on the type of motion. In the next part, we are going to see how the choice of initial conditions and the fractional order influence the dynamics of the particle.

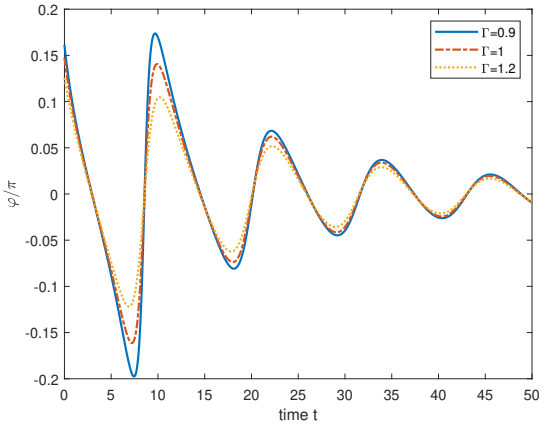
3.4.3 The effect of initial conditions and fractional order on dynamics

Let's analyse this more deeply to see how the order of the derivative can influence the three regimes. It is known that the initial conditions Γ has a big impact on the two types of motions selected (TB and VB) [2]. Herein, we have plotted in Figure 3.7 the dynamic of the orientation angle for three distinct Γ values, as well as several α values and when the parameter χ is fixed. When $\alpha = 1$ (i.e., the classical derivative), the orientation angle of the rigid sphere reveals a periodic regime [2], which corresponds to the TB or VB regime depending on the value of Γ. However, when $0 < \alpha < 1$, it is obvious that the parameter Γ has completely lost its impact on the two types of motion where the curves predict oscillations with decreasing amplitudes as α decreases. Whatever the value of Γ, which is the same thing for the shape deviation, which also represents a cosine form with decreasing amplitudes as α decreases, as illustrated in Figure 3.8 with three different values of Γ and varied α values.
As a result, the fractional derivative considers not only the initial shape but also the entirety of

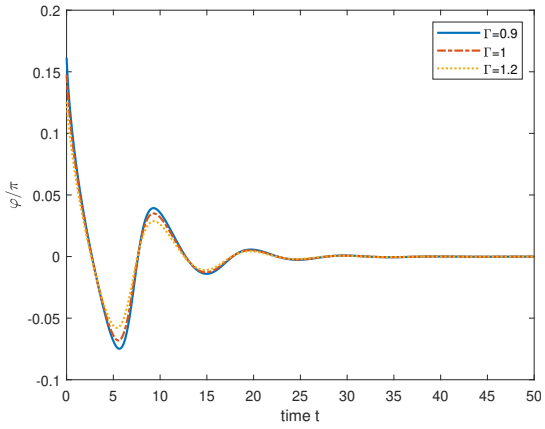
the instant, during which it is expected that some degree of memory would be conserved. Further, these graphics indicate that when α increases, we tend more slowly toward equilibrium.



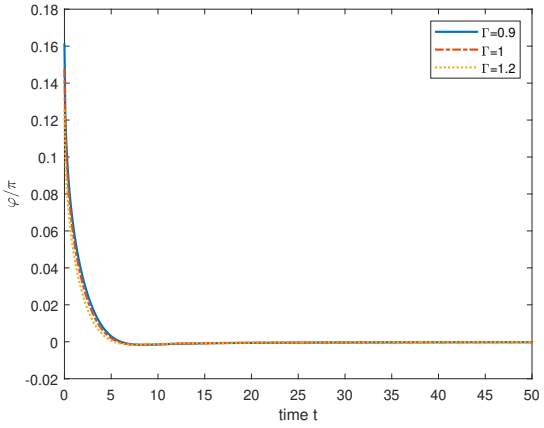
((a)) Dynamics of the orientation angle φ when $\alpha = 1$.



((b)) Dynamics of the orientation angle φ when $\alpha = 0.95$.

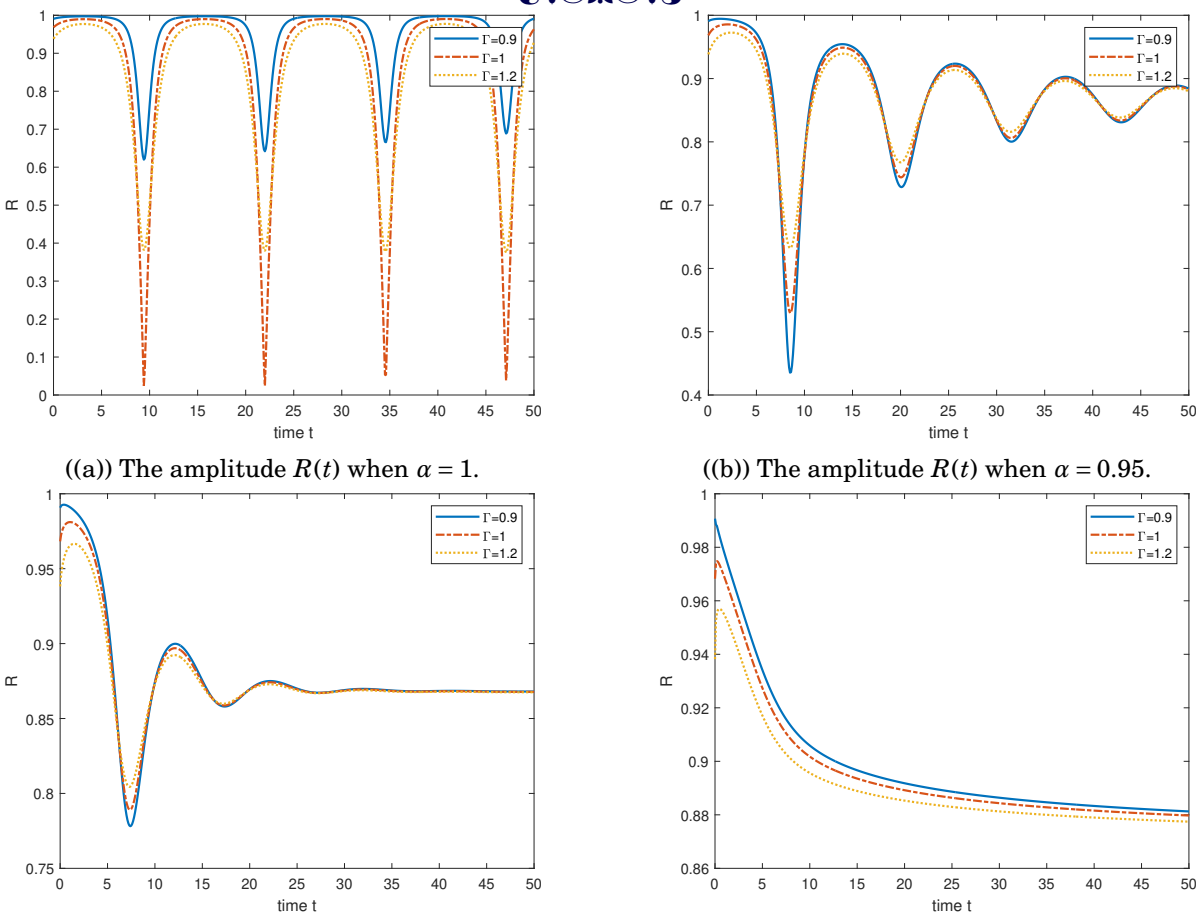


((c)) Dynamics of the orientation angle φ when $\alpha = 0.75$.



((d)) Dynamics of the orientation angle φ when $\alpha = 0.55$.

Figure 3.7: The behavior of the orientation angle φ for four arbitrary values of fractional order. Parameters are : $\chi = 2/\sqrt{3}, \gamma = 1$ with $\Gamma = 0.9$, $\Gamma = 1$ and $\Gamma = 1.2$.



((a)) The amplitude $R(t)$ when $\alpha = 1$.

((b)) The amplitude $R(t)$ when $\alpha = 0.95$.

((c)) The amplitude $R(t)$ when $\alpha = 0.75$.

((d)) The amplitude $R(t)$ when $\alpha = 0.55$.

Figure 3.8: The dynamic of the particle contour for four arbitrary values of fractional order. Parameters are : $\chi = 2/\sqrt{3}, \gamma = 1$ with $\Gamma = 0.9$, $\Gamma = 1$ and $\Gamma = 1.2$.

Figures 3.7 and 3.8 indicate that the orientation angle and shape deformation represent cosine forms with decreasing amplitude as α decreases for any value of Γ (whatever the beginning conditions). In other words, these regimes can be described by TT with over-damped vesicle oscillations (TT-OD) and TT with under-damped vesicle oscillations (TT-UD). Moreover, Figures 3.8(b) and 3.7(b) reveal that when α approaches 1, there are oscillations through the equilibrium that indicate TT-UD oscillations, which signifies that the TT mode is on the verge of losing its stability to the VB mode.

3.5 Conclusion

Given that vesicle dynamics involve memory, in this work we provide an analysis based on the memory effect specifically on fractional-order derivatives of mapping vesicle dynamics onto rigid particles in five dimensions using the Caputo fractional operator. We have adopted the Adams-Bashforth-Moulton predictor-corrector scheme (often called the fractional Adams method) to

demonstrate numerically that the fractional model gives more interesting and accurate outcomes.

We demonstrated that when $\chi < 1$, the fractional order α has no effect on the stability of the equilibria, but it does affect the time required to reach the steady states. Therefore, the analytical and numerical results demonstrate that, for increasing values of α, the solution converges more quickly to its stationary state. Herein, the vesicle predicts a TT regime. On the other hand, when $\chi > 1$, we have proved the stability of the two equilibrium points, which was not obtained in the case of the classical order (i.e., $\alpha = 1$), where nothing can be deduced about the stability.

Moreover, as a result of using the fractional Caputo derivative, the vesicle exhibits small oscillations instead of the pure TT, VB, or TB motion that we have represented here by the tank-treading with over-damped (TT-OD) and under-damped (TT-UD) vesicle oscillations, depending on the value of α, which influences the two regimes regardless of the value of Γ (i.e., the initial conditions). This proves the existence of intermediate regimes between TT and VB that cannot be observed using the classical derivative.

CHAPTER 4

ANALYTICAL INVESTIGATION OF VESICLE DYNAMICS VIA THE MODIFIED RIEMANN–LIOUVILLE FRACTIONAL DERIVATIVE: MITTAG-LEFFLER FUNCTION SOLUTION AND COMPARATIVE ANALYSIS WITH CAPUTO'S DERIVATIVE

Contents

4.1 Introduction **81**

4.2 From fractional general orientation equations to fractional five-dimensional mapping **82**

4.3 Exact Solutions and Interpretation of Fractional Mapping Equations **84**

4.3.1 TT-mode 85

4.3.2 Damping-TT modes 89

4.4 Comparative analysis of the two fractional derivatives **96**

4.5 Conclusion **105**

4.1 Introduction

In the previous chapter, we utilized the Caputo derivative to approximate solutions for vesicle dynamics under shear flow. This approach provided valuable insights into the behavior of vesicles, particularly in understanding their deformation and orientation in the presence of memory effects. While the Caputo derivative offered a robust framework for these approximations, it was not sufficient to capture the full complexity of the system, especially when aiming for exact analytical solutions.

In this chapter, we advance our analysis by employing the modified Riemann-Liouville derivative, which enables us to derive exact solutions for the vesicle's motion. This method not only enhances the mathematical rigor of our model but also allows for a detailed comparison with the previously obtained approximate results. By contrasting these two approaches Caputo's approximation and the exact solutions provided by the Riemann-Liouville derivative we aim to shed light on the impact of memory effects on vesicle dynamics and assess the suitability of fractional calculus in accurately describing these complex physical systems.

Moreover, this comparative analysis between the Caputo and modified Riemann-Liouville derivatives serves as a critical step in determining the most effective mathematical tool for modeling vesicle behavior. The Caputo derivative, widely used for its ability to handle initial conditions in a physically meaningful way, provided approximate solutions that were insightful for capturing general trends. However, the modified Riemann-Liouville derivative, with its distinct properties, offers a more precise and comprehensive representation of systems with memory effects, enabling us to resolve the vesicle's orientation and shape dynamics exactly.

Through this chapter, we not only aim to highlight the advantages of achieving exact solutions but also to explore the implications of using different fractional operators in modeling complex biological systems. This comparative framework will deepen our understanding of the underlying mechanisms governing vesicle dynamics, offering clearer insights into the role of memory and non-local effects in such systems.

This chapter is organized as follows: Section 4.2 presents the formulation of the fractional evolution equation and the mapped fractional equation, alongside an analysis of the local stability of equilibrium points. Section 4.3, which constitutes the central part of our study, focuses on the computation of exact solutions and an in-depth discussion of the dynamic modes observed. Section 4.4 offers a comparative analysis of the modified Riemann-Liouville and Caputo fractional derivatives within the framework of vesicle dynamics. Finally, Section 4.5 concludes the study, summarizing key insights from the preceding sections. The results of this chapter are based on the paper [12].

4.2 From fractional general orientation equations to fractional five-dimensional mapping

For the reader's convenience, in this section, we will offer a detailed overview of the fractional vesicle model within the scope of small deformation theory. This comprehensive overview aims to facilitate a deeper understanding of the model central to this chapter. The objective is to replace the classical derivative in the evolution equation (8) with Jumarie's fractional derivative, and this substitution leads to

$$ {}^{\mathcal{J}}D_t^{\alpha}F_{2m} = \gamma\left\{-i\frac{m}{2}\delta_{2|m|}h + i\frac{m}{2}F_{2m} - h\sqrt{\frac{6}{5\pi}}\mathscr{C}_{\kappa}^{-1}(6+\sigma_0)F_{2m}\right\}, \tag{4.1}$$

where ${}^{\mathcal{J}}D_t^{\alpha}$ is the Jumarie's modified Riemann-Liouville derivative, $0 < \alpha \leq 1$.
Using the fixed total area constraint (6) and the basic properties of the Jumarie derivative, the expression for σ_0 is derived as follows,

$$ \sigma_0 = i\Delta^{-1}\mathscr{C}_{\kappa}\sqrt{\frac{10\pi}{3}}\,(F_{22} - F_{2-2}) - 6. \tag{4.2}$$

Therefore, by substituting σ_0 into the fractional evolution equation (4.1), we observe that the equation remains independent of the bending parameter, $\mathscr{C}_{\kappa}$,

$$ {}^{\mathcal{J}}D_t^{\alpha}F_{2m} = \gamma\left\{-i\frac{m}{2}\delta_{2|m|}h + i\frac{m}{2}F_{2m} + \frac{4h}{\Delta}\left(F_{22}^{*} - F_{22}\right)F_{2m}\right\}, \tag{4.3}$$

where F_{22}^{*} is the complex conjugate of F_{22}. It describes the evolution of quasi-spherical vesicle shapes, a topic that has been previously explored in references [2, 37, 64] within a classical framework.
Additionally, the evolution of the vesicle shape over time in the shear plane is described by the dynamics of F_{22}. It is obvious that the vesicle can deviate from the shear plane, the F_{20} and F_{21} modes describe the out of shear plane. Furthermore, we find from the evolution equation that F_{21} can be determined through the information provided by F_{20}, which is an efficient property confirmed from equation (4.3). Indeed, F_{21} fulfil the following expression:

$$ {}^{\mathcal{J}}D_t^{\alpha}\left(E_{\alpha}(-\frac{i\gamma}{2}t^{\alpha})F_{21}\right) = \gamma\left\{\frac{4h}{\Delta}\,\mathrm{Im}(F_{22})F_{21}E_{\alpha}(-\frac{i\gamma}{2}t^{\alpha})\right\}. \tag{4.4}$$

It is evident that the F_{20} mode and the function $E_{\alpha}(-i\gamma/2t^{\alpha})F_{21}$ satisfy the identical equation. This specifically implies that:

$$ {}^{\mathcal{J}}D_t^{\alpha}\left(E_{\alpha}(-\frac{i\gamma}{2}t^{\alpha})F_{21}F_{20}^{-1}\right) = 0. \tag{4.5}$$

As a consequence, there is a complex parameter, denoted as C, which verifies

$$ F_{21} = C.E_{\alpha}(\frac{i\gamma}{2}t^{\alpha})F_{20}. \tag{4.6}$$

In this context, we explore the transformation of the vesicle problem into that of a rigid sphere. To derive the transformed equation, the approach involves decomposing complex amplitudes into their real and imaginary parts, as detailed in (11), this decomposition results in the following fractional mapped equation,

$$ {}^{\mathscr{J}}D_t^{\alpha}\boldsymbol{p} = \gamma\left\{\Omega\cdot\boldsymbol{p} + \Lambda^{-1}(e_2 - e_2\cdot\boldsymbol{p}\boldsymbol{p})\right\}. \tag{4.7} $$

Here, $\boldsymbol{p}$ is defined as $\boldsymbol{p} = \frac{2}{\sqrt{\Delta}}\left(f_{22}, \tilde{f}_{22}, f_{20}, f_{21}, \tilde{f}_{21}\right), e_2 = (0,1,0,0,0), \Lambda = \sqrt{\Delta}/(2h)$, incorporating all the physical parameters, and a vorticity tensor Ω is expressed as (14) which is antisymmetric, ensuring that for every vector $\boldsymbol{p}$, we have $\boldsymbol{p}.\Omega.\boldsymbol{p} = 0$. When discussing vesicle behaviour under the small deformation approach, we observe that vesicle behaviour is entirely determined by the vector $\boldsymbol{p}$ in $\mathbb{R}^5$ ($\boldsymbol{p}$ is a unit vector from the constraint (6)). Moreover, the preservation of its norm is assured; by using (4.7), we automatically get $\boldsymbol{p}.{}^{\mathscr{J}}D_t^{\alpha}\boldsymbol{p} = 0$.
To enable a quality discussion regarding the various motions, it is more practical to transform the equation that has been mapped into the subsequent two systems

$$ \begin{aligned} {}^{\mathscr{J}}D_t^{\alpha}\boldsymbol{p}_1 &= \gamma\left(\boldsymbol{p}_2 - \Lambda^{-1}\boldsymbol{p}_2\boldsymbol{p}_1\right), \\ {}^{\mathscr{J}}D_t^{\alpha}\boldsymbol{p}_2 &= \gamma\left(\Lambda^{-1} - \boldsymbol{p}_1 - \Lambda^{-1}\boldsymbol{p}_2^2\right), \\ {}^{\mathscr{J}}D_t^{\alpha}\boldsymbol{p}_3 &= \gamma\left(-\Lambda^{-1}\boldsymbol{p}_2\boldsymbol{p}_3\right), \end{aligned} \tag{4.8} $$

$$ \begin{aligned} {}^{\mathscr{J}}D_t^{\alpha}\boldsymbol{p}_4 &= \gamma\left(-\Lambda^{-1}\boldsymbol{p}_2\boldsymbol{p}_4 - \frac{1}{2}\boldsymbol{p}_5\right), \\ {}^{\mathscr{J}}D_t^{\alpha}\boldsymbol{p}_5 &= \gamma\left(\frac{1}{2}\boldsymbol{p}_4 - \Lambda^{-1}\boldsymbol{p}_2\boldsymbol{p}_5\right). \end{aligned} \tag{4.9} $$

System (4.8) describes dynamics within the shear plane, where $F_{2\mp1} = 0$, while system (4.9) describes dynamics outside the plane, with $F_{2\mp1} \neq 0$. The equation (4.7), which has been mapped, was exactly solved in Reference [2] using the classical derivative. Furthermore, the fractional mapped equation, utilising the Caputo fractional derivative. It is worth noting that the system above has equilibrium points that depend on the parameter Λ:

$$ \left(\Lambda, \pm\sqrt{1-\Lambda^2}, 0, 0, 0\right), $$

for $\Lambda < 1$ where $\left(\Lambda, \sqrt{1-\Lambda^2}, 0, 0, 0\right)$, is asymptotically stable and $\left(\Lambda, -\sqrt{1-\Lambda^2}, 0, 0, 0\right)$ is completely unstable, and for $\Lambda > 1$,

$$ \left(\Lambda^{-1}, 0, \pm\sqrt{1-\Lambda^{-2}}, 0, 0\right), $$

which are stable. We have investigated the local stability of fractional system solutions using the Theorem 1.2.3, where we have demonstrated that in this case we can deduce the stability in contrast to the classical derivative, where nothing can be deduced 3.

4.3 Exact Solutions and Interpretation of Fractional Mapping Equations

The purpose of this part is to find all solutions that ensure the physical constraints (**??**), which means finding all physical solutions. Therefore, in this part, we provide exact solutions to systems (4.8), as well as system (4.9) by using the fundamental properties of the modified Riemann-Liouville fractional derivative outlined in Chapter 1. Our objective is to evaluate the influence not only of the parameter Λ but also of the fractional derivative α, aiming to elucidate the effects of the memory phenomenon on the vesicle's mobility.
We will next introduce the function

$$\phi = \frac{\boldsymbol{p}_1 - \Lambda^{-1}}{\boldsymbol{p}_2}, \tag{4.10}$$

from (4.8) and (4.10), we deduce that,

$$^{\mathscr{J}}D_t^{\alpha}\phi = \gamma\left(\phi^2 + 1 - \Lambda^{-2}\right), \tag{4.11}$$

With D_t^{α} representing the Jumarie's modified Riemann-Liouville fractional operator of order $0 < \alpha \leq 1$, and $\Lambda = \frac{\sqrt{\Lambda}}{2h}$, our research centers on the precise instance where $\gamma = 1$. Zang et al. initially proposed five solutions to equation (4.10) in [92], depending on the sign of $1 - \Lambda^{-2}$. The following expressions for the solution are particularly intriguing for our investigation:

$$\phi(t) = -B\frac{E_{\alpha}(Bt^{\alpha}) + C_1 E_{\alpha}(-Bt^{\alpha})}{E_{\alpha}(Bt^{\alpha}) - C_1 E_{\alpha}(-Bt^{\alpha})}, \tag{4.12}$$

for $\Lambda < 1$, and for $\Lambda > 1$,

$$\phi(t) = B\tan_{\alpha}\left(B^{\frac{1}{\alpha}}t + C_1'\right), \tag{4.13}$$

where, C_1 and C_1' are constant that depend on initial conditions , and $B = \sqrt{|1 - \Lambda^{-2}|}$.
After obtaining explicit formulations for ϕ, the subsequent step involves solving system (4.8) and undertaking a comprehensive analytical exploration of the distinct regimes, which were investigated numerically in [15]. The incorporation of expressions (4.12) and (4.13) into system (4.8) results once more in the formulation of a fractional differential equation.

$$^{\mathscr{J}}D_t^{\alpha}\boldsymbol{p}_2 = -\phi(t)\boldsymbol{p}_2 - \Lambda^{-1}\boldsymbol{p}_2^2. \tag{4.14}$$

As mentioned in the introduction, the system (12) was initially solved analytically, employing the classical derivative [2, 37]. In this context, we aim to extend the order of the derivative using the modified Riemann-Liouville fractional derivative in order to provide the analytical solution in cases where $F_{2\pm1} \neq 0$, utilising the modified Riemann-Liouville fractional operator.

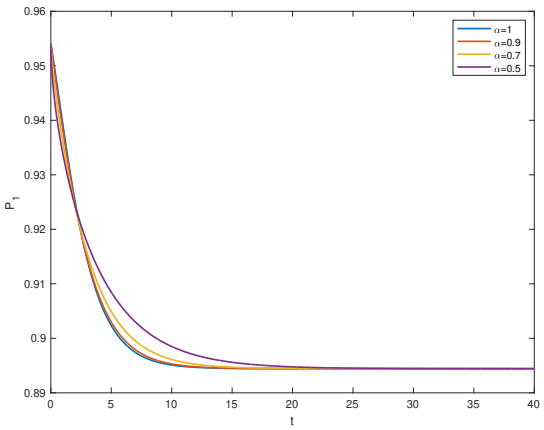
4.3.1 TT-mode

In this part, we delve into the intriguing tank-treading mode (TT-mode), a distinctive behaviour that emerges in specific scenarios. This behaviour is explored through the utilisation of the key function of the fractional derivative, Mittag-Leffler, known for its significance in fractional calculus. With the combined insights from the Mittag-Leffler and the Jumarie fractional derivatives, the ensuing expressions indicate the emergence of the tank-treading mode,

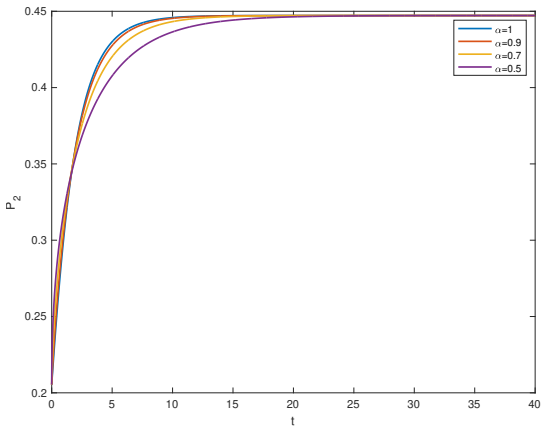
$$\boldsymbol{p}_1 = \Lambda.\frac{C_2\Lambda^{-1} + E_\alpha(Bt^\alpha) + C_1E_\alpha(-Bt^\alpha)}{C_2 + E_\alpha(Bt^\alpha) + C_1E_\alpha(-Bt^\alpha)}, \tag{4.15}$$

$$\boldsymbol{p}_2 = B\Lambda.\frac{E_\alpha(Bt^\alpha) - C_1E_\alpha(-Bt^\alpha)}{C_2 + E_\alpha(Bt^\alpha) + C_1E_\alpha(-Bt^\alpha)}, \tag{4.16}$$

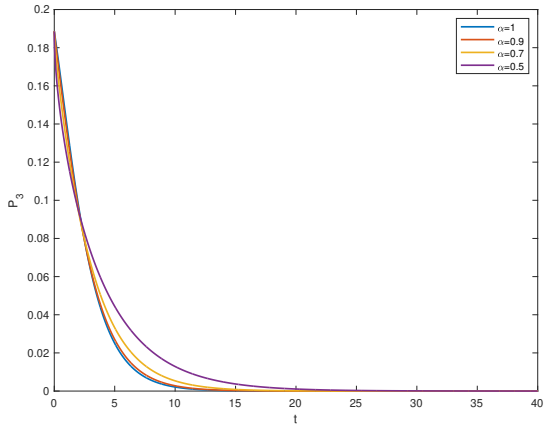
$$\boldsymbol{p}_3 = \frac{BC_3}{C_2 + E_\alpha(Bt^\alpha) + C_1E_\alpha(-Bt^\alpha)}, \tag{4.17}$$



((a)) The time evolution of p_1 for the Modified Riemann-Liouville operator.



((b)) The time evolution of p_2 for the Modified Riemann-Liouville operator.



((c)) The time evolution of p_3 for the Modified Riemann-Liouville operator.

Figure 4.1: The depiction of the exact solutions for the fractional mapped equation acquired for $\boldsymbol{p}_1, \boldsymbol{p}_2$ and $\boldsymbol{p}_3$ is presented for four distinct values of α , denoting the fractional order.

Moreover, through the introduction of the novel function

$$g = \boldsymbol{p}_4 + i\boldsymbol{p}_5, \tag{4.18}$$

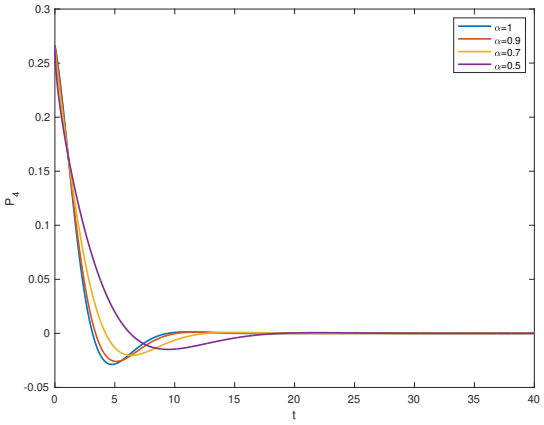
which satisfies the following equation

$${}^{\mathcal{J}}D_t^{\alpha} g = \left(-\Lambda^{-1}\boldsymbol{p}_2 + \frac{i}{2}\right)g, \tag{4.19}$$

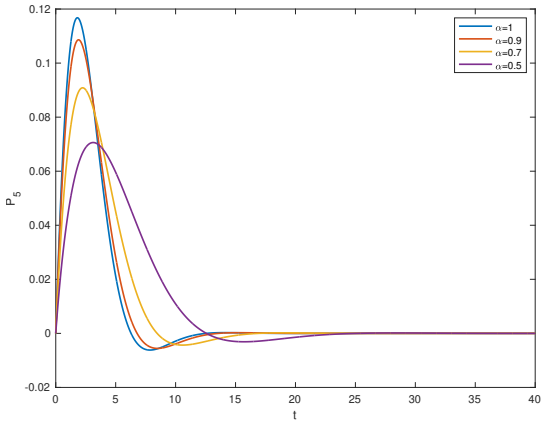
by employing the properties of the Jumarie's modified Riemann-Liouville derivative and the formulation of $\boldsymbol{p}_2$, we can determine the expressions for $\boldsymbol{p}_4$ and $\boldsymbol{p}_5$,

$$\boldsymbol{p}_4 = \frac{C_4 cos_{\alpha}\left(\left(\frac{1}{2}\right)^{\frac{1}{\alpha}} t\right)}{C_2 + E_{\alpha}(Bt^{\alpha}) + C_1 E_{\alpha}(-Bt^{\alpha})}, \tag{4.20}$$

$$\boldsymbol{p}_5 = \frac{C_4 sin_{\alpha}\left(\left(\frac{1}{2}\right)^{\frac{1}{\alpha}} t\right)}{C_2 + E_{\alpha}(Bt^{\alpha}) + C_1 E_{\alpha}(-Bt^{\alpha})}. \tag{4.21}$$



((a)) The time evolution of p_4 for the Modified Riemann-Liouville operator.



((b)) The time evolution of p_5 for the Modified Riemann-Liouville operator.

Figure 4.2: The depiction of the exact solutions for the fractional mapped equation acquired for F_{21} modes is presented for four distinct values of α , denoting the fractional order.

Figure 4.1 illustrates the dynamics of $\boldsymbol{p}_1$,$\boldsymbol{p}_2$, and $\boldsymbol{p}_3$ converging toward a stable point. In contrast, Figure 4.2 demonstrates the dynamics of $\boldsymbol{p}_4$ and $\boldsymbol{p}_5$, which exhibit oscillations approaching zero asymptotically as t tends to ∞. The insights derived from Figures 4.1 and 4.2 indicate that the Jumarie operator's of $\boldsymbol{p}$ predicts the tank-treading regime for vesicles.

As highlighted above, the orientation angle characterizes the different motions of vesicles. The first motion, TT, involves ψ converging towards a constant value over an extended period. The second motion, TB, entails the vesicle completing a full rotation, where the angle oscillates between $\frac{-\pi}{2}$ and $\frac{\pi}{2}$. In this context, a rotation through an angle of π is considered a full rotation, as the vesicle remains unchanged under such rotation. The third motion, VB, ψ oscillates within

two values in $[\frac{-\pi}{4}, \frac{\pi}{4}]$.

To clarify how the dynamics of a rigid body translate into the dynamics of a deformable particle, we raise the following question:If the behavior of a deformed object, such as a vesicle, is depicted on a rigid body (rigid sphere), where does the deformation remain concealed? This question will be examined in more detail during the upcoming discussions.

To answer this question, we represent the two-dimensional projection $\mathbf{p}_\perp$ of $\boldsymbol{p}$ in the (e_1, e_2) plane, which is given by (15) with φ is the angle formed by the vector $\mathbf{p}_\perp$ and the e_1 axis, represents the orientation angle, as illustrated in Figure 4.3, where $\varphi \in [-\pi, \pi]$.

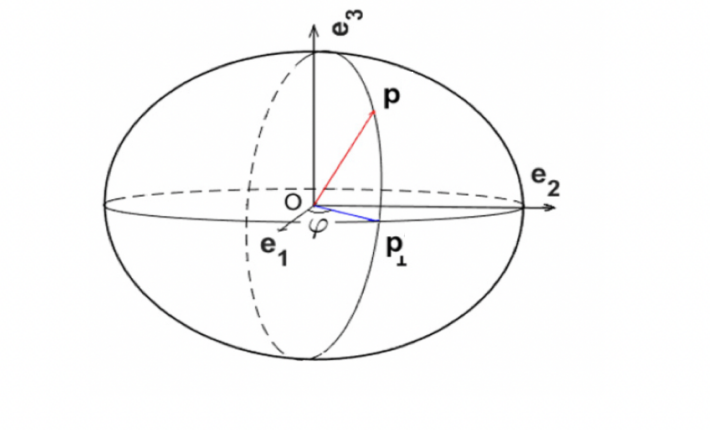


Figure 4.3: The projection of $\mathbf{p}$ onto the plane is denoted as $\mathbf{p}_\perp$, forming an angle φ with the e_1 axis [2].

Therefore, the deformation amplitude ($\mathscr{R}$) and the orientation angle (φ) satisfy a system analogous to (2.1)

$$\begin{aligned} {}^{\mathscr{J}}D_t^{\alpha}\mathscr{R} &= \gamma\left\{\Lambda^{-1}\sin(\varphi)\left(1-\mathscr{R}^2\right)\right\}, \\ {}^{\mathscr{J}}D_t^{\alpha}\varphi &= \gamma\left\{-1+\frac{\Lambda^{-1}}{\mathscr{R}}\cos(\varphi)\right\}, \end{aligned} \tag{4.22}$$

Subsequently, the projection $\mathbf{p}_\perp$ of the polarisation vector $\boldsymbol{p}$ from the rigid body allows for an understanding of the connection between the two systems. Moreover, the norm of $\mathbf{p}_\perp$ is equal to $\mathscr{R}$, while φ represents twice the angle formed by the vesicle's principal axis with the direction of the flow. When the projection $\mathbf{p}_\perp$ maintains a constant orientation in the plane (e_1, e_2), it implies that φ is constant. Furthermore, the norm of $\mathbf{p}_\perp$ remains fixed, indicating a constant deformation of the shape $\mathscr{R}$. If the angle φ and $\mathscr{R}$ remain constant, it signifies that the vector $\boldsymbol{p}$ retains a constant orientation.

Our results show that the run mode is connected to $F_{2\pm1}$ mode oscillations, even without deformation along the vorticity axis. Specifically, $\boldsymbol{p}_4$ and $\boldsymbol{p}_5$ (or equivalently, the $F_{2\pm1}$ modes) undergo an infinite number of oscillations through 0 and asymptotically approach 0.

Now, let's examine how the dynamics of $\boldsymbol{p}$ in the rigid sphere problem can be linked with the

tank-treading mode for vesicles, particularly when $\Lambda < 1$.
The shape deformation fulfils

$$\mathscr{R}^2(t) = \Lambda^2 \frac{\left(C_2\Lambda^{-1} + E_\alpha(Bt^\alpha) + C_1E_\alpha(-Bt^\alpha)\right)^2 + B^2\left(E_\alpha(Bt^\alpha) - C_1E_\alpha(-Bt^\alpha)\right)^2}{\left(C_2 + E_\alpha(Bt^\alpha) + C_1E_\alpha(-Bt^\alpha)\right)^2}, \tag{4.23}$$

and the inclination angle can be expressed in the following form

$$\varphi(t) = \arctan\left(B\Lambda \frac{E_\alpha(Bt^\alpha) - C_1E_\alpha(-Bt^\alpha)}{C_2\Lambda^{-1} + E_\alpha(Bt^\alpha) - C_1E_\alpha(-Bt^\alpha)}\right). \tag{4.24}$$

To achieve this goal, we define $\varphi = \arctan(\frac{\boldsymbol{p}_2}{\boldsymbol{p}_1})$ and $\mathscr{R} = \sqrt{\boldsymbol{p}_1^2 + \boldsymbol{p}_2^2}$. These definitions provide exact expressions corresponding to the angle that $\mathbf{p}_\perp$ makes with the e_1 axis. While System (**??**) may initially appear intricate for vesicles, the primary objective is to simplify it. We aim for an exact analytical solution by introducing innovative coordinates, thereby transforming System (**??**) into a more straightforward form. From (**??**) and (11), we deduce

$$\boldsymbol{p}_1 = \mathscr{R}\cos(2\psi), \quad \boldsymbol{p}_2 = \mathscr{R}\sin(2\psi). \tag{4.25}$$

This relationship is expressed in terms of $\mathscr{R}$ and ψ providing a clearer representation of the system. Expanding on this, the angle φ for a rigid particle conveys the identical information as ψ does for the vesicle. This insight enables us to comprehend the relationship between the behaviour of a rigid sphere and a vesicle. Specifically for vesicles, the angle between the main axis and the fluid flow direction is expressed as follows

$$\psi(t) = \frac{1}{2}\arctan\left(B\Lambda \frac{E_\alpha(Bt^\alpha) - C_1E_\alpha(-Bt^\alpha)}{C_2\Lambda^{-1} + E_\alpha(Bt^\alpha) - C_1E_\alpha(-Bt^\alpha)}\right). \tag{4.26}$$

These formulas provide a clear understanding of the link between the rigid particle and vesicle behaviours, highlighting the intricate relationship between the angles φ and ψ in the given context.
Moreover, it is observed that as t approaches infinity, $\mathscr{R}$ converges to $\sqrt{\Delta}/2$, and the orientation angle φ monotonically tends towards $\psi(\infty) = \frac{1}{2}\arctan(B)$, which means that ψ the orientation angle is always less than $\frac{\pi}{4}$. These findings imply that the orientation angle of the vesicle is constant across different values of α which corresponds to the TT regime in vesicle language.

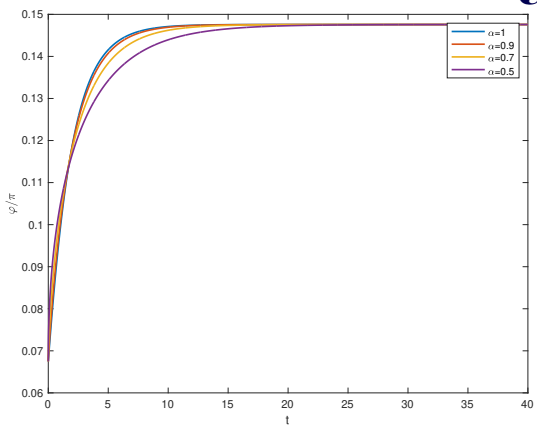


Figure 4.4: The particle's orientation angle φ for four different fractional order values.

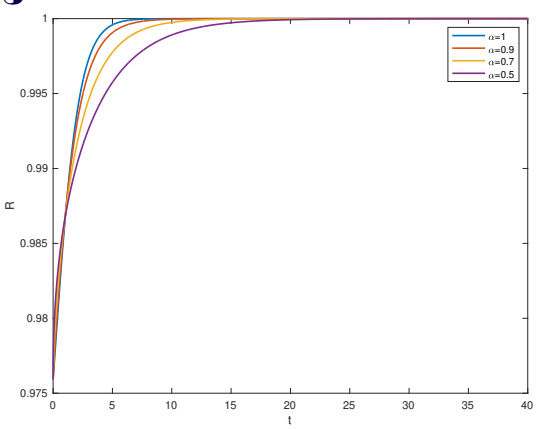


Figure 4.5: The particle's shape deformation $\mathscr{R}$ for four different fractional order values.

Furthermore, to strengthen these theoretical findings, we have illustrated in Figures 4.4 and 4.5 the orientation angle and the shape deviation for various values of α. In these figures, it becomes clear that $\mathscr{R}$ approaches 1, while φ remains constant across different α values. This indicates that the vector $\boldsymbol{p}$ exhibits a running motion equivalent to the pure TT regime for vesicles.

In this context, it is evident from the figures discussed above that the fractional order does not impact the stability of the equilibrium. Consequently, an increase in the value of α, representing a longer memory time, facilitates a quicker convergence of solutions to the steady state. This implies that the dynamics of rigid particles are significantly influenced by the strength of α-controlled memory effects. As a result, the vesicle's dynamics depend on both the current time and the time history, and these aspects can be effectively captured using fractional calculus concepts. By including the adapted Modified Riemann-Liouville fractional derivative, a more realistic model is introduced.

4.3.2 Damping-TT modes

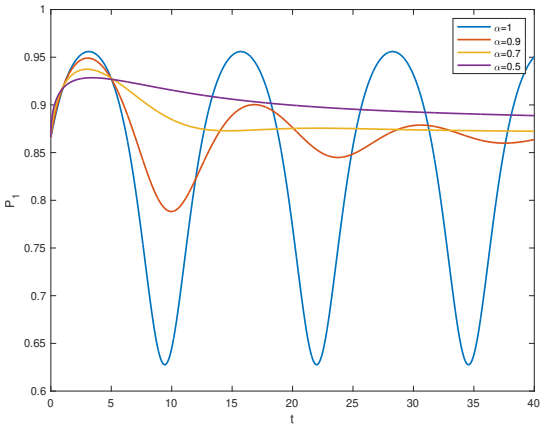
Embarking on the most crucial part of our research, we now turn our focus to the oscillatory solution, described and studied in the classical case by the authors in [2, 37], where $\Lambda > 1$. In their investigation, oscillatory solutions were uncovered, delineating the TB and VB modes. Their findings also underscored the significant impact of initial conditions on the discerned motion types. Taking our exploration a step further in the present chapter, we delve into the computation of exact solutions, accounting for the memory effect manifested by the fractional derivative of Jumarie. Just as in the case where $\Lambda < 1$, our goal is to solve equation (4.14) using the expression of ϕ in (4.13). Following rigorous calculations, we reveal the following expressions

$$\boldsymbol{p}_1 = \Lambda.\frac{\Gamma + sin_\alpha(B^{\frac{1}{\alpha}}t + C_1')}{C_2' + sin_\alpha(B^{\frac{1}{\alpha}}t + C_1')}, \tag{4.27}$$

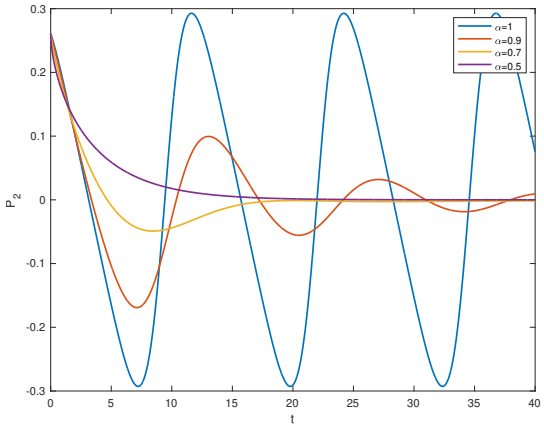
(4.28) $$\boldsymbol{p}_2 = B\Lambda.\frac{cos_\alpha(B^{\frac{1}{\alpha}}t + C_1')}{C_2' + sin_\alpha(B^{\frac{1}{\alpha}}t + C_1')},$$

(4.29) $$\boldsymbol{p}_3 = B\Lambda^2.\frac{C_3'}{C_2' + sin_\alpha(B^{\frac{1}{\alpha}}t + C_1')},$$

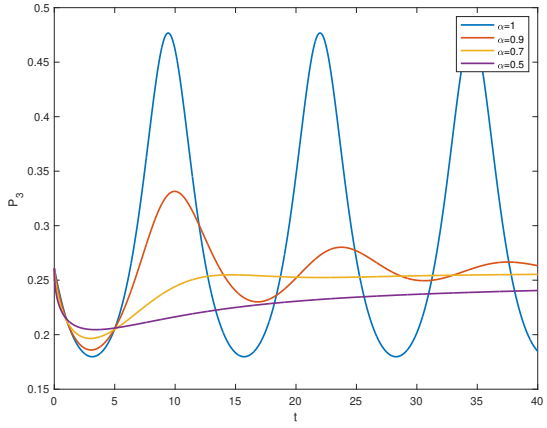
which are in relation to the distinct fractional $\cos_\alpha$ and $\sin_\alpha$ functions defined in (1.10) and where $\Gamma = C_2'\Lambda^{-2}$. The incorporation of these well-established functions provides a novel perspective, emphasising the intricate nature of the oscillatory phenomena under examination. Through rigorous mathematical analysis and compelling calculations, we unveil the derived expressions, therefore giving our work a significant and valuable contribution to the understanding of these complex dynamics.



((a)) The time evolution of p_1 for the Modified Riemann-Liouville operator.



((b)) The time evolution of p_2 for the Modified Riemann-Liouville operator.



((c)) The time evolution of p_3 for the Modified Riemann-Liouville operator.

Figure 4.6: The depiction of the exact solutions for the fractional mapped equation acquired for $\boldsymbol{p}_1, \boldsymbol{p}_2$ and $\boldsymbol{p}_3$ is presented for four distinct values of α , denoting the fractional order.

Meanwhile, to align with our theoretical findings, we have visually depicted an instance of the evolution in time of the amplitudes $\boldsymbol{p}_1$, $\boldsymbol{p}_2$, and $\boldsymbol{p}_3$ for the Jumarie operator in Figure 4.6, with the parameter Λ set to $2/\sqrt{3}$, considering four distinct values of α.
These figures illustrate a cosine form which varies based on the fractional derivative order, α. It is noteworthy that when $\alpha = 1$, there are oscillations in the $\boldsymbol{p}_1$, $\boldsymbol{p}_2$, and $\boldsymbol{p}_3$ components (corresponding to the F_{22} and F_{20} modes). However, a crucial aspect of this investigation is that, for values of $0 < \alpha < 1$, we observe a decline in amplitude as α decreases.
For components $\boldsymbol{p}_4$ and $\boldsymbol{p}_5$, it is sufficient to solve the following system

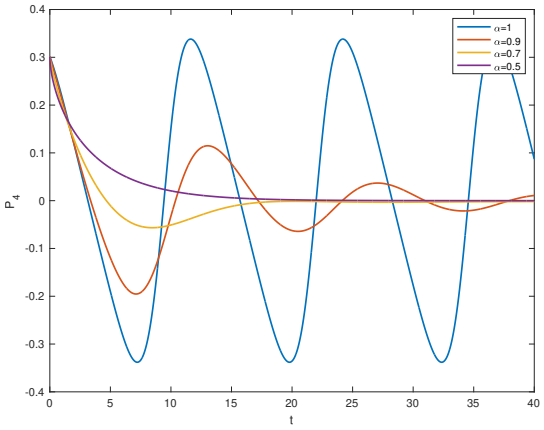
$$
\begin{aligned}
{}^{\mathcal{J}}D_t^{\alpha}\boldsymbol{p}_4 &= \gamma\left(-B\frac{cos_{\alpha}(B^{\frac{1}{\alpha}}t + C_1')}{C_2' + sin_{\alpha}(B^{\frac{1}{\alpha}}t + C_1')}\boldsymbol{p}_4 - \frac{1}{2}\boldsymbol{p}_5\right),\\
{}^{\mathcal{J}}D_t^{\alpha}\boldsymbol{p}_5 &= \gamma\left(-B\frac{cos_{\alpha}(B^{\frac{1}{\alpha}}t + C_1')}{C_2' + sin_{\alpha}(B^{\frac{1}{\alpha}}t + C_1')}\boldsymbol{p}_5 + \frac{1}{2}\boldsymbol{p}_4\right).
\end{aligned}
\tag{4.30}
$$

Furthermore, by integrating (4.19) using the fractional Riemann-Liouville integral and applying the properties of the Jumarie derivative and the Mittag-Leffler function as outlined in Chapter 1, we obtain the expressions for $\boldsymbol{p}_4$ and $\boldsymbol{p}_5$:

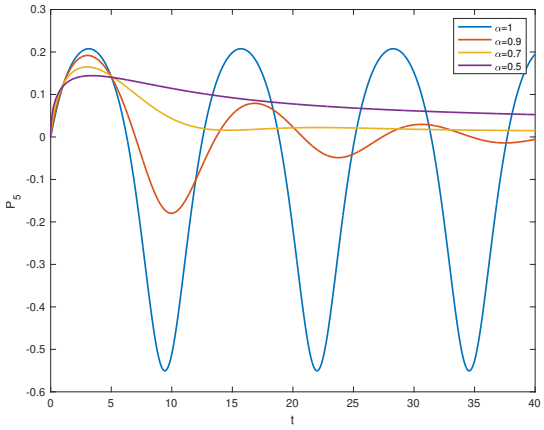
$$
\boldsymbol{p}_4 = C_4'\Lambda^2 B.\frac{cos_{\alpha}\left(\left(\frac{1}{2}\right)^{\frac{1}{\alpha}}t\right)}{C_2' + sin_{\alpha}(B^{\frac{1}{\alpha}}t + C_1')},
\tag{4.31}
$$

$$
\boldsymbol{p}_5 = C_4'\Lambda^2 B.\frac{sin_{\alpha}\left(\left(\frac{1}{2}\right)^{\frac{1}{\alpha}}t\right)}{C_2' + sin_{\alpha}(B^{\frac{1}{\alpha}}t + C_1')}.
\tag{4.32}
$$

By elucidating the expression in (4.31) and (4.32), it becomes apparent that $F_{2\pm1}(t) \neq 0$ throughout its temporal evolution depends on an initial of $F_{2\pm1}(0) \neq 0$. This revelation holds significance as it signifies that if the vesicle's main axis is initially situated outside the shear plane, it does not return to the shear plane. This crucial insight directly answers the pivotal inquiry raised in the introduction. Consequently, our attention is now directed towards cases where the principal axis of the vesicle does not return to the plane, signifying $F_{2\pm1} \neq 0$.



((a)) The time evolution of p_4 for the Modified Riemann-Liouville operator.



((b)) The time evolution of p_5 for the Modified Riemann-Liouville operator.

Figure 4.7: The depiction of the exact solutions for the fractional mapped equation acquired for F_{21} modes is presented for four distinct values of α , denoting the fractional order.

Figure 4.7 illustrates the $F_{2\pm1}$ modes for four distinct values of α. When $\alpha = 1$, the $\boldsymbol{p}_4$ and $\boldsymbol{p}_5$ components predict an oscillation mode corresponding to VB or TB. However, for $0 < \alpha < 1$, the amplitudes decrease, revealing that the rigid particle exhibits a different motion distinct from pure VB or TB. The idea is to distinguish the type of regime that the rigid particle predicts in this case. To achieve this, a deeper understanding of the movement and deformation of the particle is needed. Specifically, we must now find expressions for $\mathscr{R}$, the deformation of the shape, and φ, the orientation angle defined in (15). As previously explained, considering the relationship between $\boldsymbol{p}_1$, $\boldsymbol{p}_2$, $\mathscr{R}$, and φ, we can easily determine that

$$\mathscr{R}^2(t) = \Lambda^2 . \frac{B^2 cos_\alpha^2(B^{\frac{1}{\alpha}}t + C_1') + \left(\Gamma + sin_\alpha(B^{\frac{1}{\alpha}}t + C_1')\right)^2}{\left(C_2' + sin_\alpha(B^{\frac{1}{\alpha}}t + C_1')\right)^2}, \tag{4.33}$$

$$\varphi(t) = \arctan\left(B . \frac{cos_\alpha(B^{\frac{1}{\alpha}}t + C_1')}{\Gamma + sin_\alpha(B^{\frac{1}{\alpha}}t + C_1')}\right). \tag{4.34}$$

Furthermore, for vesicles, the angle representing the orientation between the principal axis and the shear flow direction, as defined in (4.25), is expressed as follows

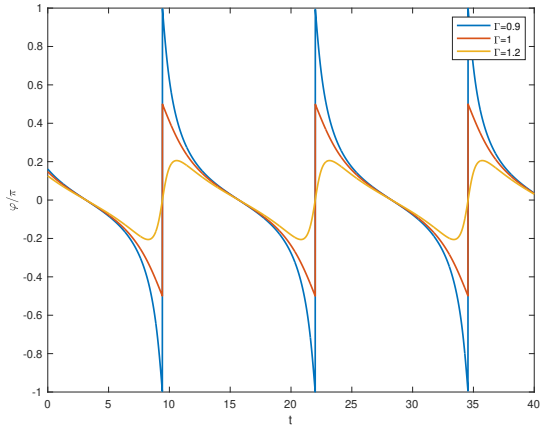
$$\psi(t) = \frac{1}{2}\arctan\left(B . \frac{cos_\alpha(B^{\frac{1}{\alpha}}t + C_1')}{\Gamma + sin_\alpha(B^{\frac{1}{\alpha}}t + C_1')}\right), \tag{4.35}$$

where C_2' depends on the initial conditions. Through a straightforward algebraic manipulation of (4.27) and (4.28) when $t = 0$, the expression is expressed as follows

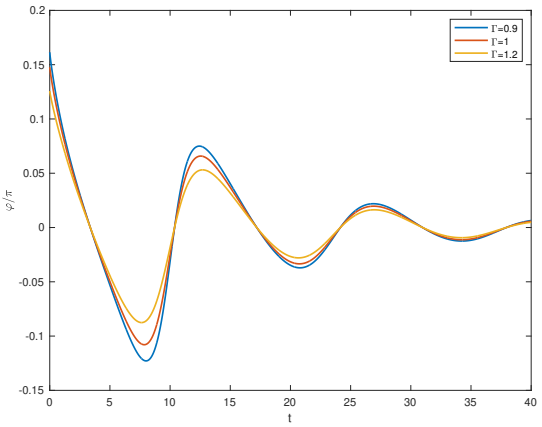
$$C_2' = \pm \frac{\Lambda - \boldsymbol{p}_1(0)}{\sqrt{[B\boldsymbol{p}_2(0)]^2 + [\boldsymbol{p}_1(0) - \Lambda^{-1}]^2}}, \tag{4.36}$$

Subsequently, by using equations (12) and (51), it becomes apparent that $\left|C_2'\right| \geqslant \Lambda$, and consequently, $\left|C_2'\right| > 1$ given that $\Lambda > 1$. Thus, the components $\boldsymbol{p}_1$, $\boldsymbol{p}_2$ and $\boldsymbol{p}_3$ remain finite for all times, and the parameter Γ fulfils to the condition $|\Gamma| \geqslant \Lambda^{-1}$.

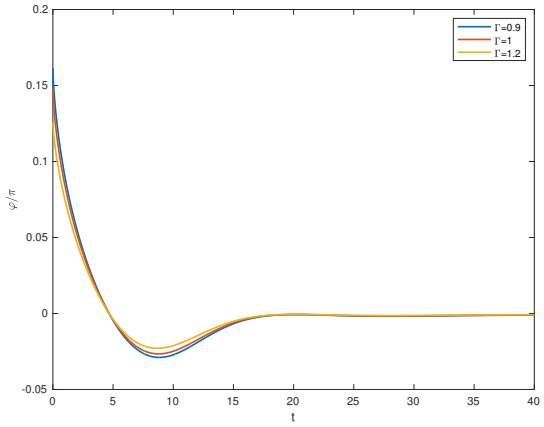
Equation (4.34) indicates that the time evolution of the angle φ is controlled by the parameter Γ. Now, we will explore the impact of Γ ($|\Gamma| \geqslant \Lambda^{-1}$), while keeping the parameters Λ fixed. As discussed earlier, for $\Lambda < 1$, every initial condition converges to the same endpoint, in contrast to the case where $\Lambda > 1$. In this case, the selection of initial conditions, particularly Γ, influences the nature of the motion. Within this context, we will examine how the dynamics of the particle are influenced by the choice of initial conditions and the fractional order.



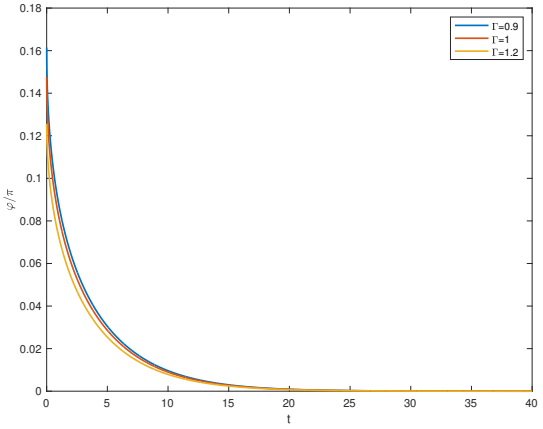
((a)) The orientation angle φ when $\alpha = 1$.



((b)) The orientation angle φ when $\alpha = 0.9$.



((c)) The orientation angle φ when $\alpha = 0.7$.



((d)) The orientation angle φ when $\alpha = 0.5$.

Figure 4.8: The particle's orientation angle φ for four different fractional order values with $\Gamma = 0.9$, $\Gamma = 1$ and $\Gamma = 1.2$.

If the vector undergoes precession around a specific axis, its projected norm will exhibit temporal oscillations, signifying either vesicle vacillating breathing (VB) or tumbling (TB) phenomena within the vesicle dynamics. It's important to note that Gamma can be either positive or negative $\left(\text{i.e., } \Gamma = \pm\sqrt{\Lambda^{-2} + C_3'^2 + C_4'^2}\right)$ but for convenience, and without loss of generality, we assume Γ to be positive. Figure 4.8 illustrates the behaviour of the orientation angle φ (Where

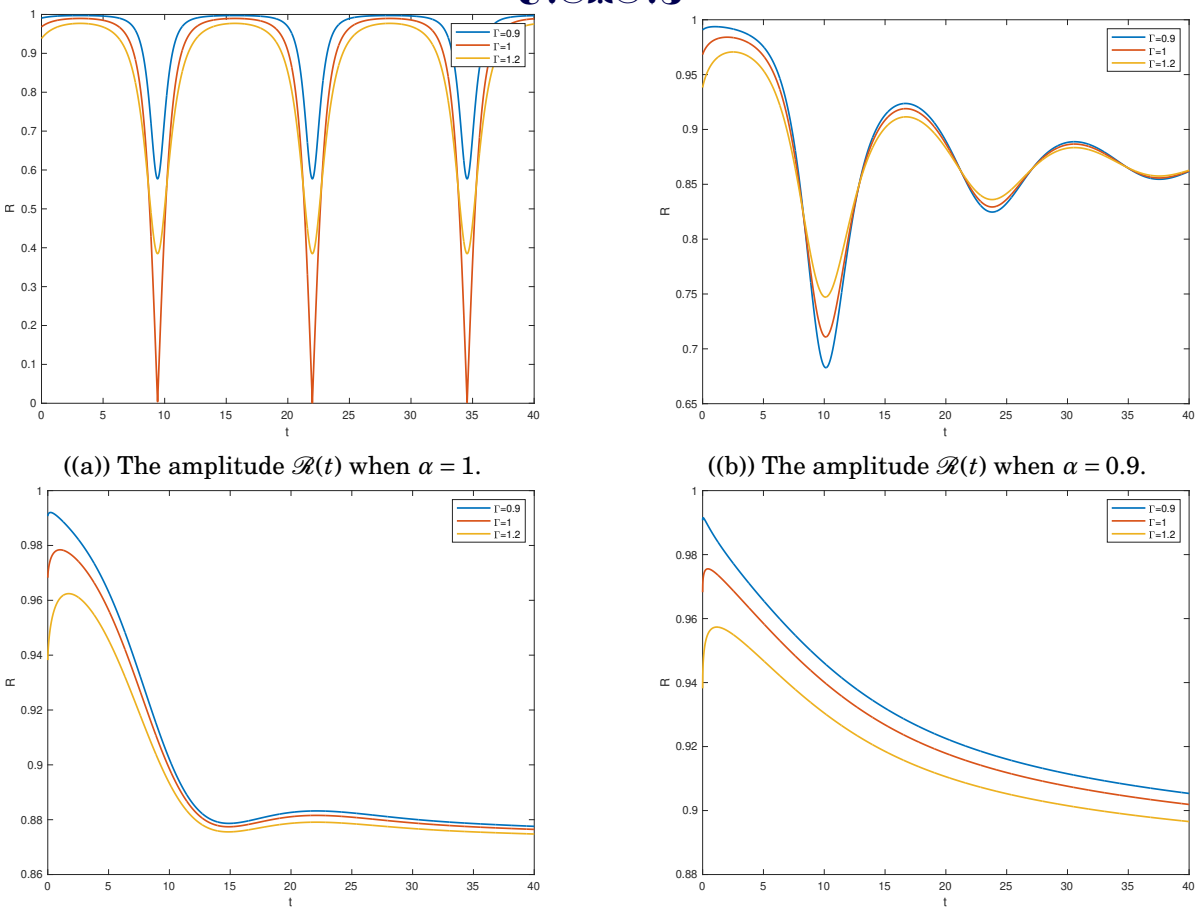
ψ, representing the angle between the main axis and the direction of the fluid flow, is equal to half of φ).

Specifically, Figure 4.8(a) provides a diagram of the angle φ under different regimes when $\alpha = 1$. In this case, the shear flow induces the rotation of vector $\boldsymbol{p}$ around a particular axis, leading to two distinct cases based on the constant Γ (the initial conditions). As depicted in Figure 4.6, the projection of the vector $\boldsymbol{p}$ into the (e_1, e_2) plane signifies the oscillation of the deformation amplitude in the vesicle problem over time. Simultaneously, the angle φ varies within $[-\frac{\pi}{2}, \frac{\pi}{2}]$, corresponding to the initially discussed Vesicle Vacillating-Breathing regime in [64]. The second case arises when the angle φ varies within $[-\pi, \pi]$ with oscillations in the norm $\mathbf{p}_\perp$, representing Tumbling regime.

This indicates that the prevalence of vesicle vacillating breathing or tumbling depends on initial conditions. It is evident from Figure 4.8(a) that when $\Gamma < 1$, the particle exhibits the tumbling mode, characterised by sudden discontinuous jumps of the angle φ over time. Conversely, in the VB regime, represented by $\Gamma > 1$, the evolution is continuous. An interesting case arises when the principal axis of the vesicle is initially positioned outside the plane for $\Gamma < 1$, referred to as the Kayaking-TB (KTB) mode. Similar to classical TB mode, the KTB regime involves the particle's contour oscillation in the shear plane if $\Gamma \neq \Lambda^{-1}$, as indicated by

$$\mathscr{R}^2 = \left(\Lambda^{-2} - \Gamma^2\right) \frac{\Lambda^4 B^2}{\left[\Gamma\Lambda^2 + \sin_\alpha(B^{\frac{1}{\alpha}} t + C_1')\right]^2} + 1. \tag{4.37}$$

This motion is accompanied by $\mathscr{R}$'s oscillation. The time-dependent behaviour of $\mathscr{R}$ for three different values of Γ is illustrated in Figure 4.9, demonstrating a periodic regime similar to the classical VB mode for deformable particles when projected into the shear plane.



((a)) The amplitude $\mathscr{R}(t)$ when $\alpha = 1$.

((b)) The amplitude $\mathscr{R}(t)$ when $\alpha = 0.9$.

((c)) The amplitude $\mathscr{R}(t)$ when $\alpha = 0.7$.

((d)) The amplitude $\mathscr{R}(t)$ when $\alpha = 0.5$.

Figure 4.9: The particle's shape deformation $\mathscr{R}$ for four different fractional order values with $\Gamma = 0.9$, $\Gamma = 1$ and $\Gamma = 1.2$.

Moreover ,the angle φ undergoes continuous evolution, as shown in Figure 4.8. In cases where initially $F_{2\pm1}(0) \neq 0$, the dynamics correspond to Kayaking-VB (KVB). Thus, for $\Gamma > 1$, the KTB regime transforms into the KVB regime. However, when $0 < \alpha < 1$, oscillations with decreasing amplitudes occur, whatever the initial conditions, indicating the presence of a different regime distinct from pure TB or VB. Notably, the parameter Γ loses its impact on both types of motion, leading to oscillations with decreasing amplitudes as α decreases. This behaviour is apparent in Figure 4.9, which shows three different values of Γ and varying values of α.

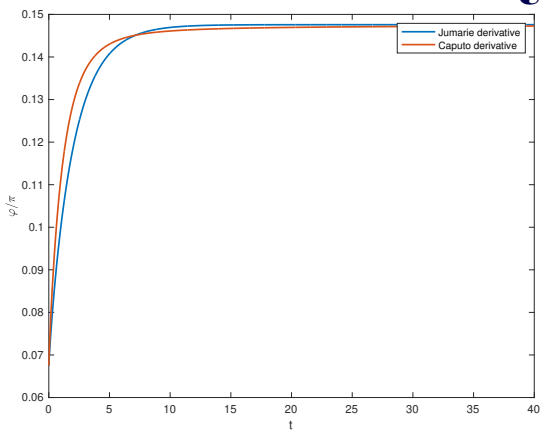
Therefore, the fractional derivative takes into account not only the initial shape but also the entirety of the entire instant, preserving a certain degree of memory. Additionally, these graphical representations suggest that as α increases, the approach to equilibrium becomes slower. Figures 4.8 and 4.9 illustrate that both the orientation angle and shape deformation follow cosine forms with decreasing amplitude as α decreases for any value of Γ.

These regimes can be described as tank-treading with under-damped vesicle oscillations (TT-UD) and tank-treading with over-damped vesicle oscillations (TT-OD). Furthermore, Figures 4.8(a)

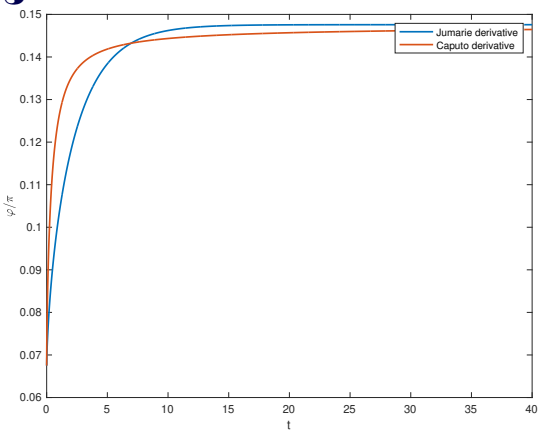
and 4.9(a) show that as α approaches 1, oscillations through the equilibrium indicate TT-UD motion, signifying that the tank-treading mode (TT) is on the verge of losing stability to the vacillating-breathing mode (VB).

4.4 Comparative Analysis of the Modified Riemann-Liouville and Caputo Fractional Derivatives in Vesicle Dynamics

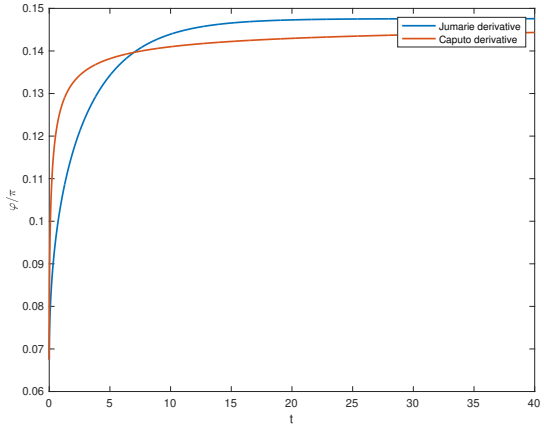
In investigating the persistent question of the choice of fractional derivative, this section conducts a comparative analysis between the Jumarie and Caputo fractional derivatives in the study of vesicle dynamics. The objective is to discern, within this context, which derivative proves more pertinent for this study. Notably, when employing the Caputo derivative, the solution was approximated using the Adams-Bashforth method [15] due to its limited properties. In contrast, the selection of the Jumarie derivative in this instance is motivated by the prospect of using its properties to obtain the exact solution, as demonstrated in the preceding section.
As previously mentioned, whether in the case of vesicles or rigid particle motion, the most relevant aspect is the examination of the orientation angle φ and shape deviation $\mathscr{R}$. Thus, this comparison focuses on evaluating these two functions for different values of α (the fractional order) and for both types of derivatives.



((a)) The orientation angle φ when $\alpha = 0.9$.



((b)) The orientation angle φ when $\alpha = 0.7$.

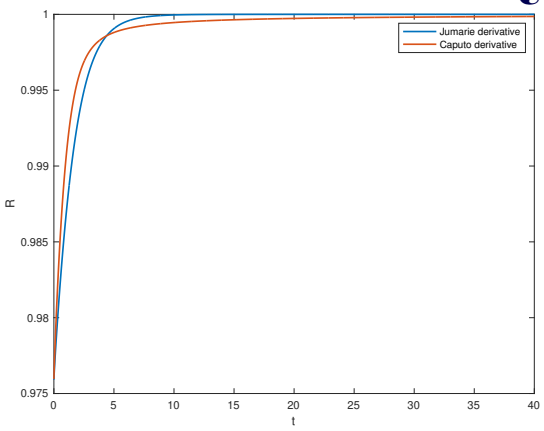


((c)) The orientation angle φ when $\alpha = 0.5$.

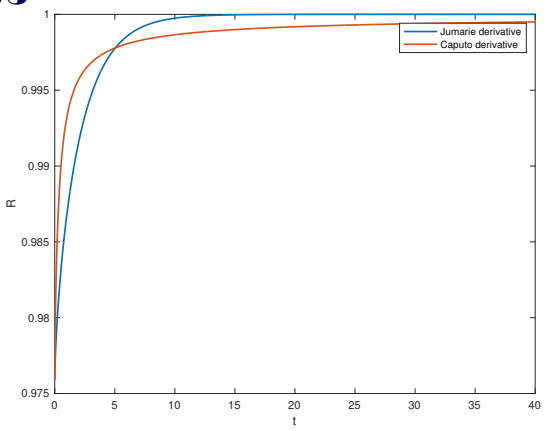
Figure 4.10: The dynamics of the Orientation Angle φ for three arbitrary values of fractional order using Caputo and Modified Riemann-Liouville Fractional Derivatives. Parameters are : $\Lambda = 0.4\sqrt{5}, \gamma = 1$.

In Figures 4.10 and 4.11, we illustrate the dynamics of the orientation angle (φ) and shape deformation ($\mathscr{R}$) for three arbitrarily chosen fractional derivatives, employing both the Caputo derivative and the Modified Riemann-Liouville fractional derivative with respect to the parameter Λ.

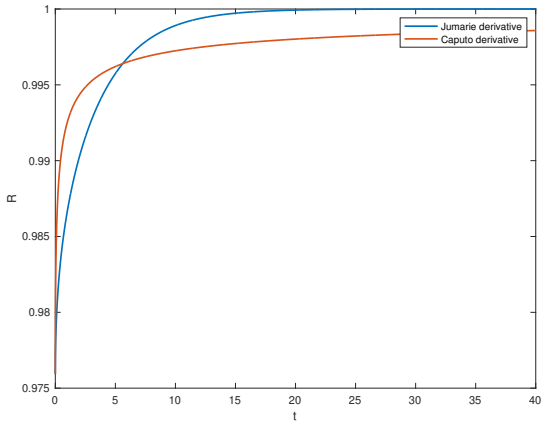
When $\Lambda < 1$, our previous discussions elucidate the vesicle's motion in this case, characterized by the tank-treading mode. Both derivatives demonstrate convergence of the orientation angle and amplitude to a stable point. However, a comparative analysis between the two derivatives, as depicted in Figures 4.10 and 4.11, reveals that the Jumarie derivative exhibits a faster convergence towards equilibrium than its Caputo counterpart. This observation suggests that, in this context, the Jumarie derivative proves to be the more advantageous choice, facilitating quicker convergence and, consequently, time efficiency to reach stability. In this way of thought, we believe that the so-called Caputo derivative is not quite always suitable, and this is the reason why we have used the modified Riemann-Liouville derivative.



((a)) The amplitude $\mathscr{R}$ when $\alpha = 0.9$.



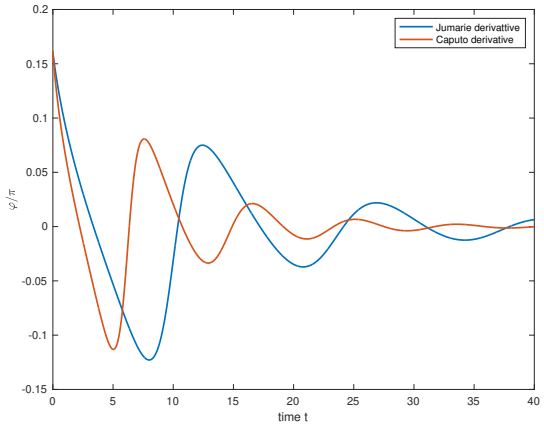
((b)) The amplitude $\mathscr{R}$ when $\alpha = 0.7$.



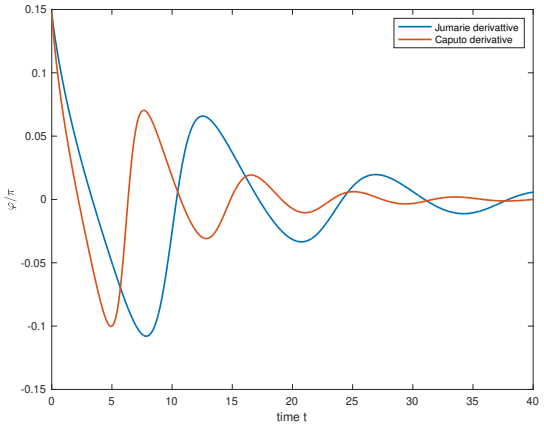
((c)) The amplitude $\mathscr{R}$ when $\alpha = 0.5$.

Figure 4.11: The dynamics of the particle contour $\mathscr{R}$ for three arbitrary values of fractional order using Caputo and Modified Riemann-Liouville Fractional Derivatives. Parameters are : $\Lambda = 0.4\sqrt{5}, \gamma = 1$.

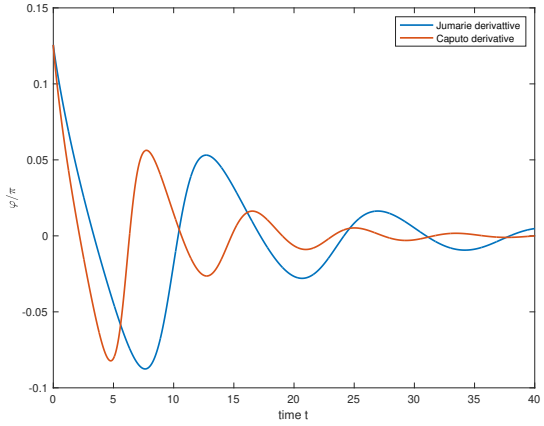
Furthermore, it is noteworthy that the use of the modified Riemann-Liouville derivative contributes not only to achieving faster convergence but also to obtaining the exact solution as opposed to providing a simple approximation. The Exact solution is expressed in terms of the Mittag-Leffler function, a generalisation of the exponential function, along with generalised trigonometric functions. This approach provides a more comprehensive understanding of the system dynamics, offering a solution that encompasses a broader class of mathematical functions. We will now turn our attention to the most crucial case, which involves oscillations or periodic behaviour ($\Lambda > 1$), particularly in the classical case (i.e., $\alpha = 1$). Using the classical derivative, we can identify the regime based on initial conditions, and we have observed damping tank-treading for $0 < \alpha < 1$, where we demonstrated that initial conditions no longer influence the types of motion. Instead, only α impacts the motion exhibited by the vesicle for both the Jumarie and Caputo derivatives.



((a)) The orientation angle φ when $\alpha = 0.9$ and $\Gamma = 0.9$.

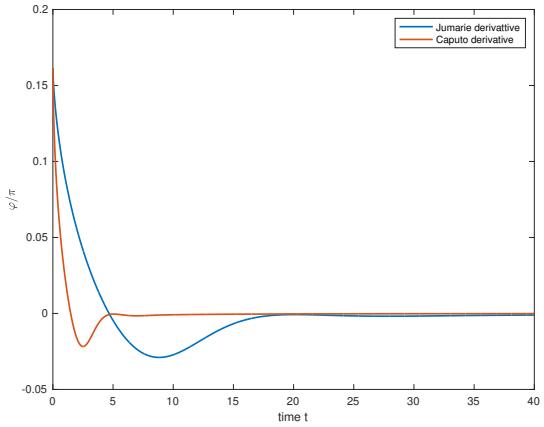


((b)) The orientation angle φ when $\alpha = 0.9$ and $\Gamma = 1$.

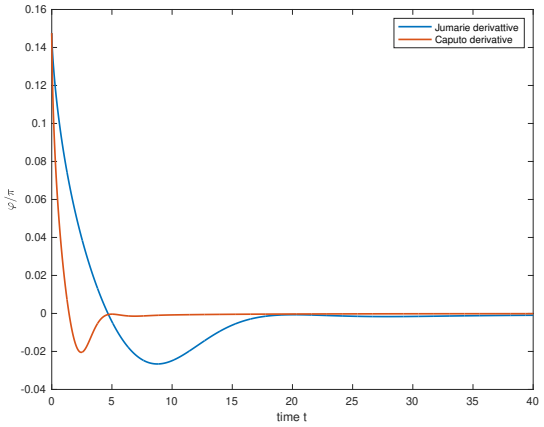


((c)) The orientation angle φ when $\alpha = 0.9$ and $\Gamma = 1.2$.

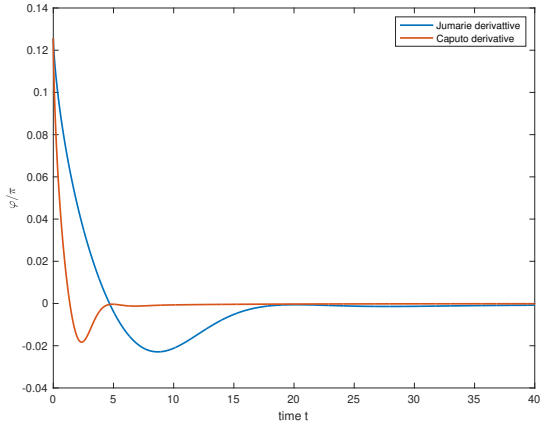
Figure 4.12: The orientation angle dynamics φ for $\alpha = 0.9$ with Caputo and Modified Riemann-Liouville Fractional Derivatives and Three Different Γ Values at $\Lambda = 2/\sqrt{3}$.



((a)) The orientation angle φ when $\alpha = 0.7$ and $\Gamma = 0.9$.

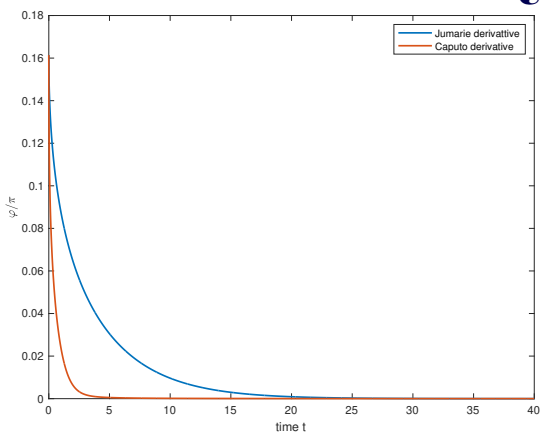


((b)) The orientation angle φ when $\alpha = 0.7$ and $\Gamma = 1$.

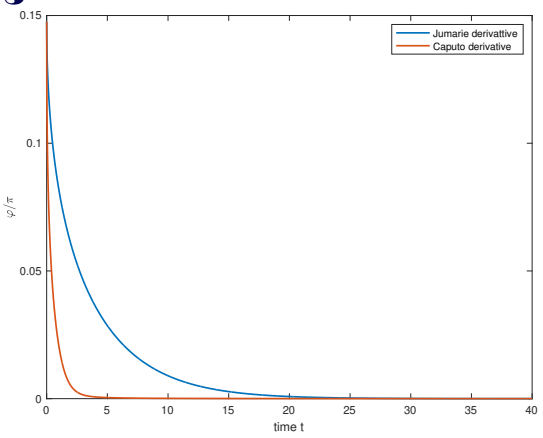


((c)) The orientation angle φ when $\alpha = 0.7$ and $\Gamma = 1.2$.

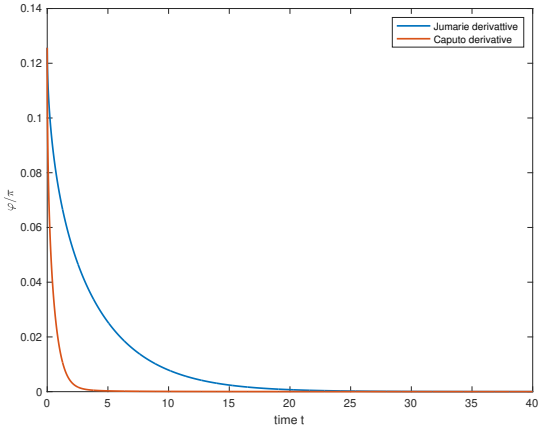
Figure 4.13: The orientation angle dynamics φ for $\alpha = 0.7$ with Caputo and Modified Riemann-Liouville Fractional Derivatives and Three Different Γ Values at $\Lambda = 2/\sqrt{3}$.



((a)) The orientation angle φ when $\alpha = 0.5$ and $\Gamma = 0.9$.



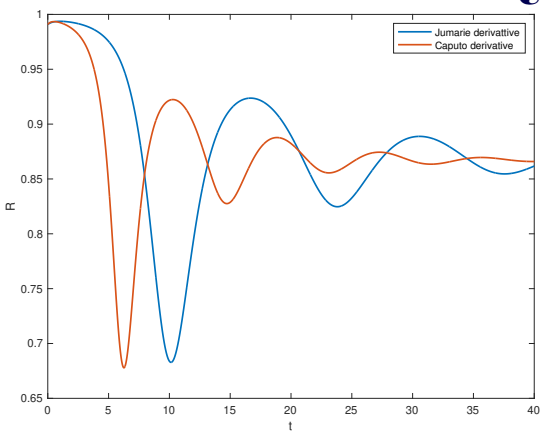
((b)) The orientation angle φ when $\alpha = 0.5$ and $\Gamma = 1$.



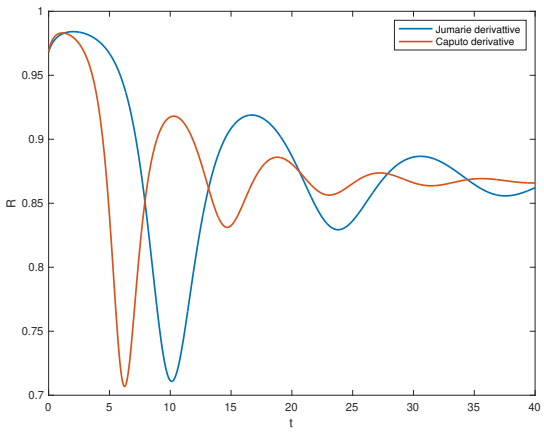
((c)) The orientation angle φ when $\alpha = 0.5$ and $\Gamma = 1.2$.

Figure 4.14: The orientation angle dynamics φ for $\alpha = 0.5$ with Caputo and Modified Riemann-Liouville Fractional Derivatives and Three Different Γ Values at $\Lambda = 2/\sqrt{3}$.

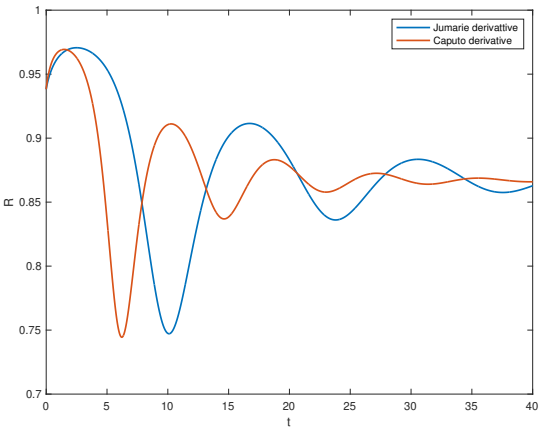
To delve deeper into this observation, we have presented the dynamics of the orientation angle in Figures 4.12, 4.13, and 4.14 for three different initial conditions (Γ values) and various α values while keeping Λ fixed at $\Lambda > 1$. The shape deformation is depicted in Figures 4.15, 4.16, and 4.17.



((a)) The amplitude $\mathscr{R}(t)$ when $\alpha = 0.9$ and $\Gamma = 0.9$.

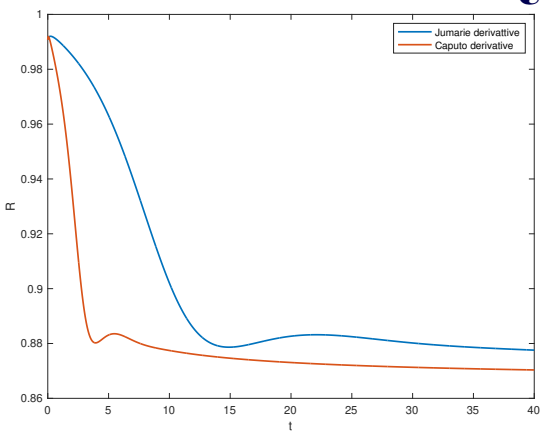


((b)) The amplitude $\mathscr{R}(t)$ when $\alpha = 0.9$ and $\Gamma = 1$.

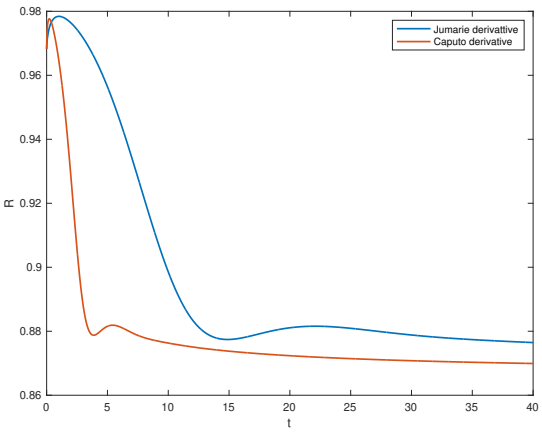


((c)) The amplitude $\mathscr{R}(t)$ when $\alpha = 0.9$ and $\Gamma = 1.2$.

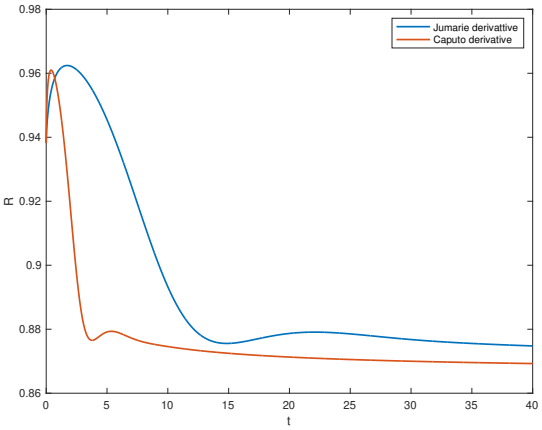
Figure 4.15: The dynamics of the shape deformation $\mathscr{R}$ for $\alpha = 0.9$ with Caputo and Modified Riemann-Liouville Fractional Derivatives and Three Different Γ Values at $\Lambda = 2/\sqrt{3}$.



((a)) The amplitude $\mathscr{R}(t)$ when $\alpha = 0.7$ and $\Gamma = 0.9$.

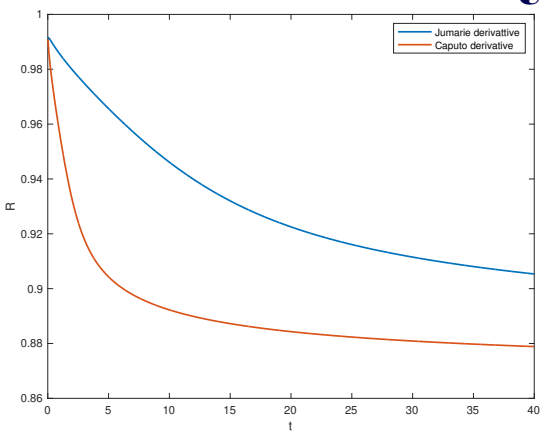


((b)) The amplitude $\mathscr{R}(t)$ when $\alpha = 0.7$ and $\Gamma = 1$.

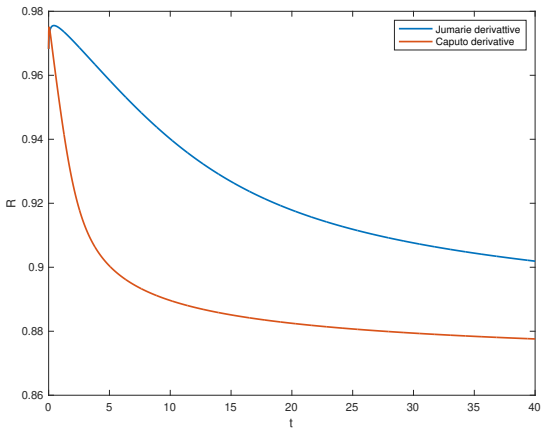


((c)) The amplitude $\mathscr{R}(t)$ when $\alpha = 0.7$ and $\Gamma = 1.2$.

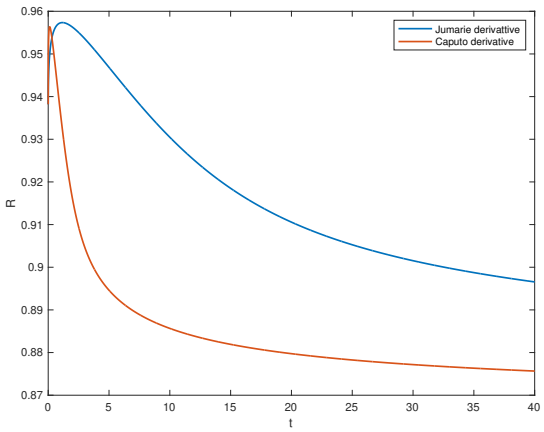
Figure 4.16: The dynamics of the shape deformation $\mathscr{R}$ for $\alpha = 0.7$ with Caputo and Modified Riemann-Liouville Fractional Derivatives and Three Different Γ Values at $\Lambda = 2/\sqrt{3}$.



((a)) The amplitude $\mathscr{R}(t)$ when $\alpha = 0.5$ and $\Gamma = 0.9$.



((b)) The amplitude $\mathscr{R}(t)$ when $\alpha = 0.5$ and $\Gamma = 1$.



((c)) The amplitude $\mathscr{R}(t)$ when $\alpha = 0.5$ and $\Gamma = 1.2$.

Figure 4.17: The dynamics of the shape deformation $\mathscr{R}$ for $\alpha = 0.5$ with Caputo and Modified Riemann-Liouville Fractional Derivatives and Three Different Γ Values at $\Lambda = 2/\sqrt{3}$.

Upon closer examination, it becomes evident that, as α decreases, Caputo yields more relevant results, and convergence is faster in this context. Oscillations decrease rapidly, leading to stabilisation towards the equilibrium point and the emergence of a new damping movement.
It is worth noting that this comparison highlights the difference between the speed of convergence and the relevance of results, emphasising the sensitivity of the vesicle's behaviour to the choice of fractional derivative.
In this case, as α get away from 1, the vesicle's behaviour predicts damping-TT for both types of derivatives. However, the Caputo derivative converges more rapidly, allowing us to discern the time difference in achieving convergence or stability between the two derivatives. This phenomenon is indicative of the Caputo derivative's ability to capture and highlight the system's intrinsic characteristics, especially during the transition from oscillatory behaviour to stabilization.
These observations underscore the challenge of determining which derivative is better suited

for this type of system; For $\Lambda < 1$, we have observed that the Jumarie derivative enhances time efficiency, while for $\Lambda > 1$, the emergence of the new motion (damping-TT) is noticeable more rapidly with Caputo. Each derivative exhibits distinctive characteristics, and notably, one feature of the Jumarie derivative that has captured our attention is its capability to obtain the exact expression as opposed to providing a simple approximation.

4.5 Conclusion

Overall, thischapter serves as a significant step forward in the study of vesicle dynamics, offering a valuable tool that can be used to gain deeper insights into the behaviour of vesicles in multi-dimensional spaces, thereby advancing our knowledge of essential biological processes and their practical applications. especially those that involve real cell-like behaviours, such as those exhibited by red blood cells, and their relevance in the low Reynolds number, viscous-dominated Stokes regime.

Thechapter presents a comprehensive analytical exploration of vesicle dynamics, employing Jumarie's Modified Riemann-Liouville Fractional Derivative as a novel mathematical framework. The study includes a detailed examination of the memory effect observed in lipid vesicles, which undergo persistent shape changes resembling real cells, especially red blood cells.

Grounded in a five-dimensional fractional rigid sphere model, our analytical analysis, employing Jumarie's fractional derivative, produces an exact solution using the key function Mittag-Leffler of fractional calculus. This solution enables a comprehensive understanding of the intricate dynamics and enduring shape alterations in lipid vesicles. It reveals alternative regimes, namely, tank-treading with over-damped and under-damped (respectively, TT-OD and TT-UD), depending on the order of the derivative, representing intermediary regimes between TT and VB that classical derivatives are unable to detect.

Furthermore, thechapter features a rigorous comparative analysis with Caputo's derivative, aiming to discern the relative efficacy of the two fractional derivatives in capturing the essential features of vesicle dynamics. This comparative study contributes not only to the theoretical understanding of vesicle behaviour but also has practical implications in the broader context of applied mathematics, particularly in the field of biophysical systems.

The findings presented herein contribute to the growing body of knowledge in fractional calculus applications, specifically within the realm of biophysical systems. The insights gained from this analytical investigation offer a valuable foundation for future research and applications in understanding the complex dynamics exhibited by vesicles and related biological structures.

CHAPTER 5

UNVEILING MEMORY-DRIVEN DYNAMICS: FRACTIONAL CALCULUS AND MICROSWIMMER TRAJECTORIES IN 1D SHEAR FLOW

Contents

5.1 Introduction **107**
5.2 Fractional Model and Stability Analysis **108**
5.3 Extending Bretherton's Approach **109**
5.3.1 run mode 112
5.3.2 Damping mode 114
5.3.3 Special Case: No Preferred Swimming Direction ($\chi = 0$) 118
5.4 Memory Effects on Swimming Trajectories **119**
5.4.1 Trajectories in the run regime 119
5.4.2 Trajectories in the Tumbling regime 120
5.4.3 Trajectories in the special case $\chi = 0$ 121
5.5 Conclusion and Future Perspectives **124**

5.1 Introduction

As mentioned in the introduction, microswimmers, microscopic entities capable of navigating fluid environments are of significant interest due to their applications in fields such as biophysics and targeted drug delivery. These microswimmers, often modeled after biological organisms like bacteria and algae, exhibit complex dynamic behaviors when interacting with their surrounding fluids. Understanding their trajectories and orientations is essential for optimizing practical applications and advancing our knowledge of transport phenomena in microfluidics and environmental science.

Microorganisms often exhibit responses to both fluid flow and various external stimuli, such as gravity (gyrotaxis), magnetic fields (magnetotaxis), and light (phototaxis). The interplay between fluid flow and these external forces results in a range of complex movements. To date, most trajectories of these microswimmers have been determined through numerical methods, as detailed below. In the presence of both flow and an external field, the dynamics of a spherical microswimmer are described by the following equations for the orientation vector $\boldsymbol{p}$ and the position vector $\mathbf{x}$

$$\begin{aligned} \frac{d\boldsymbol{p}}{dt} &= \frac{1}{2}\boldsymbol{\omega}\times\boldsymbol{p} + \chi\left[\mathbf{e}^{\star} - (\boldsymbol{p}\cdot\mathbf{e}^{\star})\boldsymbol{p}\right], \\ \frac{d\mathbf{x}}{dt} &= \mathbf{u}_0(\mathbf{x}) + \mathbf{v}_{\mathbf{s}}, \end{aligned} \tag{5.1}$$

where $\boldsymbol{\omega}$ represents the fluid vorticity vector, and $\mathbf{e}^{\star}$ denotes the applied external field, with χ characterizing its strength (where $\chi = 0$ indicates no external field). The parameter χ is often associated with external forces such as gravity for a particle with a non-coincident center of mass, such as a heavy-bottom particle (i.e., when the center of mass is offset from the center of the sphere) [19, 39].

Building on this foundational overview, this chapter explores the dynamics of spherical microswimmers subjected to one-dimensional shear flow. We employ fractional calculus, specifically Jumarie's fractional derivative, to account for memory effects that influence microswimmer behavior. This approach allows us to derive exact analytical solutions for both the orientation and trajectory of microswimmers, providing a more detailed understanding of their motion under shear forces. By extending Bretherton's method, we aim to improve the accuracy of microswimmer models and offer deeper insights into their interactions with fluid environments. This methodological advancement not only bridges the gap between classical and fractional calculus but also underscores the transformative potential of fractional derivatives in modeling complex biological systems.

The results presented in this chapter have important implications for the design and application of microswimmers in biophysics and medical technologies. By examining the interplay between microswimmers and their trajectories through a fractional calculus framework, we contribute to the development of more effective strategies for manipulating and utilizing these microscopic

entities in various practical applications.

The structure of this chapter is as follows: Section 5.2 focuses on the formulation of the fractional model and includes a detailed stability analysis. In Section 5.3, we extend Bretherton's approach to the fractional orientation evolution equation, introducing a new framework for studying particle dynamics. Section 5.4 examines the impact of memory effects on swimming trajectories in a 1D shear flow, highlighting the complex behaviors of microswimmer motion under these conditions. Finally, Section 5.5 offers concluding remarks and suggests avenues for future research.

5.2 Fractional Model and Stability Analysis

In this section, we present the fractional model by substituting the fractional derivative with an integer-order derivative. This approach allows us to analyze the system's dynamics while maintaining the essential characteristics of the original model (5.1). Let us consider the dynamics of an isolated rigid spherical microswimmer in a 1D shear flow. The swimmer moves with a velocity $\mathbf{v}_s = v_s \boldsymbol{p}$, where $\boldsymbol{p}$ is the unit orientation vector and v_s is the constant magnitude of the swimming velocity. Using Faxén's second law and considering the equilibrium of torques while assuming negligible inertial forces, we modify the system (5.1) by replacing the integer-order derivative with Jumarie's modified Riemann-Liouville fractional derivative.

Moreover $\boldsymbol{\omega} \times \boldsymbol{p}$ can be replaced by $\boldsymbol{\Omega} \cdot \boldsymbol{p}$

$$
\begin{aligned}
{}^{\mathcal{J}}D_t^{\alpha} \boldsymbol{p} &= \frac{1}{2}\left[\Omega \cdot \boldsymbol{p} + \chi\left(\mathbf{e}^* - \left(\mathbf{e}^* \cdot \boldsymbol{p}\right)\boldsymbol{p}\right)\right], \\
{}^{\mathcal{J}}D_t^{\alpha} \mathbf{x} &= \mathbf{u}_0(\mathbf{x}) + \mathbf{v}_s,
\end{aligned} \tag{5.2}
$$

where ${}^{\mathcal{J}}D_t^{\alpha}$ denotes Jumarie' fractional derivative of order $\alpha, \boldsymbol{\Omega}$ is the vorticity tensor defined as

$$
\boldsymbol{\Omega} = \begin{pmatrix} 0 & -\omega_3 & \omega_2 \\ \omega_3 & 0 & -\omega_1 \\ -\omega_2 & \omega_1 & 0 \end{pmatrix}, \tag{5.3}
$$

$\boldsymbol{e}^*$ is an arbitrary unit vector, $\mathbf{u}_0(x)$ is the fluid velocity, and $\boldsymbol{\omega} = (\omega_1, \omega_2, \omega_3)$ is the fluid vorticity vector.

The introduction of fractional derivatives in the equations above allows us to model the memory effect, where the system's current state depends on its past states. This modification leads to a generalized model that can capture more complex and realistic behaviors of microswimmers in fluid flows.

This equation has been analytically solved when $\alpha = 1$, as shown in [38]. The solution of this classical model of ordinary differential equations (ODEs) does not depend on past instants due to the lack of memory effect. Fractional calculus, however, is effective in describing real-life phenomena with memory effects.

We can easily observe that the first equation in system (5.1) is similar to equation (12), which

we previously used in Chapters 3 and 4 to study the mapping equation for vesicles to study the dynamics of quasi-spherical vesicles under shear flow using Caputo and modified Riemann-Liouville fractional derivatives. It was demonstrated that, similar to the classical case, the shape evolution equation in the fractional case can also be mapped onto that of a rigid sphere, similar to the equation above, with an appropriate χ in five dimensions and a corresponding fictitious vorticity Ω.

Based on this mapping and our previous exact analytical solutions for vesicles, we can solve the equation (5.2). Here, instead of the method used in Chapter 4, we provide a more general analytical approach that can be extended to other physical situations, such as arbitrary orientations of external fields.

To analyze the stability of the system described by these fractional equations, we examine the equilibrium points and the corresponding eigenvalues of the Jacobian matrix derived from the system. The stability conditions can be summarized as follows:

It is noteworthy that the system above possesses equilibrium points dependent on the parameter $\tilde{\chi}$, where $\tilde{\chi} = \dfrac{\chi}{\gamma} = -\dfrac{\chi}{\omega_3}$,

$$\left(\tilde{\chi}^{-1}, \pm\sqrt{1-\tilde{\chi}^{-2}}, 0\right),$$

for $\tilde{\chi} > 1$, where $\left(\tilde{\chi}^{-1}, \sqrt{1-\tilde{\chi}^{-2}}, 0\right)$ is asymptotically stable and $\left(\tilde{\chi}^{-1}, -\sqrt{1-\tilde{\chi}^{-2}}, 0\right)$ is completely unstable. For $\tilde{\chi} < 1$, the equilibrium points are:

$$\left(\tilde{\chi}, \pm\sqrt{1-\tilde{\chi}^{2}}, 0\right),$$

which are stable. We have examined the local stability of the solutions to the fractional system using Lemma 1.2.3, demonstrating that stability can be inferred in this case, unlike with classical derivatives where stability conclusions are not as straightforward.

This stability analysis is crucial for understanding the behavior of the microswimmers under various external influences, as it reveals how the memory effects captured by the fractional derivative impact the system's dynamics. The insights gained from this assessment pave the way for further exploration of the intricate interactions between microswimmers and their fluid environments.

5.3 Extending Bretherton's Approach to the Fractional Orientation Evolution Equation

The authors in [38] presented a comprehensive analytical approach based on the Bretherton method [20]. However, their analysis did not account for the time history or memory effect. Motivated by these studies, we propose extending this approach using the modified Riemann-Liouville fractional derivative. This extension can be readily applied to various physical scenarios,

such as arbitrary orientations of external fields. The primary objective of this chapter is to analytically solve a family of equations of the form

$$ {}^{\mathcal{J}}D_t^{\alpha}\boldsymbol{p} = \frac{1}{2}\left[\boldsymbol{\Omega}\cdot\boldsymbol{p} + \chi\left(\mathbf{e}^{\star} - \mathbf{e}^{\star}\cdot\boldsymbol{p}\boldsymbol{p}\right)\right], \tag{5.4} $$

where ${}^{\mathcal{J}}D_t^{\alpha}$ is the Jumarie's modified Riemann-Liouville derivative, $0 < \alpha \leq 1$. Our aim is to transform this equation into a form conducive to straightforward analysis, inspired by the Bretherton method [20] as discussed in [38]. However, it is not immediately evident how to directly apply this method to our fractional equation. To solve (5.4), we use the following approach

$$ \boldsymbol{p} = \boldsymbol{p}_0 + \beta(t)q, \tag{5.5} $$

which necessitates the decomposition into three fundamental equations for comprehensive analysis.
First, we have

$$ \Omega\cdot\boldsymbol{p}_0 + \chi\mathbf{e}^{\star} - \chi\mathbf{e}^{\star}\cdot\boldsymbol{p}_0\boldsymbol{p}_0 = 0, \tag{5.6} $$

The solution provided by the authors in [38] offers further insights into this equation by elucidating the relationship between the orientation dynamics of the microswimmer and the external flow conditions. Specifically, they derived explicit analytical expressions for the orientation vector $\boldsymbol{p}_0$. In this chapter, we focus on the swimming direction in 1D linear shear flow. Based on the results presented in [38], we obtain a one-parameter family of solutions for the orientation vector given by

$$ \boldsymbol{p}_0 = \xi\boldsymbol{k} + \tilde{\chi}\boldsymbol{i}, \tag{5.7} $$

It can be verified that, in this context, the parameter ξ does not affect (5.7) and can be set to zero. Consequently, the exact expression for the orientation vector simplifies to:

$$ \boldsymbol{p}_0 = \tilde{\chi}\boldsymbol{i}. \tag{5.8} $$

This formulation allows us to analyze the fundamental dynamics of the swimming direction in 1D linear shear flow. We now turn to the second equation, which is given by

$$ \beta(t){}^{\mathcal{J}}D_t^{\alpha}q = \frac{1}{2}\Omega\cdot\beta(t)q - \chi\mathbf{e}^{\star}\cdot\beta(t)q\boldsymbol{p}_0. \tag{5.9} $$

To simplify this equation, we divide each term by $\beta(t)$, yielding

$$ {}^{\mathcal{J}}D_t^{\alpha}q = \frac{1}{2}\Omega\cdot q - \chi\mathbf{e}^{\star}\cdot q\boldsymbol{p}_0. \tag{5.10} $$

In this simplified form, we can now address the resolution of equation (5.10). The equation is more manageable, with ${}^{\mathcal{J}}D_t^{\alpha}q$ representing the fractional derivative of q. To solve this, we utilize

the Laplace Transform of the modified Riemann-Liouville fractional derivative, as outlined in (5.13), along with the properties detailed in Section 1. Specifically, we have

$$ {}^{\mathscr{J}}D_t^{\alpha} q(t) = \mathbf{A}q, \tag{5.11} $$

where the operator $\mathbf{A}$ is given by

$$ \mathbf{A} = \frac{1}{2}\left(\Omega - \chi \boldsymbol{p}_0 \mathbf{e}^{\star T}\right). \tag{5.12} $$

Applying the Laplace Transform to equation (5.10) and using the definition of the modified Riemann-Liouville fractional derivative (5.13), we obtain

$$ \mathscr{L}({}^{\mathscr{J}}D_t^{\alpha} q(t))(s) = s^{\alpha} Q(s) - s^{\alpha-1} q(0), \tag{5.13} $$

where $Q(s)$ is the Laplace transform of$q(t)$ and $q(0)$ is the initial condition.
By performing the inverse Laplace Transform as described in Definition 1.1.6, we find the solution to be

$$ q(t) = E_{\alpha}(\mathbf{A}t^{\alpha}) q(0). \tag{5.14} $$

where E_{α} denotes the Mittag-Leffler function of order α.
Having addressed the second equation, we now turn our attention to the third equation. The third equation is given by

$$ {}^{\mathscr{J}}D_t^{\alpha} \beta(t) = -\frac{\chi}{2}\left[\beta \mathbf{e}^{\star} \cdot \boldsymbol{p}_0 + \beta^2 \mathbf{e}^{\star} \cdot q\right], \tag{5.15} $$

For the third equation (5.15), we can utilize the properties of the modified Riemann-Liouville fractional derivative described in Chapter 1 to find a solution. Specifically, by applying these properties, we obtain the following result

$$ \beta^{-1}(t) = \beta^{-1}(0) E_{\alpha}(\frac{\chi}{2}\mathbf{e}^{\star} \cdot \boldsymbol{p}_0 t^{\alpha}) + \frac{\chi}{2} E_{\alpha}(\frac{\chi}{2}\mathbf{e}^{\star} \cdot \boldsymbol{p}_0 t^{\alpha}) I_0^{\alpha}\left(E_{\alpha}(-\frac{\chi}{2}\mathbf{e}^{\star} \cdot \boldsymbol{p}_0 t^{\alpha})\right)\mathbf{e}^{\star} \cdot q. \tag{5.16} $$

From (5.5), we can finally derive the expression for $\boldsymbol{p}$

$$ \boldsymbol{p}(t) = \boldsymbol{p}_0 + \frac{q(0) E_{\alpha}(\mathbf{A}t^{\alpha})}{\beta^{-1}(0) E_{\alpha}(\frac{\chi}{2}\mathbf{e}^{\star} \cdot \boldsymbol{p}_0 t^{\alpha}) + \frac{\chi}{2} E_{\alpha}(\frac{\chi}{2}\mathbf{e}^{\star} \cdot \boldsymbol{p}_0 t^{\alpha}) I_0^{\alpha}\left(E_{\alpha}(-\frac{\chi}{2}\mathbf{e}^{\star} \cdot \boldsymbol{p}_0 t^{\alpha})\mathbf{e}^{\star} \cdot q\right)}. \tag{5.17} $$

For the particular and interesting case in which $\mathbf{e}^{\star}$ and $\boldsymbol{p}_0$ are perpendicular. The general solution of (5.4) can be written as,

$$ \boldsymbol{p}(t) = \boldsymbol{p}_0 + \frac{q(0) E_{\alpha}(\mathbf{A}t^{\alpha})}{\beta^{-1}(0) + \frac{\chi}{2} I_0^{\alpha}\left(\mathbf{e}^{\star} \cdot E_{\alpha}(\mathbf{A}t^{\alpha}) q(0)\right)}. \tag{5.18} $$

As mentioned in the introduction, we will focus on a specific case where the imposed fluid velocity is given by

$$ \boldsymbol{u}_0 = \left(\gamma y, 0, 0\right), \tag{5.19} $$

where γ represents the steady rate of shear. For this case, we assume that the external field is aligned with $\mathbf{e}$, meaning $\mathbf{e}^\star = \boldsymbol{j}$. Consequently, the fluid vorticity is $\omega = -\gamma\vec{k}$.
Additionally, we define $\Lambda = \sqrt{|\tilde{\chi}^{-2} - 1|}$.
Furthermore, after obtaining the exact analytical solutions to the system (5.5), which incorporates run and tumble dynamics, our objective is to quantify the effects of the parameter χ and the fractional order derivative α on heavy bottom particle regimes at leading order in the fractional case. Building on these results and the properties of the Jumarie derivative, the following sections will derive the analytical solutions for $\boldsymbol{p}_x$, $\boldsymbol{p}_y$, and $\boldsymbol{p}_z$ as functions of the parameters χ and α for both the run and tumble modes. Additionally, we propose an alternative approach to generating these motions by assigning random values, either greater or less than unity, to these parameters. This analysis will enable us to explore the exact expressions for φ. The behavior of these solutions will be illustrated using MATLAB software.

5.3.1 run mode

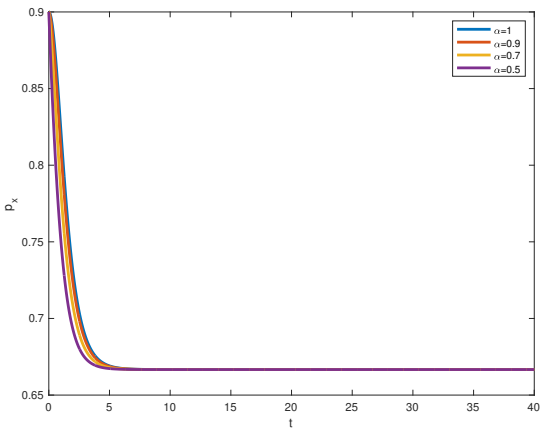
Notably, we explore the intriguing run mode, a distinct behavior that emerges under specific conditions, similar to the TT-mode observed in vesicles, where the orientation angle remains constant. Through the combined insights of the Mittag-Leffler function and Jumarie fractional derivative, the resulting expressions indicate the emergence of the run mode.

$$\boldsymbol{p}_x = \tilde{\chi} - \frac{\Lambda^2}{\tilde{\chi}} \frac{E_\alpha\left(\frac{\gamma\Lambda t^\alpha}{2}\right) + c_2 E_\alpha\left(-\frac{\gamma\Lambda t^\alpha}{2}\right)}{c_1 + E_\alpha\left(\frac{\gamma\Lambda t^\alpha}{2}\right) + c_2 E_\alpha\left(-\frac{\gamma\Lambda t^\alpha}{2}\right)}, \tag{5.20}$$

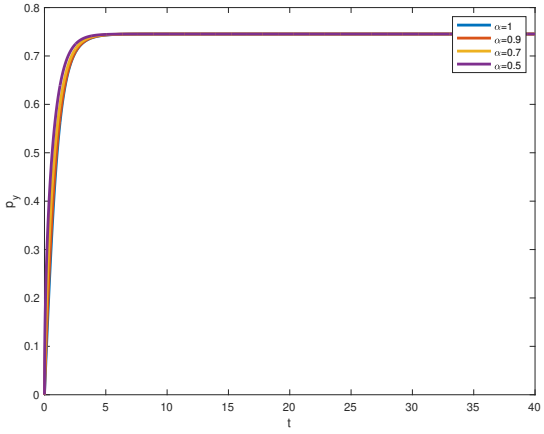
$$\boldsymbol{p}_y = \frac{\Lambda}{\tilde{\chi}} \frac{E_\alpha\left(\frac{\gamma\Lambda t^\alpha}{2}\right) - c_2 E_\alpha\left(-\frac{\gamma\Lambda t^\alpha}{2}\right)}{c_1 + E_\alpha\left(\frac{\gamma\Lambda t^\alpha}{2}\right) + c_2 E_\alpha\left(-\frac{\gamma\Lambda t^\alpha}{2}\right)}, \tag{5.21}$$

$$\boldsymbol{p}_z = \frac{\Lambda}{\tilde{\chi}} \frac{c_3}{c_1 + E_\alpha\left(\frac{\gamma\Lambda t^\alpha}{2}\right) + c_2 E_\alpha\left(-\frac{\gamma\Lambda t^\alpha}{2}\right)}, \tag{5.22}$$

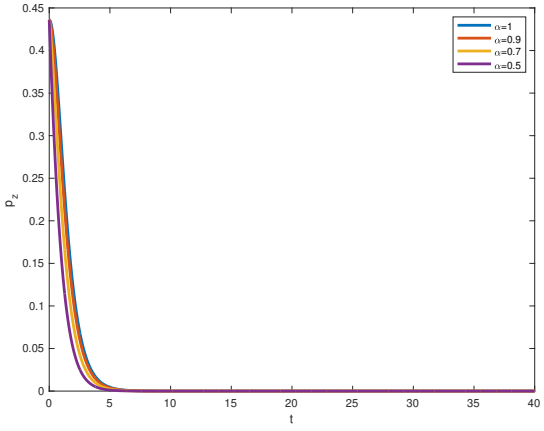
where $c_3 = \pm\sqrt{4c_2 - \tilde{\chi}^2 c_1^2}$.



((a)) The time evolution of $\boldsymbol{p}_x$ for the Modified Riemann-Liouville operator.



((b)) The time evolution of $\boldsymbol{p}_y$ for the Modified Riemann-Liouville operator.



((c)) The time evolution of $\boldsymbol{p}_z$ for the Modified Riemann-Liouville operator.

Figure 5.1: The depiction of the exact solutions for the fractional mapped equation acquired for $\boldsymbol{p}_x, \boldsymbol{p}_y$ and $\boldsymbol{p}_z$ is presented for four distinct values of α , denoting the fractional order.

Figure 5.1 illustrates the dynamics of $\boldsymbol{p}_x$, $\boldsymbol{p}_y$, and $\boldsymbol{p}_z$ as they converge toward the stable point $\left(\tilde{\chi}^{-1}, \sqrt{1-\tilde{\chi}^{-2}}, 0\right)$, regardless of the initial orientation. This behavior aligns perfectly with our theoretical findings regarding the stability of this equilibrium, confirming that the terminal vector lies within the shear plane. This corresponds to the pure run regime, showing that the particle orientation tends to the unique stable orientation.

As discussed earlier, the orientation angle φ characterizes the particle's motion, and since $\boldsymbol{p}_x$ and $\boldsymbol{p}_y$, are related to the orientation angle φ within the shear plane, we have:

$$\varphi(t) = \tan^{-1}\left(\frac{\boldsymbol{p}_y}{\boldsymbol{p}_x}\right), \tag{5.23}$$

leading to the following analytical expression of φ

$$\varphi(t) = tan^{-1}\Big(\Lambda \frac{E_\alpha\Big(\frac{\gamma\Lambda t^\alpha}{2}\Big) + c_2 E_\alpha\Big(-\frac{\gamma\Lambda t^\alpha}{2}\Big)}{\tilde{\chi}^2 c_1 + E_\alpha\Big(\frac{\gamma\Lambda t^\alpha}{2}\Big) + c_2 E_\alpha\Big(-\frac{\gamma\Lambda t^\alpha}{2}\Big)}\Big), \tag{5.24}$$

From this, we observe that the alignment angle $0 < \varphi < \frac{\pi}{2}$ between the microswimmer's orientation $\boldsymbol{p}$ and the external force $\boldsymbol{j}$ confirms that the unit vector $\boldsymbol{p}$ exhibits run motion, which is characteristic of the run phase.

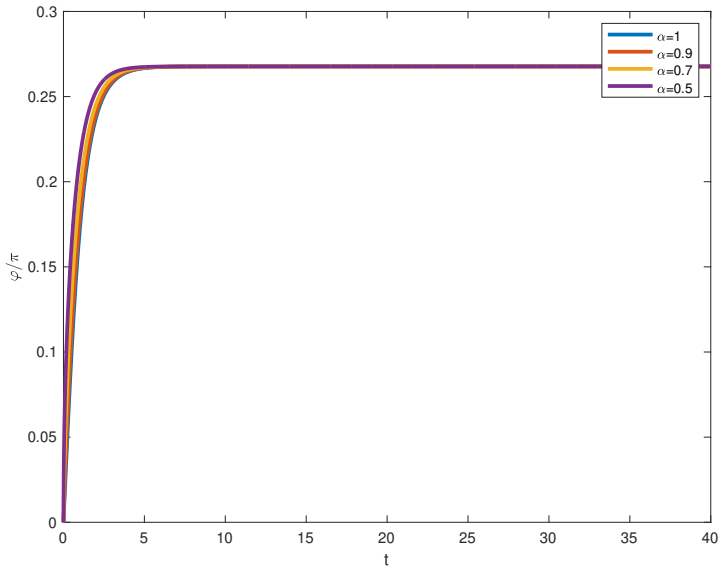


Figure 5.2: The particle's orientation angle φ for four different fractional order values.

Figure 5.2 further illustrates this relationship by presenting the orientation angle φ for various values of α. The solutions indicate that φ remains constant across different α values. During the run motion, the alignment angle $0 < \phi < \frac{\pi}{2}$ between the microswimmer's orientation $\boldsymbol{p}$ and the external force $\boldsymbol{j}$ demonstrates that the unit vector $\boldsymbol{p}$ exhibits run motion.

5.3.2 Damping mode

Considering the most essential part of our research, we direct our focus to the oscillatory solution, previously analyzed in the classical framework by the authors in [38] for the case where $\tilde{\chi} < 1$. Their study identified oscillatory solutions that delineate the TB mode. Building on this foundation, our work advances to the computation of exact solutions, incorporating the memory effect captured by the fractional derivative of the modified Riemann-Liouville. Through rigorous calculations, we derive the following expressions

$$\boldsymbol{p}_x = \tilde{\chi} + \frac{\Lambda^2}{\tilde{\chi}} \frac{\sin_\alpha\Big(\Big(\frac{\gamma\Lambda}{2}\Big)^{1/\alpha} t + c_2'\Big)}{c_1' + \sin_\alpha\Big(\Big(\frac{\gamma\Lambda}{2}\Big)^{1/\alpha} t + c_2'\Big)}, \tag{5.25}$$

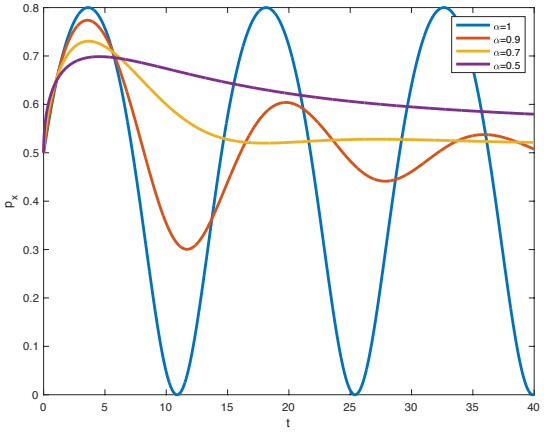
$$\boldsymbol{p}_y = \frac{\Lambda}{\tilde{\chi}} \frac{\cos_\alpha\left(\left(\frac{\gamma\Lambda}{2}\right)^{1/\alpha} t + c_2'\right)}{c_1' + \sin_\alpha\left(\left(\frac{\gamma\Lambda}{2}\right)^{1/\alpha} t + c_2'\right)}, \tag{5.26}$$

$$\boldsymbol{p}_z = \frac{\Lambda}{\tilde{\chi}} \frac{c_3'}{c_1' + \sin_\alpha\left(\left(\frac{\gamma\Lambda}{2}\right)^{1/\alpha} t + c_2'\right)}. \tag{5.27}$$

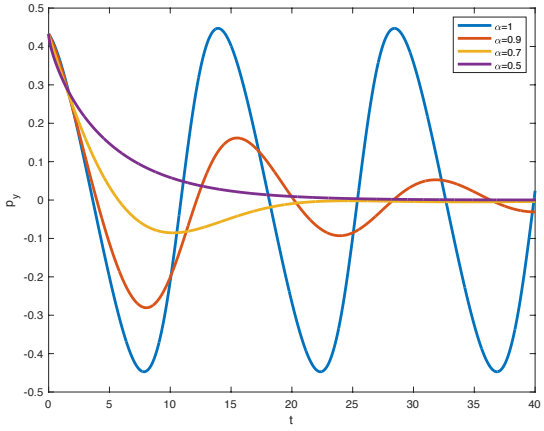
These expressions are connected to the distinct fractional $\cos_\alpha$ and $\sin_\alpha$ functions introduced in Definition 1.10, where $c_3' = \pm\sqrt{\tilde{\chi}^2 c_1' - 1}$. The incorporation of these well-established functions offers a novel perspective, highlighting the intricate nature of the oscillatory phenomena under study. Through rigorous mathematical analysis and detailed calculations, we present the derived expressions, thus providing a significant and valuable contribution to the understanding of these complex dynamics.

Our theoretical findings demonstrate that the fractional-order derivative α has a substantial impact on the stability of the equilibrium. In contrast, in the classical case ($\alpha = 1$), no conclusions can be drawn regarding stability.

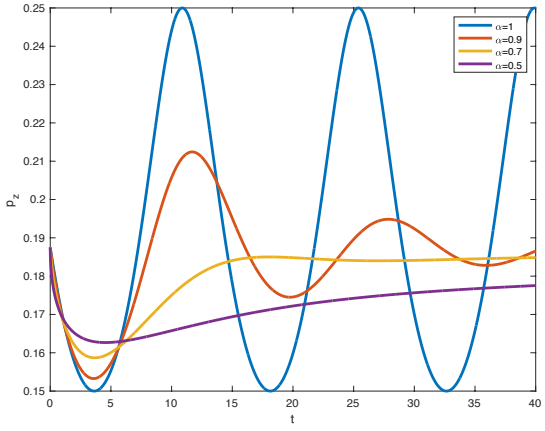
To further illustrate our findings, we present a visual depiction of the time evolution of the amplitudes $\boldsymbol{p}_x, \boldsymbol{p}_y$, and $\boldsymbol{p}_z$ for the Jumarie operator in Fig. 5.3, considering four distinct values of α. The subsequent graphical representations align with our theoretical results.



((a)) The time evolution of $\boldsymbol{p}_x$ for the Modified Riemann-Liouville operator.



((b)) The time evolution of $\boldsymbol{p}_y$ for the Modified Riemann-Liouville operator.



((c)) The time evolution of $\boldsymbol{p}_z$ for the Modified Riemann-Liouville operator.

Figure 5.3: The depiction of the exact solutions for the fractional mapped equation acquired for $\boldsymbol{p}_x, \boldsymbol{p}_y$ and $\boldsymbol{p}_z$ is presented for four distinct values of α , denoting the fractional order.

These figures depict a cosine form that varies with the fractional derivative order α. Notably, when $\alpha = 1$, oscillations are present in the $\boldsymbol{p}_x, \boldsymbol{p}_y$, and $\boldsymbol{p}_z$ components. However, for $0 < \alpha < 1$ there is a noticeable reduction in amplitude as α decreases, indicating that the microswimmer motion diverges from pure TB. This highlights the need to identify the specific regime predicted by the rigid particle in these conditions. To achieve this, a more in-depth analysis of the specific movement and deformation is necessary. In particular, we need to derive expression for φ (the orientation angle defined in (5.23)). Therefore, utilizing the relationship between $\boldsymbol{p}_x, \boldsymbol{p}_y$, and φ will enable us to determine these characteristics

$$\varphi(t) = \tan^{-1}\left(\Lambda \frac{\cos_\alpha\left(\left(\frac{\gamma\Lambda}{2}\right)^{1/\alpha} t + c_2'\right)}{\Gamma + \sin_\alpha\left(\left(\frac{\gamma\Lambda}{2}\right)^{1/\alpha} t + c_2'\right)}\right). \tag{5.28}$$

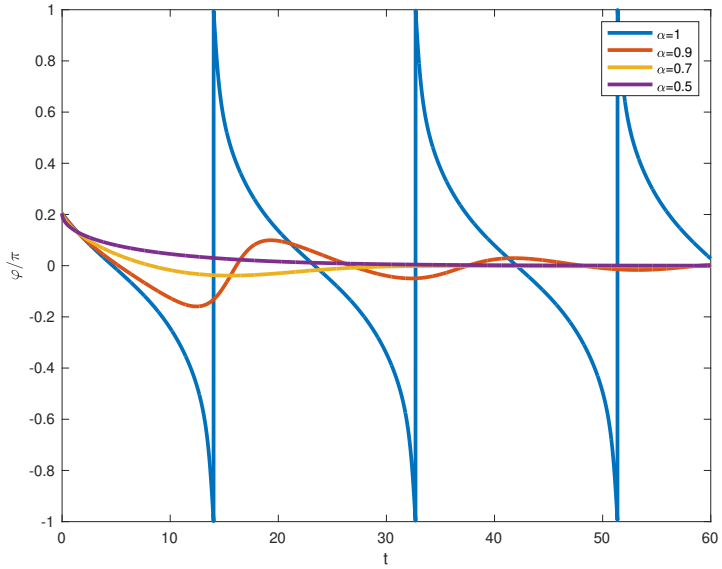


Figure 5.4: The particle's orientation angle φ for four different fractional order values with four different values of α.

Figure 5.4 presents the orientation angle φ for four distinct values of α under the condition $\tilde{\chi} < 1$. In the classical case where $\alpha = 1$, the particle exhibits tumbling behavior, consistent with the observations reported in [38]. However, for $0 < \alpha < 1$, the application of the modified Riemann-Liouville fractional derivative introduces an extended damping period and greater alignment with the flow as α decreases, eventually leading to a stationary orientation. This observation yields several significant conclusions, particularly in the context of incorporating the memory effect and the transition of the particle from tumbling to stationary motion within shear flows. This innovative approach not only illuminates the nuanced behavior exhibited by microswimmers in fluid environments but also advances the broader discourse on fluid-particle dynamics, highlighting the intricate interplay between particle shape, motion, and environmental factors. The memory effect is pivotal in determining how particles respond and orient themselves over time, as fractional-order derivatives allow us to study how particles react based on their recent history, thereby influencing their current orientation and enabling them to adapt dynamically to environmental changes.

In summary, the damping of the orientation angle with the introduction of fractional-order derivatives reveals a more complex and adaptive system dynamic, characterized by significant memory effects and emergent properties. Understanding and interpreting these changes are essential for accurately modeling and predicting system behavior. By incorporating Jumarie's modified Riemann-Liouville derivative, we present a more realistic and comprehensive model. In the following section, we will examine the influence of memory effects on swimming trajectories in one-dimensional shear flow.

5.3.3 Special Case: No Preferred Swimming Direction ($\chi = 0$)

To transition from the general case to a specific scenario, we consider the situation where there is no preferred swimming direction, represented by χ. This condition can arise in two distinct circumstances: either due to strong rotational motion that prevents a defined swimming direction or because there is no external torque acting on the microswimmer. In this particular case, the dynamics differ significantly, as the absence of a preferred direction leads to distinct behavioural patterns that must be examined separately from the general analysis. As a result, we obtain the following expressions for the components of the swimming trajectory

$$\boldsymbol{p}_x = C' \cos_\alpha \left(\left(\frac{\gamma}{2} \right)^{1/\alpha} t + C \right), \tag{5.29}$$

$$\boldsymbol{p}_y = C' \sin_\alpha \left(\left(\frac{\gamma}{2} \right)^{1/\alpha} t + C \right), \tag{5.30}$$

$$\boldsymbol{p}_z = \pm \sqrt{1 - C'^2}. \tag{5.31}$$

These expressions take into account the fractional derivative order α, which incorporates the memory effect, influencing the oscillatory motion of the system. In this fractional context, the memory effect modifies the swimming trajectories, reflecting the system's dependence on past states, thus providing a more comprehensive understanding of the particle's behavior under these specific conditions. These graphs will visualize the impact of the fractional derivative order α on the components $\boldsymbol{p}_x$,$\boldsymbol{p}_y$, and $\boldsymbol{p}_z$, enabling a more detailed analysis of the system's oscillatory behavior in this specific scenario.

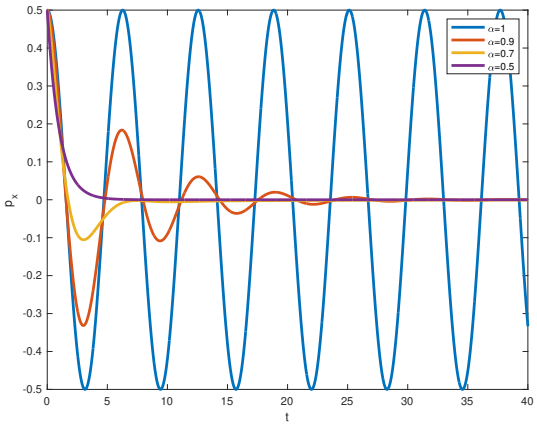


Figure 5.5: The time evolution $\boldsymbol{p}_x$ for the Modified Riemann-Liouville operator ($\chi = 0$).

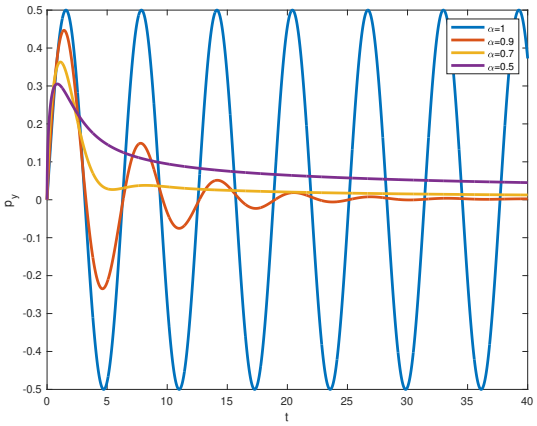


Figure 5.6: The time evolution $\boldsymbol{p}_y$ for the Modified Riemann-Liouville operator ($\chi = 0$).

Figures 5.5 and 5.6 illustrate the time evolution of the amplitudes $\boldsymbol{p}_x$ and $\boldsymbol{p}_y$ for the modified RiemannLiouville operator under the condition $\chi = 0$, analyzed for four distinct values of the fractional order α. The results reveal a cosine-like behavior dependent on the order of the derivative

α, analogous to the general case where $\chi \neq 0$. Notably, when $\alpha = 1$, the $\boldsymbol{p}_x$ and $\boldsymbol{p}_y$ components exhibit sustained oscillations. In contrast, for $0 < \alpha < 1$, which is central to this investigation, the amplitudes decrease progressively as α is reduced. This pattern suggests that in the specific scenario where $\chi = 0$, corresponding to the absence of external torque, the spherical particle exhibits a damped motion within the shear plane.

5.4 Memory Effects on Swimming Trajectories in 1D Shear Flow

The aim of this section is to explore the long-term particle transport in simple shear flow within the framework of fractional calculus. As previously explained, the time evolution of the center of mass position is governed by

$$ {}^{\mathscr{J}}D_t^{\alpha}\mathbf{x} = \mathbf{u}_0(\mathbf{x}) + \mathbf{v_s}, \tag{5.32}$$

where $\mathbf{vs} = v_s\boldsymbol{p}$ denotes the swimming velocity vector relative to the fluid, and $v_s = |\mathbf{vs}|$ is assumed constant. Various physical forces can influence particle trajectories. For instance, as mentioned earlier, a gyrotactic cell may maintain a fixed orientation or tumble [38, 50, 75]. By utilizing explicit expressions for the orientation vector $\boldsymbol{p}$, we derive exact expressions here for the swimmer's position $\boldsymbol{x} = (x, y, z)$ by solving the system of equations

$$ {}^{\mathscr{J}}D_t^{\alpha}x(t) = \gamma y + v_s\boldsymbol{p}_x, \quad {}^{\mathscr{J}}D_t^{\alpha}y(t) = v_s\boldsymbol{p}_y, \quad {}^{\mathscr{J}}D_t^{\alpha}z(t) = v_s\boldsymbol{p}_z. \tag{5.33}$$

We will explore three distinct cases: the trajectories under the run regime, the damping regime, and a specific instance with $\chi = 0$. For the latter, we have plotted the trajectory to facilitate the reader's understanding of how memory effects influence the swimmer's position.

5.4.1 Trajectories in the run regime

In the general run regime, we perform a comprehensive analysis using the properties of the modified Riemann-Liouville fractional derivative. This approach yields exact solutions for the swimmer's position relative to its initial coordinates. Specifically, we have

$$\begin{aligned} x(t) - x(0) &= \gamma\left[y(0) + \frac{v_s}{\tilde{\chi}} - \frac{2v_s}{\tilde{\chi}}\ln(C_1 + C_2 + 1)\right]\frac{t^{\alpha}}{\Gamma(\alpha+1)} \\ &+ \frac{2\gamma v_s}{\tilde{\chi}} I_0^{\alpha}\ln\left(C_1 + E_{\alpha}\left(\frac{\Lambda t^{\alpha}}{2}\right) + C_2 E_{\alpha}\left(\frac{-\Lambda t^{\alpha}}{2}\right)\right) \\ &- \frac{\Lambda v_s}{\tilde{\chi}}\frac{2c_1}{\sqrt{c_2 - \left(\frac{c_1}{2}\right)^2}}\left[\arctan\left(\frac{E_{\alpha}\left(\frac{\Lambda t^{\alpha}}{2}\right) + \frac{c_1}{2}}{\sqrt{c_2 - \left(\frac{c_1}{2}\right)^2}}\right) - \arctan\left(\frac{1 + \frac{c_1}{2}}{\sqrt{c_2 - \left(\frac{c_1}{2}\right)^2}}\right)\right] \end{aligned} \tag{5.34}$$

This reflects how the shear rate, swimming speed, and memory effect collectively shape the longitudinal motion of the swimmer. Similarly, for the lateral displacement $y(t)$, the solution is

given by

$$y(t)-y(0)=\frac{2v_s}{\tilde{\chi}}\ln\left(\frac{C_1+E_2\left(\frac{\Lambda t^\alpha}{2}\right)+C_2E_1\left(-\frac{\Lambda t^\alpha}{2}\right)}{C_1+C_2+1}\right), \tag{5.35}$$

This expression highlights the memory effect, evident here, indicates that past movements significantly influence the present position, making the path of the swimmer more intricate over time. Finally, the vertical position $z(t)$ is described by

$$z(t)-z(0)=\frac{2\Lambda b}{\tilde{\chi}\sqrt{1-a^2}}v_s\left[\arctan\left(\frac{E_\alpha\left(\frac{\Lambda t^\alpha}{2}\right)+a}{\sqrt{1-a^2}}\right)-\arctan\left(\frac{1+a}{\sqrt{1-a^2}}\right)\right], \tag{5.36}$$

where a and b depend on the constant c_1,c_2 and c_3. The $z(t)$ expression shows a dependence on the arctangent of Mittag-Leffler functions, revealing how the swimmer's vertical motion is modulated by the fractional dynamics and the memory effect. This results in a more complex vertical trajectory, where the cumulative history of motion plays a critical role.

For the classical case where $\alpha = 1$, these expressions simplify to those of a spherical gyrotactic particle, as studied in [38, 82]. In this scenario, the trajectories are determined solely by the current forces acting on the particle, with no memory effect. However, when $0 < \alpha < 1$, the solutions reveal a significant departure from classical behavior. The fractional derivative introduces a memory effect, meaning the particle's current position is influenced not only by the present forces but also by the entire history of the system's dynamics. This results in more complex trajectories in the x, y, and z directions, where past movements affect the present, showcasing the non-local and cumulative nature of the memory effect. These exact solutions provide deep insight into the dynamics of particles under the influence of memory effects, even though the complexity of the expressions precludes simple graphical representation.

5.4.2 Trajectories in the Tumbling regime

Let us now return to the central focus of our study. For a general damping trajectory, by employing the Riemann-Liouville fractional integral, we derive the following exact expressions for the particle's position. While these solutions are complex, and plotting the corresponding curves was not feasible, the derivation of these exact forms is a noteworthy achievement, providing valuable insights into the particle dynamics governed by fractional calculus.

For the x-component of the position, the expression is given by

$$\begin{aligned}x(t)-x(0)=&\left[\gamma y(0)-\gamma\frac{2v_s}{\tilde{\chi}}\ln\left(c_1'\right)+\frac{v_s}{\tilde{\chi}}\right]\frac{t^\alpha}{\Gamma(\alpha+1)}+\frac{2v_s}{\tilde{\chi}}I_0^\alpha\ln\left(c_1'+\sin_\alpha\left(\left(\frac{\gamma\Lambda}{2}\right)^{1/\alpha}t\right)\right)\\&-\frac{v_s}{\tilde{\chi}}\frac{4c_1'\Lambda}{\sqrt{{c_1'}^2-1}}\left[\arctan\left(\frac{c_1'\tan_\alpha\left(\left(\frac{\gamma\Lambda}{4}\right)^{1/\alpha}t\right)+1}{\sqrt{{c_1'}^2-1}}\right)-\arctan\left(\frac{1}{\sqrt{{c_1'}^2-1}}\right)\right]\end{aligned} \tag{5.37}$$

For the y-component, the expression is

$$y(t) - y(0) = \frac{2v_s}{\tilde{\chi}} \ln\left(\frac{c_1' + \sin_\alpha\left(\left(\frac{\Lambda}{2}\right)^{1/\alpha} t + c_3'\right)}{c_1'} \right), \tag{5.38}$$

The z-component of the position is given by

$$z(t) - z(0) = v_s \frac{c_2'}{\tilde{\chi}} \frac{4}{\sqrt{c_1'^2 - 1}} \left[\arctan\left(\frac{c_1' \tan_\alpha\left(\left(\frac{\Lambda}{4}\right)^{1/\alpha} t\right) + 1}{\sqrt{c_1'^2 - 1}} \right) - \arctan\left(\frac{1}{\sqrt{c_1'^2 - 1}} \right) \right]. \tag{5.39}$$

The resulting equations, though challenging to visualize, are essential for understanding the full scope of fractional dynamics, paving the way for future studies that may explore numerical methods or approximations to better capture these complex trajectories visually. Unlike classical systems where the future trajectory depends only on the current state, these fractional systems encapsulate a rich history of past states. These results demonstrate, as anticipated, that the y and z components exhibit periodic behavior with amplitudes that decrease as α decreases, while the x component remains unbounded over time. This historical dependence is reflected in the mathematical complexity of the expressions, highlighting how each infinitesimal moment contributes to the evolving state of the particle.

These findings emphasize the importance of considering fractional models in describing systems where memory and hereditary properties are significant. As we continue to unravel these intricate dynamics, the mathematical formulations we develop not only enhance our theoretical understanding but also provide a foundation for practical applications in fields ranging from physics to biology and beyond.

5.4.3 Trajectories in the special case $\chi = 0$

We now examine the specific case where we assume $\chi = 0$, indicating the absence of external forces acting on the system. By solving the set of equations in (5.33) using the properties outlined in Chapter 1, we derive exact expressions for the swimmer's position $\mathbf{X} = (x, y, z)$. These exact solutions are crucial for understanding how the swimmer behaves when only internal dynamics, such as gyrotaxis and self-propulsion, influence its movement without any external perturbations.

For the x-component of the position, we have

$$x(t) - x(0) = \left[\gamma y(0) + 2C' v_s \cos_\alpha(C)\right] \frac{t^\alpha}{\Gamma(\alpha+1)} + \frac{2C' v_s}{\gamma} \left[\sin_\alpha(C) - \sin_\alpha\left(\left(\frac{\gamma}{2}\right)^{1/\alpha} t + C\right)\right]. \tag{5.40}$$

The y-component is given by

$$y(t) - y(0) = \frac{2C' v_s}{\gamma} \left[\cos_\alpha(C) - \cos_\alpha\left(\left(\frac{\gamma}{2}\right)^{1/\alpha} t + C\right)\right]. \tag{5.41}$$

For the z-component, we derive

$$z(t) - z(0) = \pm v_s \sqrt{1 - C'^2} \frac{t^\alpha}{\Gamma(\alpha + 1)}. \tag{5.42}$$

By focusing on these exact solutions, we uncover the detailed trajectory behavior under the influence of memory. The expressions for $x(t)$, $y(t)$, and $z(t)$ reveal how the swimmer's position evolves over time, not just due to instantaneous forces, but as a result of all prior motions. This emphasizes the importance of memory effects in accurately describing the system's dynamics, making fractional calculus an essential tool for modeling such systems. Unlike classical systems, where motion is purely a function of the immediate instant, the fractional dynamics encapsulate a memory effect, meaning the swimmer's current position is a cumulative result of its entire path history. This makes the system more realistic in capturing phenomena where past states play a significant role, such as in biological systems or complex fluids.

The trajectories reveal how the system's dynamics, characterized by fractional calculus, lead to unique motion patterns. They provide a tangible means to explore and interpret the influence of memory on the swimmer's behavior. This visual representation not only confirms the theoretical predictions but also offers valuable insights into the dynamics of fractional-order systems. By illustrating these trajectories, we gain a deeper understanding of how fractional dynamics shape the system's behavior, paving the way for further exploration and application of fractional calculus in various scientific and engineering fields. Figure 5.7 shows an instance of the trajectories

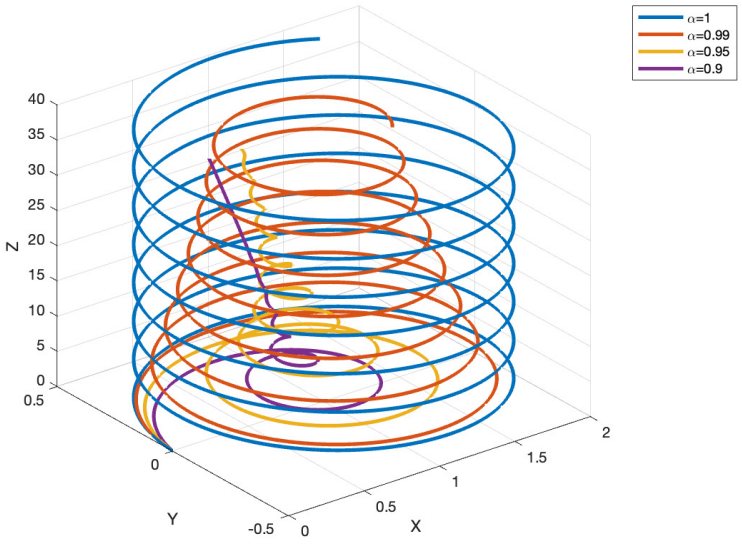


Figure 5.7: Example of a trajectory for the fractional case in the absence of external torque (Eqs. (5.40)-(5.42)) with four arbitrary values of α. The parameters are $C = \frac{\pi}{2}, C' = 0.5, v_s = 1$, and $\gamma = 2$.

for large t of a swimmer in the absence of external torque. In the case where $\alpha = 1$, corresponding to the classical scenario, the swimmer's trajectory exhibits a periodic helical structure, with the

helix pitch oriented along the z-axis. This configuration results in a well-ordered and repetitive motion, indicative of a stable trajectory in the absence of external torques.

As α decreases, entering the fractional regime where $0 < \alpha < 1$, the previously tight helical trajectory begins to expand. The influence of memory effects inherent in fractional derivatives disrupts the periodic nature of the motion. Notably, in this fractional case, the radius of the helical trajectory decreases over time, progressively shrinking as the swimmer moves forward. This reduction in radius eventually leads the trajectory to approach a linear path. As α approaches zero, the trajectory deviates increasingly from the initial helical form, with the radius decreases until the motion becomes nearly straight. This behavior implies that the swimmer oscillates infinitely around the rotation axis, ultimately converging towards this axis as $t \to \infty$. In the second sce-

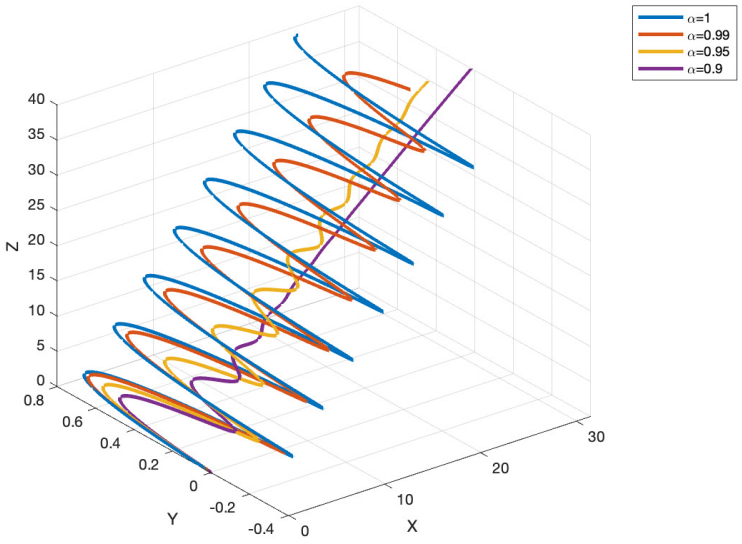


Figure 5.8: Example of a trajectory for the fractional case in the absence of external torque (Eqs. (5.40)-(5.42)) with four arbitrary values of α. The parameters are $C = \frac{\pi}{3}, C' = 0.5, v_s = 1$, and $\gamma = 2$.

nario where $\dfrac{\gamma y(0) + 2C' v_s \cos_\alpha(C)}{\Gamma(\alpha+1)} \neq 0$, the swimmer's trajectory becomes unbounded in both the x and z directions (see Figure 5.8). In conclusion, the decrease in α fundamentally alters the nature of the trajectory, transitioning it from a regular, tightly coiled swirl to a more open and eventually linear motion, thereby illustrating the growing influence of memory effects within the system.

For the particular case where $\chi = 0$, indicating the absence of external torque, the spherical particle exhibits a tumbling motion. When $\alpha = 1$, the resulting trajectory is a cycloid within the shear plane. In contrast, for the fractional case where $0 < \alpha < 1$, the particle predicts a damping effect, leading the cycloidal trajectory to gradually decrease in radius over time, eventually evolving into a linear path.

In the context of dynamical systems, such behavior is analogous to the effects of damping, which

typically lead to a reduction in oscillatory energy, resulting in diminished amplitude or altered motion over time. The memory effects introduced by the fractional order act similarly to a dissipative force, modifying the swimmer's trajectory. The resulting motion transitions from a helical structure to a more linear path, akin to the effect of damping on a classical oscillator where oscillations progressively decrease.

Understanding the influence of memory effects on microswimmer trajectories has significant implications for the design and optimization of these systems. This knowledge is particularly vital for applications such as targeted drug delivery, where precise control over microswimmer motion is critical. Our findings establish a foundation for optimizing microswimmer designs tailored to specific applications, thereby enhancing their efficiency and effectiveness. Notably, in the presence of memory effects, the final trajectory depends not only on the initial conditions but also on the value of α.

5.5 Conclusion and Future Perspectives

This chapter highlights the transformative potential of fractional calculus in unraveling the complex dynamics of spherical microswimmers within a 1D shear flow. The exact solutions we have derived not only deepen our understanding of the memory effects that shape microswimmer trajectories but also provide a robust framework for analyzing their behavior under varying conditions. While the intricate nature of these solutions poses visualization challenges, our targeted approach has yielded practical insights that can be readily applied in real-world scenarios.

As we look to the future, exciting opportunities await in the exploration of microswimmers in external fluids. We plan to investigate their dynamics in more complex flow environments, including turbulent and non-Newtonian fluids, which will enhance our comprehension of their performance in realistic settings. This exploration will be crucial for optimizing microswimmer designs for applications in targeted drug delivery, environmental remediation, and advanced micro-robotics.

Moreover, expanding our research to encompass a diverse array of microswimmer types, including nonspherical and biologically inspired models, will broaden the scope and impact of our findings. By integrating fractional calculus with a variety of fluid dynamics scenarios, we aim to push the boundaries of current knowledge and foster innovations that can revolutionize the field of microswimmer research. Ultimately, this work not only contributes to theoretical advancements but also holds the promise of significant practical applications that can benefit society at large.

In conclusion, the use of fractional calculus in the study of microswimmer dynamics opens up new avenues for research and technological advancements. The incorporation of memory effects through fractional derivatives provides a more accurate and comprehensive description of these systems, paving the way for innovative approaches in biophysics and fluid dynamics.

CHAPTER 6

EFFECT OF FAMILY AND PUBLIC HEALTH EDUCATION IN DRUG TRANSMISSION: AN EPIDEMIOLOGICAL MODEL WITH MEMORY

Contents

6.1 Introduction **126**
6.2 Formulation of the fractional order model **127**
6.3 Results **129**
6.3.1 The existence, positivity and boundedness of solutions of the fractional model 129
6.3.2 The basic reproduction number, existence, and stability of equilibrium 130
6.3.3 Numerical method for Caputo-fractional derivative 137
6.3.4 Model parameter sensitivity analysis in relation to the basic reproduction number 141
6.4 Discussion **146**
6.4.1 Memory effect 146
6.4.2 The influence of model parameters 147
6.4.3 Sensitivity analysis of model parameters 148
6.5 Conclusion **148**

6.1 Introduction

Having studied the complex dynamics of vesicles and red blood cells in shear flows in the previous chapters, we now shift focus to a macroscopic phenomenon: drug abuse in populations. The same fractional calculus models, which capture memory effects in cellular systems, can be applied to epidemiology. This chapter explores how these tools help us understand the spread of drug abuse by incorporating memory into epidemiological models.

Drug abuse, also known as drug addiction, is a major health and social problem globally, with complex impacts on health, public safety, crime, economics, and politics. Drug use contributes to the spread of contagious diseases like AIDS and hepatitis [68, 71]. Recognized as a new epidemic, drug abuse shares characteristics with classical epidemics (SIR, SEIR, etc. [22, 34, 35]. Various mathematical models have been developed to understand the mechanisms of drug transmission and to design effective countermeasures [21, 40, 62, 66, 70]. For example, in [88] they presented a heroin model highlighting the importance of prevention over treatment, while the authors in [60], used distributed delays in their model to show the relation between stability of equilibrium and the basic reproduction number $\mathscr{R}_0$. [67] analyzed the global stability of a SIRS model considering both light and heavy drugs.

Some epidemic models also incorporate public health education alongside classical treatments like vaccination and isolation. Studies have shown that health education initiatives can significantly reduce the spread of diseases [6, 54, 65, 78, 89]. Recently, fractional derivatives have been used in epidemiological models to account for memory effects, offering more accurate interpretations than integer-order models [27, 31, 76, 80].

In this chapter, we examine the six-dimensional drug model incorporating family and public health education introduced by [54], studying the effect of memory using the Caputo fractional derivative order. The Caputo fractional derivative, as discussed in the Introduction, is frequently used for modeling real-world problems due to its ability to incorporate traditional initial conditions and its similarity to ordinary derivatives.

The current chapter is organized as follows: We investigate the dynamical transmission process of the drug spread by utilizing Caputo operator. In the following section we introduce the classical and fractional models. “Results” section contains the main findings of this chapter, where we have proved the existence and uniqueness of the solution for the fractional drug mode, as well as the local stability of the disease-free and endemic equilibrium points. Moreover, with the help of Lyapunov functions, the global stability of the two equilibrium points is proven according to the basic reproduction number $\mathscr{R}_0$. The modified trapezoidal rule and the fractional Euler’s method are employed to support our analytical findings. Further, the parameter’s sensitivity was examined. In “Discussion” section, we depict our principal results with graphical representations and discuss the memory effect, the influence of model parameters, and the sensitivity analysis of model parameters. The conclusions are given in “Conclusion” section. The results of this chapter are based on the paper [9].

6.2 Formulation of the fractional order model

We consider in this section that the drug transmission model combines public health education and family education [54]. Individuals under the age of 15 receive drug safety education primarily from their families, while those over the age of 15 receive it from society or school, which could be referred as public health education.

The total population N is divided into six groups, namely, susceptible drug users who accept public health education (S), susceptible drug users who accept public health education (C), as well as individuals who use light drugs (L), individuals who use heavy drugs (H), individuals in treatment for drug addiction (T), and individuals who have permanently quit drugs (R).

Therefore, the proposed classical non-linear system of ODEs takes the following form [54],

$$
\begin{cases}
\frac{\mathrm{d}S}{\mathrm{d}t} = (1-q)d\Lambda - \alpha_1 SL - \alpha_2 SH - (d+\tau)S, \\
\frac{\mathrm{d}C}{\mathrm{d}t} = qd\Lambda + \tau S - \alpha_1 \varepsilon CL - \alpha_2 \varepsilon CH - (d+\chi)C, \\
\frac{\mathrm{d}L}{\mathrm{d}t} = \alpha_1 SL + \alpha_2 SH + \alpha_1 \varepsilon CL + \alpha_2 \varepsilon CH - e_1 L, \\
\frac{\mathrm{d}H}{\mathrm{d}t} = \sigma L + \mu T - e_2 H, \\
\frac{\mathrm{d}T}{\mathrm{d}t} = \theta H + \gamma L - e_3 T, \\
\frac{dR}{dt} = \chi C + mT - dR.
\end{cases} \tag{6.1}
$$

Figure 6.1 depicts the transfer diagram for this model. A proportion $q \quad (0 < q < 1)$, of the general population accept the family health education, whereas a proportion $1-q$ do not accept family education. In the meanwhile, a susceptible person easiest to capture by a heavy drug addict; this presupposes that $\alpha_2 > \alpha_1$. Therefore, public health education causes persons who are susceptible (C) to become light addicts at rate $\varepsilon\alpha_1$ and $\varepsilon\alpha_2$, where $\varepsilon \in (0,1)$.

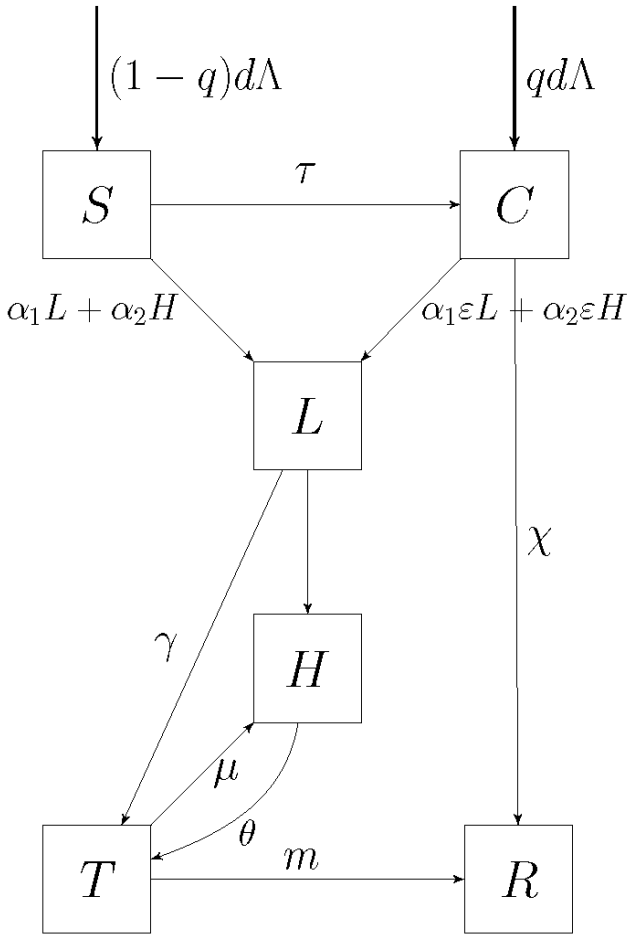


Figure 6.1: Schematic diagram of drug model and parameters with health education according to [54]

The above ordinary differential system (6.1) was analysed by [54]; it does not depend on the previous instant. As mentioned above, the non-locality of the fractional operator plays a very important role in including not only the time instant but also the time history, as drug spreading dynamics exhibited strong different temporal memories, thus motivating the application of fractional derivative methods. In the next part, the system is further extended to a fractional-order one.

For our present model, we use as mentioned before the Caputo fractional derivative instead of the classical one. In this case, we obtain

$$
\begin{cases}
{}^{C}D_t^{\alpha} S(t) = (1-q)d\Lambda - \alpha_1 SL - \alpha_2 SH - (d+\tau)S \\
{}^{C}D_t^{\alpha} C(t) = qd\Lambda + \tau S - \alpha_1 \varepsilon CL - \alpha_2 \varepsilon CH - (d+\chi)C, \\
{}^{C}D_t^{\alpha} L(t) = \alpha_1 SL + \alpha_2 SH + \alpha_1 \varepsilon CL + \alpha_2 \varepsilon CH - e_1 L, \\
{}^{C}D_t^{\alpha} H(t) = \sigma L + \mu T - e_2 H, \\
{}^{C}D_t^{\alpha} T(t) = \theta H + \gamma L - e_3 T, \\
{}^{C}D_t^{\alpha} R(t) = \chi C + mT - dR,
\end{cases}
\tag{6.2}
$$

where D^{α}, denotes the Caputo-fractional operator of order $0 < \alpha \leq 1$. System (6.2) will be analysed under the following initial conditions

$$\begin{aligned} &S(0) = S_0 > 0, \quad C(0) = C_0 > 0, \quad L(0) = L_0 > 0, \\ &H(0) = H_0 > 0, \quad T(0) = T_0 > 0, \quad R(0) = R_0 > 0. \end{aligned} \tag{6.3}$$

Moreover, parameters in system (6.2) are the same as those of the classical model (6.1) (see Table 6.1).

Table 6.1: The parameters used in the drug transmission model

Parameters	Symbol
Natural birth and dead rate	d
The total size of new recruits	Λ
popularizing rate of family education	q
The rate that susceptible individuals accept public health education	τ
The effective contact rate that susceptible individuals contact with light drug addicts	α_1
The effective contact rate that susceptible individuals contact with heavy drug addicts	α_2
The factor which results the effective contact rates decrease	ε
The death rate related the light drug addiction	β_1
The death rate related the heavy drug addiction	β_2
The treatment rate of light drug addicts	γ
The transformation rate from light addicts to heavy addicts	σ
The permanent quit drug rate because of public health education	χ
The treatment rate of heavy addicts	θ
The relapse rate after treatment	μ
The permanent quit drug rate after treatment	m

The total population $N(t) = S(t) + C(t) + L(t) + H(t) + T(t) + R(t)$.

It has been shown by [54], that the dynamics of system (6.1), can be studied in the following biologically feasible region denoted by :

$$D = \{(S, C, L, H, T, R) \mid S \geq 0, C \geq 0, L \geq 0, H \geq 0, T \geq 0, R \geq 0, S + C + L + H + T + R \leq \Lambda\}.$$

6.3 Results

6.3.1 The existence, positivity and boundedness of solutions of the fractional model

Since the variables $S(t), C(t), L(t), H(t)$, and $T(t)$ determine the human population, it is critical to prove that all variables are positive when $t \geq 0$.

Theorem 6.3.1.

The initial value problem of Caputo-fractional order (6.2) *has a unique solution* $x(t) = (S(t), C(t), L(t), H(t), T(t), R(t))$ *in the positively set* D.

Proof. Using Theorem 3.1 presented in [41] and Lemma 1.2.3, the existence and uniqueness of the $x(t) = (S(t), C(t), L(t), H(t), T(t), R(t))$ corresponding to the system (6.2) is proved.
To show that D for the fractional model (6.2) is positively invariant, we must demonstrated that any solution trajectory beginning in D persists in D on $[0, \infty)$.
First, we notice that

$$\begin{aligned}
{}^{C}D_t^{\alpha} S|_{S=0} &= (1-q)d\Lambda \geq 0,\\
{}^{C}D_t^{\alpha} C|_{C=0} &= qd\Lambda + \tau S \geq 0,\\
{}^{C}D_t^{\alpha} L|_{L=0} &= \alpha_2 SH + \alpha_2 \varepsilon CH \geq 0,\\
{}^{C}D_t^{\alpha} H|_{H=0} &= \sigma L + \mu T \geq 0,\\
{}^{C}D_t^{\alpha} T|_{T=0} &= \theta H + \gamma L \geq 0,\\
{}^{C}D_t^{\alpha} R|_{R=0} &= \chi C + mT \geq 0.
\end{aligned}$$

Thus, the vector field points to D in each hyperplane surrounding the non-negativity of the solutions. The evidence will then be established based on Lemma 1.2.2.
We have,

$$D^{\alpha} N(t) = {}^{C}D_t^{\alpha} S(t) + {}^{C}D_t^{\alpha} C(t) + {}^{C}D_t^{\alpha} L(t) + {}^{C}D_t^{\alpha} H(t) + {}^{C}D_t^{\alpha} T(t) + {}^{C}D_t^{\alpha} R(t),$$

Moreover, to verify the boundedness of the solution components, it can easily be seen that

$$\begin{aligned}
{}^{C}D_t^{\alpha} N &= d\Lambda - dN(t) - \beta_1 L(t) - \beta_2 H(t)\\
&\leqslant d\Lambda - dN(t).
\end{aligned}$$

We acquire upon figuring out $N(t)$

$$N(t) \leqslant N(0) E_{\alpha}\left(-dt^{\alpha}\right) + \Lambda\left(1 - E_{\alpha}\left(-dt^{\alpha}\right)\right).$$

Consequently, if $N(0) \leqslant \Lambda$, then the total population $N(t)$ is bounded between 0 and Λ. Hence the boundedness of all the solution components.
Therefore, the set D is positively invariant and the system (6.2) is well-posed. ■

6.3.2 The basic reproduction number, existence, and stability of equilibrium

We solve the drug transmission models to identify their equilibrium.

$$\begin{aligned}
&(1-q)d\Lambda - \alpha_1 SL - \alpha_2 SH - (d+\tau)S = 0,\\
&qd\Lambda + \tau S - \alpha_1 \varepsilon CL - \alpha_2 \varepsilon CH - (d+\chi)C = 0,\\
&\alpha_1 SL + \alpha_2 SH + \alpha_1 \varepsilon CL + \alpha_2 \varepsilon CH - e_1 L = 0,\\
&\sigma L + \mu T - e_2 H = 0,\\
&\theta H + \gamma L - e_3 T = 0,\\
&\chi C + mT - dR = 0.
\end{aligned}$$

The drug-free equilibrium is given by $\mathscr{E}_0 = (S_0, C_0, L_0, H_0, T_0, R_0)$, where, $L_0 = H_0 = T_0 = R_0 = 0$, $S_0 = \frac{(1-q)d\Lambda}{d+\tau}$ and $C_0 = \frac{(\tau+qd)d\Lambda}{(d+\chi)(d+\tau)}$.
The basic reproduction number, indicated by $\mathscr{R}_0$, is expressed as follows by using the method presented in [85],

$$\mathscr{R}_0 = (S_0 + \varepsilon C_0)\frac{\alpha_1\mathscr{F} + \alpha_2}{e_1\mathscr{F}}, \tag{6.4}$$

where $\mathscr{F} = \frac{e_2e_3 - \mu\theta}{e_3\sigma + \mu\gamma}$.
Furthermore, the system (6.2) admits a unique endemic steady state

$$\mathscr{E}^* = (S^*, C^*, L^*, H^*, T^*, R^*),$$

where

$$S^* = \frac{(1-q)d\Lambda}{(\alpha_1\mathscr{F} + \alpha_2)H^* + d + \tau}, \quad C^* = \frac{d(\Lambda - S^*) - e_1\mathscr{F}H^*}{d+\chi} \quad T^* = \frac{\sigma\theta + e_2\gamma}{e_3\sigma + \mu\gamma}H^*, \tag{6.5}$$

$$L^* = \mathscr{F}H^*, \quad R^* = \frac{\chi(\Lambda - S^*)}{d+\chi} + \left[\frac{m\left(\sigma\theta + e_2\gamma\right)}{d\left(e_3\sigma + \mu\gamma\right)} - \frac{\chi e_1\mathscr{F}}{d\left(d+\chi\right)}\right]H^*, \tag{6.6}$$

where the value of H^* is the positive root of the given algebraic equation

$$AH^2 + BH + C = 0, \tag{6.7}$$

with

$$\begin{aligned} A &= (\alpha_1\mathscr{F} + \alpha_2)^2\varepsilon e_1\mathscr{F}, \\ B &= (\alpha_1\mathscr{F} + \alpha_2)\left((d+\tau)\varepsilon e_1\mathscr{F} - (\alpha_1\mathscr{F} + \alpha_2)\varepsilon d\Lambda + e_1\mathscr{F}(d+\chi)\right), \\ C &= (d+\tau)(d+\chi)e_1\mathscr{F}(1-\mathscr{R}_0). \end{aligned}$$

Theorem 6.3.2. *The drug transmission model* (6.2) *admits a unique drug addiction equilibrium whenever* $\mathscr{R}_0 > 1$ *given by*

$$\mathscr{E}^* = (S^*, C^*, L^*, H^*, T^*, R^*),$$

where S^*, C^*, L^*, T^* *and* R^* *are given in* (6.5) *and* (6.6)*, and* $H^* = \frac{-B + \sqrt{B^2 - 4AC}}{2A}$.

6.3.2.1 The fractional model's local stability analysis

In this part, we investigate the local stability of the drug-free and endemic equilibrium points of the drug transmission model (6.2). Since $R(t)$ does not appear in the first five equations, the system (6.2) can be written as

$$\begin{cases} {}^{C}D_t^{\alpha}S(t) = (1-q)d\Lambda - \alpha_1 SL - \alpha_2 SH - (d+\tau)S \\ {}^{C}D_t^{\alpha}C(t) = qd\Lambda + \tau S - \alpha_1\varepsilon CL - \alpha_2\varepsilon CH - (d+\chi)C, \\ {}^{C}D_t^{\alpha}L(t) = \alpha_1 SL + \alpha_2 SH + \alpha_1\varepsilon CL + \alpha_2\varepsilon CH - e_1 L, \\ {}^{C}D_t^{\alpha}H(t) = \sigma L + \mu T - e_2 H, \\ {}^{C}D_t^{\alpha}T(t) = \theta H + \gamma L - e_3 T, \end{cases} \tag{6.8}$$

where

$$S(0)=S_0>0,\quad C(0)=C_0>0,\quad L(0)=L_0>0,$$
$$H(0)=H_0>0,\quad T(0)=T_0>0,\quad R(0)=R_0>0.$$

prove the Caputo model's local asymptotic stability, prove that all eigenvalues λ_1, λ_2, λ_3, λ_4 and λ_5 of the Jacobian matrix calculated at the equilibrium point verify the requirement

$$|\arg(\lambda_i)|>\frac{\alpha\pi}{2},\quad i=1,2,3,4,5 \tag{6.9}$$

this outcome is demonstrated in [91].

Theorem 6.3.3. *The drug-free equilibrium* $\mathscr{E}_0=(S_0,C_0,L_0,H_0,T_0,R_0)$ *of the system* (6.2) *is locally asymptotically stable if* $\mathscr{R}_0<1$.

Proof. At the equilibrium $\mathscr{E}_0$, the Jacobian matrix $J(\mathscr{E}_0)$ for the fractional model provided by (6.8) is given by:

$$J(\mathscr{E}_0)=\begin{pmatrix} -(d+\tau) & 0 & -\alpha_1 S_0 & 0 & 0\\ \tau & -(d+\chi) & -\alpha_1\varepsilon C_0 & -\alpha_2\varepsilon C_0 & 0\\ 0 & 0 & \alpha_1 S_0+\alpha_1\varepsilon C_0-e_1 & \alpha_2 S_0+\alpha_2\varepsilon C_0 & 0\\ 0 & 0 & \sigma & -e_2 & \mu\\ 0 & 0 & \gamma & \theta & -e_3 \end{pmatrix}. \tag{6.10}$$

We get the eigenvalues by solving the following characteristic equation

$$\det(J(\mathscr{E}_0)-\lambda Id)=0.$$

Therefore, we find the following equation

$$(d+\tau+\lambda)(d+\chi+\lambda)(\lambda^3+r_1\lambda^2+r_2\lambda+r_3)=0, \tag{6.11}$$

where

$$\begin{aligned} r_1 &= e_1+e_2+e_3-\alpha_1(S_0+\varepsilon C_0),\\ r_2 &= (e_2e_3-\mu\theta)-(\alpha_1(S_0+\varepsilon C_0)-e_1)(e_2+e_3)-\alpha_2\sigma(S_0+\varepsilon C_0),\\ r_3 &= -(\alpha_1(S_0+\varepsilon C_0)-e_1)(e_2e_3-\mu\theta)-\alpha_2(S_0+\varepsilon C_0)(e_3\sigma+\mu\gamma). \end{aligned}$$

To determine the stability of the free-drug equilibrium, we employ the Routh-Hurwitz stability criterion. It is clear that if $\mathscr{R}_0<1$, then

$$\begin{aligned} r_1 &= (e_2+e_3)+\frac{e_1\alpha_2+e_1\alpha_1\mathscr{F}(1-\mathscr{R}_0)}{\alpha_1\mathscr{F}+\alpha_2}>0,\\ r_2 &= (e_2e_3-\mu\theta)+\frac{e_1(e_2+e_3)\alpha_1\mathscr{F}(1-\mathscr{R}_0)}{\alpha_1\mathscr{F}+\alpha_2}\\ &\quad+\frac{\alpha_2e_1}{\alpha_1\mathscr{F}+\alpha_2}\left(e_3+\frac{e_2\mu\gamma+\mu\theta+e_2e_3\sigma(1-\mathscr{R}_0)}{e_3\sigma+\mu\gamma}\right)>0,\\ r_3 &= e_1(e_2e_3-\mu\theta)(1-\mathscr{R}_0)>0, \end{aligned}$$

and

$$r_1r_2-r_3=(e_2+e_3)r_2+\frac{e_1(e_2e_3-\mu\theta)}{\alpha_1\mathscr{F}+\alpha_2}\mathscr{R}_0\alpha_2+\frac{e_1\alpha_2+e_1\alpha_1\mathscr{F}(1-\mathscr{R}_0)}{\alpha_1\mathscr{F}+\alpha_2}\times$$
$$\left(\frac{e_1(e_2+e_3)\alpha_1\mathscr{F}(1-\mathscr{R}_0)}{\alpha_1\mathscr{F}+\alpha_2}+\frac{e_1\alpha_2}{\alpha_1\mathscr{F}+\alpha_2}\left(e_3+\frac{e_2\mu\gamma+\mu\theta+e_2e_3\sigma(1-\mathscr{R}_0)}{e_3\sigma+\mu\gamma}\right)\right)>0.$$

All of the eigenvalues have negative real parts according to the Routh-Hurwitz criterion [53]. Then

$$|\arg(\lambda_i)|=\pi>\frac{\pi}{2}>\frac{\alpha\pi}{2},\quad i=1,2,3,4,5.$$

Next, we use the discriminant of the characteristic equation, denoted by

$$\Delta=r_1^2r_2^2+18r_1r_2r_3-4r_2^3-4r_1^3r_3-27r_3^2, \tag{6.12}$$

and the following lemma to complete the proof of the theorem 6.3.3.

Lemma 6.3.1. *Assume that $\mathscr{R}_0<1$, then the system's drug-free equilibrium $\mathscr{E}^0$ of* (6.8) *is asymptotically stable if one of the following conditions is hold:*
(1) $\Delta>0, r_1>0, r_2>0$ *and* $r_1r_2-r_3>0$,
(2) $\Delta<0, r_1\geq 0, r_2\geq 0, r_3>0$ *and* $0<\alpha\leq\frac{2}{3}$.

For the proof of this lemma we refer to [4]. As a result, the drug-free equilibrium $\mathscr{E}_0=(S_0,C_0,L_0,H_0,T_0,R_0)$ is locally asymptotically stable. ■

Theorem 6.3.4. *The drug addiction equilibrium,*

$$\mathscr{E}^*=(S^*,C^*,L^*,H^*,T^*,R^*)$$

of the system (6.2) *is locally asymptotically stable if* $\mathscr{R}_0>1$.

Proof. The Jacobian matrix $J(\mathscr{E}^*)$ for the fractional model at the equilibrium $\mathscr{E}^*$ provided from (6.8) is given by :

$$J\left(\mathscr{E}^*\right)=\begin{pmatrix} A_1 & 0 & A_2 & A_3 & 0\\ A_4 & A_5 & A_6 & A_7 & 0\\ A_8 & A_9 & A_{10} & A_{11} & 0\\ 0 & 0 & A_{12} & A_{13} & A_{14}\\ 0 & 0 & A_{15} & A_{16} & A_{17}\end{pmatrix}, \tag{6.13}$$

where,

$$\begin{array}{lll} A_1=-\alpha_1L^*-\alpha_2H^*-(d+\tau), & A_2=-\alpha_1S^*, & A_3=-\alpha_2S^*,\\ A_4=\tau, & A_5=-\alpha_1\varepsilon L^*-\alpha_2\varepsilon H^*-(d+\chi), & A_6=-\alpha_1\varepsilon C^*,\\ A_7=-\alpha_2\varepsilon C^* & A_8=\alpha_1L^*+\alpha_2H^*, & A_9=\alpha_1\varepsilon L^*+\alpha_2\varepsilon H^*,\\ A_{10}=\alpha_1S^*+\alpha_1\varepsilon C^*-e_1, & A_{11}=\alpha_2S^*+\alpha_2\varepsilon C^*, & A_{12}=\sigma,\\ A_{13}=-e_2, & A_{14}=\mu, & A_{15}=\gamma,\\ A_{16}=\theta & A_{17}=-e_3. & \end{array}$$

By solving the characteristic equation provided below, we may determine the eigenvalues

$$\det(J(\mathscr{E}^*) - \lambda Id) = 0.$$

Consequently, we obtain the bellow equation

$$\lambda^5 + \omega_1\lambda^4 + \omega_2\lambda^3 + \omega_3\lambda^2 + \omega_4\lambda + \omega_5 = 0, \tag{6.14}$$

where

$$\begin{aligned}
\omega_1 &= -A_1 - A_5 - A_{10} - A_{13} - A_{17},\\
\omega_2 &= A_1(A_5 + A_{10}) - A_2A_8 + A_5A_{10} - A_9A_6 - A_{14}A_{16} + A_{13}A_{17} - A_{11}A_{12}\\
&\quad + (A_{13} + A_{17})(A_1 + A_5 + A_{10}),\\
\omega_3 &= -A_{11}(A_{14}A_{15} - A_{12}A_{17}) + (A_{14}A_{16} - A_{13}A_{17})(A_1 + A_5 + A_{10})\\
&\quad + (A_{13} + A_{17})(A_9A_6 - A_5A_{10} + A_2A_8 - A_1(A_{10} + A_5))\\
&\quad - A_{12}(A_9A_7 - A_5A_{11} + A_3A_8) - A_2(A_9A_4 - A_5A_8) + A_1(A_{11}A_{12} - A_9A_6),\\
\omega_4 &= (A_9A_6 - A_5A_{10} + A_2A_8 - A_1A_{10} - A_1A_5)(A_{14}A_{16} - A_{13}A_{17})\\
&\quad - (A_9A_7 - A_5A_{11} + A_3A_8 - A_1A_{11})(A_{14}A_{15} - A_{12}A_{17})\\
&\quad + A_3A_{12}(A_5A_8 - A_9A_4) - (A_2A_5A_8 - A_9A_2A_4\\
&\quad + A_9A_1A_6 - A_1A_5A_{10})(A_{13} + A_{17}) + A_1A_{12}(A_9A_7 - A_5A_{11}),\\
\omega_5 &= (A_1(A_5A_{11} - A_9A_7) + A_3(A_9A_4 - A_5A_8)(A_{12}A_{17} - A_{14}A_{15})\\
&\quad - (A_1(A_5A_{10} - A_9A_6) + A_2(A_9A_4 - A_5A_8))(A_{13}A_{17} - A_{14}A_{16}).
\end{aligned}$$

The proof of theorem is completed by the following lemma.

Lemma 6.3.2. *Assume that $\mathscr{R}_0 > 1$ and one of the below requirements are met*
1- $\omega_i > 0, i = 1,2,3,4,5$.
2- $\omega_1\omega_2\omega_3 > \omega_3^2 + \omega_1^2\omega_4$.
Then by using Lienard-chipart test [55], the equilibrium $\mathscr{E}^*$ of the drug transmission model with Caputo derivative is locally asymptotically stable.

■

6.3.2.2 The fractional model's global stability analysis

In this part, we study the global stability of our model's equilibriums and show that the drug-free $\mathscr{E}_0$ and drug-addiction $\mathscr{E}^*$ equilibrium points are globally asymptotically stable under certain conditions.

Theorem 6.3.5. *The drug-free equilibrium $\mathscr{E}_0 = (S_0, C_0, L_0, H_0, T_0, R_0)$ of the system (6.2) is globally asymptotically stable if $\mathscr{R}_0 < 1$.*

Proof. The Lyapunov function is defined as follows:

$$L_0 = S - S_0 - S_0 \ln\frac{S}{S_0} + C - C_0 - C_0 \ln\frac{C}{C_0} + L + e_3\mathcal{K}H + \mu\mathcal{K}T, \tag{6.15}$$

where $\mathcal{K} = \frac{e_1-\alpha_1(S_0+\varepsilon C_0)}{\sigma e_3+\mu\gamma}$.
The Caputo fractional derivative of L_0 along the solutions of system (6.2) satisfies

$$\begin{aligned}{}^{C}D_0^{\alpha}L_0(t) =& {}^{C}D_0^{\alpha}\big(S_0 - S_0\ln\frac{S}{S_0}\big) + {}^{C}D_0^{\alpha}\big(C - C_0 - C_0\ln\frac{C}{C_0}\big) + {}^{C}D_0^{\alpha}L\\ &+e_3\frac{e_1-\alpha_1(S_0+\varepsilon C_0)}{\sigma e_3+\mu\gamma}{}^{C}D_0^{\alpha}H + \mu\frac{e_1-\alpha_1(S_0+\varepsilon C_0)}{\sigma e_3+\mu\gamma}{}^{C}D_0^{\alpha}T.\end{aligned}$$

By using the Caputo fractional derivative's linearity property and [86] we get,

$$\begin{aligned}{}^{C}D_0^{\alpha}L_0(t) \le& \big(1-\frac{S}{S_0}\big){}^{C}D_0^{\alpha}S + \big(1-\frac{C}{C_0}\big){}^{C}D_0^{\alpha}C + {}^{C}D_0^{\alpha}L\\ &+e_3\frac{e_1-\alpha_1(S_0+\varepsilon C_0)}{\sigma e_3+\mu\gamma}{}^{C}D_0^{\alpha}H + \mu\frac{e_1-\alpha_1(S_0+\varepsilon C_0)}{\sigma e_3+\mu\gamma}{}^{C}D_0^{\alpha}T,\\ =&\tau S_0\big(\frac{S}{S_0} - \frac{C_0S}{CS_0} - \frac{C}{C_0} + 1\big) + (1-q)d\Lambda\big(2 - \frac{S_0}{S} - \frac{S}{S_0}\big)\\ &+qd\Lambda\big(2 - \frac{C_0}{C} - \frac{C}{C_0}\big) + H\big((\alpha_1\mathcal{F}+\alpha_2)(S_0+\varepsilon C_0) - e_1\mathcal{F}\big),\\ =&\tau S_0\big(3 - \frac{S_0}{S} - \frac{C_0S}{CS_0} - \frac{C}{C_0}\big) + dS_0\big(2 - \frac{S_0}{S} - \frac{S}{S_0}\big)\\ &+qd\Lambda\big(2 - \frac{C_0}{C} - \frac{C}{C_0}\big) + e_1\mathcal{F}H(\mathcal{R}_0 - 1).\end{aligned}$$

Therefore, $\mathcal{R}_0 < 1$ ensures that, ${}^{C}D_0^{\alpha}L_0(t) \le 0$, for all $t \ge 0, C, S > 0$, and if $\mathcal{R}_0 = 1$ then the largest invariant set of $\{(S,C,L,H,T,R) \in \mathbb{R}^6, {}^{C}D_0^{\alpha}L_0(t) = 0\}$ is only the singleton $\{\mathcal{E}_0\}$. By LaSalle invariance principle [41], we conclude that $\mathcal{E}_0 = (S_0, C_0, L_0, H_0, T_0, R_0)$ of the system (6.2) is globally asymptotically stable. ■

Theorem 6.3.6. *The drug addiction equilibrium*

$$\mathcal{E}^* = (S^*, C^*, L^*, H^*, T^*, R^*)$$

of the system (6.2) *is globally asymptotically stable if* $\mathcal{R}_0 > 1$ *and* $\frac{(e_3\sigma+\mu\gamma)d\Lambda}{e_3\sigma(d+\tau)} < \frac{e_1\mathcal{F}}{\alpha_1\mathcal{F}+\alpha_2} < \frac{qd}{\alpha_2}$.

Proof. The Lyapunov function is defined as follows:

$$\begin{aligned}L_1(t) =& S - S^* - S^*\ln\frac{S}{S^*} + C - C^* - C^*\ln\frac{C}{C^*} + L - L^* - L^*\ln\frac{L}{L^*}\\ &+\frac{\alpha_2(S^*+\varepsilon C^*)}{e_2e_3-\mu\theta}\Big(e_3(H - H^* - H^*\ln\frac{H}{H^*}) + \mu(T - T^* - T^*\ln\frac{T}{T^*})\Big).\end{aligned} \tag{6.16}$$

Then we calculate the Caputo fractional derivative of L_1 along the solution of the system (6.2),

$$\begin{aligned}D_0^{\alpha}L_1(t) =& D_0^{\alpha}(S - S^* - S^*\ln\frac{S}{S^*}) + D_0^{\alpha}(C - C^* - C^*\ln\frac{C}{C^*}) + D_0^{\alpha}(L - L^* - L^*\ln\frac{L}{L^*})\\ &+\frac{\alpha_2(S^*+\varepsilon C^*)}{e_2e_3-\mu\theta}\Big(e_3D_0^{\alpha}(H - H^* - H^*\ln\frac{H}{H^*}) + \mu D_0^{\alpha}(T - T^* - T^*\ln\frac{T}{T^*})\Big),\end{aligned}$$

by using Lemma 3.1 in [86], we have

$$D_0^\alpha L_1(t) \le (1-\frac{S^*}{S})D_0^\alpha S + (1-\frac{L^*}{L})D_0^\alpha L + e_3\frac{\alpha_2(S^*+\varepsilon C^*)}{e_2e_3-\mu\theta}\left(1-\frac{H^*}{H}\right)D_0^\alpha H + \mu\frac{\alpha_2(S^*+\varepsilon C^*)}{e_2e_3-\mu\theta}\left(1-\frac{T^*}{T}\right)D_0^\alpha T,$$

$$\begin{aligned}
&=(1-\frac{S^*}{S})\left((d+\tau)S^*\left(1-\frac{S}{S^*}\right)+\alpha_1 S^*L^*\left(1-\frac{SL}{S^*L^*}\right)+\alpha_2 S^*H^*\left(1-\frac{SH}{S^*H^*}\right)\right)\\
&+(1-\frac{C^*}{C})\left(\tau S^*\left(\frac{S}{S^*}-1\right)+(d+\chi)C^*\left(1-\frac{C}{C^*}\right)+\alpha_1\varepsilon C^*L^*\left(1-\frac{CL}{C^*L^*}\right)\right.\\
&\left.+\alpha_2\varepsilon C^*H^*\left(1-\frac{CH}{C^*H^*}\right)\right)+(1-\frac{L^*}{L})\left(e_1L^*\left(1-\frac{L}{L^*}\right)+\alpha_1S^*L^*\left(\frac{SL}{S^*L^*}-1\right)\right.\\
&\left.+\alpha_2S^*H^*\left(\frac{SH}{S^*H^*}-1\right)+\alpha_1\varepsilon C^*L^*\left(\frac{CL}{C^*L^*}-1\right)+\alpha_2\varepsilon C^*H^*\left(\frac{CH}{C^*H^*}-1\right)\right)\\
&+e_3\frac{\alpha_2(S^*+\varepsilon C^*)}{e_2e_3-\mu\theta}(1-\frac{H^*}{H})\left(e_2H^*\left(1-\frac{H}{H^*}\right)+\sigma L^*\left(\frac{L}{L^*}-1\right)+\mu T^*\left(\frac{T}{T^*}-1\right)\right)\\
&+\mu\frac{\alpha_2(S^*+\varepsilon C^*)}{e_2e_3-\mu\theta}(1-\frac{T^*}{T})\left(e_3T^*\left(1-\frac{T}{T^*}\right)+\theta H^*\left(\frac{H}{H^*}-1\right)+\gamma L^*\left(\frac{L}{L^*}-1\right)\right)\\
&=-\mu\gamma\frac{\alpha_2(S^*+\varepsilon C^*)}{e_2e_3-\mu\theta}L^*\left(\frac{H^*T}{HT^*}+\frac{LT^*}{L^*T}+\frac{CL^*H}{C^*LH^*}+\frac{C^*}{C}\right)\\
&-\alpha_2S^*H^*\left(\frac{S^*}{S}+\frac{SL^*H}{S^*LH^*}+\frac{LH^*}{L^*H}\right)-\tau S^*\left(\frac{S^*}{S}+\frac{SC^*}{S^*C}+\frac{C}{C^*}\right)\\
&-\left(e_3\sigma\frac{\alpha_2(S^*+\varepsilon C^*)}{e_2e_3-\mu\theta}L^*-\alpha_2S^*H^*\right)\left(\frac{C^*}{C}+\frac{CL^*H}{C^*LH^*}+\frac{LH^*}{L^*H}\right)\\
&-\left(\alpha_1L^*+d\right)S^*\left(\frac{S^*}{S}+\frac{S}{S^*}\right)-\left(qd\Lambda-\alpha_2\varepsilon C^*H^*\right)\left(\frac{C^*}{C}+\frac{C}{C^*}\right)\\
&-\mu\theta\frac{\alpha_2(S^*+\varepsilon C^*)}{e_2e_3-\mu\theta}H^*\left(\frac{H^*T}{HT^*}+\frac{HT^*}{H^*T}\right)+(\tau+2d)S^*+2(d+\chi)C^*\\
&+2e_1L^*+e_3e_2\frac{\alpha_2(S^*+\varepsilon C^*)}{e_2e_3-\mu\theta}H^*+\mu e_3\frac{\alpha_2(S^*+\varepsilon C^*)}{e_2e_3-\mu\theta}T^*.
\end{aligned}$$

Since $\frac{(e_3\sigma+\mu\gamma)d\Lambda}{e_3\sigma(d+\tau)} < \frac{e_1\mathscr{F}}{\alpha_1\mathscr{F}+\alpha_2} < \frac{qd}{\alpha_2}$, then

$$-\left(qd\Lambda-\alpha_2\varepsilon C^*H^*\right)<0 \quad \text{and} \quad -\left(e_3\sigma\frac{\alpha_2(S^*+\varepsilon C^*)}{e_2e_3-\mu\theta}L^*-\alpha_2S^*H^*\right)<0.$$

Through using the Inequality of arithmetic and geometric means,

$$\left(\frac{H^*T}{HT^*}+\frac{LT^*}{L^*T}+\frac{CL^*H}{C^*LH^*}+\frac{C^*}{C}\right)>4, \quad \left(\frac{S^*}{S}+\frac{SL^*H}{S^*LH^*}+\frac{LH^*}{L^*H}\right)>3,$$
$$\left(\frac{S^*}{S}+\frac{SC^*}{S^*C}+\frac{C}{C^*}\right)>3, \quad \left(\frac{C^*}{C}+\frac{CL^*H}{C^*LH^*}+\frac{LH^*}{L^*H}\right)>3,$$
$$\left(\frac{H^*T}{HT^*}+\frac{HT^*}{H^*T}\right)>2, \quad \left(\frac{C^*}{C}+\frac{C}{C^*}\right)>2,$$
$$\left(\frac{S^*}{S}+\frac{S}{S^*}\right)>2.$$

We obtain

$$\begin{aligned}
D_0^{\alpha} L_1(t) \leq & 2e_1 L^* - 2\alpha_1 \varepsilon C^* L^* - 2\alpha_1 L^* S^* + e_3 \sigma \frac{\alpha_2(S^* + \varepsilon C^*)}{e_2 e_3 - \mu\theta}(e_3 T^* - \theta H^*) \\
& - 2L^* \frac{\alpha_2(S^* + \varepsilon C^*)}{e_2 e_3 - \mu\theta}(e_3\sigma + \mu\gamma) - \mu\gamma \frac{\alpha_2(S^* + \varepsilon C^*)}{e_2 e_3 - \mu\theta} L^* \\
= & -\mu \frac{\alpha_2(S^* + \varepsilon C^*)}{e_2 e_3 - \mu\theta}(\theta H^* + \gamma L^* - e_3 T^*) + 2(e_1 L^* - \alpha_1 L^* S^* - \alpha_2 S^* H^* \\
& - \alpha_1 \varepsilon C^* L^* - \alpha_2 \varepsilon C^* H^*) \\
= & 0.
\end{aligned}$$

Therefore, the largest set of $\{(S,C,L,H,T,R) \in \mathbb{R}^6, {}^C D_0^{\alpha} L_1(t) = 0\}$ is only the singleton $\{\mathscr{E}^*\}$. By LaSalle's invariance principle [41], $\{\mathscr{E}^*\}$ is globally asymptotically stable. ■

6.3.3 Numerical method for Caputo-fractional derivative

In this section, we will use an algorithm based on the modified trapezoidal rule and the fractional Euler's method [73] to present numerical solution of the fractional drug transmission equation. For this purpose we use the following notations for the right side of the fractional system (6.2),

$$\begin{aligned}
f_1(t,S(t)) &= (1-q)d\Lambda - \alpha_1 SL - \alpha_2 SH - (d+\tau)S, \\
f_2(t,C(t)) &= qd\Lambda + \tau S - \alpha_1 \varepsilon CL - \alpha_2 \varepsilon CH - (d+\chi)C, \\
f_3(t,L(t)) &= \alpha_1 SL + \alpha_2 SH + \alpha_1 \varepsilon CL + \alpha_2 \varepsilon CH - e_1 L, \\
f_4(t,H(t)) &= \sigma L + \mu T - e_2 H, \\
f_5(t,T(t)) &= \theta H + \gamma L - e_3 T, \\
f_6(t,R(t)) &= \chi c + mT - dR.
\end{aligned} \tag{6.17}$$

Consider the Caputo fractional differential equation

$$\begin{cases} {}^C D_0^{\alpha} x(t) = F(t,x(t)), \quad 0 < \alpha < 1, \\ x(0) = x_0, \end{cases} \tag{6.18}$$

where $F(t,x(t)) = \begin{pmatrix} f_1(t,S(t)) \\ f_2(t,C(t)) \\ f_3(t,L(t)) \\ f_4(t,H(t)) \\ f_5(t,T(t)) \\ f_6(t,R(t)) \end{pmatrix}$ and $x_0 = (S_0, C_0, L_0, H_0, T_0, R_0)$ is the initial condition vector.

Using the Riemann-Liouville integral, we get

$$x(t) = x(0) + I_0^{\alpha}(F(t,x(t))), \tag{6.19}$$

this implies

$$x(t) = x(0) + \frac{1}{\Gamma(\alpha)} \int_0^t (t-s)^{\alpha-1} f(s) ds, \tag{6.20}$$

we consider $t_0 = 0 < t_1 < \ldots t_k \ldots < t_N = T$ an uniform discretization of interval $[0,T]$ in $N+1$ points. Let $h = \frac{T}{N}$ is the step size. We will use the modified trapezoidal [72] to approximate the fractional integral

$$I_0^{\alpha}(F(t,x(t))) \simeq T(F,h,\alpha), \tag{6.21}$$

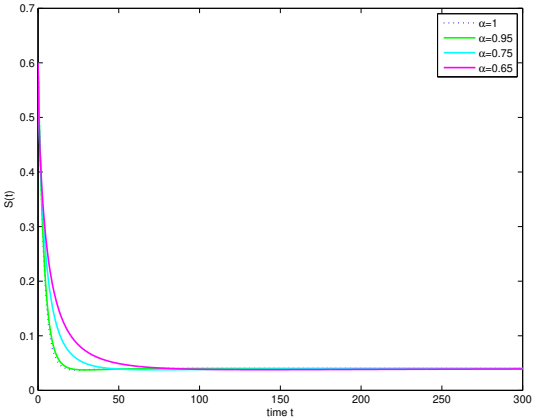
where

$$\begin{aligned} T(F,h,\alpha) = &\left((N-1)^{\alpha+1} - (N-\alpha-1)N^{\alpha}\right) \frac{h^{\alpha} F(0,x(0))}{\Gamma(\alpha+2)} + \frac{h^{\alpha} F(T,x(T))}{\Gamma(\alpha+2)} \\ &+ \sum_{k=1}^{N-1} \left((N-k+1)^{\alpha+1} - 2(N-k)^{\alpha+1} + (N-k-1)^{\alpha+1}\right) \frac{h^{\alpha} F(t_k,x(t_k))}{\Gamma(\alpha+2)}. \end{aligned} \tag{6.22}$$

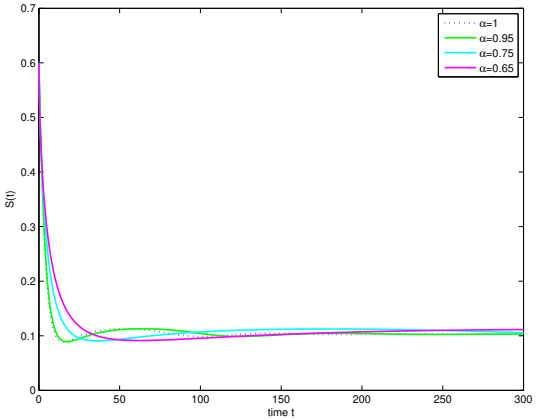
We obtain at the point $t_{n+1} = (n+1)h, h = t_{n+1} - t_n$, we have

$$\begin{aligned} x(t_{n+1}) = &x(0) + \frac{h^{\alpha}}{\Gamma(\alpha+2)} \left(n^{\alpha+1} - (n-\alpha)(n+1)^{\alpha}\right) F(0,x(0)) \\ &+ \frac{h^{\alpha}}{\Gamma(\alpha+2)} \sum_{k=1}^{n} \left((n-k+2)^{\alpha+1} - 2(n-k+1)^{\alpha+1} + (n-k)^{\alpha+1}\right) F(t_k,x(t_k)) \\ &+ \frac{h^{\alpha}}{\Gamma(\alpha+2)} F(t_{n+1},x(t_{n+1})). \end{aligned} \tag{6.23}$$

To illustrate the preceding theoretical results, numerical simulations are provided. We have used [47, 54] as a reference point for some parameters, with the remainder of the parameters' values estimated to meet the model's numerical requirements. Numerical model simulations for two cases and four arbitrary fractional order values are carried out using MATLAB software, the first case to show the stability of the disease-free equilibrium and the second case to show the stability of the endemic equilibrium point.

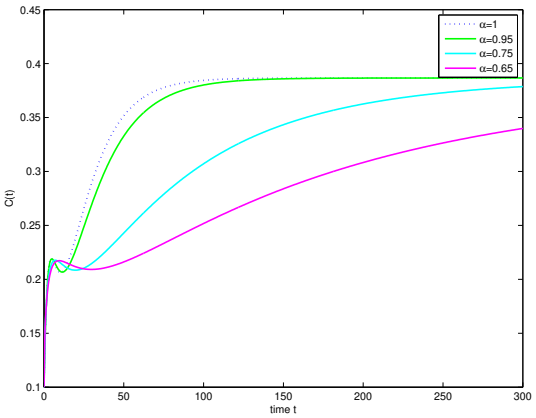


((a)) The time evolution of S when $\mathscr{R}_0 < 1$.

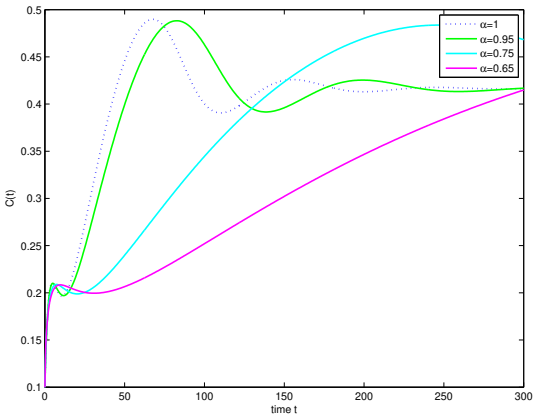


((b)) The time evolution of S when $\mathscr{R}_0 > 1$.

Figure 6.2: The depiction of the numerical solution of the fractional model produced for the the susceptible persons who do not accept the public health education $S(t)$ for four arbitrary fractional order values.

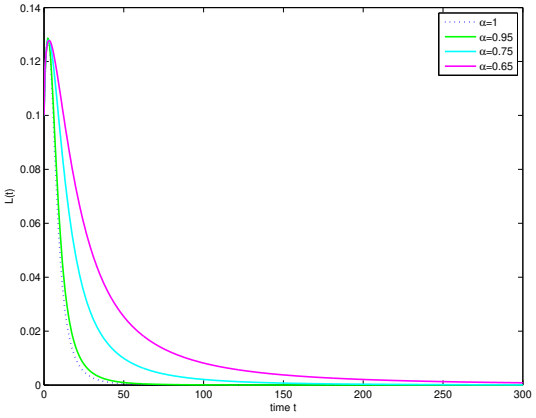


((a)) The time evolution of C when $\mathscr{R}_0 < 1$.

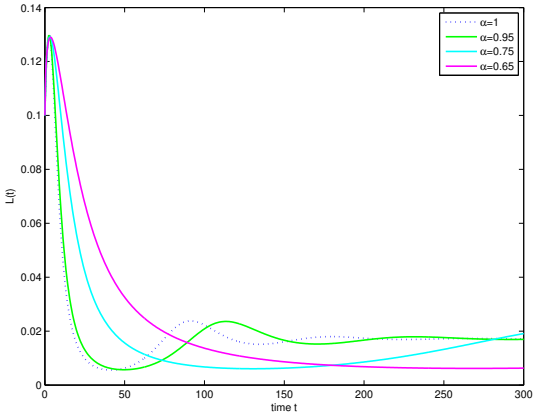


((b)) The time evolution of C when $\mathscr{R}_0 > 1$.

Figure 6.3: The depiction of the numerical solution of the fractional model produced for the susceptible persons who accept the public health education $C(t)$ for four arbitrary fractional order values.

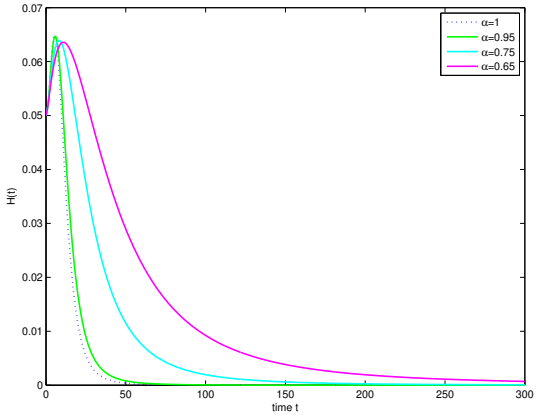


((a)) The time evolution of L when $\mathscr{R}_0 < 1$.

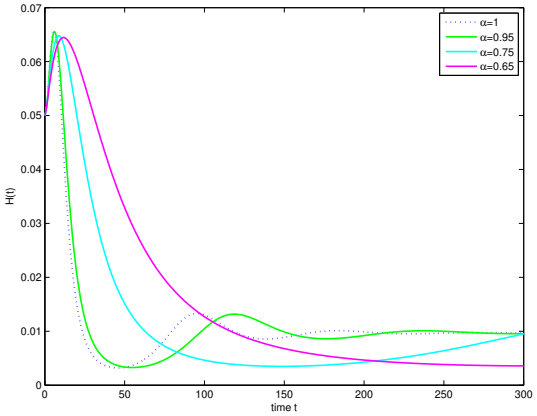


((b)) The time evolution of L when $\mathscr{R}_0 > 1$.

Figure 6.4: The depiction of the numerical solution of the fractional model produced for the light drug addicts persons $L(t)$ for four arbitrary fractional order values.

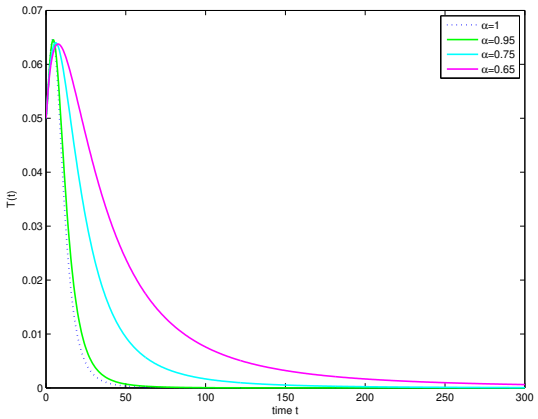


((a)) The time evolution of H when $\mathscr{R}_0 < 1$.

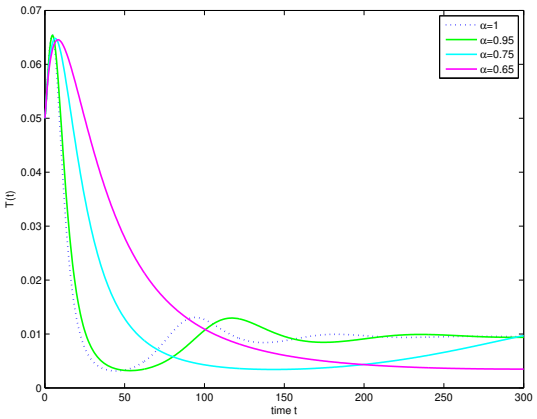


((b)) The time evolution of H when $\mathscr{R}_0 > 1$.

Figure 6.5: The depiction of the numerical solution of the fractional model produced for the heavy drug addicts persons $H(t)$ for four arbitrary fractional order values.

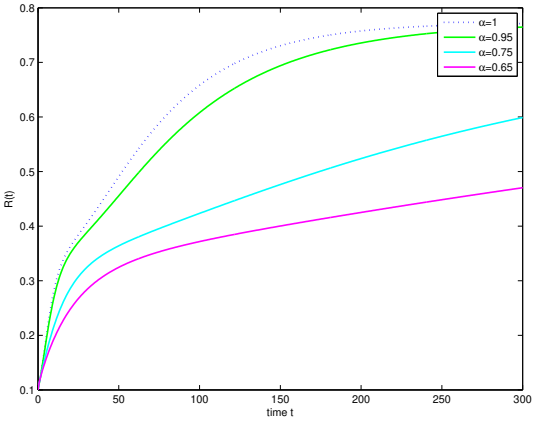


((a)) The time evolution of T when $\mathscr{R}_0 < 1$.

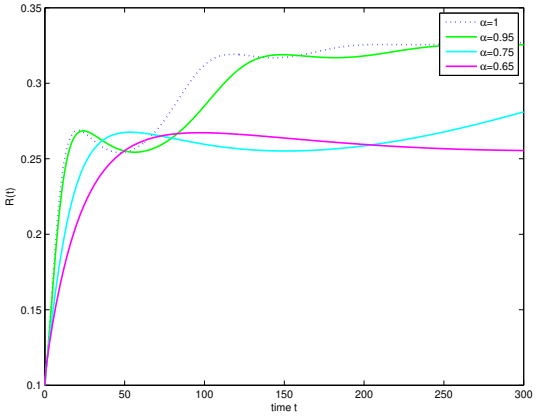


((b)) The time evolution of T when $\mathscr{R}_0 > 1$.

Figure 6.6: The depiction of the numerical solution of the fractional model produced for the drug users in treatment persons $T(t)$ for four arbitrary fractional order values.



((a)) The time evolution of R when $\mathscr{R}_0 < 1$.



((b)) The time evolution of R when $\mathscr{R}_0 > 1$.

Figure 6.7: The depiction of the numerical solution of the fractional model produced for the permanent quit drug persons $R(t)$ for four arbitrary fractional order values.

6.3.4 Model parameter sensitivity analysis in relation to the basic reproduction number

It is vital to understand the relative relevance of the many components involved in disease transmission and prevalence in order to investigate viral control parameters, that is, to attempt to raise or reduce some factors that affect disease transmission.

Sensitivity analysis is one method for assessing the relevance of each parameter in disease transmission.

To be more explicit, we adopt the concept of the sensitivity index, which represents the relevance of the variable associated with each parameter of the model in minimizing disease, as established by [25].

Definition 6.3.1. *The normalized forward sensitivity index of variable $\mathscr{R}_0$, that relies on parameter α is formulated as having:*

$$\Upsilon_{\alpha}^{\mathscr{R}_0} = \frac{\partial \mathscr{R}_0}{\partial \alpha} \frac{\alpha}{\mathscr{R}_0}. \tag{6.24}$$

The sensitivity index for $\mathscr{R}_0$ in relation to the parameters α_1, Λ, α_2, m, τ, q, θ, ε, χ, β_1, β_2,

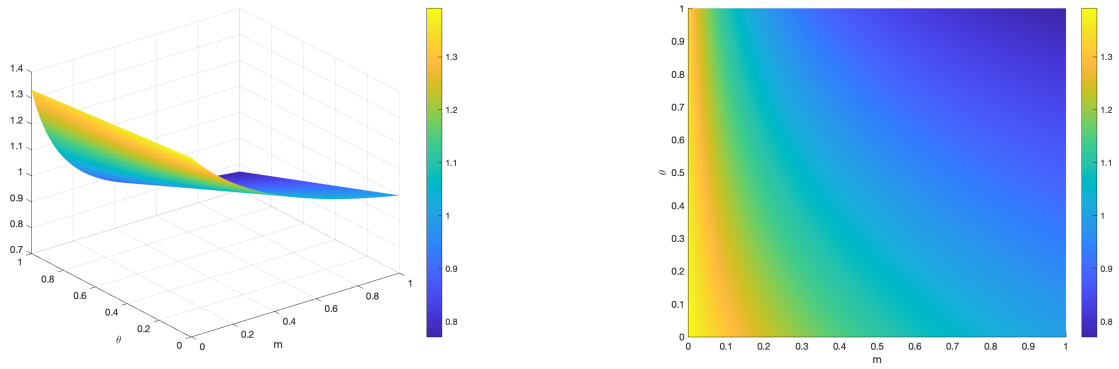
and μ will be calculated as follow

$$\begin{aligned}
\Upsilon_{\alpha_1}^{\mathscr{R}_0} &= \frac{\alpha_1(S_0+\varepsilon C_0)}{e_1 R_0},\\
\Upsilon_{\Lambda}^{\mathscr{R}_0} &= \frac{(S_0+\varepsilon C_0)(\alpha_1\mathscr{F}+\alpha_2)}{e_1 R_0 \mathscr{F}} = 1,\\
\Upsilon_{\alpha_2}^{\mathscr{R}_0} &= \frac{\alpha_2(S_0+\varepsilon C_0)}{e_1 R_0 \mathscr{F}},\\
\Upsilon_{m}^{\mathscr{R}_0} &= \frac{-\alpha_2 m\mu(S_0+\varepsilon C_0)(\theta\sigma+e_2\gamma)}{R_0 e_1 \mathscr{F}^2(e_3\sigma+\mu\gamma)^2},\\
\Upsilon_{\tau}^{\mathscr{R}_0} &= \frac{-d\Lambda\tau(\alpha_1\mathscr{F}+\alpha_2)(1-q)(\chi+d(1-\varepsilon))}{R_0 e_1 \mathscr{F}(d+\chi)(d+\tau)^2},\\
\Upsilon_{q}^{\mathscr{R}_0} &= \frac{-d\Lambda q(\alpha_1\mathscr{F}+\alpha_2)(\chi+d(1-\varepsilon))}{R_0 e_1 \mathscr{F}(d+\chi)(d+\tau)},\\
\Upsilon_{\theta}^{\mathscr{R}_0} &= \frac{-\alpha_2\theta(S_0+\varepsilon C_0)(e_3-\mu)}{e_1 R_0 \mathscr{F}^2(e_3\sigma+\mu\gamma)},\\
\Upsilon_{\varepsilon}^{\mathscr{R}_0} &= \frac{C_0\varepsilon(\alpha_1\mathscr{F}+\alpha_2)}{e_1 R_0 \mathscr{F}},\\
\Upsilon_{\chi}^{\mathscr{R}_0} &= \frac{-d\Lambda\varepsilon\chi(\tau+qd)(\alpha_1\mathscr{F}+\alpha_2)}{e_1 R_0 \mathscr{F}(d+\chi)(d+\tau)},\\
\Upsilon_{\beta_1}^{\mathscr{R}_0} &= \frac{-\beta_1(S_0+\varepsilon C_0)(\alpha_1\mathscr{F}+\alpha_2)}{R_0\mathscr{F}^2},\\
\Upsilon_{\beta_2}^{\mathscr{R}_0} &= \frac{-\alpha_2 e_3\beta_2(S_0+\varepsilon C_0)}{e_1\mathscr{F}^2 R_0(e_3\sigma+\mu\gamma)},\\
\Upsilon_{\mu}^{\mathscr{R}_0} &= \frac{\mu\alpha_2(S_0+\varepsilon C_0)(m+d)(\sigma\theta+e_2\gamma)}{R_0\mathscr{F}^2 e_1(e_3\sigma+\mu\gamma)^2}.
\end{aligned}$$

The sign per each index indicates whether the parameter raises (positive sign) or lowers (negative sign) the quantity of $\mathscr{R}_0$.

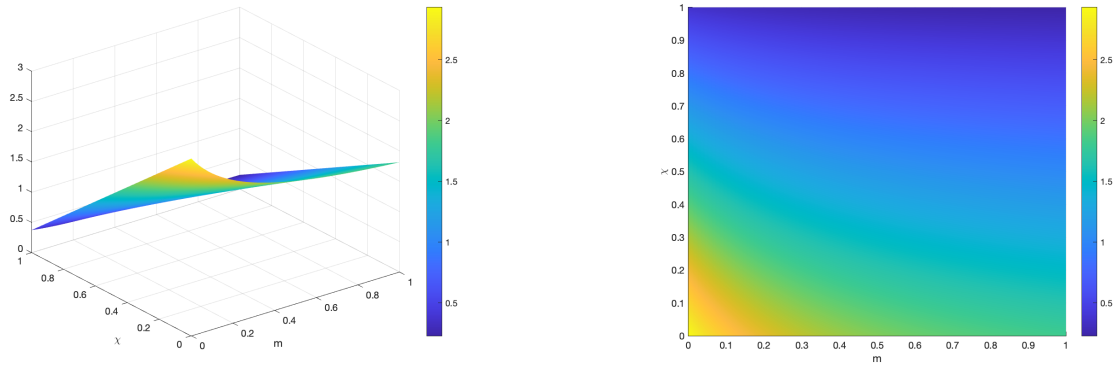
Parameters	Instance
α_1	+0.6081
Λ	+1
α_2	0.3919
m	-0.1589
τ	-0.0521
q	-0.0417
θ	-0.1050
ε	+0.8438
χ	-0.0084
β_1	-0.6449
β_2	-0.2689
μ	+0.1716

The graphical illustrations of $\mathscr{R}_0$ sensitivity indices for Caputo model parameters are presented in Figure 6.17.



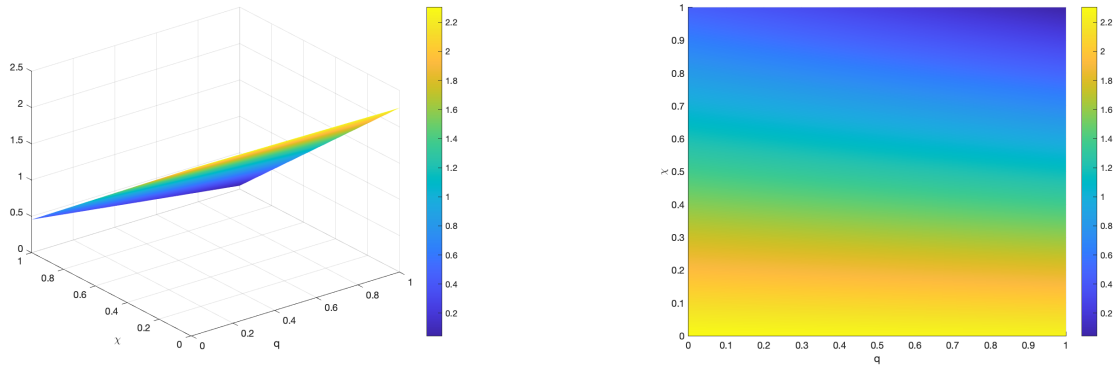
((a)) ((b))

Figure 6.8: Graphical illustration of the reproduction number $\mathscr{R}_0$ as a function of m and θ.



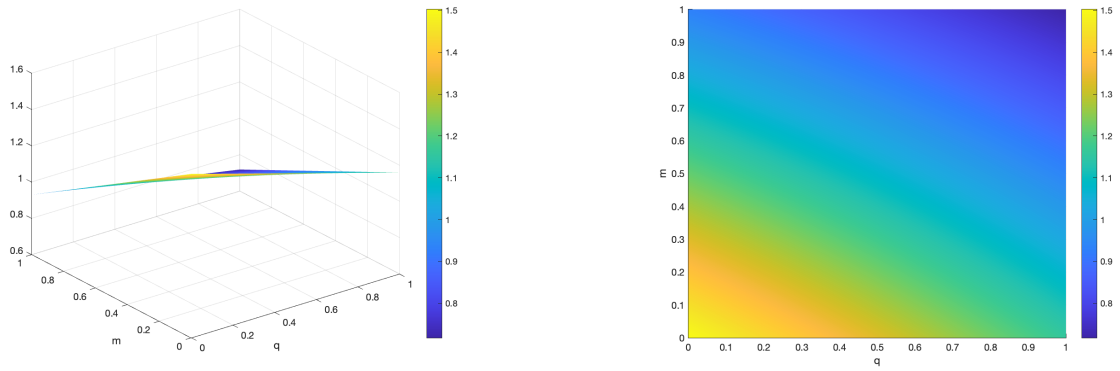
((a)) ((b))

Figure 6.9: Graphical illustration of the reproduction number $\mathscr{R}_0$ as a function of m and χ.



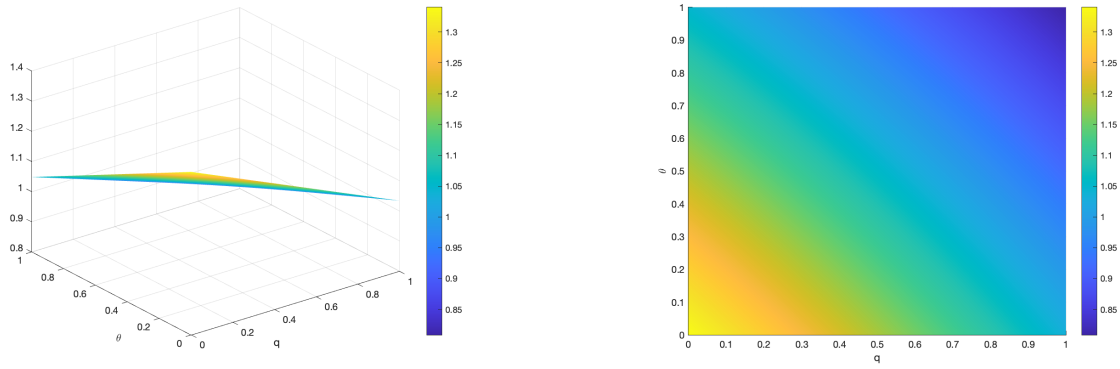
((a)) ((b))

Figure 6.10: Graphical illustration of the reproduction number $\mathscr{R}_0$ as a function of q and χ.



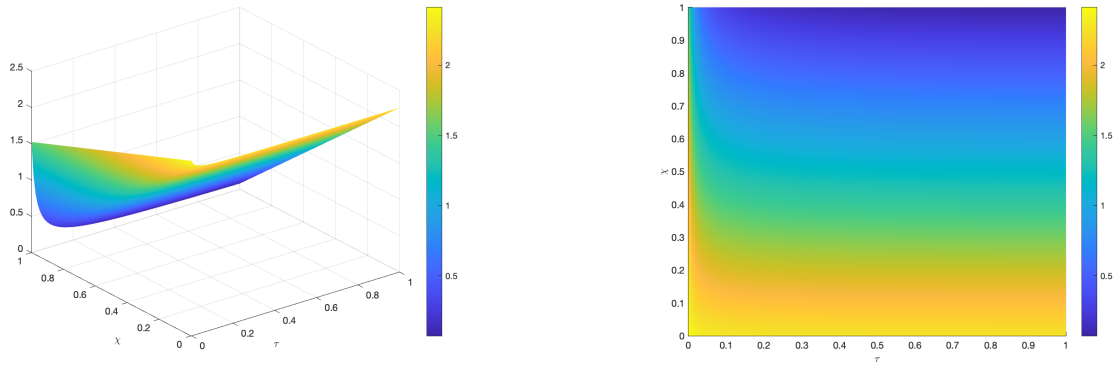
((a)) ((b))

Figure 6.11: Graphical illustration of the reproduction number $\mathscr{R}_0$ as a function of q and m.



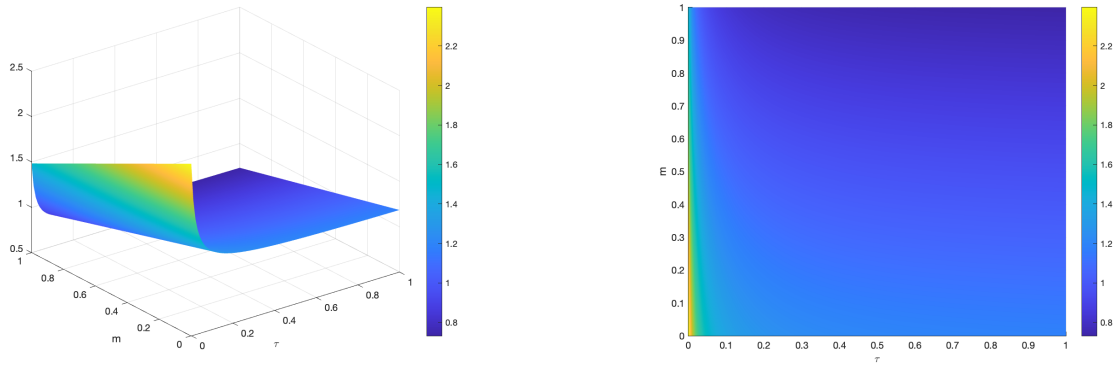
((a)) ((b))

Figure 6.12: Graphical illustration of the reproduction number $\mathscr{R}_0$ as a function of q and θ.



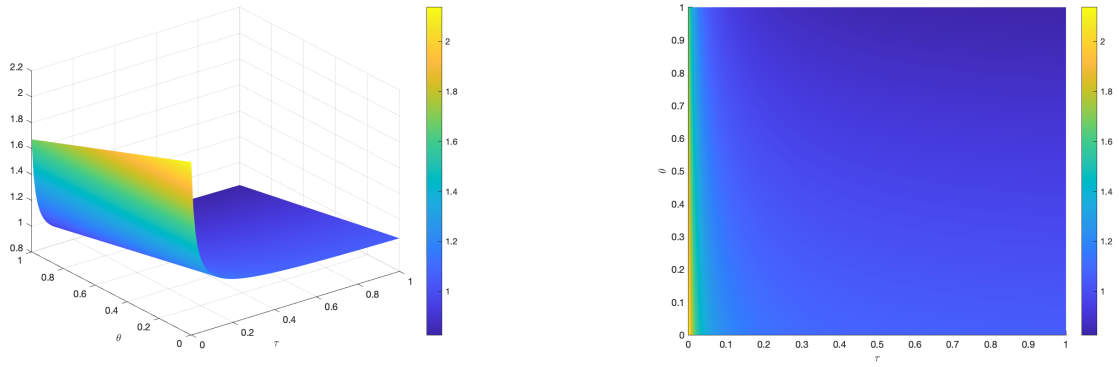
((a)) ((b))

Figure 6.13: Graphical illustration of the reproduction number $\mathscr{R}_0$ as a function of τ and χ.



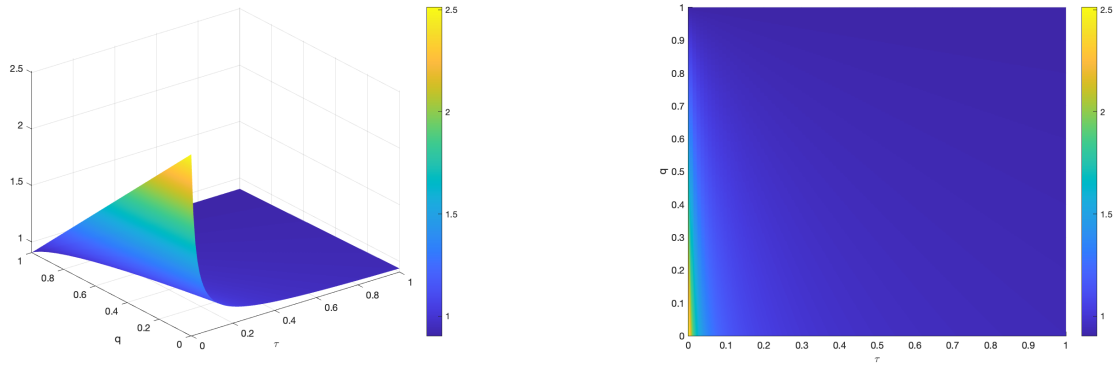
((a)) ((b))

Figure 6.14: Graphical illustration of the reproduction number $\mathscr{R}_0$ as a function of τ and m.



((a)) ((b))

Figure 6.15: Graphical illustration of the reproduction number $\mathscr{R}_0$ as a function of τ and θ.



((a)) ((b))

Figure 6.16: Graphical illustration of the reproduction number $\mathscr{R}_0$ as a function of τ and q.

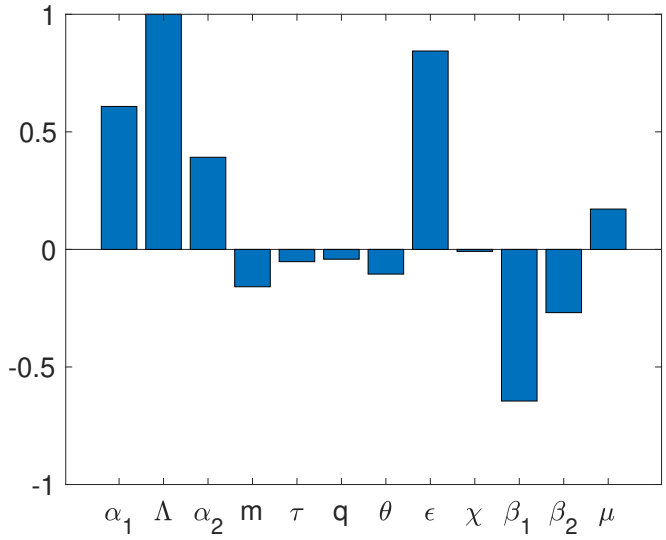


Figure 6.17: Graphical illustration of $\mathscr{R}_0$ sensitivity indices for Caputo model parameters.

6.4 Discussion

We have introduced the Caputo fractional derivative instead of the classical derivative in order to analyse the effect of family and public health education while taking the memory effect into account. We calculated the value of the reproductive number $\mathscr{R}_0$ and plotted some figures that show the change of solutions in terms of these variables to understand the effect of some parameters on drug spread as well as the effect of the fractional order.

6.4.1 Memory effect

As indicated in the introduction, the fractional order of the derivation can be explained by the memory effect, because the Caputo derivation that we used is non-local. To compare the classical

model (order one) with several different fractional order models, we solved our model using the fractional Euler numerical method for different values of the fractional order.

Figure 6.2 for susceptible peoples who do not accept the public health education S(t), Figure 6.3 for susceptible peoples who accept the public health education $C(t)$, Figure 6.4 for the light drug addicts peoples $L(t)$, Figure 6.5 for the heavy drug addicts persons $H(t)$, Figure 6.6 for the drug users in treatment $T(t)$ and Figure 6.7 for the permanent quit drug persons $R(t)$.

All the graphs listed above show that the fractional models for any value of the fractional order converge to the same equilibrium point. Figures 6.2(a)–6.7(a) show that the curves converge to the drug-free steady state $\mathscr{E}_0$, $\mathscr{R}_0 = 0.812021 < 1$ in this case. Furthermore, when $\mathscr{R}_0 = 1.607399 > 1$, we see from Figures 6.2(b)–6.7(b) that the curves converge to the endemic equilibrium $\mathscr{E}^*$. This is in perfect agreement with our theoretical results concerning the stability of $\mathscr{E}_0$ and $\mathscr{E}^*$. It is transparent, from the above illustrations, the order of the fractional derivative α has no effect on the stability of the equilibrium. However, increasing the value of α, which describes the long memory time, leads the solutions to converge to the stationary state more quickly. That is, the dynamics of drug transmission are determined by the strength of memory effects, which are controlled by the order of fractional derivative α. As a result, the dynamics of the drug transmission model depend on the time instant and the time history, which can be effectively modelled using the theory of fractional calculus [80], by considering the Caputo fractional derivative, we propose a more realistic model, which makes the system more robust and can be used by public health organisations and authorities in preventing and controlling drug spread.

6.4.2 The influence of model parameters

To show the influence of the parameters in the variation of the basic reproduction number $\mathscr{R}_0$, the latter is considered as a function with two variables and some graphical presentations of this number are made. The effect of m (the permanent quit drug rate after treatment) and θ (the treatment rate of heavy addicts) in Figure 6.8, m and χ (the permanent quit drug rate because of public health education) is shown in Figure 6.9, q (popularizing rate of family education) and χ in Figure 6.10, q and m is shown in Figure 6.11, q and θ in Figure 6.12, τ (the rate that susceptible individuals accept public health education)and χ in Figure 6.13, τ and m in Figure 6.14, τ and θ in Figure 6.15 and finally, the effect of τ and q is shown in Figure 6.16.

From Figure 6.8, it is clear that θ and m have a major influence on reducing the spread of drugs. Since prevention is better than treatment, it is clear from Figure 6.9 that the impact of the permanent quit drug rate because of public health education (χ) also has a considerable impact on the decrease of the $\mathscr{R}_0$ value, which affirms the impact of education. However, the purpose of this study is to examine the impact of education on reducing the spread of drugs. In order to explore and evaluate in detail this influence, we have plotted the following curves of τ and q.

Figures 6.10–6.15 depict that both τ and q have a small influence on how drugs spread. In

contrast, we subsequently deduce from Figure 6.16 that increasing τ and q simultaneously can reduce the number of base reproductions $\mathscr{R}_0$ faster than increasing τ or q alone, which would help the government fight the spread of drugs more effectively. However, educating families and the public health is a method for reducing drug transmission.

6.4.3 Sensitivity analysis of model parameters

For further clarification, as already mentioned in Subsection 6.3.4, among the tools that allow researchers to know the parameters that must be reduced or increased to fight against epidemics, that is, to reduce the value of the basic reproduction number $\mathscr{R}_0$, we find the so-called parameter sensitivity analysis.

In Figure 6.17, we have plotted the illustration of $\mathscr{R}_0$ sensitivity indices for Caputo model parameters to discuss the parameters that control the spread of drugs, which can be counted on to reduce the effect of drug addiction.

Although, as seen previously, $\mathscr{R}_0$ is influenced by various parameters such as θ, m, and others, as is obvious from Figure 6.17, here we want to explore in detail how education, whether in the family, public health, or both, may reduce the value of $\mathscr{R}_0$.

It is clear that q and τ have a small influence in this case compared to the other parameters, which also explains the results obtained in the previous subsection. This indicates that there is an influence, but taking into account the memory effect (The Caputo fractional case), it turns out that the impact of either τ or q is small, which means that the impact of both family and public health education should be taken into account because they are both relevant; to fight against drug transmission, it is important to decrease the number of basic reproductions, and for this it is necessary to increase both q and τ.

This conclusion will allow us to use different means of education or possibly adapt a new treatment strategy to reduce the drug transmission.

6.5 Conclusion

Drug addiction is a real disease that requires treatment and education to develop healthy attitudes in populations. In this work, taking into account that drug transmission involves memory, an analysis of the drug transmission dynamics in fractional-order derivatives has been provided, incorporating public and family health education. We have used the modified trapezoidal rule and the fractional Euler's method to demonstrate numerically that the fractional drug model provides more accurate and exciting results.

Specifically, it has been demonstrated that, while the fractional-order derivative α has no effect on the stability of the drug-free and endemic equilibrium points, it does affect the time to reach the steady states for each solution.

Consequently, both the analytical and numerical results indicated that, for higher values of α,

each solution converges more quickly to its stationary state.

On the other hand, using a sensitivity analysis, we have found that both the rate at which susceptible individuals accept public health education (τ) and the popularising rate of family education (q) have an effect on how drugs spread, which confirmed that an increase in both the family and public health education parameters may decrease the prevalence of drugs.

This study can be extended to other types of models, for example, to propose other types of fractional derivatives and compare the results. Space dependence can be added to build a spatio-temporal model, and random distribution can also be used to transform this model into a stochastic model.

CONCLUSION AND PERSPECTIVES

This thesis provides a comprehensive study of vesicle deformation, rigid particle dynamics, microswimmer trajectories, and an epidemiological model, with particular emphasis on drug abuse transmission. Using fractional derivatives, specifically the Jumarie modified Riemann-Liouville and Caputo derivatives, this work bridges analytical and numerical analyses to capture the complex memory effects inherent in these systems. The research covers both physical and biological models, exploring how memory effects influence vesicle dynamics under shear flow, the behavior of rigid particles, and the transmission dynamics in drug epidemiology. By incorporating fractional calculus, this thesis introduces a more accurate and flexible approach to modeling time-dependent processes and long-term interactions in both fluid dynamics and epidemiological contexts.

Several significant findings emerged from this research. First, two new motion types were identified in vesicle dynamics under shear flow, expanding the classical tank-treading (TT), tumbling (TB), and vacillating-breathing (VB) modes. These new modes provide deeper insights into the behavior of vesicles, particularly in the presence of strong memory effects. Additionally, the study confirmed Keller and Skalak's predictions on vesicle flipping behavior, offering analytical solutions that extend our understanding of these transitions. In the realm of rigid particle dynamics, the fractional models enabled an accurate mapping of these systems to the vesicle problem, revealing new motion regimes that can be applied to various biological and synthetic materials.

Furthermore, the investigation into microswimmer trajectories in 1D shear flow demonstrated the influence of memory effects on their paths, enriching the current understanding of fractional-order models in fluid mechanics. Lastly, the epidemiological model focused on drug transmission dynamics introduced an innovative use of fractional derivatives to model the progression and control of drug abuse. This model, which integrates public and family health education, offers new perspectives on controlling drug-related epidemics by emphasizing the long-term memory effects of behavioral interventions.

The findings of this thesis open up several promising avenues for future research. One immediate direction is the investigation of spatial diffusion effects on vesicle and rigid particle dynamics, which could provide further insights into their behavior in more complex and heterogeneous environments. In addition, exploring the impact of external fields, such as electromagnetic or gravitational fields, on vesicle dynamics and microswimmer trajectories will enhance our under-

standing of their behavior under more intricate conditions. Another exciting area of exploration involves expanding this work to nonspherical and biologically inspired models, with potential applications in understanding cell and microorganism behavior in varying fluid environments.

On the epidemiological front, there is significant potential to further develop fractional models of drug transmission, particularly by incorporating machine learning techniques to predict and analyze behavioral trends based on the models derived here. These approaches could lead to more effective public health strategies and targeted interventions in controlling drug abuse. The combination of machine learning and fractional calculus offers exciting opportunities to deepen our understanding of both biological systems and public health challenges, ensuring that the foundational work presented in this thesis will continue to impact a range of scientific and engineering disciplines.

REFERENCES

[1] *Red blood cell images - pixabay*, 2024. Accessed: 2024-10-23.

[2] A. AARAB, M. GUEDDA, N. ALAA, AND C. MISBAH, *Mapping vesicle dynamics onto that of a rigid sphere in five dimensions*, Physical Review E, 98 (2018), p. 042407.

[3] A. ABIDEMI, *Optimal cost-effective control of drug abuse by students: insight from mathematical modeling*, Modeling Earth Systems and Environment, (2022), pp. 1–19.

[4] E. AHMED, A. EL-SAYED, AND H. A. EL-SAKA, *On some routh–hurwitz conditions for fractional order differential equations and their applications in lorenz, rössler, chua and chen systems*, Physics Letters A, 358 (2006), pp. 1–4.

[5] H. F. AHMED, *Fractional euler method; an effective tool for solving fractional differential equations.*, Journal of the Egyptian Mathematical Society, 26 (2018).

[6] K. AKDIM, A. EZ-ZETOUNI, AND M. ZAHID, *The influence of awareness campaigns on the spread of an infectious disease: a qualitative analysis of a fractional epidemic model*, Modeling Earth Systems and Environment, 8 (2022), pp. 1311–1319.

[7] A. ALI, F. S. ALSHAMMARI, S. ISLAM, M. A. KHAN, AND S. ULLAH, *Modeling and analysis of the dynamics of novel coronavirus (covid-19) with caputo fractional derivative*, Results in Physics, 20 (2021), p. 103669.

[8] S. ALIZADEH, D. BALEANU, AND S. REZAPOUR, *Analyzing transient response of the parallel rcl circuit by using the caputo–fabrizio fractional derivative*, Advances in Difference Equations, 2020 (2020), pp. 1–19.

[9] A. ALLA HAMOU, E. AZROUL, G. DIKI, AND M. GUEDDA, *Effect of family and public health education in drug transmission: an epidemiological model with memory*, Modeling Earth Systems and Environment, 9 (2023), pp. 2809–2828.

[10] L. AN, F. JI, Y. YIN, Y. LIU, AND C. ZHOU, *Modeling of red blood cells in capillary flow using fluid–structure interaction and gas diffusion*, Cells, 11 (2022), p. 3987.

[11] E. Azroul, S. Bouda, G. Diki, and M. Guedda, *Analytical solutions and classification of vesicle motion and deformation in shear flow: Uncovering new tank-treading modes*, Chaos: An Interdisciplinary Journal of Nonlinear Science, 34 (2024).

[12] E. Azroul and G. Diki, *Analytical investigation of vesicle dynamics via the modified riemann–liouville fractional derivative: Mittag-leffler function solution and comparative analysis with caputo's derivative*, Chaos: An Interdisciplinary Journal of Nonlinear Science, 34 (2024).

[13] E. Azroul and G. Diki, *Dynamic insights on the caputo derivative's impact in unraveling vesicle behavior*, in Proceedings of the International Conference on Fractional Calculus and Applications (ICFCA 2024), 2024. Accepted.

[14] ——, *Motion of an ellipsoidal particle in shear flow: Analyzing memory effect influence through exact solutions investigation*, in Proceedings of the International Conference on Intelligent Computing in Data Sciences (ICDS 2024), 2024. Accepted.

[15] E. Azroul, G. Diki, and M. Guedda, *Exploring the interplay between memory effects and vesicle dynamics: A five-dimensional analysis using rigid sphere models and mapping techniques*, Studies in Applied Mathematics, (2023).

[16] L. C. d. Barros, M. M. Lopes, F. S. Pedro, E. Esmi, J. P. C. d. Santos, and D. E. Sánchez, *The memory effect on fractional calculus: an application in the spread of covid-19*, Computational and Applied Mathematics, 40 (2021), pp. 1–21.

[17] R. Bellman and R. S. Roth, *The laplace transform*, vol. 3, World Scientific, 1984.

[18] H. C. Berg, *E. coli in Motion*, Springer, 2004.

[19] H. Brenner, *Rheology of a dilute suspension of dipolar spherical particles in an external field*, Journal of Colloid and Interface Science, 32 (1970), pp. 141–158.

[20] F. P. Bretherton, *The motion of rigid particles in a shear flow at low reynolds number*, Journal of Fluid Mechanics, 14 (1962), pp. 284–304.

[21] M. N. Burattini, E. Massad, F. A. B. Coutinho, R. S. d. Azevedo-Neto, R. Menezes, and L. Lopes, *A mathematical model of the impact of crack-cocaine use on the prevalence of hiv/aids among drug users*, Mathematical and computer modelling, 28 (1998), pp. 21–29.

[22] X. Cen, Z. Feng, and Y. Zhao, *Emerging disease dynamics in a model coupling within-host and between-host systems*, Journal of theoretical biology, 361 (2014), pp. 141–151.

[23] L. CHEN, Y. CHAI, R. WU, AND J. YANG, *Stability and stabilization of a class of nonlinear fractional-order systems with caputo derivative*, IEEE Transactions on Circuits and Systems II: Express Briefs, 59 (2012), pp. 602–606.

[24] Y. CHEN, F. LIU, Q. YU, AND T. LI, *Review of fractional epidemic models*, Applied mathematical modelling, 97 (2021), pp. 281–307.

[25] N. CHITNIS, J. M. HYMAN, AND J. M. CUSHING, *Determining important parameters in the spread of malaria through the sensitivity analysis of a mathematical model*, Bulletin of mathematical biology, 70 (2008), pp. 1272–1296.

[26] G. DANKER, C. VERDIER, AND C. MISBAH, *Rheology and dynamics of vesicle suspension in comparison with droplet emulsion*, Journal of non-newtonian fluid mechanics, 152 (2008), pp. 156–167.

[27] K. DIETHELM, *Efficient solution of multi-term fractional differential equations using p (ec) m e methods*, Computing, 71 (2003), pp. 305–319.

[28] K. DIETHELM AND N. J. FORD, *Analysis of fractional differential equations*, Journal of Mathematical Analysis and Applications, 265 (2002), pp. 229–248.

[29] K. DIETHELM, N. J. FORD, AND A. D. FREED, *A predictor-corrector approach for the numerical solution of fractional differential equations*, Nonlinear Dynamics, 29 (2002), pp. 3–22.

[30] A. DIN AND Y. LI, *Controlling heroin addiction via age-structured modeling*, Advances in Difference Equations, 2020 (2020), pp. 1–17.

[31] M. DU, Z. WANG, AND H. HU, *Measuring memory with the order of fractional derivative*, Scientific reports, 3 (2013), pp. 1–3.

[32] J. DUPIRE, M. SOCOL, AND A. VIALLAT, *Full dynamics of a red blood cell in shear flow*, Proceedings of the National Academy of Sciences, 109 (2012), pp. 20808–20813.

[33] E. FENDZI-DONFACK, G. W. K. TEMGOUA, Z. I. DJOUFACK, A. KENFACK-JIOTSA, J. P. NGUENANG, AND L. NANA, *Exotical solitons for an intrinsic fractional circuit using the sine-cosine method*, Chaos, Solitons & Fractals, 160 (2022), p. 112253.

[34] Z. FENG, X. CEN, Y. ZHAO, AND J. X. VELASCO-HERNANDEZ, *Coupled within-host and between-host dynamics and evolution of virulence*, Mathematical biosciences, 270 (2015), pp. 204–212.

[35] S. FUNK, M. SALATHÉ, AND V. A. JANSEN, *Modelling the influence of human behaviour on the spread of infectious diseases: a review*, Journal of the Royal Society Interface, 7 (2010), pp. 1247–1256.

[36] B. GHANBARI AND A. ATANGANA, *A new application of fractional atangana–baleanu derivatives: designing abc-fractional masks in image processing*, Physica A: Statistical Mechanics and its Applications, 542 (2020), p. 123516.

[37] M. GUEDDA, M. ABAIDI, M. BENLAHSEN, AND C. MISBAH, *Dynamic modes of quasispherical vesicles: Exact analytical solutions*, Physical Review E, 86 (2012), p. 051915.

[38] M. GUEDDA, J. CHAIBOUB, M. BENLAHSEN, AND C. MISBAH, *Exact trajectory solutions of a spherical microswimmer under flow and external fields*, Physical Review Fluids, 6 (2021), p. 074102.

[39] W. HALL AND S. BUSENBERG, *Viscosity of magnetic suspensions*, The Journal of Chemical Physics, 51 (1969), pp. 137–144.

[40] L. G. HUNT, C. D. CHAMBERS, ET AL., *The heroin epidemics: a study of heroin use in the United States, 1965-1975*, vol. 2, Halsted Press, 1976.

[41] J. HUO, H. ZHAO, AND L. ZHU, *The effect of vaccines on backward bifurcation in a fractional order hiv model*, Nonlinear Analysis: Real World Applications, 26 (2015), pp. 289–305.

[42] G. B. JEFFERY, *The motion of ellipsoidal particles immersed in a viscous fluid*, Proceedings of the Royal Society of London. Series A, Containing papers of a mathematical and physical character, 102 (1922), pp. 161–179.

[43] I. M. H. JULIUS K. K., *Bolasomen als durchbruch für die wirkstofffreisetzung?*, Deutsche Apotheker Zeitung, (2018).

[44] G. JUMARIE, *Modified riemann-liouville derivative and fractional taylor series of non-differentiable functions further results*, Computers & Mathematics with Applications, 51 (2006), pp. 1367–1376.

[45] ——, *Table of some basic fractional calculus formulae derived from a modified riemann–liouville derivative for non-differentiable functions*, Applied Mathematics Letters, 22 (2009), pp. 378–385.

[46] D. KAI, *The analysis of fractional differential equations: An application-oriented exposition using differential operators of caputo type*, in Lecture Notes in Mathematics, Springer, 2010.

[47] A. S. KALULA AND F. NYABADZA, *A theoretical model for substance abuse in the presence of treatment*, South African Journal of Science, 108 (2012), pp. 1–12.

[48] S. R. KELLER AND R. SKALAK, *Motion of a tank-treading ellipsoidal particle in a shear flow*, Journal of Fluid Mechanics, 120 (1982), pp. 27–47.

[49] W. O. KERMACK AND A. G. MCKENDRICK, *A contribution to the mathematical theory of epidemics*, Proceedings of the royal society of london. Series A, Containing papers of a mathematical and physical character, 115 (1927), pp. 700–721.

[50] J. O. KESSLER, *Hydrodynamic focusing of motile algal cells*, Nature, 313 (1985), pp. 218–220.

[51] M. KRAUS, W. WINTZ, U. SEIFERT, AND R. LIPOWSKY, *Fluid vesicles in shear flow*, Physical review letters, 77 (1996), p. 3685.

[52] G. LEDDER, *Mathematical modeling for epidemiology and ecology*, Springer, 2023.

[53] A. P. LEMOS-PAIÃO, C. J. SILVA, AND D. F. TORRES, *An epidemic model for cholera with optimal control treatment*, Journal of Computational and Applied Mathematics, 318 (2017), pp. 168–180.

[54] J. LI AND M. MA, *The analysis of a drug transmission model with family education and public health education*, Infectious Disease Modelling, 3 (2018), pp. 74–84.

[55] LIENARD, *Sur le signe de la partie réelle des racines d'une équation algébrique*, Journal de Mathématiques Pures et Appliquées, 10 (1914), pp. 291–346.

[56] W. LIN, *Global existence theory and chaos control of fractional differential equations*, Journal of Mathematical Analysis and Applications, 332 (2007), pp. 709–726.

[57] C.-S. LIU, *Counterexamples on jumarie's two basic fractional calculus formulae*, Communications in Nonlinear Science and Numerical Simulation, 22 (2015), pp. 92–94.

[58] ——, *Counterexamples on jumarie's three basic fractional calculus formulae for non-differentiable continuous functions*, Chaos, Solitons & Fractals, 109 (2018), pp. 219–222.

[59] H. LIU, *Lyapunov-type inequalities for certain higher-order difference equations with mixed non-linearities*, Advances in Difference Equations, 2018 (2018), pp. 1–14.

[60] J. LIU AND T. ZHANG, *Global behaviour of a heroin epidemic model with distributed delays*, Applied Mathematics Letters, 24 (2011), pp. 1685–1692.

[61] E. LUNGU, M. KGOSIMORE, AND F. NYABADZA, *Models for the spread of hiv/aids: Trends in southern*, in Mathematical Studies on Human Disease Dynamics: Emerging Paradigms and Challenges: AMS-IMS-SIAM Joint Summer Research Conference on Modeling the Dynamics of Human Diseases: Emerging Paradigms and Challenges, July 17-21, 2005, Snowbird, Utah, vol. 410, American Mathematical Soc., 2006, p. 259.

[62] D. R. MacKintosh and G. T. Stewart, *A mathematical model of a heroin epidemic: implications for control policies.*, Journal of Epidemiology & Community Health, 33 (1979), pp. 299–304.

[63] D. Matignon, *Stability results for fractional differential equations with applications to control processing*, in Computational engineering in systems applications, vol. 2, Lille, France, 1996, pp. 963–968.

[64] C. Misbah, *Vacillating breathing and tumbling of vesicles under shear flow*, Physical review letters, 96 (2006), p. 028104.

[65] Z. Mukandavire, W. Garira, and J. Tchuenche, *Modelling effects of public health educational campaigns on hiv/aids transmission dynamics*, Applied Mathematical Modelling, 33 (2009), pp. 2084–2095.

[66] G. Mulone and B. Straughan, *A note on heroin epidemics*, Mathematical Biosciences, 218 (2009), pp. 138–141.

[67] Y. Muroya, H. Li, and T. Kuniya, *Complete global analysis of an sirs epidemic model with graded cure and incomplete recovery rates*, Journal of Mathematical Analysis and Applications, 410 (2014), pp. 719–732.

[68] J. Mushanyu, F. Nyabadza, and A. Stewart, *Modelling the trends of inpatient and outpatient rehabilitation for methamphetamine in the western cape province of south africa*, BMC research notes, 8 (2015), pp. 1–13.

[69] P. A. Naik, M. Yavuz, S. Qureshi, J. Zu, and S. Townley, *Modeling and analysis of covid-19 epidemics with treatment in fractional derivatives using real data from pakistan*, The European Physical Journal Plus, 135 (2020), pp. 1–42.

[70] F. Nyabadza and S. D. Hove-Musekwa, *From heroin epidemics to methamphetamine epidemics: Modelling substance abuse in a south african province*, Mathematical biosciences, 225 (2010), pp. 132–140.

[71] F. Nyabadza, J. B. Njagarah, and R. J. Smith, *Modelling the dynamics of crystal meth ('tik') abuse in the presence of drug-supply chains in south africa*, Bulletin of mathematical biology, 75 (2013), pp. 24–48.

[72] Z. Odibat, *Approximations of fractional integrals and caputo fractional derivatives*, Applied Mathematics and Computation, 178 (2006), pp. 527–533.

[73] Z. M. Odibat and S. Momani, *An algorithm for the numerical solution of differential equations of fractional order*, Journal of Applied Mathematics & Informatics, 26 (2008), pp. 15–27.

[74] Z. M. Odibat and N. T. Shawagfeh, *Generalized taylor's formula*, Applied Mathematics and Computation, 186 (2007), pp. 286–293.

[75] T. J. Pedley and J. Kessler, *The orientation of spheroidal microorganisms swimming in a flow field*, Proceedings of the Royal Society of London. Series B. Biological Sciences, 231 (1987), pp. 47–70.

[76] I. Podlubny, *Fractional differential equations: an introduction to fractional derivatives, fractional differential equations, to methods of their solution and some of their applications*, Elsevier, 1998.

[77] D. Qian, C. Li, R. P. Agarwal, and P. J. Wong, *Stability analysis of fractional differential system with riemann–liouville derivative*, Mathematical and Computer Modelling, 52 (2010), pp. 862–874.

[78] R. Resmawan, N. Supu, and N. Achmad, *Dynamic model analysis of the spread of drug addicts with educational effects*, in 1st International Conference on Mathematics and Mathematics Education (ICMMEd 2020), Atlantis Press, 2021, pp. 55–64.

[79] S. R. Ross and D. Thomson, *Pseudo-Relapses in Cases of Malarial Fever During Continuous Quinine Treatment*, University Press, 1911.

[80] M. Saeedian, M. Khalighi, N. Azimi-Tafreshi, G. Jafari, and M. Ausloos, *Memory effects on epidemic evolution: The susceptible-infected-recovered epidemic model*, Physical Review E, 95 (2017), p. 022409.

[81] S. Saratha, G. S. S. Krishnan, and M. Bagyalakshmi, *Analysis of a fractional epidemic model by fractional generalised homotopy analysis method using modified riemann-liouville derivative*, Applied Mathematical Modelling, 92 (2021), pp. 525–545.

[82] G. J. Thorn and R. N. Bearon, *Transport of spherical gyrotactic organisms in general three-dimensional flow fields*, Physics of fluids, 22 (2010).

[83] R. Ud Din, K. Shah, I. Ahmad, and T. Abdeljawad, *Study of transmission dynamics of novel covid-19 by using mathematical model*, Advances in Difference Equations, 2020 (2020), pp. 1–13.

[84] S. Ullah and M. A. Khan, *Modeling the impact of non-pharmaceutical interventions on the dynamics of novel coronavirus with optimal control analysis with a case study*, Chaos, Solitons & Fractals, 139 (2020), p. 110075.

[85] P. Van den Driessche and J. Watmough, *Reproduction numbers and subthreshold endemic equilibria for compartmental models of disease transmission*, Mathematical biosciences, 180 (2002), pp. 29–48.

[86] C. VARGAS-DE-LEÓN, *Volterra-type lyapunov functions for fractional-order epidemic systems*, Communications in Nonlinear Science and Numerical Simulation, 24 (2015), pp. 75–85.

[87] W. WANG, S. LU, H. TANG, B. WANG, C. SUN, P. ZHENG, Y. BAI, Z. LU, AND Y. KANG, *A scoping review of drug epidemic models*, International Journal of Environmental Research and Public Health, 19 (2022), p. 2017.

[88] E. WHITE AND C. COMISKEY, *Heroin epidemics, treatment and ode modelling*, Mathematical biosciences, 208 (2007), pp. 312–324.

[89] H. XIANG, N.-N. SONG, AND H.-F. HUO, *Modelling effects of public health educational campaigns on drinking dynamics*, Journal of biological dynamics, 10 (2016), pp. 164–178.

[90] Q. YANG, D. CHEN, T. ZHAO, AND Y. Q. CHEN, *Fractional calculus in image processing: a review*, Fractional Calculus and Applied Analysis, 19 (2016), pp. 1222–1249.

[91] Q. ZENG, G. CAO, AND X. ZHU, *The asymptotic stability on sequential fractional order systems*, J. Shanghai Jiatong Univ., 39 (2005), pp. 346–348.

[92] S. ZHANG, *A generalized exp-function method for fractional riccati differential equations*, Communications in Fractional Calculus, 1 (2010), pp. 22–27.

[93] M. ZHAO, *Dynamics of microcapsules and red blood cells in time-dependent shear flow*, Rutgers The State University of New Jersey, School of Graduate Studies, 2011.